Autoxidation of Oilsands Bitumen: Applied, Model Compounds and Microfluidic Study

by

Muhammad Nurunnabi Siddiquee

A thesis submitted in partial fulfillment of the requirements for the degree of

Doctor of Philosophy

in

Chemical Engineering

Department of Chemical and Materials Engineering
University of Alberta

Abstract

Canada has the world's largest oilsands reserves. Part of the reserves is being considered as marginal and is not profitable to recover using current technology. Autoxidation (oxidation with air) is a potential upgrading strategy to produce more valuable products from the oilsands derived bitumen at low cost. Bitumen hardening, however, is a potential challenge to make the upgrading process viable. The interest of this study was to get a better fundamental understanding to prevent or reduce hardening as a generic problem faced by low temperature free radical conversion processes. The research documented in this thesis comprises four different studies to advance the knowledge in the field. In the first study, bitumen was autoxidized at different temperatures and times to understand the extent of hardening and corresponding chemical and physical changes due to autoxidation. Although bitumen hardening was anticipated, it was severe with an order of magnitude increase in both penetration hardness and viscosity after autoxidation at 130 °C for 229 hours. The relative aliphatic to aromatic hydrogen losses were 18:1, 30:1 and 32:1, respectively, for the bitumen autoxidation of 6 hours at 140, 150 and 160 °C. Hydrogen disproportionation occurred during autoxidation of bitumen indicating unsaturation that led to free radical addition and heavier product formation. Model compounds representing different hydrocarbon and heterocyclic compound classes were autoxidized in the second study to understand the compounds responsible for oxidative addition that potentially caused bitumen hardening and the mechanism to form addition products. The results revealed that naphthenic–aromatic compounds, pyrrolic O–containing compounds and pyrrolic N–containing compounds were susceptible to form heavier products. Five–membered naphthenic–aromatic hydrocarbons, indene and indan, were more prone to oxidative addition than even their pyrrolic analogues, indole and 2,3–dihydroindole, which were known to be prone to oxidative

addition. In all the instances, higher molecular weight products were C–C coupled by free radical addition. The third study put special emphases on the controlling of product selectivity at near constant conversion via manipulating oxygen availability by changing the hydrodynamics of a microfluidic reactor. Increasing oxygen availability in the liquid phase at near constant conversion, constant oxygen partial pressure and constant temperature increased the ketone–to–alcohol selectivity in primary oxidation products by an order of magnitude from less than 1:1 to 14:1. A crucial insight that came from the study of oxidation selectivity was that ketone–to–alcohol selectivity in primary oxidation products was an indicator of oxygen availability in the liquid phase during oxidation and the likelihood of free radical addition. In the fourth study, engineering aspects of liquid phase autoxidation were studied experimentally to confirm the oxygen level in the bulk liquid phase during the liquid phase autoxidation. Only in extreme cases, when a very high oxidation rate causes the reaction system to become severely mass transfer limited and does the oxygen level in the bulk liquid reach zero, oxidation takes place in the film. Low oxygen availability could potentially lead to increased formation of addition products, since there is insufficient oxygen to drive free radical termination by oxidation to final products. The study confirmed that liquid phase oxidation was kinetically controlled during the induction period of autoxidation of indan and reached complete saturation with air (19.2 kPa O_2) during this period. Liquid phase autoxidation was limited by mass transfer after the induction period and oxygen level decreased in the liquid phase. It was possible to determine to what extent oxidation took place in the film and in the bulk phases. The reaction rate threshold was 2.6×10^{-3} (mol/m^3.s) or 3.4×10^{-6} (mol/m^2.s) for the reaction to occur in the film instead of the bulk. The oxygen concentration in the bulk liquid phase was measured experimentally, while performing autoxidation, instead of relying on theory to predict the liquid phase oxygen

concentration. In conclusion, the main contributions made by this thesis are: (i) identifying the main compound classes responsible for free radical addition reactions with an explanation based on their reaction pathways, (ii) demonstrating how oxygen availability can be used to control oxidation selectivity independent of conversion by manipulating reactor hydrodynamics, and (iii) modifying the current theoretically predicted threshold for oxidation in the film based on the Hatta-number by performing *in situ* liquid phase oxygen measurements during autoxidation.

Preface

(Mandatory due to collaborative work)

Chapter 3 of this thesis was published partly as "Siddiquee, M. N.; De Klerk, A. Hydrocarbon addition reactions during low-temperature autoxidation of oilsands bitumen. *Energy Fuels* **2014**, *28* (11), 6848–6859" and "Siddiquee, M. N.; De Klerk, A. Continuous and prolonged oxidation of bitumen for upgrading by microbial digestion. *Prepr. Pap.-Am. Chem. Soc., Div. Energy Fuels* **2013**, *58*(2), 649–651". I was responsible for concept formation, experimental design, data collection and analysis as well as the manuscript composition. Arno de Klerk was the supervisory author and was involved with concept formation, data analysis, and manuscript composition.

Chapter 4 of this thesis was published partly as "Siddiquee, M. N.; De Klerk, A. Hydrocarbon addition reactions during low-temperature autoxidation of oilsands bitumen. *Energy Fuels* **2014**, *28* (11), 6848–6859"; and "Siddiquee, M. N.; De Klerk, A. Oxidation of naphthenic-aromatic compounds in bitumen. *Prepr.Pap.-Am. Chem. Soc., Div. Energy Fuels* **2014**, *59*(2), 572–574". I was responsible for concept formation, experimental design, data collection and analysis as well as the manuscript composition. Arno de Klerk was the supervisory author and was involved with concept formation, data analysis, and manuscript composition.

Chapter 5 of this thesis was published as "Siddiquee, M. N.; De Klerk, A. Heterocyclic addition reactions during low temperature autoxidation. *Energy Fuels* **2015**, *29* (7), 4236–4244." I was responsible for concept formation, experimental design, data collection and analysis as well as the manuscript composition. Arno de Klerk was the supervisory author and was involved with concept formation, data analysis, and manuscript composition.

Chapter 6 of this thesis was submitted to be published in Reaction Chemistry and Engineering as "Siddiquee, M. N.; De Klerk, A.; Nazemifard, N. Application of microfluidics to control product– selectivity during non-catalytic oxidation of naphthanic–aromatic hydrocarbon." I was responsible for concept formation, experimental design, data collection and analysis as well as the manuscript composition. Arno de Klerk and Neda Nazemifard were the supervisory authors and were involved with concept formation, data analysis, and manuscript composition.

Chapter 7 of this thesis was submitted to be published in Industrial and Engineering Chemistry Research as "Siddiquee, M. N.; De Klerk, A. *In situ* measurement of liquid Phase oxygen during oxidation." I was responsible for concept formation, experimental design, data collection and analysis as well as the manuscript composition. Arno de Klerk was the supervisory author and was involved with concept formation, data analysis, and manuscript composition.

Dedication

To Kanij Fatema– my beloved wife

To Nusaybah– my cuddly princes

To Noman– my delightful son

To my respectful parents

Acknowledgements

First of all, I would like to express my deepest gratitude to almighty Allah who gave me enough strength and patience to complete a successful long journey of about four and half years. I would like to extend my sincere thanks and gratitude to my supervisors, Dr. Arno de Klerk and Dr. Neda Nazemifard, for their supervision, insight, advice, and guidance throughout my graduate studies. They provided me enthusiastic supports and encouragements to apply my own ideas, which have broadened my knowledge in the area of my study and helped me to complete this research work. I am very proud to have had the opportunity to work with them.

I would like to acknowledge the funding provided by the Cenovus FCCL Ltd as Operator for FCCL partnership in conjunction with NSERC-CRD (Natural Sciences and Engineering Research Council of Canada through the Co-operative Research and Development) program. I also want to acknowledge the Faculty of Graduate studies and Research (FGSR), University of Alberta to select me for the Doctoral Requirement Scholarship (2011) and Gerald J Maier/NOVA Chemicals Corporation Graduate Recruitment Award (2015).

I offer my sincere appreciation to Dr. Domonic Sauvageau and Dr. Qi Liu of Chemical and Materials Engineering Department, and Dr. Gabriele Centi from the Industrial Chemistry Department at the University of Messina, Italy for being in my examination committee and for their assurance and informative views.

Special thanks to all my current and past research group members and friends especially Dr. Shaofeng Yang and Dr. Cibele Melo Halmenschlager for their help in purchasing some lab stuffs and equipments; Toluwanise Adesanwo and Jose García Zapata for their help to setup some early experiments, Allision De Man and Sima Hendessi for co-ordinating their parts of the research project. Help from Mikel, Chan, Xiao, and Kevan to perform image processing and calculations of some microfluidic experiments are highly appreciated.

It is a pleasure to convey my gratitude to Dr. Moshfiqur Rahman for his help with the SARA fractionation of bitumen samples and Derek Guenther, Senior R&D Scientist, Ocean Optics for his support during the development of the *in situ* oxygen partial pressure measurements in the

liquid phase. Special thanks to Lily Laser, Marion Pritchard, Walter Boddez, Les Dean, Matthew Kloster, and Kevin Heidebrecht of Chemical and Materials Engineering Department for their supports during the course of my studies.

I am deeply indebted to my parents and relatives for their support, encouragement, and guidance all over my life. I would also like to thanks my friends who help my family in different ways and made our stay enjoyable in Canada specially Md. Hosany Mobarok, S M Al-Rafia, Shah Asifur Rahman, Alaul Azim, Safa Tasneem, and Sourav Chowhury.

Last but not least, I would like to convey sincere thank and gratitude to my dear wife, *Kanij Fatema*, for providing two valuable gifts *Nusaybah* and *Noman* and for all her love, supports, understanding and patience during the course of my studies.

Table of Contents

List of Tables

List of Figures

Nomenclature

a	gas-liquid interfacial area, (m^2/m^3)
A	pre-exponential factor
A_i	peak area of model compounds
Ca	capillary number, two-phase, $Ca = U_{TP}\mu L/\sigma$
C_A^*	concentration of gas at the interface, (mol/m^3)
CASRN	chemical abstracts services registry number
C_b	concentration of gas in bulk liquid (mol/m^3)
Da	Damköhler number; $\mathrm{Da} = (k_r\, C_A^* \delta^2)/D_A$
D_A	diffusivity of oxygen in tetralin (m^2/s)
d_H	hydraulic diameter; $d_H = 2[wh/(w+h)]$, (m)
DTBP	di-tert-butyl peroxide
E_a	activation energy, (kJ/mol)
FID	flame ionization detector
Fo	Fourier number, $Fo = L_G D_A/\delta_L^2 U_G$
GC	gas chromatography
h	depth of the reactor, (m)
HCB	hexachlorobenzene
HCN	hydrogen, carbon and nitrogen
HP DSC	high-pressure differential scanning calorimeter
HPLC	high performance liquid chromatography
^{1}H NMR	proton nuclear magnetic resonance
J_A	mass transfer rate across the gas-liquid interface ($mol/m^3.s$)
k_L	mass transfer coefficient; $k_L = D_A/\delta$, (m/s)
k_La	overall mass transfer coefficient, (s^{-1})
k_r	reaction rate constant
L_G	length of gas bubble, (m)

L_S	length of liquid slug, (m)
M_H	Hatta modulus; $M_H = \delta\sqrt{k_r C_A^*/D_A}$
MS	mass spectrometry
m/z	mass-to-charge ratio
n-C_5	normal pentane
NIST	National Institute of Standards and Technology
Pe_L	Peclet number; $Pe_L = \delta_L^2 U_L/D_A$
Pe_L	Peclet number; $Pe_L = Re_L Sc_L$
PTFE	Poly tetra fluoro ethylene
Re_G	gas-phase Reynolds number; $Re_G = U_G d_H \rho_G/\mu_G$
Re_L	liquid-phase Reynolds number; $Re_L = U_L d_H \rho_L/\mu_L$
Re_{TP}	two-phase Reynolds number; $Re_{TP} = U_{TP} d_H \rho_L/\mu_L$
RF	response factor
RRF	relative response factor
RTD	residence time distribution
Sc_L	Schimdt number, $Sc_L = \mu_L/D_A\rho_L$
S_G	surface area of gas bubble, (m^2)
Sh_L	Sherwood number; $Sh_L = k_L d_H/D_A$
t	retention time of GC analysis
U_G	superficial gas bubble velocity, (m/s)
U_L	superficial liquid slug velocity, (m/s)
U_{TP}	two phase superficial velocity, (m/s)
V_G	volume of gas bubble, (m^3)
V_L	volume of liquid slug, (m^3)
w	width of the reactor, (m)
We	Wever number; $We = D_h U_{TP}^2 \rho_L/\sigma_L$
W_{HCB}	Weight % of hexachlorobenzene
W_i	Weight % of model compounds

Greek letters

δ	thickness of liquid film, (m)
ε_G	volume fraction of gas bubble
ρ_G	density of gas, (kg/m^3)
ρ_l	density of liquid, (kg/m^3)
μ_G	gas viscosity, (Pa.s)
μ_L	liquid viscosity, (Pa.s)
σ	surface tension, (N/m)

Subscripts

b	bulk
G	gas
L	liquid
TP	two-phase

CHAPTER 1 – INTRODUCTION

1.1 Background

World energy consumption is increasing day by day. Liquid fuel is advantageous over gas and solid fuels in terms of transportation and energy density. At present, most of the liquid fuels come from non-renewable conventional crude oil reserves. But, the conventional crude oil reserves are limited – they constitute only 30% of the total oil reserves (**Figure 1.1**). The remaining 70% of the total oil reserves are unconventional oils that include heavy oil (°API gravity 10-19, density 900-1000 kg/m^3, and viscosity 10^2-10^5 mPa.s); extra heavy oil (°API gravity < 10, density > 1000 kg/m^3, and viscosity < 10^5 mPa.s) and oil sands bitumen (°API gravity < 10, density > 1000 kg/m^3, and viscosity > 10^5 mPa.s) (Gray, 2015; Nji, 2010). Conventional crude oil reserves has led to extensive research to find energy from alternative non-crude feed materials.

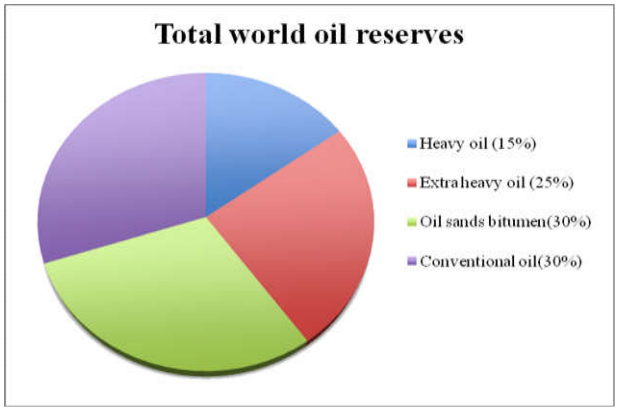

Figure 1.1. Total world oil reserves (Nji, 2010).

Energy recovery from non-crude oil reserves is technologically different and expensive compared to that from conventional crude oil resources, although the recovered oil components are sometimes less valuable than the conventional crude oils (Fedorak et al., 2009). However, unconventional crude oils are naturally abundant (Gray, 2015). A substantial effort has been made to produce fuel from bitumen in oilsands (bituminous sand).

There are large quantities of oilsands in several locations around the world. Canada has the world's largest oilsands deposits that contain approximately 2400 billion barrels of bitumen. Approximately 5 billion barrels of bitumen have been recovered and approximately 174 billion barrels of bitumen are recoverable using current technology (Gray, 2015). The average bitumen content in Canadian oilsands is 10–12 %; however, it actually varies within the range of 6–18 %. Oilsands with a low bitumen content is not considered economically feasible to process and is rejected because of the overburden. Moreover, there is no proven technology for the recovery of bitumen from oilsands deposits within 75–200 meters below the earth's surface (De Klerk et al., 2014). Hence, approximately 2200 billion barrels of bitumen resources are considered as marginal that are not profitable using current technology.

Bitumen derived from Canadian oilsands is heavy and extremely viscous (10 100 Pa.s) (De Klerk et al., 2014) and must be refined to produce usable fuels. There are some processes to upgrade oil sands derived bitumen such as thermal cracking and coking, hydroconversion, hydrocracking, hydrotreating etc. (Gray, 2015). In addition, regeneration and/or recovery of the catalysts used in upgrading processes are very difficult (Gray, 2015; Rana et al., 2007). Bitumen is fouling on account of its high organic metal content (for instance, chelates of Nickel (Ni) and Vanadium (V)) and residual mineral content (Strausz and Lown, 2003). Bitumen refining is also hydrogen intensive due to its high heteroatom content, especially sulfur. Moreover, marginal oilsands is not economically viable to upgrade using current technology. Hence, it is desirable to develop a viable bitumen recovery and upgrading process that can produce a cleaner product at lower cost.

An alternative approach that was suggested (Fedorak et al., 2009) is the conversion of the bitumen to methane by microorganisms, and the recovery of methane as a much cleaner fuel. Although at the current price of methane ($ 2.4/GJ)[a], it seems that methane production from bitumen will not be profitable, the proposed process is justified based on a longer term vision by industry.

[a]Source of gas price: http://www.energy.alberta.ca/NaturalGas/1316.asp (access on August 20, 2015)

Fedorak et al. (2009) described a hypothetical pathway (based on the known pathways for cellulose) for the conversion of heavier components of bitumen and heavy oils to methane (**Figure 1.2**). They claimed that methane could be produced from oilsands derived bitumen through partial oxidation followed by microbial digestion with appropriate microorganisms.

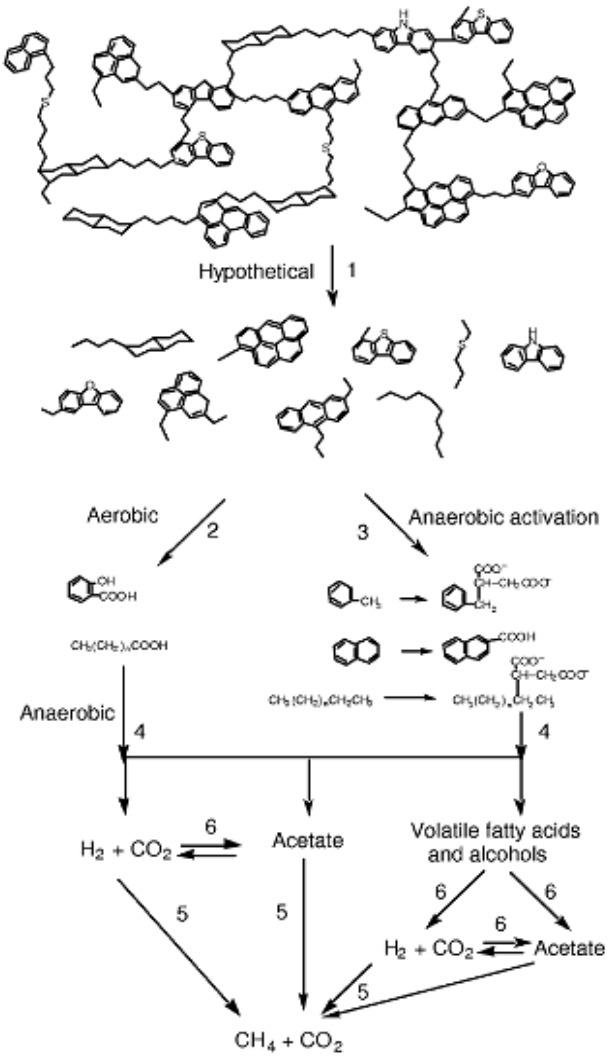

Figure 1.2. A hypothetical pathway for conversion of high-molecular weight bitumen components to methane, based on the known pathways for cellulose (Fedorak et al., 2009).

Londry et al. (2009) demonstrated the concept of methane production by oxidizing the bitumen using various chemicals and inoculating the oxidized products with sewage sludge, which resulted in higher methane formation than control cultures containing non-ozonated bitumen or no bitumen. The results indicated that bitumen without oxidation is not susceptible to bio-

conversion, and the oxidation step is the limiting factor in generating methane from bitumen. However, bitumen oxidation by using chemicals (for instance, hydrogen peroxide, pure oxygen, ozone, potassium permanganate, etc.) is not an industrially viable approach due to high cost and large volume of the oxidizing agent required (Javadli and De Klerk, 2012a). More importantly, unreacted chemicals might be toxic for the subsequent microbial steps. Therefore, it is important to consider an alternative and cost effective oxidation approach. Autoxidation (oxidation with air) is a promising strategy to limit the environmental impact and cost of the bitumen oxidation process. Hence, detailed studies of autoxidation of bitumen are of great interest to develop an alternative and cost effective bitumen upgrading process.

Although oxidation of simpler hydrocarbons (except light hydrocarbon gases) is facile, the oxidation of highly complex bitumen is challenging. The major challenges are:

1. Control of free radical addition reactions that produce heavier, more viscous and more refractory products than the feed materials.

2. Selective oxidation to obtain oxidation products that are suitable for microbial digestion.

3. Mass transfer limitations due to higher bitumen viscosity.

4. Obtaining adequate oxidation rate while minimizing energy consumption.

5. Avoiding over-oxidation to produce CO_2.

6. Finding ways for ring-opening of aromatic rings.

These challenges must be overcome for efficient bitumen oxidation. In this study, the following questions are taken into consideration and addressed to overcome part of the challenges:

Why does bitumen become hard during oxidation and how can increased hardness be limited during oxidation?

Oxidative bitumen hardening is the main challenge to achieve the ultimate goal of the project. At low temperature, heavier product formation is the dominant cause of bitumen hardening

(Petersen, 1993). It is required to investigate the compound classes responsible for addition product formation and the nature of addition product bonds being formed (C-C or C-O-C). This would help understand oxidation chemistry of bitumen and to select suitable reactor types and/or oxidation conditions to limit free radical additions.

What are the design parameters that can be manipulated to change oxidation rate?

This is both a chemistry and engineering related challenge. Temperature and pressure are the traditional operating parameters that are employed to increase rate, but can be used only to a limited extent in the present context due to their increasingly negative impact on product selectivity as severity is increased. It is desirable to explore the strategies that relate to the oxidation chemistry and improve oxidation rate without a detrimental impact on selectivity. For example, initiators can be added to reduce the time required for the initiation of oxidation reaction and to facilitate propagation that would help increase the overall reaction rate. Also, the rate of the oxidation reaction is expected to increase by increasing gas-liquid mass transfer, for example, by using microchannel reactors.

How can oxidation selectivity be controlled?

This is a chemistry related challenge, along with reaction engineering aspects. Product selectivity usually depends on conversion. In practice, autoxidation selectivity of hydrocarbons is controlled by a combination of temperature, oxygen availability and residence time (De Klerk, 2003). Temperature and oxidation time influence the product selectivity by changing the conversion. The oxygen concentration proximity to free radical intermediates mainly influences the product selectivity that is independent of conversion. Local oxygen availability can be improved by oxygen transport in liquid phase. Increasing gas-liquid interfacial area and/or mass transfer coefficient can increase mass transfer at constant temperature and pressure. Microfluidic reactor is a potential reactor to manipulate oxygen availability by changing reactor hydrodynamics.

How can mass transfer limitations be overcome?

This is an engineering challenge. In order to overcome mass transfer limitation, it is required to understand the origin of the mass transfer limitation and what is its extent. Very fast reactions

between organic free radicals and molecular oxygen can be responsible for mass transfer limitations. Moreover, the very high viscosity of the bitumen also hinders mass transfer between the gas and liquid phase. In an industrial process, naphtha is employed for bitumen dilution to reduce viscosity, but this is unlikely to be viable in a bitumen oxidation process, because the naphtha (a paraffinic mixture) is not oxidation resistant. However, this challenge can be overcome by using (i) a non-alkylated aromatic solvent (benzene) that is very refractory to oxidation and (ii) a microfluidic reactor as it has potential to overcome transport limitations (Chen et al., 2004; Kiwi-Minsker and Renken, 2005).

1.2 Objectives and Scope of Work

1.2.1 Objectives

The overall objective of the project is to produce methane and/or valuable liquid products from bitumen via oxidation followed by microbial digestion (**Figure 1.3**).

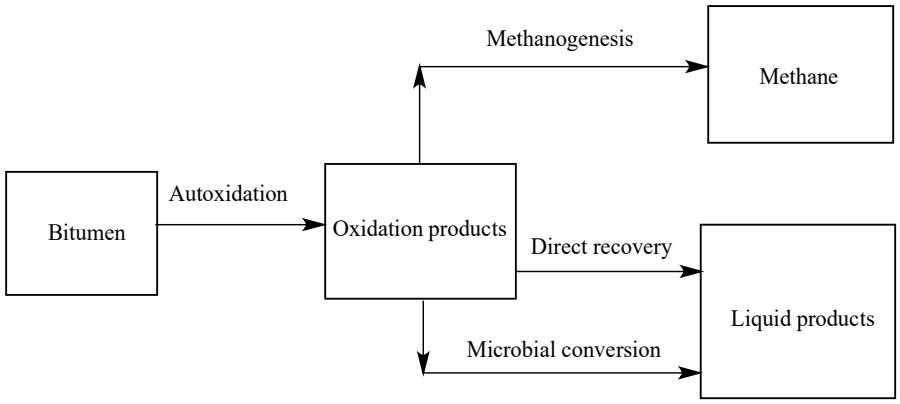

Figure 1.3. Block diagram of methane or valuable liquid production from bitumen.

Different researchers have investigated the various parts of the overall project in a collaborative effort. The main focus of the current research is to investigate low-temperature oxidation (LTO), principally to address some challenges to produce oxidation products that are suitable for microbial conversion. Hence, the specific objectives of the current research can be summarized as follows:

1. Investigate the feasibility to produce products that are amenable for microbial digestion by prolonged and continuous oxidation.

2. Investigate the fundamental oxidation chemistry underlying bitumen hardening.

3. Investigate how oxygen availability could be manipulated during gas-liquid oxidation and how it is related to both oxidation rate and product selectivity

4. Investigate whether or not the gas-liquid oxidation is mass transfer limited or kinetically controlled.

5. Investigate whether or not overcoming mass-transfer limitation reduces addition product selectivity (which potentially causes bitumen hardening).

1.2.2 Scope of work

In order to limit the scope of the investigation to oxidation strategies that may ultimately yield an economically viable industrial process, some constraining assumptions have been imposed on the research. These assumptions are validated from literature, by conceptual engineering evaluations or by experiments:

(1) Bitumen oxidation relevant to this process occurs mainly in the liquid phase. This rules out processes relying on partial vaporisation of bitumen and catalytic gas phase oxidation.

(2) Air is the only or dominant oxidant. This rules out the bulk addition of costly oxidizing agents. In some cases, the addition of small quantities of oxidants to reduce the time required for initiation of oxidation was considered.

(3) Complete bitumen conversion is not essential. This provides an additional degree of freedom to balance oxidation time, temperature, conversion and CO_2 selectivity. This degree of freedom reduces the CO_2 footprint. However, it also implies that there may be a partially upgraded bitumen stream (lower viscosity, lower sulphur content, lower nitrogen content) as oil product.

(4) Oxidation can take place at close to atmospheric pressure. In fact, a low O_2 partial

pressure has selectivity advantages. Concepts relying on high-pressure oxidation are not favored.

The following topics have been investigated in this study:

Chapter 2: Literature review. This chapter provides an overview of bitumen and compound classes available in bitumen, oxidation chemistry and related engineering aspects.

Chapter 3: Low temperature autoxidation of oilsands bitumen. In this chapter, feasibility to produce products for microbial digestion by prolonged and continuous oxidation is reported. Effect of temperatures and changes in physical and chemical properties are also discussed.

Chapter 4: Low temperature autoxidation of hydrocarbons. Fundamental oxidation chemistry underlying bitumen hardening is described in this chapter. Different hydrocarbon compounds available in oilsands bitumen are considered for the investigation.

Chapter 5: Low temperature autoxidation of heterocyclic compounds. In this chapter, fundamental oxidation chemistry underlying bitumen hardening is further discussed. Different heterocyclic compounds available in oilsands bitumen are considered for the investigation.

Chapter 6: Oxygen availability to manipulate oxidation rate and product selectivity. This chapter describes how oxygen availability can be manipulated by changing reactor hydrodynamics and how it is related to both oxidation rate and product selectivity.

Chapter 7: Engineering aspects of liquid phase autoxidation. This chapter describes whether or not the gas-liquid oxidation is mass transfer limited or kinetically controlled and what the extent of mass transfer limitation is from the experimentally determined mass transfer rate and oxidation rate.

Chapter 8: Conclusions. In this chapter, the major conclusions and new insights that will contribute to the field of oxidative upgrading of oilsands derived materials and the liquid phase autoxidation in general are highlighted.

1.3 Literature Cited

Chen, G.; Yuan, Q.; Li, H.; Li, S. CO selective oxidation in a microchannel reactor for PEM fuel cell. *Chem. Eng. J.* **2004,** *101*, 101–106.

De Klerk, A. Continuous- mode thermal oxidation of Fischer-Tropsch waxes. *Ind. Eng. Chem. Res*. **2003,** *42*, 6545–6548.

De Klerk, A.; Gray, M. R.; Zerpa, N. Unconventional oil and gas: Oilsands. In *Future Energy*, 2ed; Letcher, T. M. Ed.; Elsevier: Amsterdam, 2014; pp 95–116.

Fedorak, P. M.; Foght, J. M.; Gray, M. R. Conversion of heavy oil and bitumen to methane by chemical oxidation and bioconversion, US Patent Application 2009/0130732.

Gray, M.R. Upgrading of oilsands bitumen and heavy oil; The University of Alberta Press: Edmonton, Canada, 2015.

Javadli, R.; de Klerk, A. Desulfurization of heavy oil. *Appl. Petrochem. Res.* **2012a,** *1*, 3–19.

Kiwi-Minsker, L.; Renken, A. Microstructured reactors for catalytic reactions. *Catal. Today* **2005,** *110,* 2–14.

Londry, K.; Foght, J. M.; Fedorak, P. M.; Gray, M. R. Bioconversion of Oil Sands Bitumen, Final report to EnCana, June 11, 2009.

Nji, G. Characterization of heavy oils and bitumens. Ph.D. dissertation, University of Calgary (Canada), Canada. Retrieved January 11, 2012, from Dissertations & Theses: Full Text. (Publication No. AAT NR62165).

Petersen, J. C. Asphalt oxidation - an overview including a new model for oxidation proposing that physicochemical factors dominate the oxidation kinetics. *Fuel Sci. Technol. Int.* **1993**, *11*, 57–87.

Rana, M. S.; Sámano, V.; Ancheyta, J.; Diaz, J. A. I. A review of recent advances on processing technologies for upgrading of heavy oils and residua. *Fuel* **2007**, *86*, 1216–1231.

Strausz, O. P.; Lown, E. M. *The chemistry of Alberta oil sands, bitumens and heavy oils*; Alberta Energy Research Institute: Calgary, AB, 2003.

CHAPTER 2 – LITERATURE REVIEW

2.1 Introduction

The focus of the current research is to develop a viable oxidation process for the oxidative degradation of bitumen. In order to do so it is important to know the nature of the bitumen (Section 2.2), oxidation chemistry (Section 2.3), previous work on bitumen autoxidation (Section 2.4), role of mass transfer in liquid phase autoxidation (Section 2.5), and reactors used for liquid phase autoxidation (Section 2.6). A more detailed review of the literature focused on the experimental work and interpretation of the results is included in the respective chapters (**Chapters 3–7**). This chapter only provides the starting point of the investigation.

2.2 Nature of the Bitumen

Bitumen, the heaviest form of petroleum, is a dark brown-to-blackish, dense, slightly viscoelastic, semisolid hydrocarbon that is rich in heteroatoms, nitrogen, oxygen, sulfur, and various metals (Liu and Gunning, 1991; Strausz and Lown, 2003). In terms of properties determined at standard conditions of 15 ºC for trading of crude oils, bitumen refers to the fractions having °API gravity < 10; density > 1000 kg/m^3; and viscosity > 10^5 mPa s (Gray, 2015).

The term bitumen is also used for asphalts and asphalt-like manufactured materials used in road construction, including products from the processing of coals and/or oil shales (Yen and Chilingarian, 1994). “Asphalt” is commonly used in America, whereas “asphaltic bitumen” and “bitumen” are terms used in Europe and Canada. However, both the asphalt and bitumen are used in the literature interchangeably. In this thesis the term bitumen will be used mainly to refer to the raw heavy oil material that is recovered from oilsands deposits.

Bitumen occurs in the earth’s crust in various states like (i) disperse state, in trace quantities; and (ii) accumulations, where bitumen either impregnates the rock or occurs in pure or nearly pure form (Yen and Chilingarian, 1994). In Canadian oilsands, bitumen is mixed mainly with sands and water. It is separated from sand particles by a thin coating of water which makes it easier for recovery (De Klerk et al., 2014). Bitumen from Canadian oilsands is recovered either by open

mining or by *in situ* extraction using techniques such as steam-assisted gravity drainage (SAGD) technique (De Klerk et al., 2014).

One of the distinguishing features of bitumen derived from Canadian Oilsands is very high viscosity- typically of the order 10^4 mPa s at 40 ºC (Strausz and Lown, 2003). Such a high viscosity makes it difficult to use conventional oil drilling and production technology or to transport bitumen in its native state. Heated pipelines or railcars are used for the transportation over short distance and naphtha as solvent is used for the transportation over long distance (De Klerk et al., 2014).

Another important feature of bitumen that is important for bitumen oxidation is that it already contains stable free radicals and the amount varies depending on the origin of bitumen. Resins and asphaltenes are the most reactive fractions of bitumen and contain most of the stable free radicals (Knotnerus, 1972).

2.2.1 Composition of Canadian Oilsands Bitumen

The main elements present in bitumen are carbon (C), hydrogen (H), nitrogen (N), oxygen (O), and sulfur (S). In addition to these elements, it contains trace amounts of nickel and vanadium. Bitumen composition varies with depth and geographic position (Montgomery, 1981). **Table 2.1** shows the elemental composition of various heavy oils and bitumens derived from Canadian oilsands (Strausz and Lown, 2003).

The atomic hydrogen to carbon ratio (H/C) is an important property to determine quality of crude oils from a refining perspective. It indicates the degree of unsaturation and the decreases from conventional oils (usually greater than 1.8) to unconventional oils (typical range for heavy oils and bitumen is 1.4 to 1.6) (Gray, 2015; Strausz and Lown, 2003). The lower H/C ratio indicates the presence of a significant amount of aromatic molecules in heavy oils and bitumen. The H/C ratio of 1.5 (**Table 2.1**) supports the presence of higher concentration of naphthenic-aromatic compounds and lower amount of paraffinic compounds in Canadian oilsands bitumen (Strausz and Lown, 2003).

Table 2.1. The elemental composition of some heavy oils and bitumen (Strausz and Lown, 2003).

source	elemental composition (wt%)					
	C	H	S	O	N	H/C ratio
Athabasca	83.3	10.6	4.8	0.9	0.4	1.53
Cold Lake	83.1	10.7	4.2	1.4	0.3	1.55
Peace River	82.7	10.2	5.9	1.6	0.5	1.48
Lloydminster	83.2	10.5	4.2	0.9	0.3	1.51

2.2.2 Compound Classes Available in Oilsands Bitumen

Bitumen is classified based on the solubility or adsorption characteristics of different fractions. Asphaltenes and maltenes are the two main solubility fractions of bitumen. Bitumen is usually regarded as a suspensoid in which asphaltenes are the dispersed phase and maltenes are the dispersion medium (Thyrion, 2000). Asphaltenes are the benzene soluble and alkane insoluble parts of the bitumen. Maltenes are the parts of the bitumen that are soluble in *n*-alkane such as *n*-pentane or *n*-heptane (Gray, 2015). Maltenes are further classified as resins, saturates, and aromatics. A flow diagram that indicated how to separate different fractions of bitumen is shown in **Figure 2.1**. The class compositions of Alberta oil sands bitumen vary within the following limits: saturates 15–21%, aromatics 18–19%, resins 44–48%, and asphaltenes 14–20% (Strausz and Lown, 2003).

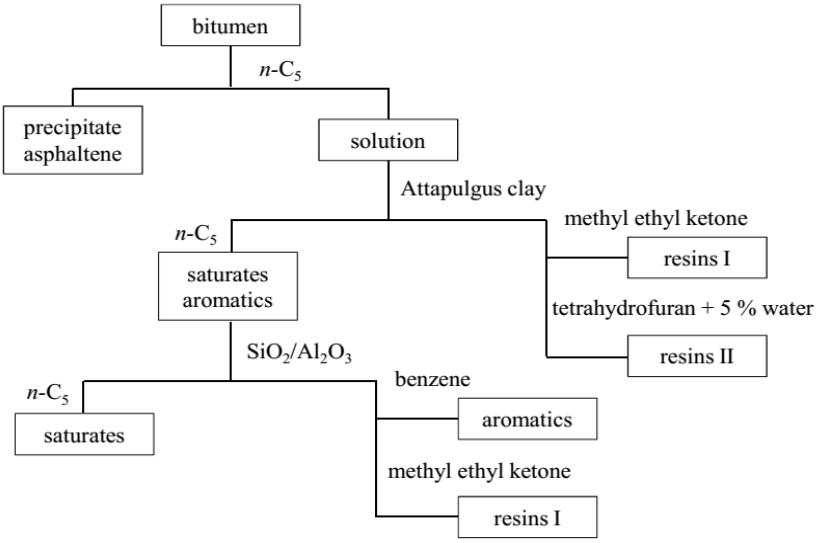

Figure 2.1. Flow diagram to separate different fractions of bitumen (Strausz and Lown, 2003).

Resins are the part of maltenes in *n*-pentane that is adsorbed on clay (Attapulgus clay, Fuller's earth). Resins consist of acidic, basic, amphoteric, and neutral components. Aromatics are the clay eluted part of maltenes in *n*-pentane that is adsorbed on silica/alumina column. Saturates are the clay eluted part of maltenes in *n*-pentane that is also eluted from silica/alumina column (Gray, 2015; Strausz and Lown, 2003). The saturate fractions contain one to six-ring hydrocarbons having low levels of aromatic or heteroatom compounds.

Bitumen consists of various functional groups and compound classes. Strausz and coworkers identified and characterized different compound classes and functional groups (**Table 2.2**.) available in Canadian oilsands bitumen (Strausz and Lown, 2003). One can anticipate that oxidation behavior of different classes in bitumen will be different.

Table 2.2. Important compound classes and functional groups in Alberta bitumen (Gray, 2015; Strausz and Lown, 2003).

compound classes	compounds/ functional groups
acyclic	*n*-alkane or *iso*-alkane ($C_nH_{2n+2;}$ where, typically n < 19)
aromatic	naphthalene, anthracene, phenanthrene, perylene, fluoranthracene, chrysene, picene, pyrene, etc.
naphthenic	decalin, cheilanthane, sterane, gammacerane, etc.
hydroaromatics (naphthenic-aromatic)	tetralin (1,2,3,4-tetrahydro naphthalene), fluorine, 9,10-dihydro phenanthrene, etc.
heteroatomic (S-containing)	thiophene, benzothiophene, dibenzothiophene, sulfide, thiol, thiacylopentane (thiolane), thiacyclohexane, sulfoxide, sulfone, sulfonic acids, etc.
heteroatomic (O-containing)	carboxylic acid, carboxylic acid ester, alcohol, ketone, ether, aldehyde, fluorenol, fluorenone, furan, benzofuran, dihydro benzofuran, etc.
heteroatomic (N-containing)	pyrrole, pyridine, carbazole, quinoline, quinolone, etc.
metal chelates	nickel and vanadyl porphyrins

2.3 Oxidation Chemistry

The concept of oxidation in organic chemistry differs from that in inorganic chemistry. In organic chemistry, oxidation usually refers to either elimination of hydrogen (e.g. the sequential dehydrogenation of ethane) or the replacement of hydrogen atom bonded to a carbon with a more electronegative element such as oxygen (e.g. oxidative transformation of methane to CO_2) (Sheldon and Kochi, 1981). Oxidation is an industrially important conversion processes to produce petrochemicals via functionalization of petroleum (Centi and Perathoner, 2002; Alsters et al., 2014, Pina et al., 2013; Sheldon and Kochi, 1981; Suresh et al., 2000; Tolman et al.; 1989; Dimitratos et al., 2014). Different oxidizing agents, catalysts and experimental conditions are employed in oxidation processes. These are discussed in brief to select a feasible oxidation process to achieve the ultimate goal of the project.

2.3.1 Oxidising Agents

Oxidising agents (oxidants) are the oxygen donor during the oxidation process. Chemicals such as permanganates or chromium salts are commonly used stoichiometric oxidants to produce fine chemicals (Centi et al., 2001). Other oxidising agents include hydrogen peroxide, pure oxygen, air, oxygen, ozone, etc. Centi et al. (2001) characterizes some commonly used oxidizing agents. Among all the oxidizing agents air is cheap and readily available. In the current respect of the research, chemical oxidation was not considered due to the two main reasons: firstly, residual chemicals could interfere with the subsequent methanogenation process and secondly, volume and cost of the oxidant that will be required (Javadli and de Klerk, 2012a). Hence, the molecular oxygen in air was selected as primary oxidising agent for the oxidation reported in this study.

2.3.2 Catalytic and Non-catalytic Oxidation

Catalysts play an important role in selective oxidation processes. It is known that the hydroperoxides formed during autoxidation can be readily decomposed in the presence of some metals that act as decomposition catalysts, mainly Fe, Mn, Co and Cu compounds (Sheldon et al., 1981). The application is less straightforward, since metals may also act as inhibitors at higher concentration (Betts et al., 1966). Catalysts used are divided into two categories: homogeneous and heterogeneous catalysts. Heterogeneous catalysts are advantageous because

these are more selective, easier recovery and product separation, and less waste generation, which is environmentally more acceptable (Centi et al., 2001; Huchnail, 1974; Hill and Kholdeeva, 2013). In spite of the advantages of using a heterogeneous catalyst for the selective oxidation, homogeneous catalyst would be advantageous for the *in situ* bitumen conversion. However, the use of a catalyst was not considered for the current research as bitumen can deactivate the homogeneous catalyst and can cause fouling and deactivation in case of heterogeneous catalyst.

2.3.3 Gas phase and Liquid Phase Oxidation

Both the gas phase and liquid phase autoxidations are reported in literature (Centi et al., 1994; Huchnail, 1974; Bharadwaj and Schmidt, 1995; Emanuel et al., 1967). Gas phase autoxidation are suitable for the lighter compounds such as C_4 hydrocarbons (Huchnail, 1974) or compounds (and products) that would remain gaseous at oxidation conditions. The current study focused on liquid phase oxidation as bitumen is not volatile and will be in liquid phase at the studied experimental conditions. Lighter fractions produced due to partial vaporisation during bitumen oxidation (Section 3.3) could oxidize in the gas phase, but it would at most be a minor contribution to the overall oxidation process.

2.3.4 Autoxidation Chemistry

The oxidation of an organic compound with molecular O_2 in air in the absence of added catalyst is referred to as autoxidation (Noller, 1966).

Liquid phase autoxidation is a free radical chain process in which the presence of an induction time, autocatalytic propagation, and zero order kinetics with respect to oxygen are commonly observed (Lundberg, 1961; Suresh et al., 2000). Induction time is the time required for sufficient concentration of free radicals to form so that oxidation can proceed at a significant rate. During this induction period the reaction rate is almost negligible (Suresh et al., 1988a). The length of the induction period depends on compound classes, experimental conditions, and presence of oxygenate impurities.

Oxidation of organic substances by molecular oxygen leads to the formation of a large number of intermediate products such as peroxides, and final oxygen-containing products such as alcohols, carbonyl compounds, acids, esters, and also bifunctional compounds (Emanuel et al., 1967). **Figure 2.2** shows the reaction network of the hydrocarbon autoxidation.

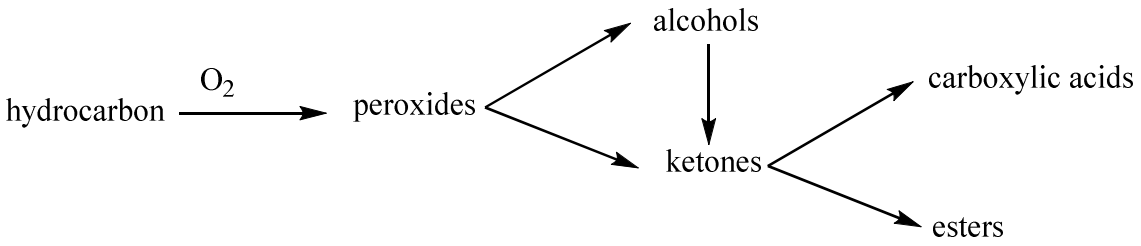

Figure 2.2. Reaction network of hydrocarbon autoxidation (De Klerk, 2011).

2.3.4.1 Mechanism of Liquid Phase Oxidation

The mechanisms of hydrocarbon oxidation are well described in literature (Emanuel et al., 1967; De Klerk, 2003; Scott, 1965; Thyrion, 2000; Tipson, 1965). Free radical oxidation reactions take place in the liquid phase and there are three steps, namely, initiation, propagation, and termination.

2.3.4.1.1 Initiation and Propagation

Initially, free radicals are formed by the reaction between hydrocarbons and molecular oxygen. Molecular oxygen abstract hydrogen from hydrocarbons to form alkyl radical and hydroperoxy radical species (Emanuel et al., 1967; De Klerk, 2003):

$$RH + O_2 \longrightarrow R^{\bullet} + HO_2^{\bullet} \qquad \text{(Reaction 2.1)}$$

The following reaction may also take place to form alkyl radical and hydrogen peroxide (Emanuel et al., 1967):

$$RH + O_2 + RH \longrightarrow 2\,R^{\bullet} + H_2O_2 \qquad \text{(Reaction 2.2)}$$

Free radicals that are formed in Reaction 2.1 react with hydrocarbons and oxygen to produce new free radicals as follows (Emanuel et al., 1967; De Klerk, 2003):

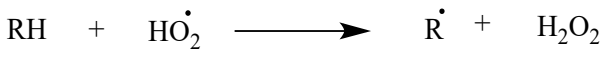
(Reaction 2.3)

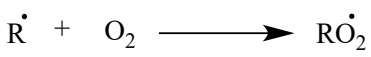
(Reaction 2.4)

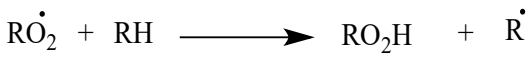
(Reaction 2.5)

Chain propagation by alkyl hydroperoxides can take place as shown in Reactions (2.6) to (2.8) (De Klerk, 2003). But, the radical induced decomposition (Reaction 2.7) is most significant (De Klerk, 2003). The homolytic fragmentation (Reaction 2.8) degenerates branching (Emanuel et al., 1967).


(bimolecular decomposition) (Reaction 2.6)

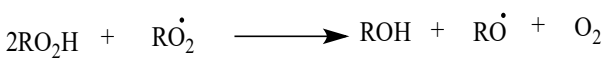
(radical induced decomposition) (Reaction 2.7)

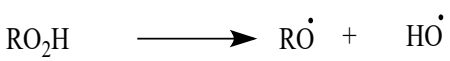
(thermal homolytic fragmentation) (Reaction 2.8)

2.3.4.1.2 Termination

The free radicals R· and ROO· are highly reactive and rapidly disappear as follows (Emanuel et al., 1967):

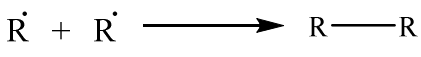
(Reaction 2.9)

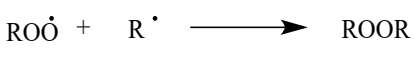
(Reaction 2.10)


(Reaction 2.11)

In the absence of initiating additives (initiators), the rate of free radical formation is extremely low. However, the use of initiator such as hydroperoxide promotes the initiation process and the use of organic salts of metals of variable valance like cobalt, manganese, iron, copper, chromium, lead, and nickel generally promote the propagation of oxidation of hydrocarbons (Emanuel et al., 1967). The product formed during termination depends on the experimental

conditions. Oxygenates are more reactive than the feed hydrocarbons and produce secondary products as shown in **Figure 2.2**. This would affect the product selectivity.

2.3.4.2 Operating Parameters that Affect Oxidation Rate and Selectivity

The main challenge in free radical autoxidation processes is to control the product selectivity. The parameters that could affect the oxidation rate and selectivity include temperature, pressure, oxidation time, light, and the presence of catalysts, initiators, and inhibitors, (Lundberg, 1961; De Klerk, 2003; Asinger, 1968). In practice, autoxidation selectivity of hydrocarbons is controlled mainly by a combination of temperature, oxygen availability and oxidation time. De Klerk (2011) explained how the product selectivity changed at different autoxidation regimes of 75 475 °C and at high and low oxygen availability.

Temperature, pressure and oxidation time influence the conversion rate and selectivity changed with the level of conversion (De Klerk, 2003; Asinger, 1968). Oxidation products are readily oxidized and produced acids (**Figure 2.2**), which can turn into CO_2. In industry, autoxidation performed at low conversion to control the product selectivity (Hermans et al., 2008).

The traditional operating parameters temperature and pressures that are employed to increase conversion rate can be used only to a limited extent in the context of current research due to their increasingly negative impact on product selectivity as severity is increased. Moreover, severe conditions (high oxygen concentration in gas phase) could lead to explosion (Centi and Perathoner, 2002). It is desirable to explore the strategies to control product selectivity that is independent on conversion.

2.4 Bitumen Autoxidation

Bitumen autoxidation refers to the reaction between bitumen and air to produce oxidation products. In a heavy oil or bitumen oxidation process, reactions occurring between air/oxygen and the fraction of heavy oil/bitumen below 300°C are generally known as low temperature oxidation (LTO) (Xu et al., 2001; Das, 2009). Bitumen oxidation follows the typical oxidation mechanisms of hydrocarbons described in Section 2.3.1 (Jha et al., 1978).

Most of the reported bitumen oxidation studies are performed to understand the *in situ* bitumen recovery process or to understand asphalt aging or hardening related to road construction. The oxidation of bitumen is associated with changes in various physical and chemical properties of bitumen. For example, oxidation of oil sands derived bitumen is often associated with an increase in asphaltene formation due to oxidation during ageing (Jha et al., 1978). An increase in asphaltene content is understandable, since the classification as asphaltenes is based on solubility; asphaltenes are defined as light hydrocarbon-insoluble material. Oxidation increases the polarity of bitumen (Xu et al., 2001) and as the bitumen becomes more polar, it becomes less soluble in apolar light hydrocarbons, which by definition translates into increased asphaltene content.

Moschophedis and Speight (1975) investigated that the asphaltene content increased significantly, and the asphaltene solubility reduced noticeably due to the oxidation of bitumen with air or oxygen in the presence of a diluent. It is suggested that one of the main factors influencing the solubility of the asphaltenes, aside from possible polymerization of asphaltenes and resins, is incorporation of oxygen groups, e.g. hydroxyl, into the asphaltenes, and consequent changes in polarity sufficient to influence asphaltene deposition. Increased asphaltene production is a negative attribute in relation to conventional upgrading and it has stifled interest in oxidation. But, in the present context oxidation is necessary for efficient bioconversion.

Noureldin et al. (1987) investigated the chemical changes due to low temperature oxidation of heavy oils using a combination of analytical pyrolysis and classical separation techniques. They reported that low temperature oxidation of maltenes isolated from heavy oil increased the acid number as well as oxygen content. They also found that organosulfur compounds were oxidized to sulfinic or sulfonic acids (Reaction 2.12), and sulfones, while hydrocarbons were oxidized to alcohols, phenols, aldehydes, ketones, carboxylic acids, and esters. Similar oxidative products are expected from the low temperature oxidation of bitumen. Oxidation products like carboxylic acids, and phenols are surface active and reduce the interfacial tension between oil and water that is believed to beneficial to oil or bitumen recovery (Montgomery, 1981).

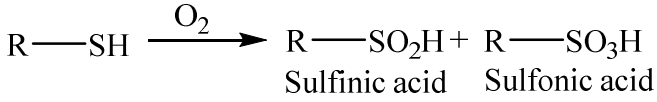

(Reaction 2.12)

Low temperature oxidation of bitumen increases viscosity, and density (Noureldin et al., 1987). Babu and Cormack (1984) investigated the effect of low temperature oxidation (47 to 97 °C) on the viscosity of Athabasca bitumen and observed that the low temperature oxidation increased the viscosity of bitumen by more than two orders of magnitude even at relatively low extent of oxidation. They finally concluded that low temperature oxidation in an oil reservoir adversely affect the oil recovery process. García Zapata and De Klerk (2014) reported oxidative bitumen hardening during bitumen autoxidation at 140 to 160 °C. Hendessi (2015) also observed viscosity increased during oxidation of Athabasca bitumen with air, oxygen and ozone. However, Xu et al. (2001) claimed that a controlled two-step oxidation process – low temperature oxidation followed by high temperature oxidation - reduces the heavy oil viscosity. Wichert (1996) found that a less viscous end product could be obtained by long, low temperature oxidation at low oxygen partial pressure. At more severe conditions, aslphalt hardening occurs (Chelton et al., 1959). The treatment of an aqueous oil sands slurry with a peroxide oxidant in the temperature range 60-100 °C has been claimed to increase hydrocarbon liberation from mineral matter and to improve the yield of lower molecular mass species (Conaway, 2001). An analogous process was suggested for upgrading of an asphaltene fraction (Duyvesteyn et al., 2007). Controlled low temperature air oxidation therefore has the potential to reduce the average molecular mass and break down the structure of bitumen. Yet, the oxidative conversion must be appropriately moderated in order to avoid free radical addition reactions and an undesirable increase in viscosity.

Air oxidation under mild conditions has in the past been used to produce carboxylic acids from heavy hydrocarbons for detergent manufacturing (Asinger, 1968). Although the feed material employed was less complex than bitumen, it illustrates industrial application of the principle for commercial production of liquid products. It is also known that some product mass is lost as light oxygenates during industrial scale autoxidation of waxes (Bolder et al., 2009) even when it is desirable not to oxidatively degrade the substrate. Again, the feed was less complex, but the work bolsters confidence that it is possible to reduce feed complexity and produce products

suitable for anaerobic digestion to methane, or an upgraded oil.

Another consequence of the autoxidation is that sulphur compounds are converted to sulfoxides and sulfones (Reaction 2.13), which makes these compounds more water-soluble. The same is true of nitrogen containing compounds, although oxidation is generally more difficult, especially when the nitrogen is part of a heterocyclic compound (Plesnicar, 1978).

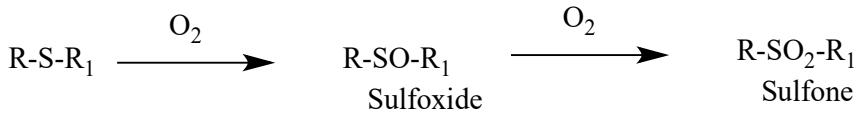

(Reaction 2.13)

Air oxidation consequently has the additional benefit of producing nutrients for the microbes, while removing some sulfur and nitrogen from the bitumen. In fact, oxidation was proposed as a method to upgrade heavy oils in this way (Webster et al., 1964). The oxidized sulfur containing compounds were more polar and could therefore be extracted in an aqueous phase. It is reasonable to expect that at least some of the oxidised sulfur and nitrogen compounds can be extracted as nutrients for the microbes. This may also enable bio-conversion that selectively targets the oxidized sulfur and nitrogen compounds to yield an oxygenate rich oil that can be recovered as an upgraded liquid product.

Literature suggested two possible outcomes of bitumen oxidation, one favorable and one unfavorable for the oxidative upgrading of oilsands bitumen. Heavier products formation that potentially caused bitumen hardening (unfavorable outcome) can be reduced by limiting oxidative addition reaction. Antioxidant is not applicable to control the addition product selectivity because it will stop the oxidation process. Moreover, commonly used antioxidants such as butylated hydroxytoluene (BHT), butylated hydroxyanisole (BHA) are larger molecule which ultimately end up with heavier products that are not suitable for bioconversion. Reaction engineering has the potential to manipulate oxygen availability and product selectivity. This premise is extensively explored in in **Chapters 6** and **7**.

2.5 Role of Mass Transfer in Liquid Phase Autoxidation

Oxidation of bitumen with air is a gas-liquid reaction (multiphase reaction). In a gas-liquid system, as reactants are present in two different phases, it is important to diffuse one of the reactants from its phase to the other phase for the reaction to take place. Gas diffusivity is higher (~10^{-5} m^2/s) compared to liquid diffusivity (~10^{-9} m^2/s) (Davis and Davis, 2003). So, it is generally assumed that gas will diffuse to liquid phase and non-volatile liquid will not appreciably diffuse to gas phase.

Gas-liquid mass transfer along with chemical reaction is well described in literature (Danckwerts, 1970; Kaštánek et al., 1993; Cussler, 2009). Three different models i.e., film model, penetration model, and surface renewal model have been proposed (Danckwerts, 1970; Kaštánek et al., 1993; Cussler, 2009; Doraiswamy and Üner, 2014). In most cases the results are very similar (Kaštánek et al., 1993; Cussler, 2009; Suresh et al., 1988b). Film theory is simple and assumed a stagnant film of uniform thickness. Based on film theory mass transfer rate can be presented as:

$$J_A = k_L a\,(C_{Ai} \quad C_b) = \frac{D_A}{\delta}\, a\,(C_{Ai} \quad C_b) \qquad \text{(Equation 2.1)}$$

J_A is mass transfer rate across the gas-liquid interface (mol/m^3.s), k_L is the liquid side mass transfer coefficient (m/s), D_A is diffusivity of gas in liquid (m^2/s) , δ is the film thickness (m), a is gas-liquid interfacial area, (m^2/m^3), C_{Ai} is the concentration of gas at the interface, (mol/m^3), and C_{bi} is the concentration of gas in bulk liquid (mol/m^3). Pressure increases the concentration differences and hence oxygen transfer to liquid phase; but increasing pressure has negative impact on product selectivity (Section 2.3.4.2). δ and a are the two most important parameters to enhance the gas-liquid mass transfer because D_A and C_{Ai} can be changed only to a limited extent. However, based on film theory δ is considered as uniform. Hence, gas-liquid interfacial area is the most important parameter to assess the role of mass transfer in the oxidation of liquid with molecular oxygen. Microfluidic reactor (Section 2.6.2) is a potential reactor to increase the gas-liquid interfacial area (a) and also to decrease film thickness (δ) which would increase mass transfer coefficient (k_L). This is advantageous to transport both oxygen and oxygenates into liquid phase.

The rate of gas-liquid reaction depends on the mass transfer through the film and on the reaction kinetics. Hence, gas-liquid reaction can be kinetically controlled; mass-transfer controlled or controlled by both kinetic and mass transfer. In kinetically controlled reactions, the rate of dissolution and diffusion of oxygen (gas) to the liquid phase is high and the concentration of oxygen in liquid phase is close to saturation. Oxidation rate in a kinetically controlled situation is slow and oxidation occurs predominantly in the bulk liquid. In diffusion controlled reaction, oxidation rate is very high and oxidation takes place predominantly at the gas-liquid interface (Emanuel et al., 1967). However, both the diffusion and reaction can also take place simultaneously (Suresh et al., 1988b). It is important to understand nature of reaction and reaction zone in order to understand how mass transfer affects the reaction.

2.6 Reactors for Liquid Phase Autoxidation

Reactor selection for liquid phase oxidation depends on several factors such as gas-liquid contact, surface area-to-volume ratio, backmixing phenomena, and material of reactor wall (Centi and Perathoner, 2002). There are many potential reactors for liquid phase autoxidation studies such as bubble column reactors, microfluidic reactors, loop reactors, and stirred tank reactor.

2.6.1 Bubble Column Reactors

Bubble column reactor is a device in which gas, in the form of bubbles, come in contact with liquid. This multiphase reactor is typically a cylindrical vessel with a gas distributor generally at the bottom of the column. If a solid phase exists, these reactors are known as slurry bubble column reactors. Bubble column reactors are mainly operated in semi-batch mode or continuous mode. In semi-batch mode, liquid is stationary and gas is introduced from the bottom. However, in continuous mode, gas introduced from the bottom of the reactor and liquid is introduced either co-currently or counter-currently of gas flow (Kantarci, 2005). A typical bubble column reactor used for the oxidation studies of bitumen or heavy oil is shown in **Figure 2.3**.

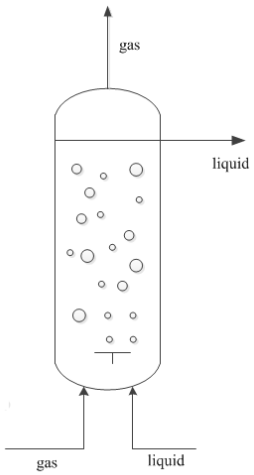

Figure 2.3. A typical bubble column reactor (Hofmann, 1983).

Bubble column reactors are widely used in chemical, petrochemical, biochemical, and metallurgical industries for the oxidation, hydrogenation, chlorination, alkylation, and polymerization (Kantarci, 2005; Degaleesan, 2001). The advantages of bubble column reactors over the other reactors are excellent mass and heat transfer characteristics, compactness of the reactor, lower operating and maintenance cost, etc. (Degaleesan, 2001). However, large column diameter, and reactor heights are required for the large gas throughputs, and good conversion efficiency, respectively. The design and scale up of a bubble column reactor are complex due to complicated multiphase fluid dynamics (Kantarci, 2005). Most of the oxidation studies of bitumen and heavy oil were conducted in bubble column reactors.

2.6.2 Microfluidic Reactors

Microfluidic reactors, also known as microchannel reactors or simply microreactors refer to miniaturized reaction devices with feature sizes in the sub–millimeter range (Liu et al., 2012). It has the potential to develop strategies to manipulate product selectivity independent of conversion by changing the hydrodynamics of reactor operation without changing operating temperature or pressure.

The advantages of microfluidic reactors include very high heat and mass transfer rates, increased product yield, and improved energy efficiency (Lerou et al., 2010; Fletcher et al., 2002). It is reported that this reactor technology can increase the rate of various chemical reactions and the

rate of heat and mass transfer by 2–3 orders of magnitude compared to conventional macroscale systems (Lerou et al., 2010; Chen et al., 2004; Liu et al., 2012; Hamano et al., 2012). This acceleration has become possible due to the higher surface area to volume ratio provided by these smaller reactors. Typically, specific surface area (surface area per volume) of microfluidic reactors are between 10 000 to 50 000 m^2. m^{-3} that are significantly higher compared to conventional reactors (100 to 2000 m^2. m^{-3}) (Wilms et al., 2008). Increasing interfacial area increases the mass transfer rate as shown in Equation (2.1). Moreover, the liquid film produced in microfluidic reactor is very thin which would also increase the mass transfer coefficient ($k_L = \frac{D_A}{\delta}$) and hence transport rate (Equation 2.1). These would be advantageous to increase local oxygen availability in the liquid phase and to decrease the chance of the addition Reaction (2.9) without changing the conversion.

Another crucial thing to improve mass transfer as well as product selectivity is efficient mixing of the reaction components. Mixing in the microreactors of laminar flow pattern is the result of diffusion at the interface of thin reactant layers (Wilms et al., 2008). Also, the direction of diffusion is toward the smaller dimension (radius). Very short radial diffusion pathway ensures better mixing and leads to narrow residence time distribution (RTD). This is advantageous for consecutive reactions (A to B to C) to enable high selectivity of the desired intermediates (Kiwi-Minsker and Renken, 2005).

Flow in a microfluidic reactor is laminar and the Reynolds number, Re, varies within ~0.01–100 (Song et al., 2003). Re is defined as $\rho vd/\mu$, where, d [m] is the diameter of the capillary, v [ms^{-1}] is velocity of the flow, ρ [$kg\ m^{-3}$] is the density, and μ [$kgm^{-1}s^{-1}$] is the viscosity of the fluid. The flow pattern in microfluidic reactors depend on the materials of construction, chemical compatibility, and the reactor geometry. Typical flow patterns in microfluidic systems are shown in **Figure 2.4**. The slug flow (also known as Taylor flow) is characterized as a liquid-gas two-phase flow. The internal circulation within the liquid slug ensures good mixing (Vanoye et al., 2013; Günther et al., 2004; Doraiswamy and Üner, 2014; Sobieszuk et al., 2012), and more importantly, could transport the oxygenates from the interface to the bulk liquid which could prevent the over oxidation. Overall, microfluidic reactor has the potential to manipulate product selectivity independent of conversion.

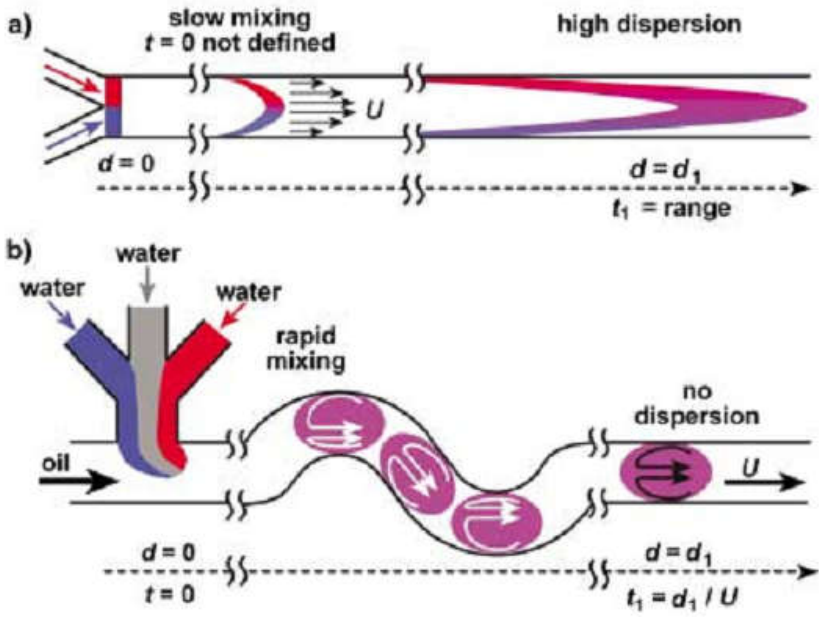

Figure 2.4. Typical flow patterns in microfluidic systems. Schematic comparison of a reaction A + B conducted (a) in a standard pressure-driven microfluidic system device, and (b) in networks of microchannels with rectangular cross sections and hydrophobic surfaces (Song et al., 2003)[a].

[a] Reprinted from Angewandte Chemie International Edition, 42(7), Song, H.; Tice, J.D.; Ismagilov, R.F.A microfluidic system for controlling reaction networks in time, 768-772, Copyright 2003, with permission from John Wiley and Sons.

2.7 Biodegradation of Oxidation Products

Some bacterial strains can biodegrade the *n*-alkanes of conventional crude oil (**Figure 2.5**). Head et al. (2003) reported that some naturally occurring microorganisms are able to produce methane by bioconversion of conventional crude oil. However, the highly complex material in bitumen cannot be easily biodegraded to methane or other upgraded products.

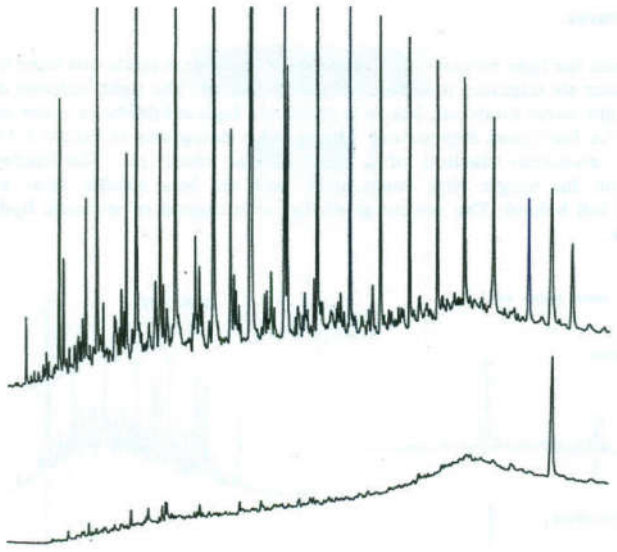

Figure 2.5. Biodegradation of Alberta sweet mix blend crude oil. Crude oil incubated without (upper curve) and with (lower curve) *Rhodococcus*sp. S+14He at 28 °C for 14 days in presence of buffer solution with shaking (Gray, 2010).

Fedorak et al. (2009) and Londry et al. (2009) reported that methane could be produced from bitumen via chemical oxidation followed by microbial conversion. De Man (2014), involved in the project, investigated the biodegradation of dibenzothiophene sulfone (oxidation product of dibenzothiophene) by using *Rhodococcus* K1bD and *Rhodococcus* EPWF to produce upgraded products.

Partially oxidized compounds (e.g. fatty acids, long chain alcohols, and aromatic carboxylic acids like benzoate) are suitable for biodegradation as these are water-soluble and have functional groups that facilitate enzymatic reactions (Londry et al., 2009). Hence, oxidatively degraded products of bitumen are a potential source for biodegradation to produce methane or other upgraded liquid products.

2.8 Literature Cited

Alsters, P. L.; Aubry, J. M.; Bonrath, W.; Daguenet, C.; Hans, M.; Jary, W.; Letinois, U.; Nardello-Rataj, V.; Netscher, T.; Rarton, R.; Schütz, J.; Van Soolingen, J.; Tinge, J.; Wüstenberg, B. Selective oxidation in DSM: Innovative catalysts and technology. In *Handbook of Advanced Methods and Processes in Oxidation Catalysis: From Laboratory to Industry*; Duprez, D., Cavani, F., Eds.; Imperial College Press: London, 2014; pp 382–419.

Asinger, F. *Paraffins Chemistry and Technology*; Pergamon: Oxford, 1968.

Babu, D. R.; Cormack, D. E. Effect of low-temperature oxidation on the composition of Athabasca bitumen. *Fuel* **1984**, *63*, 858–861.

Betts, A.T.; Uri, N.The conversion of metal catalysts into inhibitors of autoxidation. *Die Makromolekulare Chemie.***1966**, 95, 22-39.

Bharadwaj, S. S.; Schmidt, L. D. Catalytic partial oxidation of natural gas to syngas. *Fuel Process. Tech.* **1995**, *42*, 109–127.

Bolder, F. H. A.; De Klerk, A.; Visagie, J. L. Hydrogenation of oxidized wax and a process to produce olefins from paraffins by autoxidation, selective hydrogenation, and dehydration. *Ind. Eng. Chem. Res.* **2009,** *48*, 3755.

Chelton, H. M.; Traxler, R. N.; Romberg, J. W. Oxidized asphalts. *Ind. Eng. Chem.* **1959,** *51*, 1353–1354.

Chen, G.; Yuan, Q.; Li, H.; Li, S. CO selective oxidation in a microchannel reactor for PEM fuel cell. *Chem. Eng. J.* **2004,** *101*, 101–106.

Centi, G.; Cavani, F.; Triffò, F. *Selective Oxidation by Heterogeneous Catalysis*. Kluwer/Plenum: New York, 2001.

Centi, G; Perathoner, S. Selective oxidation—industrial. In *Encyclopedia of Catalysis.* Wiley, 2002.

Centi, G.; Malaguti, M.; Stella, G. Low temperature gas-phase selective oxidation of 1-butene to 2- butanone on supported Pd/V_2O_5 Catalysts. In *New Developments in Selective Oxidation II;* Corberan, V. C., Bellón, S. V., Eds.; Elsevier: Amsterdam, 1994.

Conaway, L. M. Method for recovering hydrocarbons from tar sands and oil shales. US Patent 6, 251, 290 B1, 2001.

Cussler, E. L. *Diffusion: Mass Transfer in Fluid Systems,* 3rd ed.; Cambridge University Press: Cambridge, 2009.

Danckwerts, P. V. *Gas-Liquid Reactions*; McGraw-Hill: New York, 1970.

Das, S. C. A Study of Oxidation Reaction Kinetics During an Air Injection Process. M.E.Sc. Thesis. The University of Adelaide, April 2009.

Davis, M. E.; Davis, R. J. *Fundamental of Chemical Reaction Engineering*; McGraw-Hill: New York, 2003.

Degaleesan, S.; Dudukovic, M.; Pan,Y. Experimental study of gas-induced liquid-flow structures in bubble columns. *Fluid Mech. Trans. Phenom.* **2001,** *47*(9), 1914-1931.

De Klerk, A. *Fischer-Tropsch Refining*, 1st ed. Wiley VCH: Weinheim, 2011.

De Klerk, A. Continuous- mode thermal oxidation of Fischer-Tropsch waxes. *Ind. Eng. Chem. Res*. **2003,** *42*, 6545.

De Klerk, A.; Gray, M. R.; Zerpa, N. Unconventional oil and gas: Oilsands. In *Future Energy*, 2nd ed; Letcher, T. M., Ed.; Elsevier: Amsterdam, 2014; pp 95–116.

De Man, A. Desulfurization of oxidized bitumen using microorganisms through process-based directed evolution. MSc. Thesis, University of Alberta, Canada, June 2014.

Dimitratos, N.; Lopez-Sanchez, J. A.; Hutchings, G. J. Supported metal nanoparticles in liquid-phase oxidation reactions. In *Handbook of Advanced Methods and Processes in Oxidation Catalysis: From Laboratory to Industry*; Duprez, D., Cavani, F., Eds.; Imperial College Press: London, 2014; pp 631–678.

Doraiswamy, L.K.; Üner, D. *Chemical Reaction Engineering, Beyond the Fundamentals*; CRC Press: Boca Raton, 2014.

Duyvesteyn, W. P. C.; Morley, R. L. Oxidation of asphaltenes. US Patent Application 2007/0284283.

Emanuel, N. M.; Denisov, E.T.; Maizus, Z. K. *Liquid-Phase Oxidation of Hydrocarbons*; Plenum Press: New York, 1967.

Fedorak, P. M.; Foght, J. M.; Gray, M. R. Conversion of heavy oil and bitumen to methane by chemical oxidation and bioconversion, US Patent Application 2009/0130732.

Fletcher, P.D. I.; Haswell, S. J.; Pombo-Villar, E.; Warrington, B.H.; Watts, P.; Wongc, S. Y. F.; Zhanga, X. Micro reactors: principles and applications in organic synthesis. *Tetrahedron,* **2002,** *58,* 4735–4757.

García Zapata, J. L.; De Klerk, A. Viscosity changes during mild oxidation of oilsands derived bitumen: Solvent effects and selectivity. *Energy Fuels* **2014**, *28*, 6242–6248.

Günther, A.; Khan, S. A.; Thalmann, M.; Trachsel, F.; and Jensen, K. F. Transport and reaction in microscale segmented gas–liquid flow. *Lab Chip* **2004**, *4*, 278–286.

Gray, M.R. *Upgrading of Oilsands Bitumen and Heavy Oil*; The University of Alberta Press: Edmonton, Canada, 2015.

Gray, M.R. *Fundamentals of Oil Sands Upgrading*; Course notes, University of Alberta, Edmonton, 2010.

Hamano, M.; Nagy, K. D.; Jensen, K. F. Continuous flow metal-free oxidation of picolines using air. *Chem. Comm.* **2012,** *48*, 2086–2088.

Head, I. M.; Jones, D. M.; Larter, S. R. Biological activity in the deep subsurface and the origin of heavy oil. *Nature* **2003,** 426, 344–352.

Hendessi, S. Low temperature ozonation of Canadian Athabasca bitumen. MSc. Thesis, University of Alberta, Canada, September 2015.

Hermans, I.; Peeters, J.; Jacobs, P. A. Autoxidation of Hydrocarbons: From Chemistry to Catalysis. *Top Catal.* **2008**, *50*, 124–132.

Hill, C. L.; Kholdeeva, O. A. Selective liquid phase oxidation in the presence of supported polyoxometalates. In *Liquid Phase Oxidation via Heterogeneous Catalysis: Organic Synthesis and Industrial Applications,* 1st ed.; Clerici, M. G., Kholdeeva, O. A., Eds.; Wiley: Hoboken, 2013; pp 263–319.

Hofmann, H. Reaction Engineering Problems in slurry reactors. In *Mass Transfer with Chemical Reaction in Multiphase Systems,* II: Three-Phase Systems; Alper, E., ed.; NATO ASI series: Series E: Applied Sciences-No.73, Martinus Nijhoff Publishers: The Hauge, 1983; 171–173.

Hucknall, D. J. Selective oxidation of hydrocarbons. Academic Press: London, 1974.

Javadli, R.; de Klerk, A. Desulfurization of heavy oil. *Appl. Petrochem. Res.* **2012a,** *1*, 3–19.

Jha, K. N.; Rao, P. M.; Strausz, O. P. Oxidation of Athabasca oil sand and its reactions. *Prepr. Pap. Am. Chem. Soc., Div. Fuel Chem.* **1978,** *23*(4), 91–97.

Kantarci, N.; Borak, F., Ulgen, K. O. Bubble column reactors. *Process Biochem.* **2005,** *40,* 2263-2283.

Kaštánek, F.; Zaharadník, J.; Kratochvíl, J.; Čermák, J. *Chemical Reactors for Gas-Liquid Systems*, 1st ed.; Ellis Horwood: West Sussex, 1993.

Kiwi-Minsker, L.; Renken, A. Microstructured reactors for catalytic reactions. *Catal. Today* **2005,** *110,* 2–14.

Knotnerus, J.; Bitumen durability-measurement by oxygen absorption. *Ind. Eng. Chem. Prod. Res. Develop.* **1972**, *11* (4), 411–422.

Lerou, J. J.; Tonkovich, A. L.; Silva, L.; Perry, S.; McDaniel, J. Microchannel reactor architecture enables greener processes. *Chem. Eng. Sci.* **2010,** *65,* 380.

Liu, J. K.; Gunning, H. E. Syncrude analytical methods manual for bitumen upgrading; AOSTRA, Edmonton, 1991.

Liu, X.; Jensen, K.F. Direct oxidative amidation of aromatic aldehydes using aqueous hydrogen peroxide in continuous flow microreactor systems. *Green Chem.,* **2012,** *14* (5), 1471–1474.

Londry, K.; Foght, J. M.; Fedorak, P. M.; Gray, M. R. Bioconversion of Oil Sands Bitumen, Final report to EnCana, June 11, 2009.

Lundberg, W. O. *Autoxidation and Antioxidants*, Vol I.; Wiley: New York, 1961.

Montgomery, D. S. Bitumen chemistry related to oil production and upgrading. Edmonton, Alberta, 1981.

Moschopedis, S.E.; Speight, J.G. Oxidation of bitumen. *Fuel* **1975,** *54* (3), 210–212.

Noller, R. C. *Chemistry of Organic Compounds*, 3rd ed.; W. B. Saunders Company: London, 1966.

Noureldin, N. A.; Lee, D. G.; Mourtis, F. M.; Jha, K. N. Chemical changes accompanying the low temperature oxidation of heavy oil. *AOSTRA J. Res.* **1987,** *3,* 155–161.

Pina, C. D.; Falletta, E.; Rossi, M. Liquid phase oxidation of organic compounds by supported metal-based catalysts with a focus on gold. In *Liquid Phase Oxidation via Heterogeneous Catalysis: Organic Synthesis and Industrial Applications,* 1st ed.; Clerici, M. G.; Kholdeeva, O. A., Eds.; Wiley: Hoboken, 2013, pp 221–262.

Plesnicar, B. In *Oxidation in Organic Chemistry*, 5-C; Trahanovsky, W. S., ed.; Academic Press: New York, 1978, 211–294.

Scott, G. *Atmospheric Oxidation and Antioxidants*; Elsevier Publishing Company: Amsterdam, 1981.

Sheldon, R. A.; Kochi, J. K. *Metal-Catalyzed Oxidations of Organic Compounds*; Academic Press: New York, 1981, 6.

Sobieszuk, P.; Aubin, J.; Pohorecki, R. Hydrodynamics and mass transfer in gas-liquid flows in microreactor. *Chem. Eng. Tech.* **2012**, *35*(8), 1346–1358.

Song, H.; Tice, J.D.; Ismagilov, R.F. A microfluidic system for controlling reaction networks in time. *Angew. Chem. Int. Ed.* **2003,** *42* (7), 768–772.

Strausz, O. P.; Lown, E. M. *The Chemistry of Alberta Oil Sands, Bitumens and Heavy Oils*; Alberta Energy Research Institute (AERI): Calgary, Alberta, Canada, 2003.

Suresh, A. K.; Sharma, M. M.; Sridhar, T. Engineering aspects of industrial liquid-phase air oxidation of hydrocarbon. *Ind. Eng. Chem. Res.* **2000,** *39,* 3958–3997.

Suresh, A. K.; Sridhar, T.; Potter, O. E. Mass transfer and solubility in autocatalytic oxidation of cyclohexane. *AIChE J.* **1988a**, *34*(1), 55–68.

Suresh, A. K.; Sridhar, T.; Potter, O. E. Autocatalytic oxidation of cyclohexane- mass transfer and chemical reaction. *AIChE J.* **1988b**, *34*(1), 81–93.

Thyrion, F.C. Asphalt Oxidation. In *Asphaltenes and Asphalts, 2. Developments in Petroleum Sciences, 40B*; Yen, T.F., Chilingarian, G.V., eds.; Elsevier: Amsterdam, 2000, 445–474.

Tipson, R.S. Oxidation of Polycyclic, Aromatic Hydrocarbons. A review of literature; National Bureau of Standards: NBS monograph 87, Washington, 1965; 1–49.

Vanoye, L.; Aloui, A.; Pablos, M.; Philippe, R.; Percheron, A.; Favre-Réguillon, A.; de Bellefon, C. A safe and efficient flow oxidation of aldehydes with O_2. *Org. Lett.* **2013**, *15*(23), 5978–5981.

Webster, A. B.; Small, N. J. H.; Rigby, R. Desulfurization of heavy oils. Patent US 3,163,593 (1964, Shell).

Wichert, G. C. In situ upgrading of heavy oils by low-temperature oxidation in the presence of caustic additives; MSc dissertation, University of Calgary, 1996.

Wilms, D.; Klos, J.; Frey, H. Microstructured reactors for polymer synthesis: a renaissance of continuous flow processes for Tailor-Made macromolecules? *Macromol. Chem. Phys.* **2008,** *209,* 343–356.

Xu, H. H.; Okazawa, N. E.; Moore, R. G.; Mehta, S. A.; Laureshen, C. J.; Ursenbach, C. J.; Ursenbach, M. G.; Mallory, D. G. In situ upgrading of heavy oil. *J. Can. Pet. Technol.* **2001,** *40* (8), 45–53.

Yen, T.F.; Chilingarian, G.V. Introduction. *In Asphaltenes and Asphalts,1. Developments in Petroleum Sciences,* 40A.; Yen, T.F., Chilingarian, G.V., eds.; 1994, Elsevier : Amsterdam, 1–6.

CHAPTER 3 – LOW-TEMPERATURE AUTOXIDATION OF OILSANDS BITUMEN[1, 2]

Abstract

Low temperature oxidation of bitumen with air in the temperature range 130 to 160 °C was investigated. Of particular interest was to investigate the feasibility to produce water-soluble products by prolonged and continuous autoxidation and to understand the effect of temperature on bitumen autoxidation. Oxidation extent for bitumen autoxidation at 130 °C for 229 h was ~ 6400 mg O per kg bitumen. It produced limited water-soluble products (~ 0.0007 g per gram bitumen) and resulted ~ 0.02 wt % volatile organic fractions that contained oxygenate functional groups. In spite of limited elemental composition change, density and viscosity were increased by 13 % and 11 times, respectively, and bitumen became very hard (17 times increase in penetration hardness) due to extended autoxidation of bitumen at 130 °C for 229 h. Analogous chemical and physical changes were also observed due to oxidation performed at different temperatures (140 °C, 150 °C and 160 °C). FTIR analysis confirmed the C=O as a dominant functional group in oxidized bitumen. During autoxidation of bitumen the relative aliphatic to aromatic loss of hydrogen increased from 18:1 to 30:1 when the temperature was increased from 140 to 150 °C and then remained almost the same at 160 °C. It coincided with a bitumen oxidation selectivity change reported in literature.

Keywords: Oilsands bitumen, autoxidation, bitumen hardening, free radical addition, hydrogen disproportionation

[1]Reprinted in part with permission from Siddiquee, M. N. and De Klerk, A. Hydrocarbon addition reactions during low-temperature autoxidation of oilsands bitumen. *Energy Fuels* **2014**, *28* (11), 6848–6859. Copyright 2014 American Chemical Society. http://pubs.acs.org/doi/abs/10.1021/ef501694s.

[2] Part of the work was also published as Siddiquee, M. N.; De Klerk, A. *Prepr. Pap.-Am. Chem. Soc., Div. Energy Fuels* **2013**, *58*(2), 649–651.

3.1 Introduction

Considerable effort in the recovery and upgrading of bitumen from the Canadian oilsands is directed at improving the fluidity of the bitumen. The oilsands derived bitumen has a high viscosity, of the order 10-100 Pa s (10,000-100,000 cP) (De Klerk et al., 2014). The conversion of bitumen to a more fluid product is therefore desirable.

One potential strategy to overcome the poor fluidity of bitumen is to introduce methanogens into the oilsands deposit, so that the micro-organism can convert the bitumen into methane (Fedorak et al., 2009). Methane is more easily recovered and transported. This strategy is of value to marginal oilsands reserves that cannot economically be exploited with current technology. It is a two-step process. The first step involves the *in situ* oxidation of the bitumen in the oilsands deposit to make the bitumen more susceptible to subsequent conversion by the methanogens. The second step is the introduction of methanogens to convert the bitumen under anaerobic conditions; anaerobic methanogenesis of aromatic hydrocarbons was reviewed by Foght (2008).

This study deals only with the first step in the process, namely, the low temperature (< 200 °C) oxidation of bitumen with air to increase the water solubility of the bitumen.

The study evaluated the hypothesis that prolonged low temperature autoxidation of bitumen can substantially convert the bitumen to products amenable to microbial conversion. The hypothesis was based mainly on the success that was reported with oxidative degradation of coal to water-soluble products under mild reaction conditions (Schwartz et al., 1988; Hayashi et al., 1997; Mae et al., 1997; Anderson et al., 2011; Pan et al.; 2013). Although bitumen is dissimilar to coal in various respects, previous studies on the low temperature oxidation (LTO) of bitumen indicated that oxygen is readily incorporated in the bitumen and that prolonged low temperature oxidation exhibits is first order kinetics with respect to oxygen (Jha et al., 1978; Babu and Cormack, 1983; Herrington, 2004). A yield of 30 wt % of water-soluble material was reported for chemical oxidation, albeit not autoxidation, of oilsands bitumen derived asphaltenes (Moschopedis and Speight, 1971a). The objective of the study was to empirically evaluate the changes in bitumen properties and conversion by autoxidation. The beneficial effect of water during the oxidation

process that was claimed in literature (Lee and Noureldin, 1989), was not studied and it was anticipated that at least some hardening of the bitumen would take place.

3.2 Experimental

3.2.1 Materials

Cold Lake bitumen supplied by Centre for Oil Sands Innovation (COSI), University of Alberta, Edmonton, AB, Canada was used for bitumen autoxidation studies. The properties of the bitumen used for experiments are shown in **Table 3.1**.

Table 3.1. Properties and composition of Cold Lake bitumen.

Property	Bitumen
Viscosity at 60 °C (Pa s)	10.1 ± 0.4
Density at 20 °C (kg m^{-3})	1008 ± 14
Penetration hardness (mm) [a]	1.7 ± 0.1
Water soluble fraction (g g^{-1}) [b]	≤ 0.0005
Acetone soluble fraction (g g^{-1}) [c]	≤ 0.008
SARA fractions (wt %)	
saturates	16.8 ± 2.4
aromatics	46.1 ± 2.7
resins	17.7 ± 1.2
asphaltenes	18.7 ± 0.5
Elemental composition (wt %)	
C	82.6 ± 0.1
H	10.3 ± 0.1
S	4.7 ± 0.1
N	0.6 ± 0.1
O	2.6 ± 0.3

[a] Calculated on a bitumen basis, excluding incorporated oxygen.

[b] Dissolution in excess solvent at 60 °C.

[c] Dissolution in solvent at 21 °C.

Extra-dry air was purchased from Praxair Inc., Edmonton, Canada and used as oxidizing agent.

3.2.2 Equipment and Procedure

The experimental investigation was an applied study to determine the change in bitumen properties and conversion due to extended low temperature oxidation. The equipment employed in the study is shown in **Figure 3.1**.

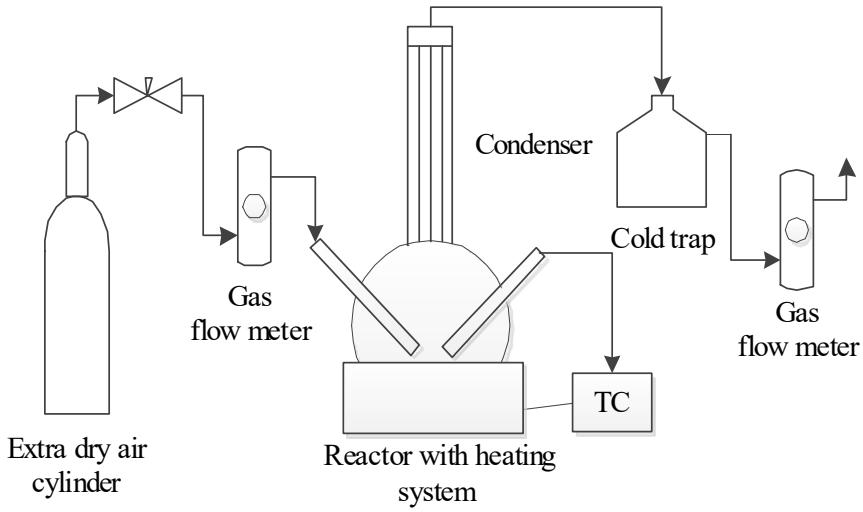

Figure 3.1. Experimental setup for bitumen autoxidation.

For the each autoxidation experiment approximately 80 g of Cold Lake bitumen was pre-heated to 90 °C and transferred to a 250 ml round bottom flask. The round bottom flask was equipped with a reflux condenser having a chilled water supply that was maintained at 10 °C. The condensed volatile products were collected. Oxidation of bitumen was conducted at different times and temperatures in the range 6 to 229 h and 130 to 160 °C. The temperature in the flask was controlled by a Heidolph MR Hei-Standard heat-on-block heater with magnetic stirring. A magnetic stirring bar was used for mixing at 500 rpm. The airflow rate was maintained at 120 mL/min, which is equivalent to 160 mL h^{-1} air per g bitumen. At the end of each reaction the airflow was stopped and the bitumen was allowed to cool down to ambient temperature. The products were weighed and characterized. Additional workup was performed on the bitumen oxidized at 130 °C for 229 h. Part of the oxidized bitumen was extracted with water (bitumen to water weight ratio 0.5) at 60 °C for 1 h while stirring at 500 rpm, and part of the oxidized

bitumen was extracted by using acetone at 21 °C. The bitumen to acetone weight ratio was 2.8 and shaking time was 5 min. All the experiments were conducted in duplicate.

3.2.3 Analyses

Bitumen and oxidized bitumen were analyzed off-line employing the following techniques and instruments:

(a) Viscosity was determined using an Anton Paar viscometer (RheolabQC, Part No. 81143139) with a cylindrical cup (model CC-17) and a cylindrical spindle (diameter = 16.664 mm, length 24.970 mm, model CC-17, part No. 28337). Shear rate was 10 s^{-1}, speed was 7.7 min^{-1} and temperature was 60 °C.

(b) Density was determined relative to the density of water. Bitumen samples were heated at 60 °C and approximately 5 g sample was transferred in a measuring flask. Measured amount of water was added to make final volume 15 ml and the mass increase was recorded. The volume of bitumen was calculated by subtracting volume of water from the final volume. The density was calculated by dividing the mass by the volume.

(c) Hardness was determined in terms of penetration values using a penetrometer, Humboldt model ML 1200. Measurements were performed with an applied load of 100 g for 0.01 s.

(d) Elemental analysis was performed with a Carlo Erba EA1108 Elemental Analyzer (Triad Scientific Inc., Manasquan, NJ, USA).

(e) The composition of the bitumen in terms of saturates, aromatics, resins and asphaltenes (SARA) fractions were determined using a modified ASTM D 2007 method (*ASTM D2007-03*). The modified ASTM method is described in detail in **Appendix A**. The main difference is the use of a 1:1 pentane: toluene mixture was used to elute the aromatic fraction, which would result in heavier aromatics also being eluted in the aromatic fraction rather than in the resin fraction.

(f) Infrared analyses were performed using an ABB MB 3000 Fourier transform infrared (FTIR) spectrometer. A small amount of sample was placed on a potassium bromide (KBr) disc and the spectrum was collected over the wave number range 4000 to 500 cm^{-1} as the average of 120

scans per sample. The spectral resolution was 2 cm^{-1}, signal strength was 70 %, the acquisition mode was absorbance and detector gain was 243.

(g) The proton nuclear magnetic resonance (^{1}H NMR) spectra of bitumen and oxidized bitumen samples were measured by a NMReady 60 spectrometer (Nanalysis Corp., Calgary, Canada). $CDCl_3$ (99.96 % deuterium, Sigma) was used for sample preparation. Samples were analyzed using standard 5 mm NMR tubes (NORELL, Landisville, USA). Experimental conditions were: frequency = 60 MHz, spectral range = 14 ppm, number of scans = 32.

(h) ^{13}C NMR spectra of bitumen and oxidized bitumen sample was recorded using Varian Inova-400 and Varian Inova-500 spectrometers operating at 100.6 and 125.7 MHz, respectively. $CDCl_3$ (99.96 % D, Sigma) was used for sample preparation. Samples were analyzed using standard 5 mm NMR tubes (NORELL, Landisville, USA).

3.3. Results and Discussion

3.3.1 Extended Low Temperature Autoxidation of Bitumen

Extended low temperature autoxidation of bitumen was conducted to determine whether bitumen could be substantially converted to water-soluble products, as well as what the impact of oxidation was on the properties of the bitumen.

Bitumen autoxidation incorporated oxygen into the feed material to produce oxidized bitumen, volatile organic products, CO_2, H_2O, SO_2 and potentially other light gases. Little oxidative degradation to produce volatile products was found during prolonged oxidation at 130 °C **(Table 3.2)**. The difference in gas flow rate was too small to accurately determine the evolution of gases and uncondensed volatile products. The yield of the oxidized bitumen, excluding the oxygen incorporated during oxidation, was determined through elemental analysis and the gas yield was determined by difference. Minor changes in elemental composition were observed, and there was little change in water and acetone solubility. In this respect the results corroborated the observations by Moschopedis and Speight (1974), who conducted prolonged oxidation at milder conditions, but also found little recovery of water-soluble products.

Table 3.2. Product yield and properties of bitumen oxidized at 130 °C for 229 h with an air flow rate of 160 mL/g bitumen.

Description	Oxidized bitumen	
	Run 1	Run 2
Oxidation extent (mg O/kg bitumen)	6260	6400
Product yield (wt %) [a]		
oxidized bitumen	97.6	97.7
volatile organic products	0.02	0.02
gases (by difference)	2.4	2.3
Water soluble fraction (g g^{-1}) [b]	0.0006	0.0008
Acetone soluble fraction (g g^{-1}) [c]	0.008	0.008
Elemental composition (wt %) [d]		
C	82.31	82.27
H	10.00	10.11
S	4.55	4.39
N	0.49	0.41
O	3.27	3.28

[a] Calculated on a bitumen basis, excluding incorporated oxygen.
[b] Dissolution in excess solvent at 60 °C.
[c] Dissolution in solvent at 21 °C.
[d] Elemental composition of oxidized bitumen only.

Considering the duration of the oxidation, the maximum observed oxygen incorporation was only 6400 mg O per kg bitumen. The conversion of bitumen to gaseous products was also low (~ 2.4 wt %).

Yet, despite the comparatively low oxidation extent, the product reflected significant hardening (**Table 3.3**) compared to the bitumen feed (**Table 3.1**). The viscosity increased by an order of magnitude and the penetration hardness decreased by an order of magnitude. Furthermore, the density increased from 1008 to 1142 kg m^{-3}. The results indicated that the impact of prolonged oxidation on viscosity and hardening were severe.

Table 3.3. Characterization of oxidized bitumen produced by autoxidation at 130 °C for 229 h.

Property	Oxidized bitumen
Viscosity at 60 °C (Pa s)	111.3 ± 5.0
Density at 20 °C (kg m^{-3})	1142 ± 31
Penetration hardness (mm) [a]	0.1 ± 0.03

[a] Penetrometer with 100 g load for 0.01 s.

Herrington (1998) reported that the increase in viscosity (μ) was correlated to the increase in the concentration of carbonyl ($x_{C=O}$) and sulfoxide ($x_{S=O}$) in the oxidized bitumen (Equation 3.1).

$$\Delta(\log \mu) = a\,(\Delta x_{C=O} + \Delta x_{S=O}) \qquad \text{(Equation 3.1)}$$

The proportionality constant (*a*) depends on the bitumen and it is independent of oxidation temperature below ~100 °C (Herrington, 1998). The method of determination employed by Herrington (1998) is briefly described. The concentration of carbonyl and sulfoxide groups in the oxidized bitumen was determined by infrared spectroscopy of a 5% solution of bitumen in chloroform ($CHCl_3$) in a liquid cell with a path length of 1 mm. The carbonyl concentration was calculated from the integrated peak area between 1805 cm^{-1} and 1643 cm^{-1}, while the sulfoxide concentration was calculated in an analogous way from the peak area between 1084 cm^{-1} and 983 cm^{-1}. The aforementioned work did not demonstrate that the correlation caused hardening. It was only inferred that hardening was caused by carbonyl and sulfoxide functional groups, because of the correlation (Equation 3.1). Likewise, in computational work, it was indicated that sulfoxides and carbonyls increased interaction with dipoles and induced dipoles, which could contribute to agglomeration (Pan et al., 2012). The computation work suggests a link between the carbonyls, sulfoxides, and hardening, but to what extent these groups explain the increase in hardening is still an open question.

3.3.2 Effect of Temperature on Low Temperature Autoxidation of Bitumen

Petersen (1993) stated that both physical and chemical effects play a role in bitumen rheology and that the nature of the hardening process is sensitive to temperature. Previous work on low-temperature bitumen oxidation also indicated that there is a change in the oxidation selectivity and kinetics at ~ 150 °C (Babu and Cormack, 1983; Javadli and De Klerk, 2012b).

The effect of oxidation temperature on the properties of oxidized bitumen was investigated by performing oxidation for only 6 hours at 140, 150 and 160 °C. The mass loss observed was in the range of 0.6 to 0.8 wt %. There was little difference between the elemental compositions of the oxidized bitumen samples (**Table 3.4**) and that of the bitumen feed (**Table 3.1**).

Table 3.4. Elemental analysis of oxidized bitumen after 6 h oxidation at different temperatures and an air flow rate of 160 mL/g bitumen.

Description	Oxidized bitumen					
	140 °C		150 °C		160 °C	
	Run 1	Run 2	Run 1	Run 2	Run 1	Run 2
Oxidized bitumen yield (wt %)	99.2	99.3	99.4	99.3	99.3	99.4
Elemental composition (wt %)						
C	82.2	82.5	82.9	82.7	83.2	83.1
H	10.0	10.3	10.0	10.2	10.2	10.4
S	4.5	4.4	4.3	4.1	4.6	4.4
N	0.7	0.6	0.6	0.5	0.5	0.5
O	2.8	2.5	2.8	2.8	2.6	2.3

Yet, the physical properties of the oxidized bitumen reflected the influence of oxidation (**Table 3.5**). The density increased with increasing oxidation temperature. The values for viscosity and penetration hardness were higher than that of the bitumen feed (**Table 3.1**), but the differences were too small to be statistically meaningful. Thus, the change in density, rather than viscosity, was the primary indicator that oxidation temperature affected the physical properties differently.

Table 3.5. Characterization of oxidized bitumen produced by autoxidation for 6 h at different temperatures and an air flow rate of 160 mL/g bitumen.

Property	Oxidized bitumen		
	140 °C	150 °C	160 °C
Viscosity at 60 °C (Pa s)	17.5 ± 0.1	17.4 ± 0.1	17.3 ± 0.2
Density at 20 °C (kg m^{-3})	1038 ± 8	1040 ± 12	1047 ± 13
Penetration hardness (mm) [a]	1.1 ± 0.1	1.1 ± 0.1	1.0 ± 0.1

[a] Penetrometer with 100 g load for 0.01 s.

Many spectroscopic techniques were not able to provide sufficient differentiation between the oxidized bitumen samples to elucidate the effect of temperature on the oxidized bitumen. The exception was NMR spectroscopy (**Table 3.6**), which was interpreted based on literature (Silverstein et al., 2005). In the ^{1}H NMR spectra the proton shift-values of $\delta = 0$ to 4.5 ppm was assigned to aliphatic hydrogen and the proton shift-values of $\delta = 6.3$ to 8.5 ppm was assigned to aromatic hydrogen. In the ^{13}C NMR spectra the carbon shift-values of $\delta = 0$ to 60 ppm was

assigned to aliphatic carbon and the carbon shift-values of δ = 110 to 160 ppm was assigned to aromatic carbon. The regions outside of these indicated ranges contained no peaks.

Table 3.6. NMR analyses of the bitumen feed and bitumen oxidized for 6 h at different temperatures.

Property	Bitumen feed	Oxidized bitumen		
		140 °C	150 °C	160 °C
Aliphatic hydrogen (wt %)	90.4	89.4	87.6	87.1
Aromatic hydrogen (wt %)	9.6	10.6	12.4	12.9
Aliphatic carbon (wt %)	68	68	69	68
Aromatic carbon (wt %)	32	32	31	32

The results (**Table 3.6**) indicated that the ratio of aliphatic to aromatic hydrogen decreased, but this change was not accompanied by a change in the relative amount of aliphatic to aromatic carbon. The decrease in the ratio of aliphatic to aromatic hydrogen indicated that the ratio of oxidative hydrogen loss from aliphatic carbons was at least an order of magnitude higher than the oxidative hydrogen loss from aromatic carbons. It can be calculated that for every aromatic hydrogen removed during oxidation at 140 °C, 18 aliphatic hydrogens were removed. At 150 °C the ratio of aromatic to aliphatic hydrogen loss was 1:30 and at 160 °C it was 1:32.

Most of the hydrogen lost during oxidation is lost as water and must be either due to carbonyl formation, or due to olefin formation, since the formation of alcohols is not associated with hydrogen loss. This can be applied to the results that were presented (**Table 3.6**). For every aromatic carbonyl (quinonoid) formed, which accounted for the loss of one aromatic hydrogen, between 9 and 16 aliphatic carbonyls (ketones, esters, carboxylic acids) or olefins were formed, which each accounted for the loss of two aliphatic hydrogens in the form of water. This was an important observation, because it implied that temperature affected the selectivity of carbonyl and/or olefin formation. Oxidation at 140 °C resulted in a lower aliphatic to aromatic oxidation ratio than oxidation at 150 and 160 °C, which had higher, but almost the same aliphatic to aromatic oxidation ratio. The NMR results corroborated the previously reported change in bitumen oxidation selectivity around 150 °C (Babu and Cormack, 1983; Javadli and De Klerk, 2012b).

The question that was not resolved, was whether the carbonyl formation caused the increase in viscosity, or did it just happen to correlate with the viscosity increase (**Equation 3.1**).

The results (**Tables 3.4, 3.5** and **3.6**) suggested that the increase in carbonyl content was not what caused the increase in viscosity, because little change in viscosity was observed despite a significant change in hydrogen distribution. Carbonyl formation was not the only cause of aliphatic hydrogen loss. Hydrogen could also be lost by elimination to produce olefins. Unfortunately the NMR spectra of bitumen were too complex to confirm the carbonyl to olefin ratio. There was insufficient evidence to make a strong conclusion.

As outlined in the introduction, it was anticipated that oxidative addition reactions could also cause bitumen hardening. Carbonyl compounds are capable of aldol condensation, which in turn result in addition. Carbonyl compounds are also capable of keto-enol tautomerism, which can result in addition through the C=C of the enol, although the addition product now contains an alcohol group. Thus, the correlation of carbonyl content to viscosity increase (Equation 3.1) might be causal in nature. However, because olefinic compounds are capable of free radical addition any olefinic compounds that were formed by hydrogen elimination could result in hardening. If olefin formation is meaningful compared to carbonyl formation, the correlation of carbonyl content to viscosity increase (Equation 3.1) might just be an indirect measure of olefin formation and not the cause of the viscosity increase, or not the only cause of viscosity increase. In order to resolve this uncertainty, a model compound study was performed that focused on the nature of the oxidative addition reactions in different hydrocarbon classes (**Chapter 4**).

3.3.3 Oxygenate Classes in Oxidized Bitumen

Oxidized bitumen contains oxygenate functional groups due to incorporation of oxygen during oxidation. Oxygenate classes in oxidized bitumen were identified by using an FTIR. **Table 3.7** shows infrared absorption frequencies of different oxygenate functional groups. It was complex to identify exact functional groups due to the overlapping of some absorption frequencies.

Table 3.7. Infrared absorption frequencies of different oxygenate functional groups (Williams and Fleming, 1989; Colthup et al., 1990; Silverstein et al., 2005).

Compounds	Functional groups	Frequency ranges, cm^{-1}, (wave number)
Ester	C=O	1750-1735 (s) for saturated ester 1730-1715 for aryl and αβ-unsaturated ester 1755-1740 for α-keto ester
	C O	1210-1160 (s) stretch
Carboxylic acid	C=O	1725-1700 for saturated acid 1715-1690 for αβ-unsaturated acid 1700-1680 for aryl ketone
	C O	1315-1200 (s) 1440-1395 (w)
	O H	3000-2500, stretching 1440-1395 bending
Ketone	C=O	1725-1705 for saturated ketone 1685-1665 for αβ-unsaturated ketone 1750-1740 for five-ring ketone 1760 and 1730 for 1,2-diketones s-cis, six ring 1775 and 1760 for 1,2-diketones s-cis, five ring
Aldehyde	C=O	1740-1720 (s) for aliphatic aldehyde 1710-1685 for aromatic aldehyde 1705-1680 for αβ-unsaturated aldehyde
Alcohol	O H	3710 for water in solution 3650-3590 (v) sharp, stretch; for free O H 3600-3200 (b) stretch ; for H-bonded O H 1410-1260 (s) bending
	C O	1150-1040 (s) stretching
Ether	C O	1150-1070 (s), stretching
Sulfoxide	S=O	1060-1040 (s)
Sulfone	O=S=O	1350-1310 (s) 1160-1120 (s)
v, variable; s, strong; b, broad; w, weak; wave number=1/wavelength		

The FTIR spectra of bitumen and oxidized bitumen are shown in **Figure 3.2**. As shown in **Figure 3.2**, there were some oxidative functional groups in the region of 1710 cm^{-1}, and in the region of 1180 cm^{-1} that developed during oxidation.

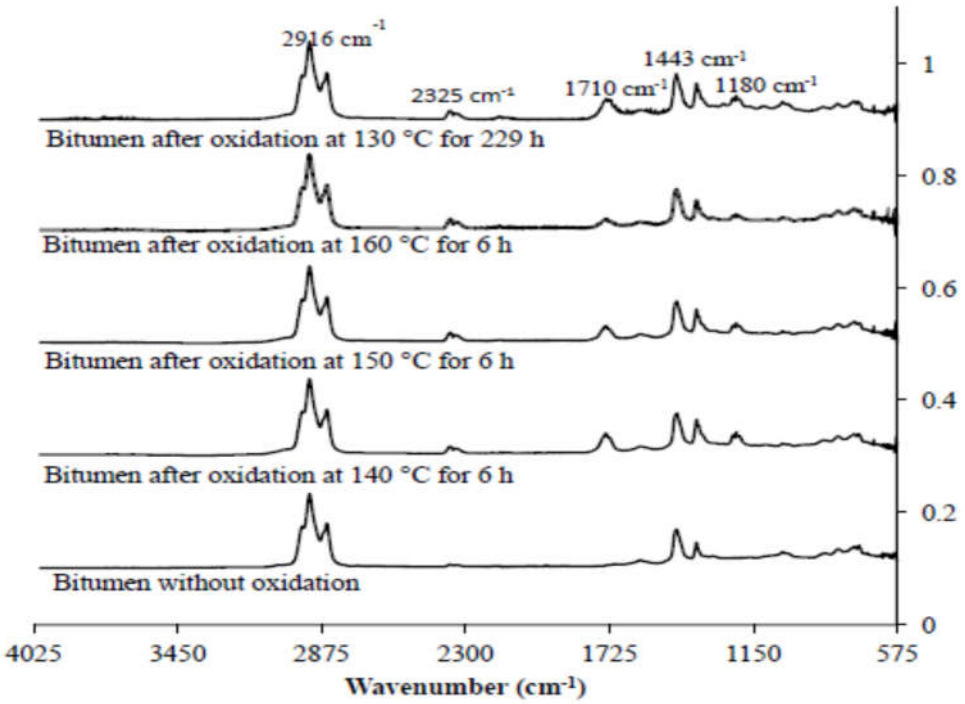

Figure 3.2. FTIR spectra of bitumen and oxidized bitumen.

In order to have a closer look for oxygenate functionalities, infrared spectra of bitumen and oxidized bitumen were redrawn (**Figure 3.3**) in the spectral region 1850 to 1650 and 1350 to 950 cm^{-1}.

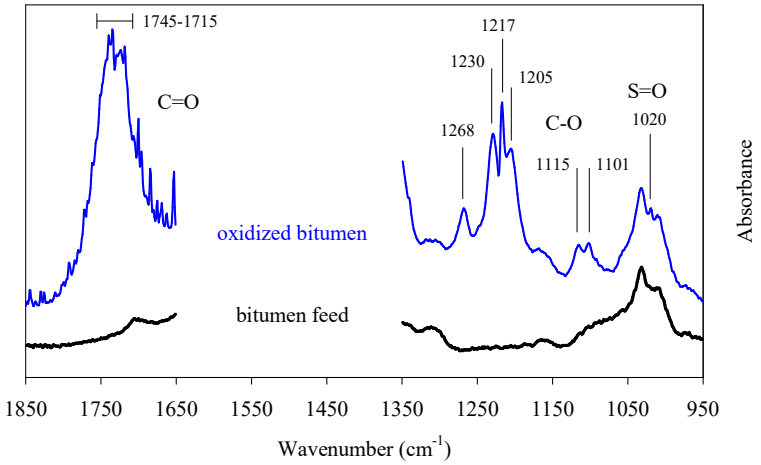

Figure 3.3. Infrared spectra of bitumen and oxidized bitumen in the spectral region 1850 to 1650 and 1350 to 950 cm^{-1}.

A comparison of the infrared spectra of the oxidized bitumen and the bitumen feed showed that there was a considerable increase in carbonyl formation, but that the increase in sulfoxides was minor. The only indication of sulfoxide formation was the absorption at 1020 cm^{-1}, which is typical of aliphatic sulfoxides (Dolphin and Wick, 1977). The spectrum in the 1800 to 1650 cm^{-1} region was convoluted, with the highest absorption found in the range 1745 to 1715 cm^{-1}. It was clear that there was incorporation of carbonyl groups in the oxidized bitumen and the infrared spectrum indicated that there was considerable diversity in the chemical environment of the carbonyl groups. There was also a marked increase in C–O functionality, with prominent absorption peaks at 1268, 1230, 1217, 1205, 1115 and 1101 cm^{-1}. Although no quantification over time was performed, the infrared analysis suggested that carbon oxidation was more likely to be a cause of hardening than sulfur oxidation.

Oxygenate classes in volatile organic fractions (distillates) and water-soluble fractions were also identified by using an FTIR. According to FTIR spectra of bitumen and lighter fractions (**Figure 3.4**) and interpretation of FTIR spectra of oxidized bitumen (**Figure 3.3)**, it is clear that lighter fractions contain oxygenate functional groups. Like oxidized bitumen, carbonyl groups (1718 cm^{-1}) and C–O functionality (1260 and 1100 cm^{-1}) were dominant over sulfoxide functionality (1018 cm^{-1}).

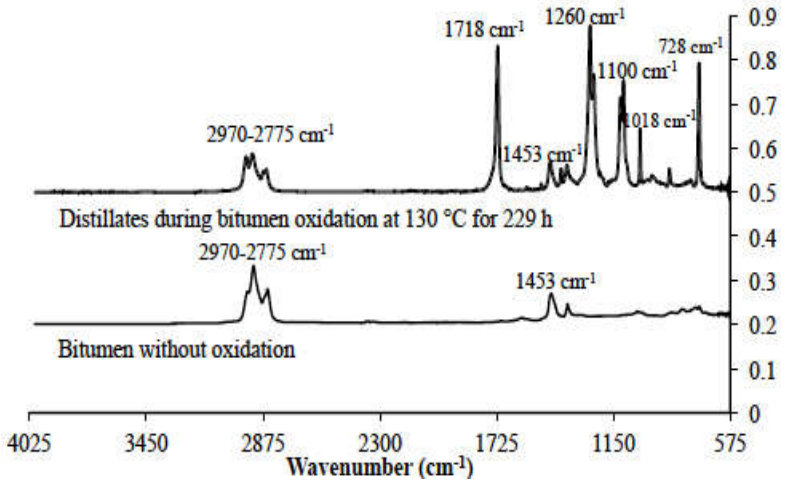

Figure 3.4. FTIR spectra of bitumen, and volatile organic fractions obtained during bitumen autoxidation at 130 °C for 229 h.

As anticipated, water-soluble fractions also contained oxygenate functional groups (**Figure 3.5**). Like oxidized bitumen (**Figure 3.3**) and volatile organic fractions (**Figure 3.4**), carbonyl group (1720 cm^{-1}) and C–O functionality (1260 and 1100 cm^{-1}) were dominant over sulfoxide functionality (1018 cm^{-1}).

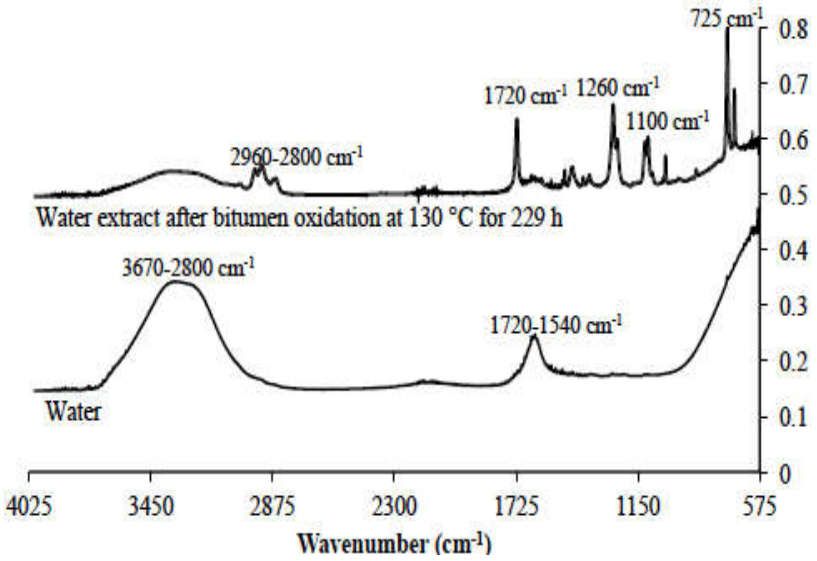

Figure 3.5. FTIR spectra of water, and water extract of oxidized bitumen at 130 °C for 229 h.

3.4 Conclusions

Autoxidation of oilsands bitumen were presented in this Chapter by performing experiment at 130 °C for 229 h and also in the temperature range 130 to 160 °C for 6 h. In all cases, oxidation resulted in undesirable physical changes and comparatively minor chemical changes. It was postulated that the physical changes were at least in part caused by addition reactions.

The main observations and conclusions from this study are the following:

(a) Autoxidation of bitumen at low temperature resulted in physical property changes. Viscosity and density increased due to autoxidation. These changes were not accompanied by increased water-solubility of the oxidized bitumen, which is required for bitumen upgrading by microbial digestion.

(b) The most notable chemical change as result of low temperature bitumen autoxidation was the decrease in aliphatic to aromatic hydrogen ratio in the oxidized bitumen. It indicated that the

relative aliphatic to aromatic hydrogen loss was changed from 18:1 to 30:1 when the temperature was increased from 140 to 150 °C, but remained almost the same, 32:1, when the temperature was increased from 150 to 160 °C. The change around 150 °C coincided with a reported change in bitumen oxidation selectivity (Babu and Cormack, 1983; Javadli and De Klerk, 2012b).

(c) There was an increase in the oxygenate functionality in the oxidized bitumen. An increase in both C–O and C=O bonds were apparent from infrared spectroscopy, with some increase in S=O also being noted. The elemental composition was not significantly changed by autoxidation at low temperature, even after prolonged oxidation.

(d) The increase in bitumen viscosity due to oxidation was reportedly correlated to the increase in carbonyl content of bitumen (Herrington, 1998). This study showed that this correlation is not causal and that the increase in carbonyl content was not the cause of addition reactions. Hence, unless carbonyl groups are responsible for physical changes that cause a viscosity increase, which was not investigated by this study, an increase in carbonyl content does not cause an increase in viscosity, even though it may be correlated.

3.5 Literature Cited

Anderson, K. B.; Crelling, J. C.; Huggett, W. W.; Perry, D.; Fullinghim, T.; McGill, P.; Kaelin, P. Oxidative hydrothermal dissolution (OHD) of coal and biomass. *Prepr. Pap.-Am. Chem. Soc., Div. Fuel Chem.* **2011**, *56*(2), 310 311.

Babu, D. R.; Cormack, D. E. Low temperature oxidation of Athabasca bitumen. *Can. J. Chem. Eng.* **1983**, *61*, 575 580.

Colthup, N. B.; Daly, L. H.; Wiberley, S. E. *Introduction to infrared and Raman spectroscopy*, 3rd ed; Academic Press: San Diego, CA, 1990.

De Klerk, A.; Gray, M. R.; Zerpa, N. Unconventional oil and gas: Oilsands. In *Future Energy*, 2nd ed; Letcher, T. M. Ed.; Elsevier: Amsterdam, 2014, p. 95 116.

Dolphin, D.; Wick, A. *Tabulation of infrared spectral data*; Wiley-Interscience: New York, 1977.

Fedorak, P. M.; Foght, J. M.; Gray, M. R. Conversion of heavy oil and bitumen to methane by chemical oxidation and bioconversion. US Patent Application 2009/0130732 A1, May 21, 2009.

Foght, J. M. Anaerobic biodegradation of aromatic hydrocarbons: pathways and prospects. *J. Mol. Microbiol. Biotechnol.* **2008**, *15*, 93 120.

Hayashi, J.; Matsuo, Y.; Kusakabe, K.; Morooka, S. Depolymerization of lower rank coals by low-temperature O_2 oxidation. *Energy Fuels* **1997**, *11*, 227 235.

Herrington, P. R. Oxidation of bitumen in the presence of a constant concentration of oxygen. *Petrol. Sci. Technol.* **1998**, *16*, 1061 1084.

Herrington, P. R. Effect of concentration on the rate of reaction of asphaltenes with oxygen. *Energy Fuels* **2004**, *18*, 1573 1577.

Javadli, R.; De Klerk, A. Desulfurization of heavy oil - Oxidative desulfurization (ODS) as potential upgrading pathway for oil sands derived bitumen. *Energy Fuels* **2012b**, *26*, 594 602.

Jha, K. N.; Rao, P. M.; Strausz, O. P. Oxidation of the Athabasca oil sand and its fractions. *Prepr. Pap.-Am. Chem. Soc., Div. Fuel Chem.* **1978**, *23*(4), 91 97.

Lee, D. G.; Noureldin, N. A. Effect of water on the low-temperature oxidation of heavy oil. *Energy Fuels* **1989**, *3*, 713 715.

Mae, K.; Maki, T.; Araki, J.; Miura, K. Extraction of low-rank coals oxidized with hydrogen peroxide in conventionally used solvents at room temperature. *Energy Fuels* **1997**, *11*, 825 831.

Moschopedis, S. E.; Speight, J. G. Water-soluble derivatives of Athabasca asphaltenes. *Fuel* **1971a**, *50*, 34 40.

Moschopedis, S. E.; Speight, J. G. Oxidation of bitumen in relation to its recovery from tar-sand formations. *Fuel* **1974**, *53*, 21 25.

Pan, T.; Lu, Y.; Lloyd, S. Quantum-chemistry study of asphalt oxidative aging: An XPS-aided analysis. *Ind. Eng. Chem. Res.* **2012**, *51*, 7957 7966

Pan, C.-X.; Wei, X.-Y.; Shui, H.-F.; Wang, Z.-C.; Gao, J.; Wei, C.; Cao, X.-Z.; Zong, Z.-M., Investigation on the macromolecular network structure of Xianfeng lignite by a new two-step depolymerization. *Fuel* **2013**, *109*, 49 53.

Petersen, J. C. Asphalt oxidation - an overview including a new model for oxidation proposing that physicochemical factors dominate the oxidation kinetics. *Fuel Sci. Technol. Int.* **1993**, *11*, 57 87.

Schwartz, D.; Hall, P. J.; Marsh, H. Macromolecular and chemical changes induced by air-oxidation of a medium volatile bituminous coal. *Prepr. Pap.-Am. Chem. Soc., Div. Fuel Chem.* **1988**, *33*(2), 343 351.

Silverstein, R. M.; Webster, F. X.; Kiemle, D.J. *Spectrometric Identification of Organic Compounds,* 7th ed.; John Wiley: New York, 2005.

Williams, D. H.; Fleming. *Spectrometric Methods in Organic Chemistry,* 4th ed. revised; McGraw-Hill: New York, 1989.

CHAPTER 4 – HYDROCARBON ADDITION REACTIONS DURING LOW-TEMPERATURE AUTOXIDATION[3, 4]

Abstract

Low temperature oxidation of a naphthenic-aromatic hydrocarbon (tetralin) with air in the temperature range 120 to 165 °C was investigated. Of particular interest were to investigate the oxidative physical and chemical changes of naphthenic-aromatic part of bitumen and to understand whether it was responsible for bitumen hardening or not. Instrumental analyses confirmed the possible formation of heavier compounds and oxygen-containing functional groups. Acid number and conductivity were also increased due to autoxidation. Various chemical changes caused some physical changes in tetralin such as change in colour and increase in density. The oxidation of naphthenic-aromatic compounds in bitumen would also result in similar chemical changes that might lead to analogous physical changes in bitumen. The study was expanded to incorporate a range of hydrocarbon classes: five member ring naphthenic-aromatic, naphthenic, aromatic, alkane, and alkyl aromatic. Oxidation of different hydrocarbon classes at 130 °C for 6 h confirmed that the hydrocarbon class responsible for the most addition reactions during bitumen oxidation is the naphthenic-aromatic class. The study also found no addition products during paraffin oxidation, low addition product selectivity for naphthenic and alkylaromatic compounds and no measurable oxidation of aromatics without alkyl groups. It was proposed that the dominant pathway for addition reactions of hydrocarbons is hydrogen disproportionation of free radicals to produce olefins. Free radical addition to olefins through the formation of C–C bonds explained all of the oxidation selectivity observations from the model compound studies, as well as the addition products identified from their mass spectra. It could also be applied to explain the bitumen oxidation results in this and other studies.

Keywords: hydrocarbon, autoxidation, free radical addition, hydrogen disproportionation, oxidative coupling

[3]Reprinted in part with permission from Siddiquee, M. N. and De Klerk, A. Hydrocarbon addition reactions during low-temperature autoxidation of oilsands bitumen. *Energy Fuels* **2014**, *28* (11), 6848–6859. Copyright 2014 American Chemical Society. http://pubs.acs.org/doi/abs/10.1021/ef501694s.

[4]Part of the work published also as Siddiquee, M. N.; De Klerk, A. Oxidation of naphthenic-aromatic compounds in bitumen. *Prepr.Pap.-Am. Chem. Soc., Div. Energy Fuels* **2014**, *59*(2), 572–574.

4.1 Introduction

Bitumen autoxidation reported in **Chapter 3** showed several physical and chemical changes that are related to bitumen hardening. As mentioned before, a number of bitumen oxidation studies also remarked on the increase of viscosity, or hardening of the bitumen, even though the oxidation was conducted at low temperature (Babu and Cormack, 1984; Jia et al., 2005; Javadli and De Klerk, 2012b). In order to facilitate oxidative bitumen upgrading, the bitumen hardening process must be understood and overcome.

Oxidation caused an increase the microstructure of the bitumen (Petersen, 1993), which is a physical effect. The increased microstructure is in turn associated with a change in the effective volume of solvation of the aggregated species, which causes the viscosity to increase (Lesueur, 2009). The increased viscosity was correlated to the formation of carbonyl (C=O) and sulfoxide (S=O) functional groups in the bitumen (Herrington, 1998). However, the causal nature of the correlation was not demonstrated per se. Quantum chemistry of the oxidation process calculations pointed to the loss of lighter material, as well as the formation of carbonyls and sulfoxides as the main oxidative aging mechanism (Pan et al., 2012). Experimental corroboration for the formation of the functional groups was provided by X-ray photoelectron spectroscopy (XPS) and the causal relationship between the observed changes and hardening was attributed to the increased interaction of carbonyls and sulfoxides with other dipoles, which, in turn, caused association and agglomeration. Another potential cause of hardening is free-radical addition reactions, which is a chemical effect, which was the working hypothesis for the study reported here. In order to understand the role of oxidative coupling better, a model compound study was performed.

It is reported in **Table 2.1** that typical H/C ratio of Canadian oilsands bitumen is 1.5. This indicates dominant naphthenic-aromatic character and low paraffinic character of bitumen (Strausz and Lown, 2003). As bitumen shows naphthenic-aromatic character, it is important to investigate oxidation behavior of naphthenic-aromatic compounds to understand the bitumen hardening process. Tetralin as a representative of the naphthenic-aromatic part of the bitumen was oxidized by using air as an oxidizing agent at temperatures in the range 120-165 °C for 24 h and 48 h. The objectives were to investigate the oxidative physical and chemical changes of

naphthenic-aromatic compounds in bitumen, and to understand whether this combination of functional groups of bitumen is responsible for bitumen hardening or not.

The tetralin autoxidation study confirmed that oxidative addition was taking place (Siddiquee, et al. 2014a). In order to understand the role of oxidative coupling better, the study was further extended considering different hydrocarbon classes found in bitumen. The hydrocarbon classes studied were: five member ring naphthenic-aromatic, naphthenic, aromatic, alkane, and alkyl aromatic. Oxidation was performed with air at 130 °C for 6 h. The objective was to establish the nature of the coupling, C–C or C–O–C, as well as the hydrocarbon compound classes responsible for cross-coupling reactions. This work was subsequently published (Siddiquee, et al. 2014b). The investigation in Chapter 4 was limited to hydrocarbon compound classes and **Chapter 5** describes oxidation of heteroatom-containing compound classes.

4.2 Experimental

4.2.1 Materials

Model compounds that represented different hydrocarbon compound classes found in bitumen were selected for the oxidative coupling studies (**Table 4.1**). Tetralin, indan and indene represented the naphthenic-aromatic compound class, decalin represented the naphthenic compound class, naphthalene represented aromatic compound class, *p*-cymene represented the alkylaromatic compound class and *n*-decane represented the acyclic paraffinic compound class. The model compounds were selected to be within a narrow carbon number range (C_9–C_{10}) and boiling point range (174 to 218 °C) to facilitate analysis and comparison.

In order to facilitate identification of the oxidized products, a number of additional compounds were used as standards. Tetralin 1,2,3,4-tetrahydro-1-naphthol (97 %, Aldrich), alpha-tetralone (97 %, Aldrich), 1-indanol (98 %, Aldrich), 1-indanone (≥99 %, Aldrich), *cis*-decahydro-1-naphthol (99 %, Aldrich), 1-decalone (97 %, Aldrich) were used for the identification of oxidation products by gas chromatography coupled with mass spectrometry (GC-MS). Chloroform (98 %, HPLC grade, Fisher Scientific) was used as a general solvent for analyses. Hexachlorobenzene (99 %, analytical standard, Supleco) was used as internal standard for

chromatographic analyses. Extra-dry air was purchased from Praxair Inc., Edmonton, Canada and used as oxidizing agent.

Table 4.1. List of model compounds used for oxidative coupling.

Name	CASRN [a]	Formula	Normal boiling point (°C)	Purity (wt %)		Supplier
				supplier [b]	analysis [c]	
tetralin	119-64-2	$C_{10}H_{12}$	207	99	98.89	Sigma-Aldrich
indan	496-11-7	C_9H_{10}	176	95	96.68	Aldrich
indene	95-13-6	C_9H_8	181	≥99	98.69	Aldrich
n-decane	124-18-5	$C_{10}H_{22}$	174	≥99	99.67	Sigma-Aldrich
cis/*trans*-decalin [d]	91-17-8	$C_{10}H_{18}$	196 / 187	≥99	51.40 / 48.59	Sigma-Aldrich
naphthalene	91-20-3	$C_{10}H_8$	218	99	99.84	Aldrich
p-cymene	99-87-6	$C_{10}H_{14}$	177	99	99.98	Aldrich

[a] CASRN = Chemical Abstracts Services Registry Number.
[b] This is the purity of the material guaranteed by the supplier.
[c] This is the purity based on peak area obtained by GC-FID analysis.
[d] Mixture of *cis*- and *trans*-decalin; values reported in the same order.

4.2.2 Equipment and Procedure

The equipment shown in **Figure 3.1** of **Chapter 3** was modified to accommodate various online analyzers for the oxidation reported in this Chapter (**Figure 4.1**). In each experiment approximately 50 g of the model compound was used and the oxidation was conducted using a similar procedure as described in **Chapter 3**.

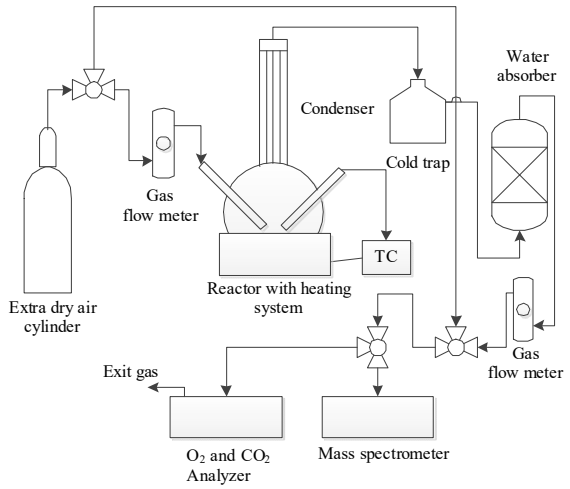

Figure 4.1. Experimental setup for autoxidation of model compounds.

Tetralin oxidations were conducted with an airflow rate of 250 mL/min at temperature in the range 120 - 165 °C for 24 and 48 h. A cold trap was used to ensure liquid free off-gas. The liquid-free off-gas was then passed through pre-weighed and pre-dried calcium chloride ($CaCl_2$) bed to absorb the water vapor. Oxygen consumption and CO_2 production was monitored by continuously measuring the off-gas using an O_2 and CO_2 analyzer (Series 9600, Alpha Omega Instruments, Lincoln, RI 02865, USA). In parallel the off-gas was analyzed by a mass spectrometer (Extorr XT Series RGA, XT300 M, Extorr Inc., New Kensington, PA 15068, USA). Both of these measurements were carried out on-line in a continuous fashion.

Oxidations of different hydrocarbon compound classes were conducted with an airflow rate of 120 mL/min at 130 °C for 6 hours. Samples were collected at different time intervals to monitor oxidation products formed at different oxidation times. Sample sizes were kept small (approximately 0.5 g) so that the ratio of feed to oxidant was not greatly affected.

4.2.3 Analyses

In addition to the on-line analyzers described as part of the equipment, the products were also analyzed off-line employing the following techniques and instruments:

(a) Quantitative analyses of model compounds and oxidized model compounds were performed by gas chromatography with flame ionization detector (GC-FID). An Agilent GC-FID (Agilent 7890A GC system) equipped with DB-5 MS column 30 m × 0.25 mm × 0.25 μm column was employed for this purpose. The GC injector temperature was 250 °C, the split ratio was 10:1. Column flow of He as carrier gas was 2 mL/min and was kept constant. The oven temperature was 75 °C for 0.5 min and then temperature was increased from 75 °C to 325 °C at the rate of 20 °C/min, and finally, temperature was kept constant at 325 °C for 5 min. The samples were prepared using chloroform as solvent and hexachlorobenzene was added as an internal standard. The FID response factors for key compounds were experimentally determined and the calculated relative response factors are very close the response factors reported in literature (Dietz, 1967; Huang et al. 1990; Katritzky et al., 1994).

Table 4.2. FID response factors of studied model hydrocarbons.

Compound Name	Retention Time (minute)	Response factor (RF)	Reported RF value
Heptane	1.72	1.00 ± 0.00	1.00 (Dietz, 1967)
$CHCl_3$	1.52	0.09 ± 0.01	
Hexachlorobenzene	8.67	0.36 ± 0.01	0.31(Huang et al. 1990)
Tetralin	4.90	1.07 ± 0.01	1.02 (Katritzky et al., 1994)
Indan	3.82	1.06 ± 0.01	1.03 (Katritzky et al., 1994)
Indene	3.92	1.08 ± 0.01	
cis/*trans*-Decalin[a]	3.99/ 4.37	1.06 ± 0.02	
Naphthalene	5.08	1.12 ± 0.01	1.07 (Katritzky et al., 1994)
p-Cymene	3.68	1.07 ± 0.01	
n-Decane	3.41	1.02 ± 0.01	0.97(Katritzky et al., 1994)

[a] Response factor of decalin was calculated by adding the area of *trans*-decalin and *cis*-decalin

(b) Identification of oxidized model compounds was performed by GC-MS using an Agilent 7820A GC system (Agilent Technologies Canada Inc., Mississauga, ON) and an Agilent 5977E MSD (Agilent Technologies Canada Inc., Mississauga, ON) mass spectrometer (MS). The products were separated on an HP-5 30 m × 0.25 mm × 0.25 µm column. The same temperature program as for GC-FID analyses were used; the HP-5 and DB-5 MS columns also have similar separation characteristics. Product identification was performed based on the analysis of model compounds that were anticipated as oxidation products and interpretation of the electron ionization mass spectra. Identification was aided by use of the National Institute of Standards and Technology (NIST) library of electron ionization mass spectra.

(c) Infrared analyses were performed using an ABB MB 3000 Fourier transform infrared (FTIR) spectrometer. A small amount of sample was placed on a potassium bromide (KBr) disc and the spectrum was collected over the wave number range 4000 to 500 cm^{-1} as the average of 120 scans per sample. The spectral resolution was 2 cm^{-1}, signal strength was 70 %, the acquisition mode was absorbance and detector gain was 243.

(d) Raman analyses were performed with a Snowy Range Raman, using a laser power 35 mW, integration time of 20 s, and each spectrum was the average of 5 scans.

(e) A HPLC (High Performance Liquid Chromatography) having Waters e 2695 Separation Module, Waters 2998 Photodiode Array Detector, and Waters 2414 Refractive Index Detector was used for the analyses of tetralin and oxidized tetralin. HPLC grade hexane is being used as a mobile phase, and the flow rate of mobile phase was 1 ml/min.

(f) A density meter (Anton Paar, DMA 4500M) was employed to measure density of tetralin and oxidized tetralin.

(g) Acid number of tetralin and oxidized tetralin were measured by using a Mettler Toledo Titration Excellence T50 (Mettler-Toledo AG Analytical, Switzerland).

(h) A conductivity meter (Seven Compact^{TM} Conductivity S230, Mettler-Toledo AG, Switzerland) was used to measure conductivity of tetralin and oxidized tetralin.

4.2.4 Calculations

(a) The Dietz-method (Dietz, 1967) was used to calculate the FID response factors:

$$\text{Response factor (RF)}_{\text{Dietz}} = \frac{(\text{area of compound})(\text{mass of standard})}{(\text{mass of compound})(\text{area of standard})} \qquad \text{(Equation 4.1)}$$

Heptane was used as the standard and its response factor was 1.00.

(b) The percentage conversion was calculated as follows:

$$W_i = \frac{A_i * W_{HCB}}{A_{HCB} * RRF_{i,HCB}} \qquad \text{(Equation 4.2)}$$

Where, $RRF_{i,HCB} = RF_i / RF_{HCB}$ (Dietz, 1967) (Equation 4.3)

= Relative response factor of model compounds with respect to hexachlorobenzene (internal standard)

RF_{HCB} = Response factor of hexachlorobenzene with respect to heptane

RF_i = Response factor of model compound with respect to heptane

W_i = Weight % of model compounds

W_{HCB} = Weight % of hexachlorobenzene
A_i = Peak area of model compounds
A_{HCB} = Peak area of hexachlorobenzene

(c) Product selectivity was calculated from the relative peak area of the products as follows:

$$\text{product selectivity (\%)} = \frac{\text{relative peak area of specific product}}{\text{sum of relative peak area of all the products}} \text{ x } 100\% \qquad \text{(Equation 4.4)}$$

4.3. Results and Discussion

4.3.1 Oxidation of Tetralin to Investigate Physical and Chemical Changes

Oxidation of tetralin (representative of naphthenic-aromatic part of bitumen) results in physical changes (e.g. change in color and density), and chemical changes (e.g. change in functional groups, heavier product formation, change in conductivity and acid number, etc.). These are discussed in following sections.

4.3.1.1 Change in Color

Tetralin (colorless) was turned to brown color due to oxidation at 135 °C for 24 h (**Figure 2B**) and turned to dark color as a result of oxidation at 150 °C for 48 h (**Figure 2C**). This change in color might be due to the formation of heavier products and/or compounds having different functional groups.

(A) (B) (C)

Figure 4.2. (A) Tetralin; (B) tetralin oxidized at 135 °C for 24 hour and (C) tetralin oxidized at 150 °C for 48 hour.

4.3.1.2 Change in Density

Density of tetralin and oxidized tetralin are reported in **Table 4.3.**

Table 4.3. Physical and chemical changes during tetralin autoxidation at temperatures in the range 120 - 165 °C for 24 and 48 h.

series	physical change	chemical changes	
	density at 25 °C (kg/m^3)	conductivity (μS/cm)	acid number (mg KOH/g)
tetralin	965 ± 1	0	0.014 ± .003
tetralin oxidized at 165 °C for 48h	1051 ± 1	0.011 ± 0.001	29.40 ± 1.15
tetralin oxidized at 150 °C for 48h	1043 ± 5	0	18.62 ± 0.05
tetralin oxidized at 120 °C for 48h	1032 ± 1	0	9.77 ± 0.33
tetralin oxidized at 150 °C for 24h	1024 ± 3	0	6.15 ± 0.23
tetralin oxidized at 135 °C for 24h	1012 ± 1	0	3.86 ± 0.13
tetralin oxidized at 120 °C for 24h	994 ± 1	0	0.89 ± 0.12

As shown in **Table 4.3** density of tetralin increases due to the oxidation. The maximum density increase was 86 kg/m^3 (measured at 25 °C) due to the autoxidation of tetralin at 165 °C for 48 h. Density of naphthenic-aromatic part of bitumen would also be increased due to the oxidation. This also correlates with the density increase of bitumen due to oxidation shown in **Chapter 3**.

4.3.1.3 Chemical Changes

The elemental composition was changed because of oxygen consumption and loss of carbon as CO_2 and loss of hydrogen as H_2O. For instance, ~ 7 wt % of oxygen was consumed due to the tetralin oxidized at 150 °C for 48 hours. This amount includes approximately 4.2 wt % oxygen in oxidized tetralin, and approximately 0.2 wt % and 2.5 wt % present in CO_2 and in H_2O, respectively. The oxygen consumption results in the formation of different oxygen-containing functional groups.

GC-MS analyses confirmed the presence of alcohol, ketones, and addition products (described in **Section 4.3.2.1).** The change in functional group was also examined by using FTIR, and FTIR spectra of tetralin and oxidized tetralin are shown in **Figure 4.3**.

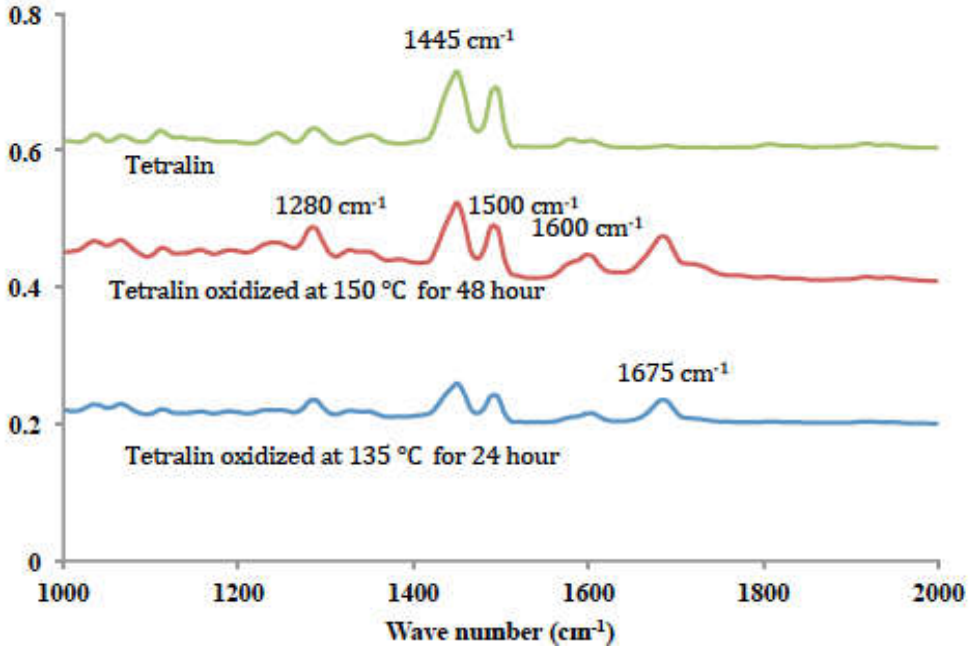

Figure 4.3. FTIR spectrum of tetralin before and after oxidation.

As shown in **Figure 4.3**, there is a promising indication of oxidative functional groups in the region of 1675 cm^{-1}. C=O bonds of aldehydes, ketones, carboxylic acids, and esters might present in the region of 1760-1670 cm^{-1} (stretch). The peaks in the region of 1600- 1500 cm^{-1} (w) stretch may be due to the presence of C=C of aromatic rings. The peak in the region of 1445 cm^{-1} may indicate the C-H of alkanes (Speight, 2006).

Heavier product formation was also confirmed by HPLC analysis. HPLC chromatograms of tetralin and oxidized tetralin of are shown in **Figure 4.4**. There are more peaks in the chromatogram of oxidized tetralin (**Figure 4.4B**) compared to tetralin (**Figure 4.4A**). Additional peaks indicate the formation of oxidative products. Also, there is a small peak at the retention time of approximately 17 minute (**Figure 4.4B**) that might be due to the formation of heavier molecules.

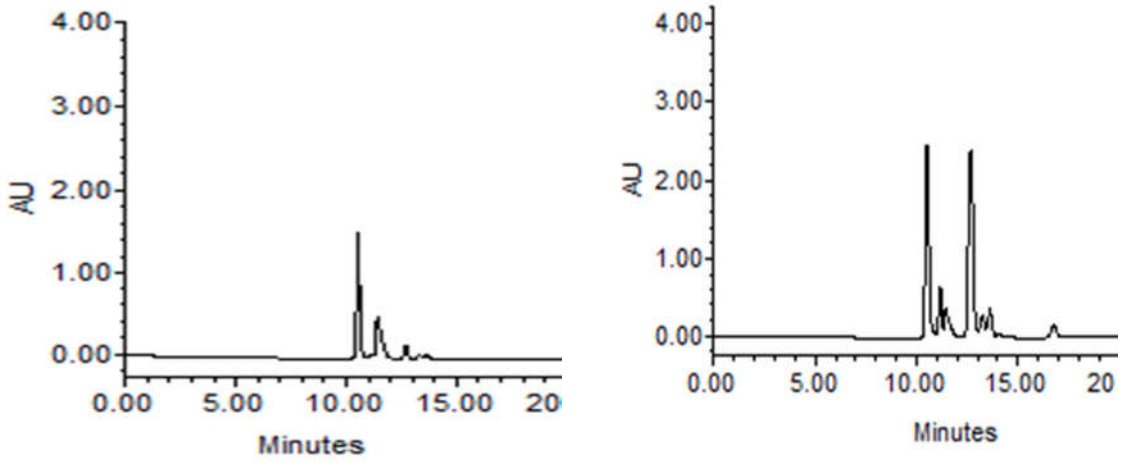

(A) **(B)**

Figure 4.4. HPLC chromatograms of (A) tetralin and (B) tetralin oxidized at 150 °C for 48 hour.

The acid numbers and conductivities of tetralin and oxidized tetralin are shown in **Table 4.3.** According to **Table 4.3**, acid number increases with the oxidation temperatures and times. This indicates C-C bond scission and the formation of acidic functional groups due to the oxidation of tetralin.

As reported in **Table 4.3**, a conductivity change was only observed due to oxidation at 165 °C for 48h. This indicates that tetralin and tetralin oxidized at less severe conditions are not in a sufficiently ionized form to affect conductivity.

The oxidation of naphthenic-aromatic compounds in bitumen would also result similar chemical changes that might lead to the various physical changes of bitumen such as bitumen hardening, viscosity and density increase.

4.3.2 Oxidation of Different Naphthenic-Aromatic Hydrocarbons

4.3.2.1 Product Identification

The first model compound class that was investigated was the naphthenic-aromatic compounds, which were represented by tetralin, indan and indene. Autoxidation was performed at 130 °C for 6 h and over time it was possible to identify three types of oxidation products, as illustrated by the chromatogram of the product from tetralin oxidation (**Figure 4.5**):

(a) Primary oxidation products, alcohols and ketones of the feed.

(b) Secondary oxidation products, which are feed molecules that have been oxidized more than once. The secondary oxidation products were mainly combinations of alcohols and ketones.

(c) Addition products that were produced by oxidative addition of two feed molecules. These products often contained one or more oxygen-containing functional groups per addition product.

The procedure that was followed to identify the oxidation products is described first by using tetralin oxidation.

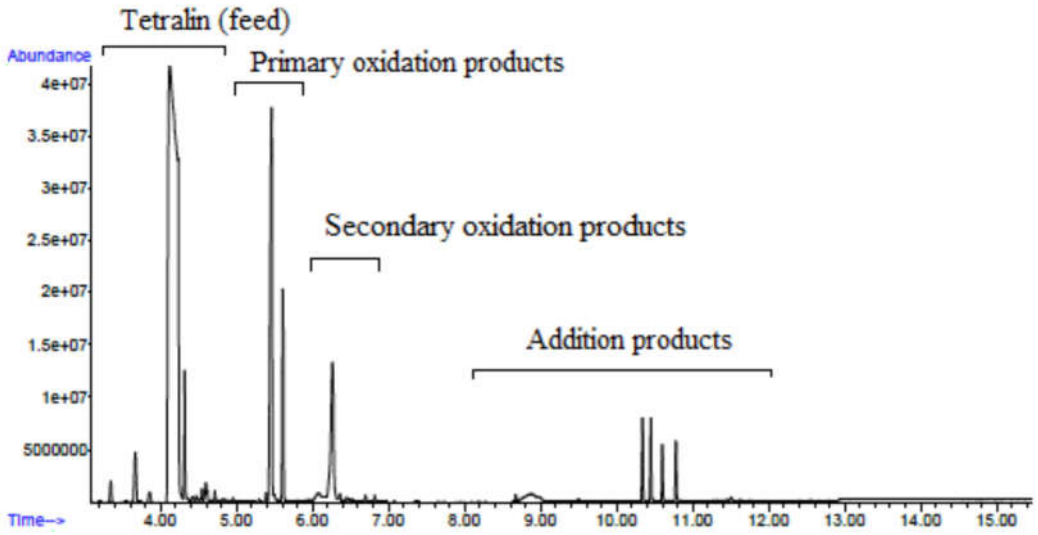

Figure 4.5. Chromatogram of tetralin oxidation products after autoxidation at 130 °C for 6 h.

All feed materials were analyzed before use (**Table 4.1**) to identify and quantify the impurities. As shown in **Figure 4.5,** peaks before a retention time of 5.0 min belonged to the tetralin (retention time 4.2 min) and its impurities. In the case of tetralin the impurities were naphthalene, decalin isomers and other close boiling hydrocarbons.

The primary oxidation products were identified based on their electron ionization mass spectra. The analysis of model compounds was used to assist with identification of compounds from the National Institute of Standards and Technology (NIST) library of electron ionization mass spectra and provide an indication of the retention time of such columns on the column used for

chromatographic separation. The model compounds 1,2,3,4-tetrahydro-1-naphthol and α-tetralone were employed to assist with the identification of alcohols and ketones derived from tetralin the model compounds.

To illustrate the procedure, the electron ionization mass spectrum of the model compound 1,2,3,4-tetrahydro-1-naphthol (**Figure 4.6**) with retention time 5.4 min, is compared with a compound from tetralin oxidation that was identified as an alcohol of tetralin (**Figure 4.7**).

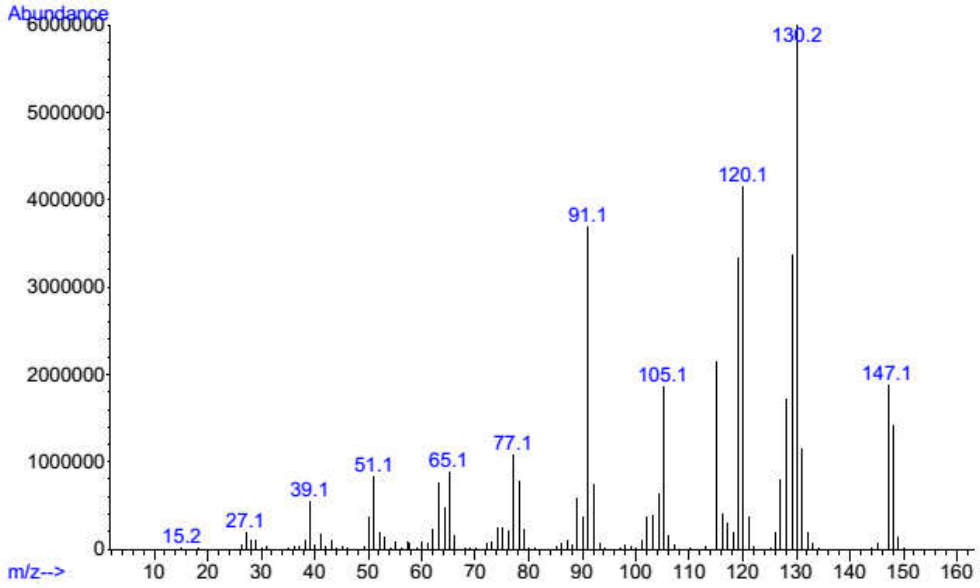

Figure 4.6. Electron ionization mass spectrum of 1,2,3,4-tetrahydro-1-naphthol (commercially obtained model compound).

In addition to the formation of simple alcohols and ketones, there were also compounds that were secondary oxidation products and had more than one functional group. Since an apolar column was employed for chromatographic separation, heavier compounds tended to elute at longer residence times. The loss of water (m/z gap of 18) from alcohols and the loss of carbon monoxide (m/z gap of 28) from carbonyls were employed as diagnostics for the interpretation of the mass spectra of secondary oxidation products.

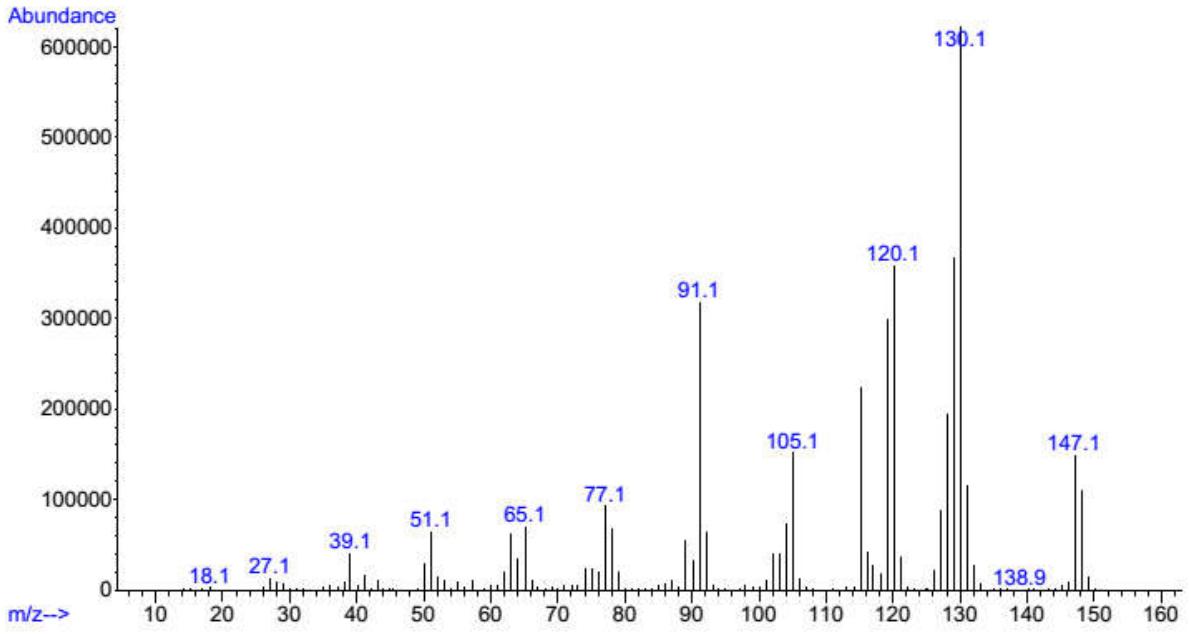

Figure 4.7. Electron ionization mass spectrum of a compound that was identified as an alcohol of tetralin that was present in the product from autoxidation of tetralin for 90 min at 130 °C.

Higher molecular weight compounds were formed due to addition reactions. These compounds were of particular interest, because their structure would provide an indication of the nature of the oxidative addition that took place. For example, one of the major addition products of tetralin oxidation is found at a retention time of 10.6 min (**Figure 4.5**) and its electron ionization mass spectrum (**Figure 4.8**) indicated that the nature of addition is through a C–C bond. The molecular ion, M^+ at m/z = 280, was less prominent than the $(M+1)^+$ protonated molecular ion at m/z = 281. Water is readily lost to produce the $(M - 18)^+$ ion at m/z = 262. This fragment not only indicated that the compound contained an alcohol functional group, but also that the tetralin dimer likely formed by C–C addition and not by an ether linkage. Unfortunately the mass spectrum on its own does not completely rule out addition through an ether linkage, because free radical recombination and a weak $(M - 18)^+$ peak are both known to occur in the electron ionization mass spectra of heavy ethers (McLafferty and Tureček, 1993).

Oxidation studies through the formation of carbocation can lead to the different reaction pathways (Poniatowski and Floreancig, 2010; Sevov and Wiest, 2010; Clausen and Floreancig, 2012; Wang et al., 2014), but any chemicals that potentially form carbocation was not considered in this study.

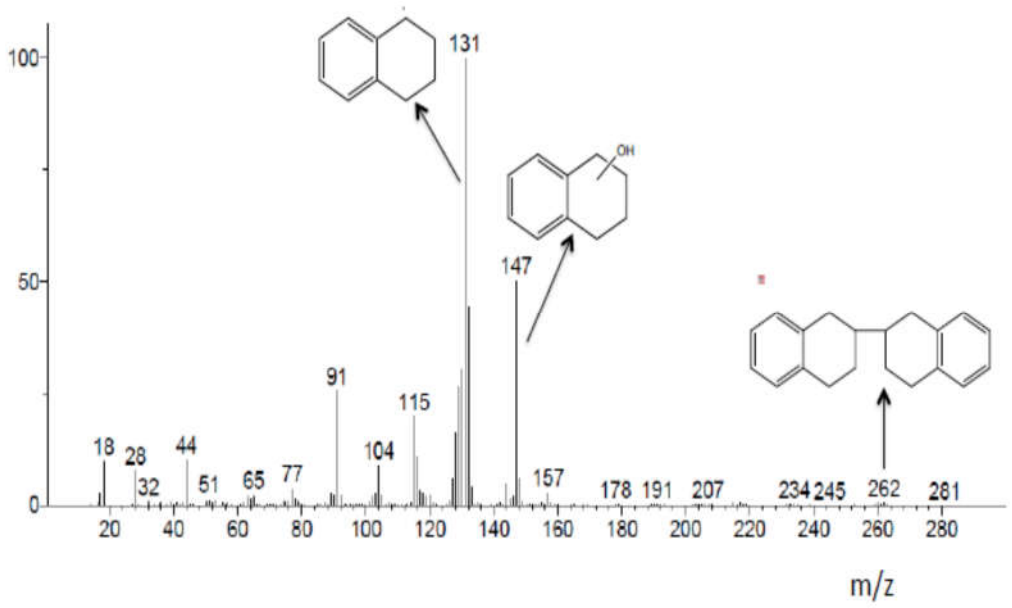

Figure 4.8. Electron ionization mass spectrum of an addition product (10.6 min retention time) formed during tetralin oxidation at 130 °C.

The chromatograms of the oxidation products from indan oxidation (**Figure 4.9**) and indene oxidation (**Figure 4.10**) illustrate that a similar grouping of oxidation products could be made as that for tetralin oxidation.

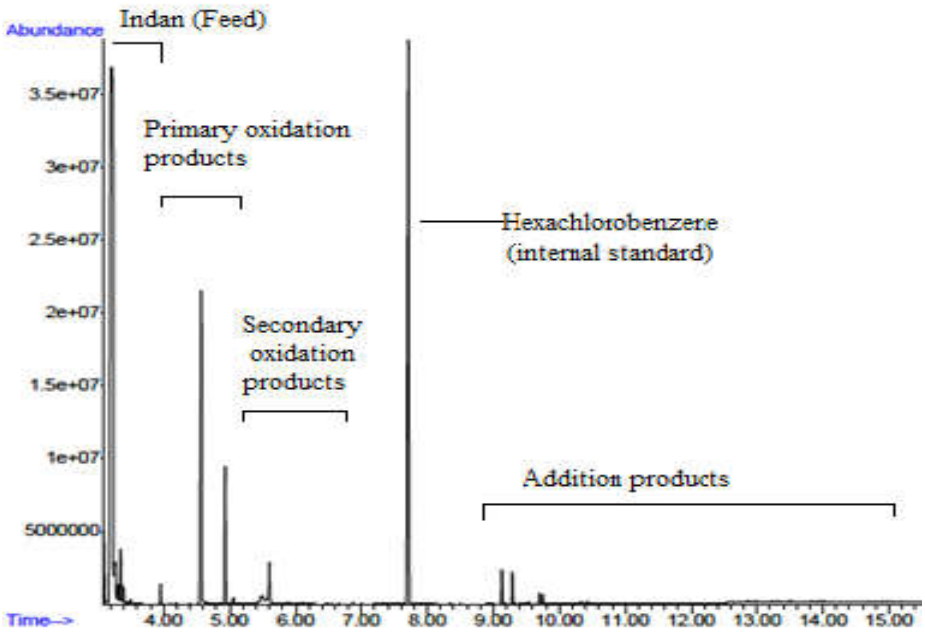

Figure 4.9. Chromatogram of the oxidation product from indan autoxidation at 130 °C for 6 h.

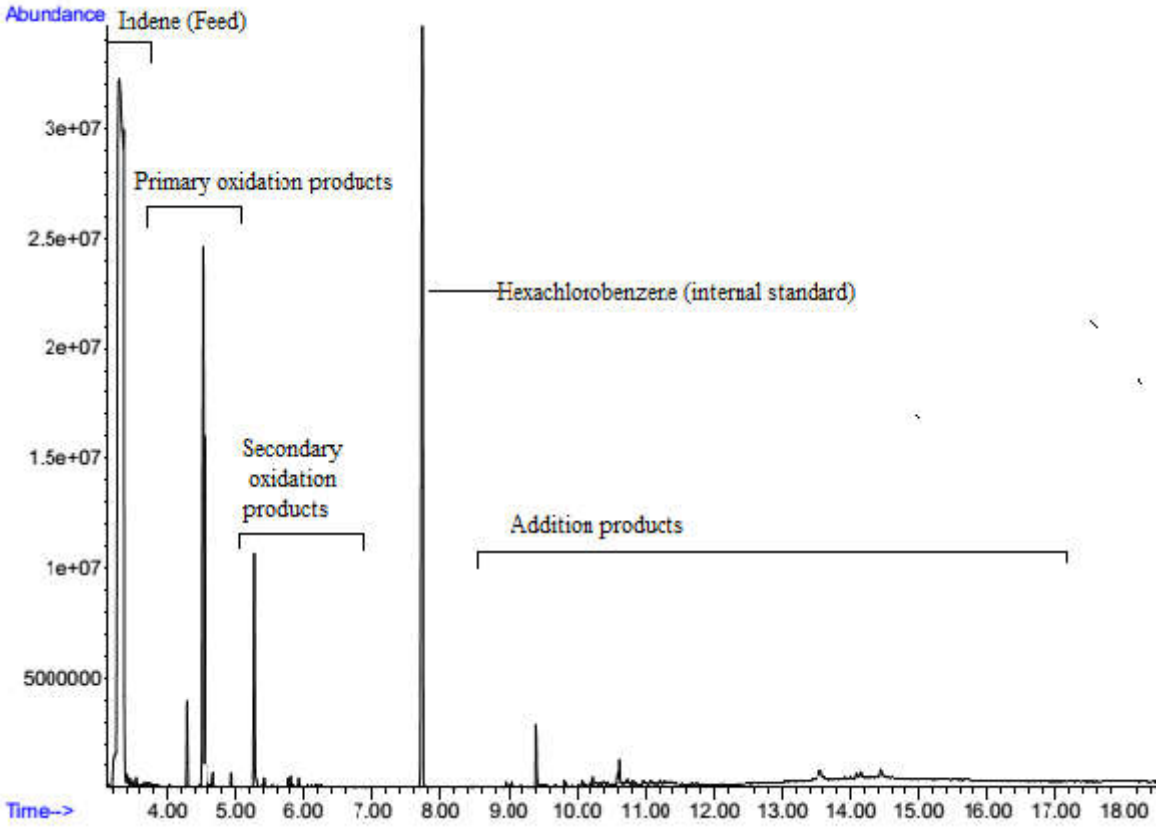

Figure 4.10. Chromatogram of the oxidation product from indene autoxidation at 130 °C for 6 h.

The addition products had similar motifs as found during tetralin oxidation. The tentative interpretation of mass spectra revealed products with C–C bonds to form dimers of the respective starting materials. For example, compare an addition product found during indan oxidation (**Figure 4.11**) with that of one in the NIST library (**Figure 4.12**). Also, compare an addition product found during indene oxidation (**Figure 4.13**) with that of one in the NIST library (**Figure 4.14**).

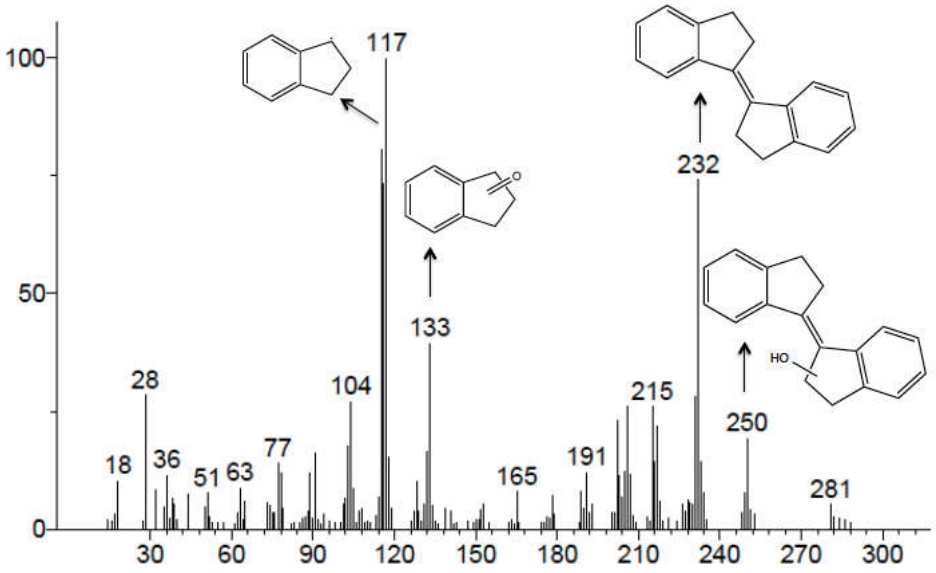

Figure 4.11. Electron ionization mass spectrum of the addition product from indan oxidation that appeared at a retention time 10.4 min.

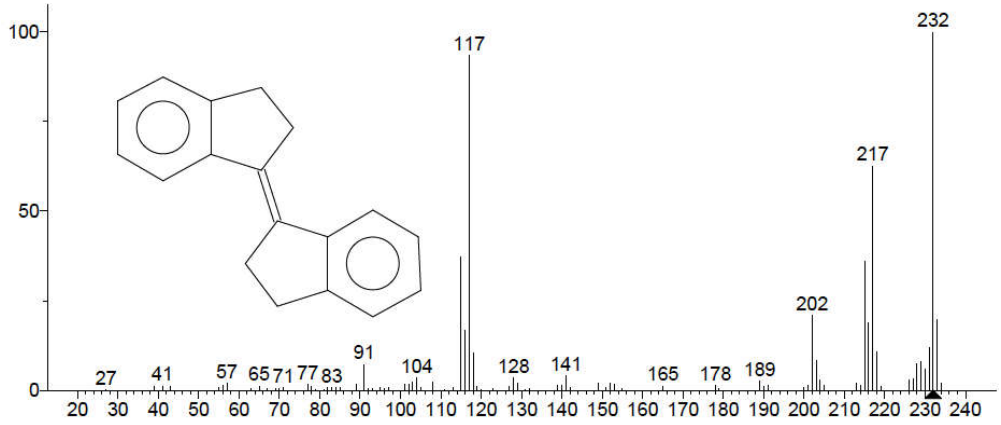

Figure 4.12. Fragmentation pattern of trans-1,1'-Bibenzoindanylidene from NIST library.

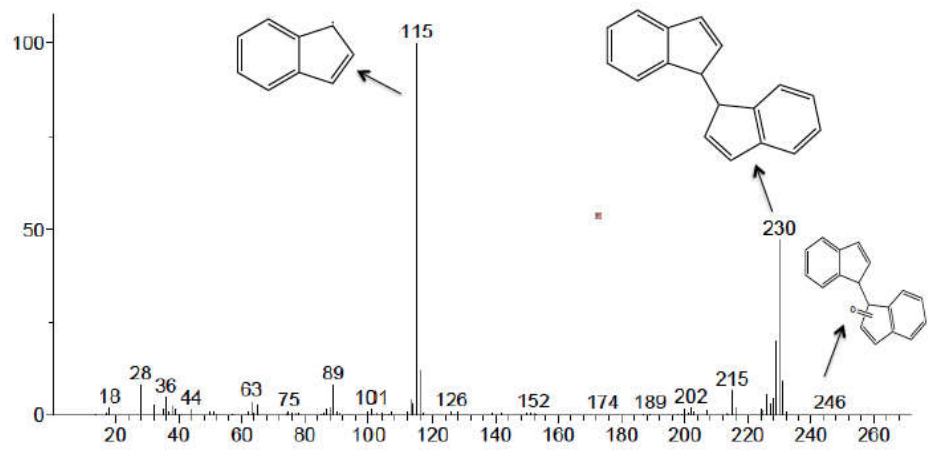

Figure 4.13. Electron ionization mass spectrum of the addition product from indene oxidation that appeared at a retention time of 8.9 min.

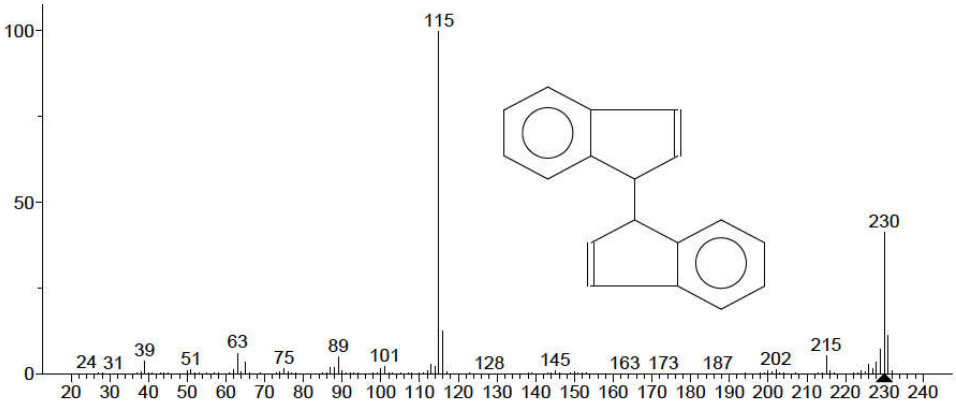

Figure 4.14. Fragmentation pattern of 1,1'-Bi-1 H indene from NIST library.

4.3.2.2 Conversion and Selectivity

The oxidative conversion of the feed materials (**Figure 4.15**) was determined. The conversion was expressed in terms of the disappearance of tetralin, indan and indene respectively and it does not reflect the extent of oxidation.

The O_2 consumption and the selectivity to primary oxidation products, secondary oxidation products, addition products, CO_2 and water was also determined (**Table 4.4**). According to the **Figure 4.15**, oxidative conversion of tetralin was linear with time, conversion of indan was fast initially and after the first 30 min of oxidation, it was linear with time. Initially, indene

conversion rate was very high, and then conversion rate decreased. Overall the indene conversion was the highest, followed by indan and tetralin conversions.

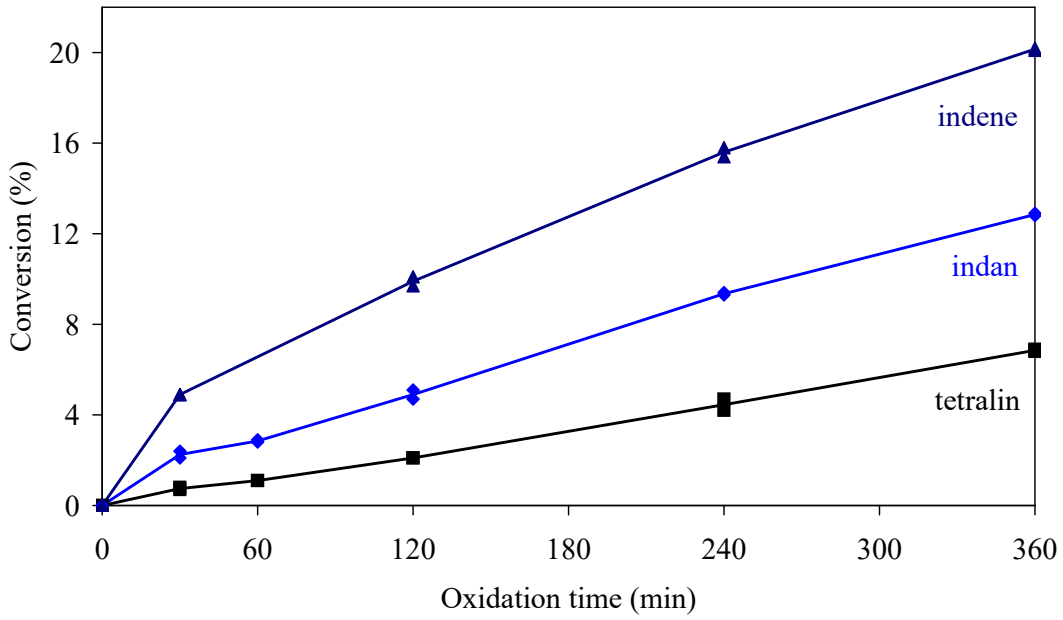

Figure 4.15. Conversion of tetralin, indan and indene by oxidation at 130 °C and air flow rate of 145-150 mL h^{-1} per g feed.

The higher conversion of indene can be explained by the presence of the nonconjugated double bond in indene. In naphthenic-aromatic compounds, oxidation preferentially takes place at C–H bond located at the α-position relative to the aromatic nucleus. Hydrocarbons that have nonconjugated double bonds, are also oxidized at the C–H bond located at α-position relative to the double bond (Emanuel et al., 1967; Waters, 1964). The radical intermediate that is formed by scission of either of these C–H bonds can be resonance stabilized by the adjacent π-electron systems (Waters, 1964). In the case of indene, the C–H that is oxidized is in the α-position with respect to both the aromatic and the olefinic double bond, making it particularly susceptible to autoxidation. The higher conversion rate of indan than tetralin was likely due to the nature and higher amount of impurities present in indan compared to tetralin (**Table 4.1**). The indan feed contained small amounts of oxidation products as impurities, suggesting that some of the close-boiling impurities in indan are more susceptible to oxidation than the mainly paraffinic impurities in tetralin. It could also explain the appearance of addition product early on during

oxidation of indan. Tetralin did not form addition products during the early stages of oxidation. However, the selectivity to addition products remained fairly constant irrespective of the oxidation extent (**Table 4.4**) and the relatively higher oxidation rate than tetralin was maintained (**Figure 4.15**). The presence of impurities would not account for these observations. The five-membered naphthenic structure in indan was inherently more susceptible to oxidation under the conditions tested.

Table 4.4. Product selectivity and O_2 consumption during the oxidation of tetralin, indan and indene at 130 °C and air flow rate of 145-150 mL h^{-1} per g feed.

Description	Selectivity [a]				
	30 min	60 min	120 min	240 min	360 min
Tetralin					
primary oxidation products (wt %) [b]	100	99	95	86	84
secondary oxidation products (wt %) [b]	0	1	5	7	5
addition products (wt %) [b]	0	0	0	7	11
CO_2 production (mg CO_2/kg feed) [c]	0	0	1	2	3
water production (mg H_2O/kg feed) [c]	- [d]	- [d]	- [d]	- [d]	970
oxygen consumption (mg O_2/kg feed) [c]	60	260	1390	3770	6080
Indan					
primary oxidation products (wt %) [b]	90	88	86	84	83
secondary oxidation products (wt %) [b]	3	4	5	5	6
addition products (wt %) [b]	8	8	9	11	11
CO_2 production (mg CO_2/kg feed) [c]	2	2	2	4	9
water production (mg H_2O/kg feed) [c]	- [d]	- [d]	- [d]	- [d]	2520
oxygen consumption (mg O_2/kg feed) [c]	810	1890	4030	7960	11660
Indene					
primary oxidation products (wt %) [b]	49	- [e]	52	54	56
secondary oxidation products (wt %) [b]	25	- [e]	20	17	15
addition products (wt %) [b]	26	- [e]	28	29	29
CO_2 production (mg CO_2/kg feed) [c]	0	1	1	1	1
water production (mg H_2O/kg feed) [c]	- [d]	- [d]	- [d]	- [d]	660
oxygen consumption (mg O_2/kg feed) [c]	1800 [f]	3020	5180	8890	11820

[a] Average of two runs

[b] Weight percentage of all oxidized products in the liquid

[c] Cumulative amount produced or consumed

[d] Measured only at the end of the run

[e] Sample formed gel as vial cap was partially opened and it was not analyzed

[f] Estimate; analytical problems during first 30 min

The presence of double bond in indene led to the formation of free radical addition products even during the initial stages of oxidation. It explained why the addition products identified were C–C bonded. The addition of a carbon centred free radical to an olefinic group results in the formation of a C–C bond and it propagates the free radical, which can readily form a peroxide radical (**Figure 4.16**).

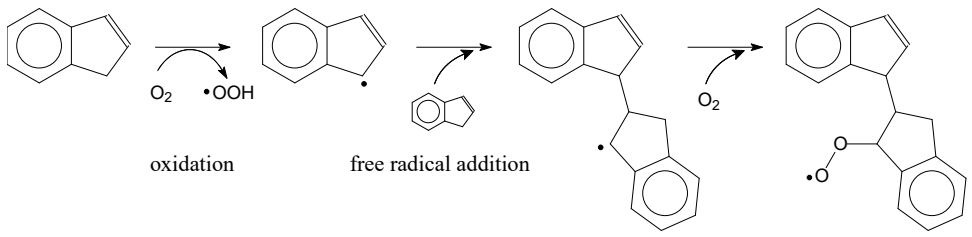

Figure 4.16. Oxidation and free radical addition reactions of indene.

The selectivity to addition products versus primary oxidation products is also illustrated by **Figure 4.16**. The second step involves addition to indene, which is in competition with addition to O_2, as shown in the last step. Once the carbon centred free radical forms, either of these reactions becomes possible and their relative rates determine the selectivity to oxidation or addition. At the conditions investigated, the selectivity to addition remained fairly constant over time, 26 to 29 % (**Table 4.4**).

It was reported that the percentage of O_2 consumed during bitumen oxidation that produces CO_x increases from 10 to 55 % with increasing temperature from 200 to 300 °C (Phillips and Hsieh, 1985). Oxidation of the model naphtenic-aromatic compounds at 130 °C produced almost no CO_2 (**Table 4.4**). CO was not measured. Indene contained an olefinic group and despite its higher conversion (**Figure 4.15**), less O_2 was consumed by dehydrogenation to produce water (**Table 4.4**) compared to tetralin and indan. As a result the O_2 consumption during indene oxidation was close to that of indan oxidation even though the conversion of indan was lower.

Overall the oxidation of the naphthenic-aromatic compounds over a 6 hour period at 130 °C was in the same range or higher than that observed for bitumen over 229 h (**Chapter 3**). This was somewhat surprizing, because it is known that oilsands bitumen is rich in such compounds (Strausz and Lown, 2003).

4.3.2.3 Confirmation of Oxygenate Functionality

The oxygenate functional groups in the oxidized naphthenic-aromatic hydrocarbons were confirmed by infrared and Raman spectroscopy. The observed infrared and Raman wavenumbers corresponding to different oxygenate functional groups are given in **Table 4.5**. The assignment of wavenumbers to specific functional groups was based on literature (Colthup et al., 1990; Silverstein et al., 2005).

Table 4.5. Oxygenate functional groups identified by infrared and Raman spectroscopy of oxidized naphthenic-aromatic compounds.

Description	Wavenumber (cm^{-1})	
	infrared	Raman
Oxidized tetralin		
C=O	1775-1705	1745-1679
O–H	3595-3236	not observed
C–O	1238-1188; 1140-1087	1232-1219; 1113-1089; 1016-1002
Oxidized indan		
C=O	1747-1662	1704-1660
O–H	3587-3160	not observed
C–O	1216-1191; 1108-1078; 1070-1000	1226-1170; 1165-1110; 1101-1063
Oxidized indene		
C=O	1710-1666	1690-1657
O–H	3565-3390; 3367-3151	not observed
C–O	1203-1166; 1164-1122; 1120-1016	1214-1172; 1126-1083

The infrared and Raman spectroscopy supported the identification of the oxidized compounds by mass spectrometry.

4.3.3 Oxidation of Naphthenic and Paraffinic Hydrocarbons

There is a considerable body of literature on paraffin oxidation (Emanuel et al., 1967). The observed conversion versus time profile (**Figure 4.17**) for *n*-decane autoxidation consisted of a prolonged induction time of more than 2 hours, followed by oxidation. This is typical for oxidation of paraffins. The C–H bonds on primary and secondary carbons are more difficult to

oxidize, because of the low stability of primary and secondary carbon centered free radicals that are formed.

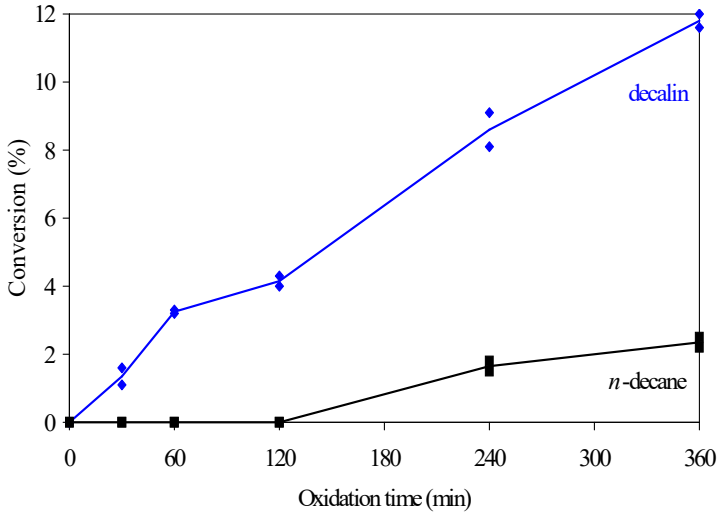

Figure 4.17. Conversion of decalin and decane by oxidation at 130 °C and air flow rate of 145-150 mL h^{-1} per g feed.

Although *n*-decane and decalin both contained eight methylene (–CH_2–) groups having C–H bonds on secondary carbons, decalin had a shorter induction time and higher conversion rate. This was because decalin also had two C–H bonds on tertiary carbons, which resulted in a more stable tertiary carbon-centred free radical after homolytic bond scission of the C–H bond (Emanuel et al., 1967; Waters, 1964).

Compared to tetralin and indan, decalin had an intermediate conversion rate (compare **Figures 4.15 and 4.17**). Tetralin and indane did not have hydrogen bonded to tertiary carbons, but the carbons in the α-position relative to the aromatic ring, can form carbon-centred free radicals that are resonance stabilized by the adjacent π-electron system, as was previously pointed out (Waters, 1964). These secondary carbon-centered free radicals are therefore more stable than the secondary carbon-centered free radicals in either *n*-decane or decalin.

The same procedure as outlined in **Section 4.3.2.1** was followed to identify the oxidation products. The oxidation rates and products from paraffin (*n*-alkane) oxidation were markedly different from that of naphthenic (cycloalkane) oxidation.

The chromatogram of the product from *n*-decane oxidation is presented in **Figure 4.18**. The absence of addition products is noteworthy.

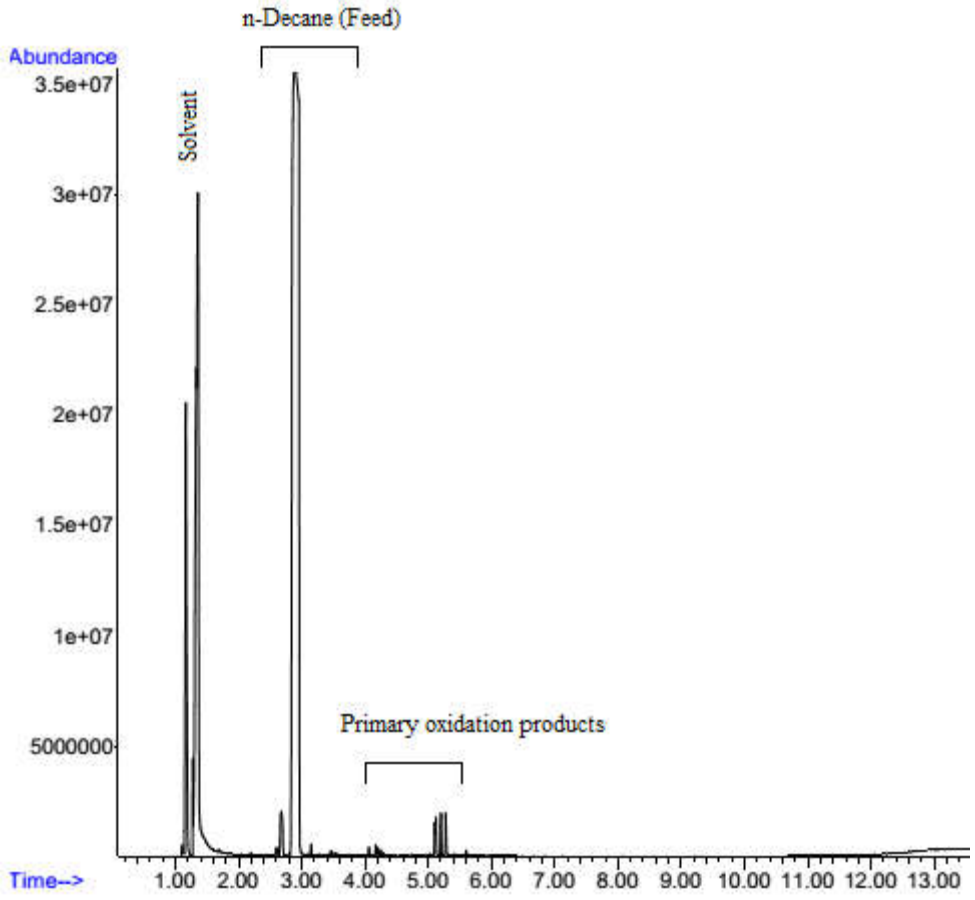

Figure 4.18. Chromatogram of the oxidation product from *n*-decane autoxidation at 130 °C for 6 h.

Initially only primary oxidation products, alcohols and ketones, were observed during the oxidation of *n*-decane (**Table 4.6**). This was partly due to the low conversion. However, after 6 h oxidation the CO_2 production was already significant, which was indicative of oxidative degradation and secondary oxidation. When the conversion time was extended to 24 h, the O_2 consumption increased by two orders of magnitude. A considerably increase in secondary oxidation was observed, as well as increase in oxidative degradation to form shorter carbon chain carboxylic acids, but no addition products.

Table 4.6. Product selectivity and O_2 consumption during the oxidation of *n*-decane and decalin at 130 °C and air flow rate of 145-150 mL h^{-1} per g feed.

Description	Selectivity [a]				
	30 min	60 min	120 min	240 min	360 min
n-Decane					
primary oxidation products (wt %) [b]	0	0	0	100	100 [d]
secondary oxidation products (wt %) [b]	0	0	0	0	0 [d]
addition products (wt %) [b]	0	0	0	0	0
CO_2 production (mg CO_2/kg feed) [c]	0	0	0	0	120
water production (mg H_2O/kg feed) [c]	- [e]	- [e]	- [e]	- [e]	- [f]
oxygen consumption (mg O_2/kg feed) [c]	60	260	1390	3770	6080
Decalin					
primary oxidation products (wt %) [b]	100	99	94	90	90
secondary oxidation products (wt %) [b]	0	1	6	10	9
addition products (wt %) [b]	0	0	0	0	1
CO_2 production (mg CO_2/kg feed) [c]	0	0	0	6	70
water production (mg H_2O/kg feed) [c]	- [e]	- [e]	- [e]	- [e]	1600
oxygen consumption (mg O_2/kg feed) [c]	80	470	1980	5270	8420

[a] Average of two runs
[b] Weight percentage of all oxidized products in the liquid
[c] Cumulative amount produced or consumed
[d] Degradation to lighter products observed, indicative of secondary oxidation
[e] Measured only at the end of the run
[f] Oxidation continued to 24 h, cumulative values: 8170 mg H_2O/kg, 3560 mg CO_2/kg and O_2 consumption of 121 000 mg O/kg.

Decalin produced primary oxidation products, secondary oxidation products, and addition products (**Table 4.6**), as was found in the naphthenic-aromatic class (**Table 4.4**). Yet, the propensity of decalin to form addition products was markedly lower than that of either tetralin or indan. Three potential contributing factors to explain the difference in addition product selectivity were identified:

(a) Longevity of the resonance stabilized free radical on the benzylic carbon of tetralin and indan compared to the tertiary carbon-centred free radical of decalin.

(b) The relative lower concentration of aliphatic (transferable) hydrogen in tetralin and indan compared to that of decalin, which reduced the chance of hydrogen transfer to terminate the free radical.

(c) The olefinic group that is formed when hydrogen disproportionation of tetralin and indan radicals takes place, is in a conjugated position with respect to the aromatic, whereas the olefinic group that is formed by disproportionation of decalin radicals is not. It is this driving force that makes tetralin the prototypical hydrogen-donor solvent. Hence, there is a larger driving force for tetralin and indan radicals to produce olefins, which in turn can lead to free radical addition reactions.

A typical chromatogram of the products after decalin was oxidized at 130 °C for 6 hour is shown in **Figure 4.19**. As shown in **Figure 4.19,** peaks before a retention time of 4.0 min were belonged to the *trans*-decalin (retention time 3.35 min), and *cis*-decalin (retention time 3.75 min). The peaks after retention time of 4.0 min in **Figure 4.19** belonged to the various oxidation products. The peak at a retention time of 5.33 min was identified as decahydro-naphthol using a reference compound to support the identification. Likewise, the peak at a retention time of 5.1 min was identified as decalone. The peak that appeared at 7.75 is hexachlolorobenzene, which was used as an internal standard. Like tetralin and indan oxidation, decalin oxidation resulted in some compounds with more than one oxygen-containing functional group. Moreover, higher molecular weight compounds were also formed due to free radical addition reactions. These higher molecular weight compounds had at least one dimer of decalin, as is illustrated by the mass spectrum in **Figure 4.20**. Of importance is that the addition products were formed by C–C addition.

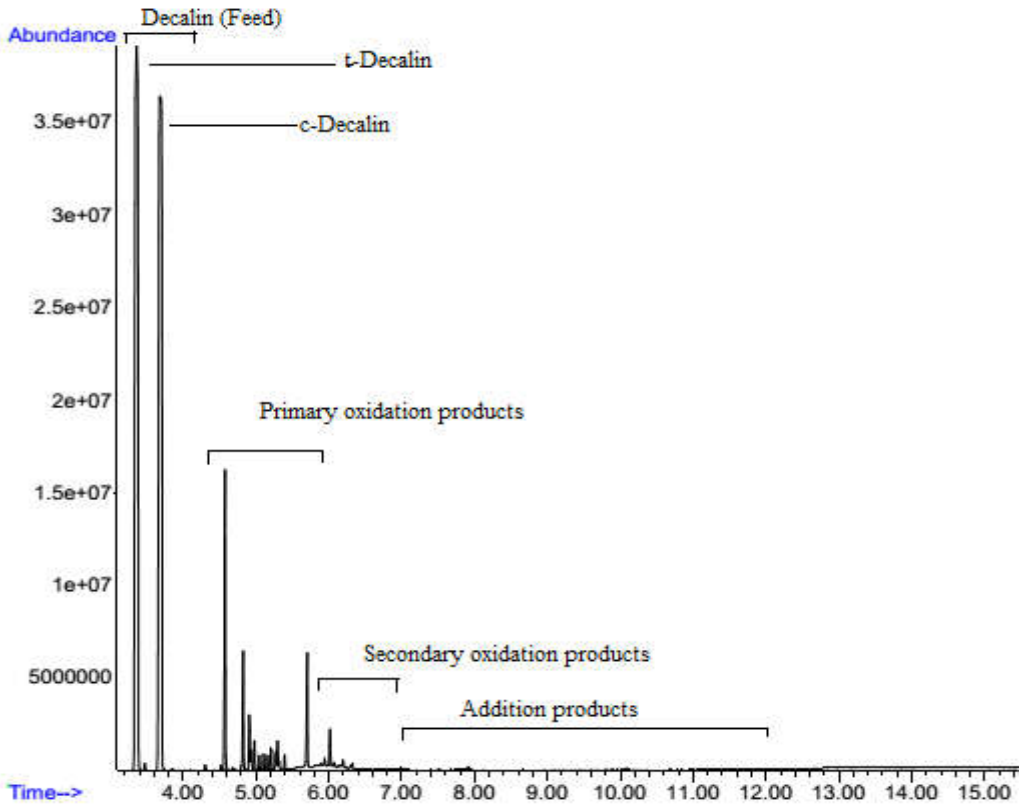

Figure 4.19. Chromatogram of the oxidation product from decalin autoxidation at 130 °C for 6 h.

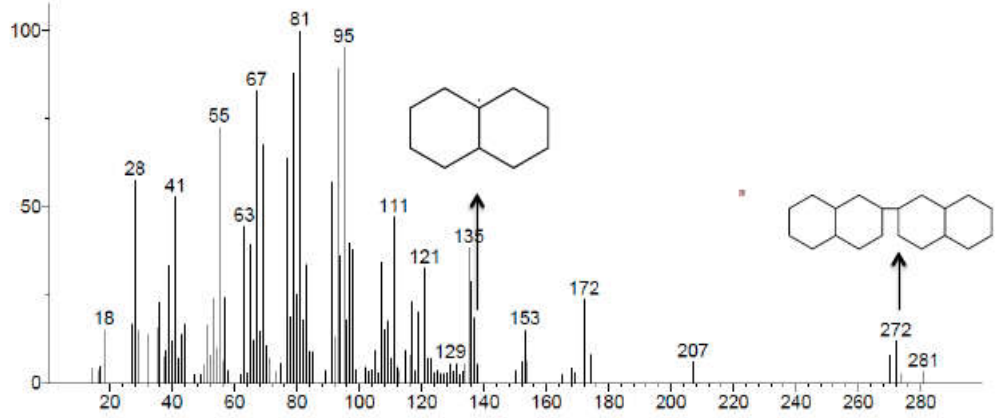

Figure 4.20. Electron ionization mass spectrum of an addition product formed during the oxidation of decalin (retention time 7.0 min in **Figure 4.19**). Despite the structure shown it is more likely that the addition took place between two tertiary carbons.

The oxygenate functional groups in the oxidized products were confirmed by infrared and Raman spectroscopy (**Table 4.7**).

Table 4.7. Oxygenate functional groups identified by infrared and Raman spectroscopy in the products from *n*-decane and decalin oxidation.

Description	Wavenumber (cm^{-1})	
	infrared	Raman
Oxidized *n*-decane		
C=O	1722-1668	1744-1688
O–H	3600-3170	Not observed
C–O	1288-1240; 1189-1155; 1097-1000	1299-1233; 1126-1086; 1073-1010
Oxidized decalin		
C=O	1760-1687	1752-1671
O–H	3581-3080	Not observed
C–O	1238-1195; 1174-1137; 1068-1008	1129-1061

4.3.4 Oxidation of Aromatic and Alkylaromatic Hydrocarbons

Naphthalene was subjected to autoxidation at 130 °C for 6 hours and no oxidation was observed, even when the oxidation time was extended to 24 hours (not shown), whereas *p*-cymene was rapidly and substantially converted (**Figure 4.21**).

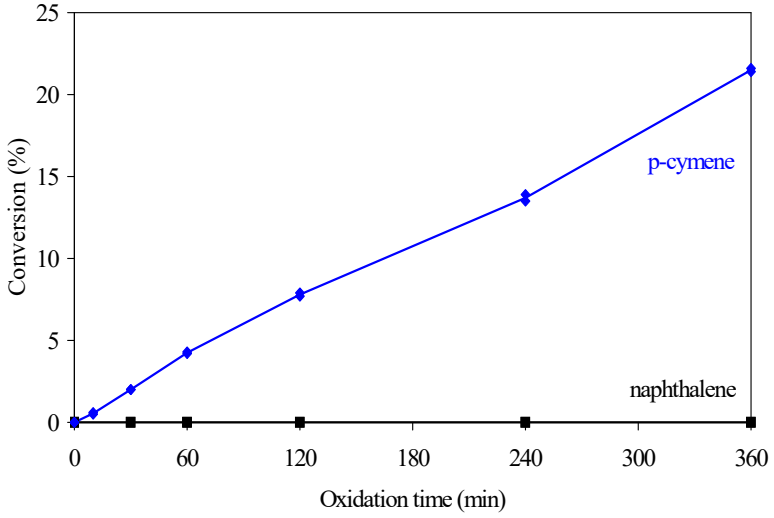

Figure 4.21. Conversion of naphthalene and *p*-cymene by oxidation at 130 °C and air flow rate of 145-150 mL h^{-1} per g feed.

As shown in **Figure 4.21**, conversion increased linearly with time and oxidation products formed early on during oxidation. The maximum *p*-cymene conversion was approximately 21.5 wt%, which was the highest conversion observed among all of the studied hydrocarbon classes. It contains two benzylic carbons and one of the benzylic carbons is also a tertiary carbon. The tertiary carbon that is also in an α-position relative to the aromatic ring, is particularly susceptible to oxidation (Emanuel et al., 1967; Waters, 1964). The hydroperoxide was readily formed and one of the oxidation products that were observed was the *p*-cymene hydroperoxide.

The chromatogram of oxidized *p*-cymene and EI spectrum of one of the addition products are shown in **Figure 4.22** and **Figure 4.23**, respectively.

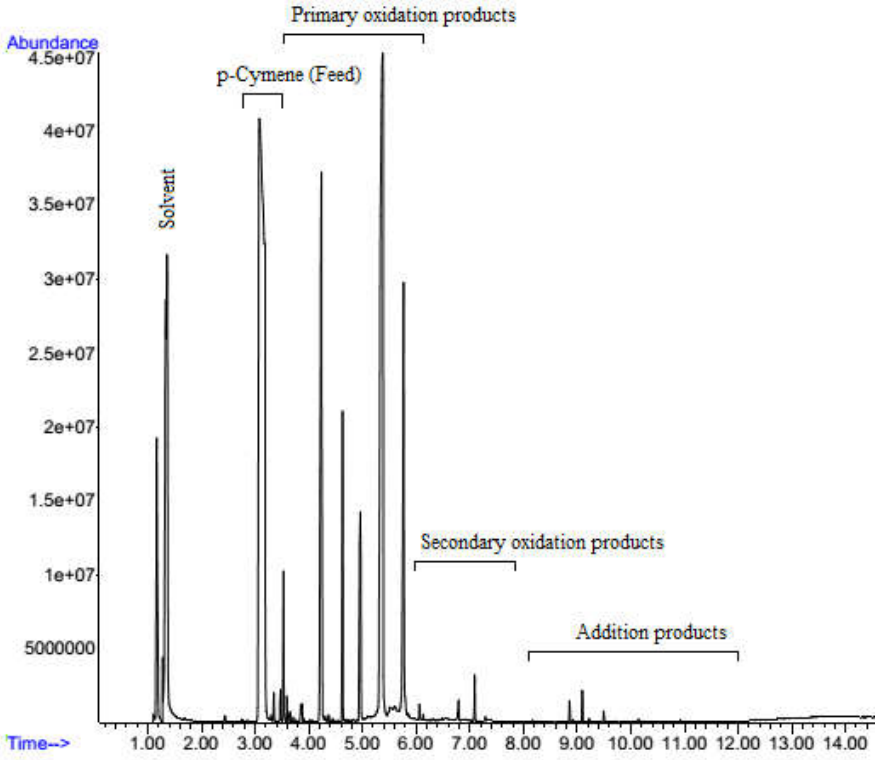

Figure 4.22. Chromatogram of the oxidation product from *p*-cymene autoxidation at 130 °C for 6 h.

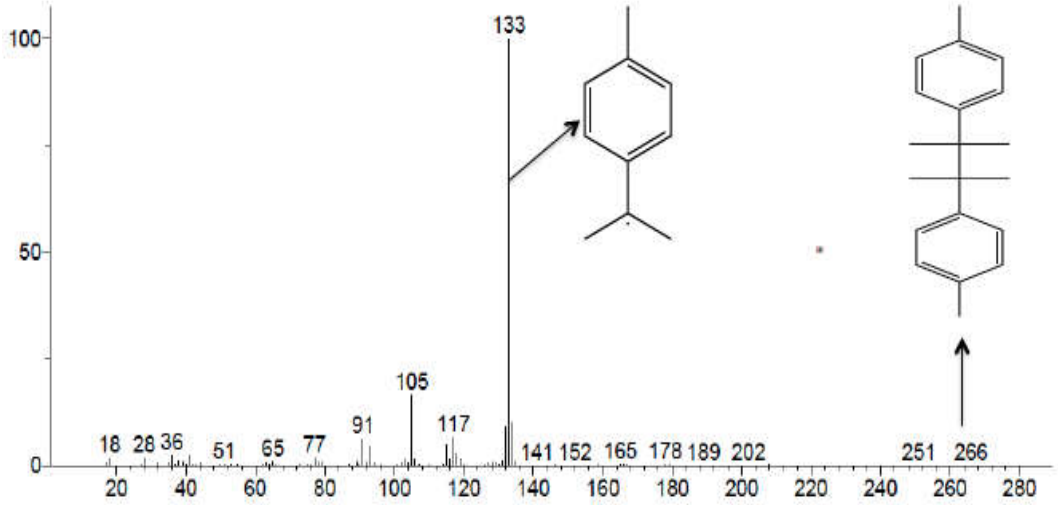

Figure 4.23. Electron ionization mass spectrum of an addition product formed during the oxidation of *p*-cymene (retention time 8.9 min in **Figure 4.22**).

Primary, secondary, and addition products were formed by the oxidation of *p*-cymene (**Table 4.8**). Despite its high conversion, the oxidation was selective to primary oxidation products, with secondary oxidation products and addition products appearing when the conversion was >10 %. Addition products formed by oxidative coupling contained at least one dimer (**Figure 4.23**). Hence, the addition products in alkylaromatic hydrocarbon class were formed by C–C linkage and was not coupled by C–O–C linkages. The C–C bond could be formed by the addition of two *p*-cymene free radicals, or by the addition reaction of a *p*-cymene free radical at a double bond that was formed by oxidative dehydrogenation. The latter is less likely to occur, because it requires scission of a C–H bond on a primary carbon (Waters, 1964). At high conversion an increasing amount of CO_2 was produced, likely due to the formation and decomposition of carboxylic acids.

Table 4.8. Product selectivity and O_2 consumption during the oxidation of *p*-cymene at 130 °C and air flow rate of 145-150 mL h^{-1} per g feed.

Description	Selectivity [a]				
	30 min	60 min	120 min	240 min	360 min
p-Cymene					
primary oxidation products (wt %) [b]	100	100	100	99.5	98.2
secondary oxidation products (wt %) [b]	0	0	0	0.5	1.3
addition products (wt %) [b]	0	0	0	0	0.4
CO_2 production (mg CO_2/kg feed) [c]	0	0	3	30	100
water production (mg H_2O/kg feed) [c]	- [d]	- [d]	- [d]	- [d]	1750
oxygen consumption (mg O_2/kg feed) [c]	780	2640	6780	15020	22780

[a] Average of two runs
[b] Weight percentage of all oxidized products in the liquid
[c] Cumulative amount produced or consumed
[d] Measured only at the end of the run

The oxygenate functional groups in the oxidized *p*-cymene were confirm by infrared and Raman spectroscopy (**Table 4.9**). It is difficult to confirm the presence of hydroperoxides by infrared spectroscopy, but it was reported that various peroxides have intense Raman bands around 885 to 877 cm^{-1} (Johnson and Siddiqi, 1970). A prominent Raman band developed at 867 cm^{-1} in the oxidized *p*-cymene, which is possibly due to O–O stretching in the *p*-cymene hydroperoxide.

Table 4.9. Oxygenate functional groups identified by infrared and Raman spectroscopy in the products from *p*-cymene oxidation.

Description	Wavenumber (cm^{-1})	
	infrared	Raman
Oxidized *p*-cymene		
C=O	1720-1670	1761-1673
O–H	3625-3180	Not observed
C–O	1189-1122; 1103-1070; 1041-1026	1207-1177, 1104-1010

4.3.5 Addition Selectivity during Hydrocarbon Oxidation

The autoxidation of different hydrocarbon classes at 130 °C resulted in marked differences with respect to selectivity to addition products (**Figure 4.24**). In general the naphthenic-aromatic

compounds were particularly susceptible to the formation of addition products during oxidation. The observed propensity for addition reactions is not due to the naphthenic ring per se, because decalin, which has two naphthenic rings, exhibited a low selectivity to addition. The proximity of the aromatic played a crucial role. The aromatic ring in the naphthenic-aromatic compounds increased the stability of carbon-centred free radicals on the benzylic carbons. However, the selectivity for addition is not just due to the benzylic carbons either. In *p*-cymene the presence of the benzylic carbons resulted in a high oxidation rate, but low addition selectivity.

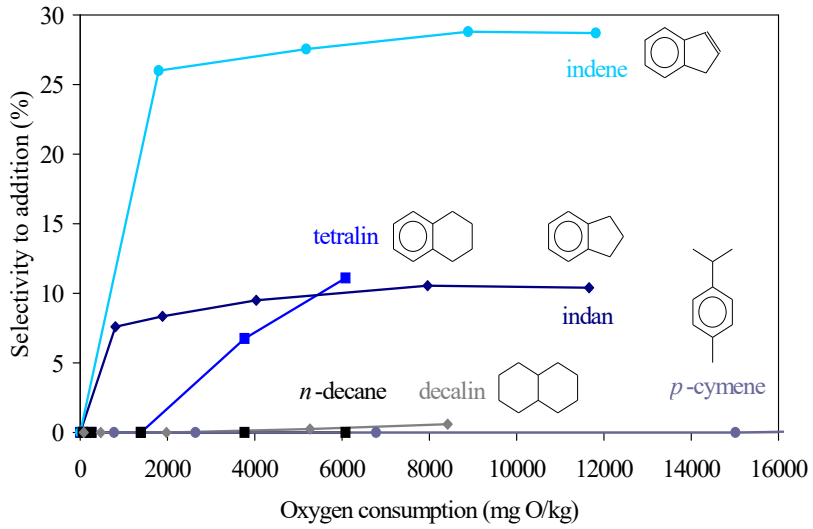

Figure 4.24. Selectivity to addition products during the autoxidation of model compounds at 130 °C.

The main difference between naphthenic-aromatic compounds and the other hydrocarbon classes is the driving force for hydrogen disproportionation. The hydrogen disproportionation reaction is illustrated by the reaction of two indan radicals (**Figure 4.25**). During the disproportionation one olefinic group is created. An analogous reaction can be envisioned whereby a peroxyradical (R–O–O•) abstracts hydrogen from a naphthenic-aromatic radical to create an olefinic group. In naphthenic-aromatic compounds this olefinic group is in a conjugated position with respect to the aromatic. The hydrogen-donor properties of such compounds are well known (Whitehurst et al., 1980). In the case of *p*-cymene the formation of an olefin by disproportionation requires abstraction of hydrogen from a primary carbon, which is more difficult.

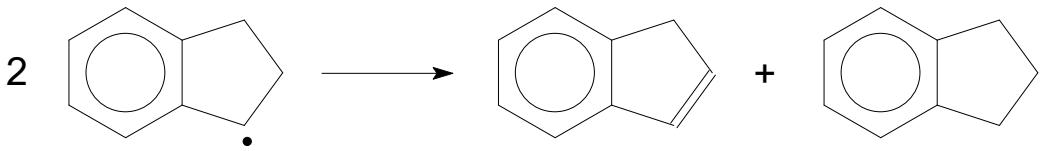

Figure 4.25. Hydrogen disproportionation of naphthenic-aromatic compounds.

The olefinic group, once formed, can readily participate in free radical addition reactions, as illustrated in **Figure 4.16**. The addition reaction proceeds through the formation of a C–C bond. Strong evidence for C–C type of bonding in the addition products was obtained from the identification of the addition products. Although the formation of C–O–C linkages could not be ruled out completely, the addition products predominantly have C–C linkages.

One of the important implications of these results is that it resolves the uncertainty around carbonyl content as possible cause for viscosity increase in bitumen, rather than just being correlated to the viscosity increase. The model compound study shows that it is not the carbonyl group that is causing increased addition selectivity, but rather the propensity for hydrogen disproportionation in the free radical species, which results in the formation of an olefinic group. It means that bitumen hardening is at least in part caused by addition reactions as a result of olefin formation during autoxidation. Unless the increase in carbonyl content is responsible for physical changes, this study indicated that the increased carbonyl content is not responsible for the increase in bitumen viscosity.

4.3.6 Implications for Oilsands Bitumen Processes

Naphthenic-aromatic compounds are abundant in oilsands derived bitumen. The increase in bitumen viscosity as a result of low temperature oxidation **(Tables 3.3 and 3.5)** is therefore understandable, because addition products are readily formed, even at low oxidation extent (**Figure 4.24**). This implies that oxidative hardening of bitumen is inevitable and cannot be avoided. It may also explain natural bitumen weathering and its impact on oilsands bitumen recovery and upgrading.

On a more positive note, if the mechanism to explain addition reactions is correct, then it should be possible to manipulate addition selectivity during oxidation. The key is to limit the

disproportionation reactions that produce olefins. Although direct free radical addition cannot be eliminated, the rate of free radical addition reactions can be reduced. The rate of direct free radical addition, as well as the rate of olefin formation by free radical disproportionation, are both dependent on the concentration of carbon-centred free radicals. Reaction engineering approaches that can limit the concentration of carbon-centred free radicals, as opposed to oxygen centred free radicals, will also decrease the selectivity to addition products.

The observations in the present work also have implications for other oilsands derived bitumen processes. Any conversion process that involves the formation of olefins and free radicals are likely to result in bitumen hardening. It would explain the considerable hardening of bitumen due to halogenation (Prado and De Klerk, 2014; Moschopedis and Speight, 1971b). It could also help to explain the non-monotonous viscosity versus conversion time behavior reported for low temperature visbreaking of oilsands bitumen (Wang et al., 2014).

4.4 Conclusions

Two sets of results were presented in this work. First, oxidation of tetralin, a naphthenic-aromatic compound, was autoxidized at different experimental conditions: temperatures 120 to 165 °C and oxidation time 24 h and 48 h, which resulted in physical and chemical changes comparable to bitumen autoxidation. Secondly, different hydrocarbons were autoxidized at 130 °C for 6 h, which provided oxidation selectivity data for naphthenic-aromatic, paraffinic, naphthenic, aromatic and alkylaromatic compound classes. These results could be used to identify the most likely addition reaction mechanism of hydrocarbons in bitumen.

The main observations and conclusions from this study are the following:

(a) Tetralin oxidation at 130 to 160 C for 24 and 48 h result various chemical changes. GC-MS and HPLC analyses confirmed the possible formation of heavier compound due to the oxidation of tetralin. These higher molecular compounds are dimerized/ oligomerized products, and/or their derivatives having oxygenate functional groups. The main oxygen-containing functional groups identified were: alcohols, and ketones. The CO_2 production and increase in acid number indicate that C-C bond cleavage and the formation of acid (-COOH), and/or other oxidation products.

(b) Chemical changes occurred during autoxidation of tetralin, which caused some physical changes in tetralin such as change in colour and increase in density. The oxidation of naphthenic-aromatic compounds in bitumen would also result similar chemical changes that might lead to the various physical changes of bitumen such as bitumen hardening, increase in viscosity and density increase. The specific cause of hardening was not established, but the investigation pointed to cross-linking and multiple functionalization as likely causes.

(c) The hydrocarbon class present in bitumen that is primarily responsible for addition reactions during oxidation, is the naphthenic-aromatic class. No addition products were observed during paraffin oxidation and no oxidation products were formed during the oxidation of aromatics without alkyl groups. Oxidation of naphthenic and alkylaromatic compounds resulted in low addition product selectivity.

(d) It was proposed that the dominant pathway for addition reactions of hydrocarbons is the hydrogen disproportionation of free radicals to produce olefins. Free radical addition to olefins through the formation of C–C bonds explained all of the oxidation selectivity observations from the model compound studies, as well as the addition products identified by GC-MS analysis.

(e) The proposed pathway for addition reactions could also explain other observations in literature, such as bitumen hardening due to halogenation and the non-monotonous viscosity versus conversion time behavior reported for low temperature visbreaking of bitumen.

4.5 Literature Cited

Babu, D. R.; Cormack, D. E. Effect of oxidation on the viscosity of Athabasca bitumen. *Can. J. Chem. Eng.* **1984**, *62*, 562–564.

Clausen, D. J.; Floreancig, P. E. Aromatic cations from oxidative carbon hydrogen bond cleavage in bimolecular carbon carbon bond forming reactions. *J. Org. Chem.* **2012**, *77*, 6574 6582.

Colthup, N. B.; Daly, L. H.; Wiberley, S. E. *Introduction to infrared and Raman spectroscopy*, 3ed; Academic Press: San Diego, CA, 1990.

Dietz, W. A. Response factors for gas chromatographic analyses. *J. Chromatogr. Sci.* **1967**, *5* (2), 68–71.

Emanuel, N. M.; Denisov, E. T.; Maizus, Z. K. *Liquid-phase oxidation of hydrocarbons*; Plenum Press: New York, 1967.

Herrington, P. R. Oxidation of bitumen in the presence of a constant concentration of oxygen. *Petrol. Sci. Technol.* **1998**, *16*, 1061–1084.

Huang, Y.; Ou, Q.; Yu, W. Characteristics of flame ionization detection for the quantitative analysis of complex organic mixtures. *Anal. Chem.* **1990**, *62* (18), 2063–2064.

Javadli, R.; De Klerk, A. Desulfurization of heavy oil - Oxidative desulfurization (ODS) as potential upgrading pathway for oil sands derived bitumen. *Energy Fuels* **2012b**, *26*, 594–602.

Jia, N.; Moore, R. G.; Mehta, S. A.; Van Fraassen, K.; Ursenbach, M. G.; Zalewski, E. Compositional changes for Athabasca bitumen in the presence of oxygen under low temperature conditions. *J. Can. Petrol. Technol.* **2005**, *44*(9), 51–56.

Johnson, R. M.; Siddiqi, I. W. *The determination of organic peroxides*; Pergamon Press: Oxford, 1970.

Katritzky, A. R.; Ignatchenko, E. S.; Barcock, R. A.; Lobanov, V. S.; Karelson, M. Prediction of gas chromatographic retention times and response factors using a general qualitative structure-property relationships treatment**.** *Anal. Chem.* **1994**, *66* (11), 1799–1807.

Lesueur, D. The colloidal structure of bitumen: Consequences on the rheology and on the mechanisms of bitumen modification. *Adv. Colloid Interface Sci.* **2009**, *145*, 42–82.

McLafferty, F. W.; Tureček, F. *Interpretation of mass spectra*, 4ed; University Science Books: Mill Valley, CA, 1993.

Moschopedis, S. E.; Speight, J. G. The halogenation of Athabasca asphaltenes with elemental halogen. *Fuel* **1971b**, *50*, 58–64.

Pan, T.; Lu, Y.; Lloyd, S. Quantum-chemistry study of asphalt oxidative aging: An XPS-aided analysis. *Ind. Eng. Chem. Res.* 2012, *51*, 7957 7966

Petersen, J. C. Asphalt oxidation - an overview including a new model for oxidation proposing that physicochemical factors dominate the oxidation kinetics. *Fuel Sci. Technol. Int.* **1993**, *11*, 57–87.

Phillips, C. R.; Hsieh, I.-C. Oxidation reaction kinetics of Athabasca bitumen. *Fuel* **1985**, *64*, 985–989.

Poniatowski, A. J.; Floreancig, P. E. Radical cation fragmentation reactions in organic synthesis. In *Carbon-Centered Free Radicals and Radical Cations: Structure, Reactivity, and Dynamics, 1st ed*; Forbes, M. D. E. Ed.; Wiley: New Jersey, 2010, p 43-60.

Prado, G. H. C.; De Klerk, A. Halogenation of oilsands bitumen, maltenes and asphaltenes. *Energy Fuels* **2014**, *28*, 4458–4468.

Sevov, C. S.; Wiest, O. Selectivity in radical cation cycloadditions. In *Carbon-Centered Free Radicals and Radical Cations: Structure, Reactivity, and Dynamics, 1st ed*; Forbes, M. D. E. Ed.; Wiley: New Jersey, 2010, p 61-82.

Siddiquee, M. N.; De Klerk, A. Oxidation of naphthenic-aromatic compounds in bitumen. *Prepr.Pap.-Am. Chem. Soc., Div. Energy Fuels* **2014a**, *59*(2), 572–574

Siddiquee, M. N. and De Klerk, A. Hydrocarbon addition reactions during low-temperature autoxidation of oilsands bitumen, *Energy Fuels* **2014b**, *28* (11), 6848–6859.

Silverstein, R. M.; Webster, F. X.; Kiemle, D.J. *Spectrometric Identification of Organic Compounds,* 7th ed.; John Wiley: New York, 2005.

Speight, J. G. *The Chemistry and Technology of Petroleum,* 4th ed.; CRC Press: Boca Raton, FL, 2006; pp 1-34.

Strausz, O. P.; Lown, E. M. *The chemistry of Alberta oil sands, bitumens and heavy oils*; Alberta Energy Research Institute: Calgary, AB, 2003.

Wang, L.; Zachariah, A.; Yang, S.; Prasad, V; De Klerk, A. Visbreaking oilsands derived bitumen in the temperature range 340-400 °C. *Energy Fuels* **2014**, *28*(8), 5014–5022.

Wang, Z. L.; Li, H. L.; Ge, L. S.; An, X. L.; Zhang, Z. G.; Luo, X.; Fossey, J. S.; Deng, W. P. DDQ-mediated oxidative coupling: an approach to 2,3-dicyanofuran (thiophene). *J. Org. Chem.* **2014**, *79*, 1156 1165.

Waters, W. A. *Mechanisms of oxidation of organic compounds*; Methuen: London, 1964.

Whitehurst, D. D.; Mitchell, T. O.; Farcasiu, M. *Coal liquefaction. The chemistry and technology of thermal processes*; Academic Press: New York, 1980.

CHAPTER 5 – HETEROCYCLIC ADDITION REACTIONS DURING LOW-TEMPERATURE AUTOXIDATION[5]

Abstract

Low temperature air oxidation affects many aspects of the fuels business: weathering, storage stability, hardening and fouling. Addition reactions taking place during the autoxidation of different heterocyclic compound classes were studied at 130 °C. This investigation reports on the conversion, product selectivity, nature of addition products and plausible mechanisms that would explain the observations subsequent to the oxidation of indole, 2,3-dihydroindole, quinoline, benzofuran, 2,3-dihydrobenzofuran and thianaphthene. Of these, indole is known to be prone to oxidative addition. Among the five-membered heterocyclic compounds, the propensity to form oxidative addition products increased in the order: S << O < N. Addition took place mainly through C–C bond formation. In comparison to hydrocarbons, it was surprising to find that indole and 2,3-dihydroindole were less prone to oxidative addition than the five-membered naphtheno-aromatic hydrocarbon analogues, indene and indan. Based on the work some implications for low temperature oxidation processes, and free radical processes in general, were discussed.

Keywords: indole, 2,3-dihydroindole, benzofuran, 2,3-dihydrobenzofuran, oxidative addition

[5]Reprinted with permission from Siddiquee, M. N. and De Klerk, A. Heterocyclic addition reactions during low temperature autoxidation. *Energy Fuels* **2015**, *29* (7), 4236–4244. Copyright 2015 American Chemical Society. http://pubs.acs.org/doi/abs/10.1021/acs.energyfuels.5b00767.

5.1 Introduction

Low temperature oxidation (autoxidation) affects many aspects of the fuels business. Storage stability of petroleum products is one of the most common topics related to autoxidation (Nixon, 1962). In transportation fuels storage stability is a regulated requirement. Weathering of raw materials exposed to air is another area where low temperature autoxidation affects storage and later on the use of the raw material. Autoxidation also affects coal. Coal weathering is undesirable, not only due to the risk of autoignition, but also due to the loss of calorific value of the coal (Van Krevelen, 1993; Green et al., 2012).

Our interest was in the impact that autoxidation had on processes related to oilsands industry. In the oilsands industry the weathering of exposed oilsands deposits is linked to reduce bitumen recovery (Ren et al., 2009). Hardening of bitumen during low temperature oxidation also poses a threat to the development of processes for oxidative desulfurization (Javadli and De Klerk, 2012b), and in situ combustion as method of oilsands bitumen recovery (Jia et al., 2005). The need to oxidize oilsands bitumen to enable recovery through microbial conversion (Fedorak et al., 2009), was also negatively affected by bitumen hardening rather than the anticipated oxidative degradation leading to solubilization.

Free radical addition reactions that take place during low temperature autoxidation could be responsible for reduced recovery of bitumen from weathered oilsands, as well as the hardening of bitumen. A systematic study of hydrocarbon addition reactions was performed and discussed in **Chapter 4** (Siddiquee and De Klerk, 2014b), which confirmed the formation of addition products and the particularly deleterious impact of molecules containing 5-membered aliphatic rings. However, oilsands bitumen does not consist of just hydrocarbons (**Chapter 2**), it also contains sulfur, nitrogen and oxygen. A typical oilsands bitumen has a sulfur content of 4.6 ± 0.5 wt% S, nitrogen content of 0.4 ± 0.1 wt% N and oxygen content of 1.1 ± 0.3 wt% O (Strausz and Lown, 2003). The composition of Cold Lake bitumen was reported in **Table 3.1**. The heteroatoms can be found in aliphatic and heterocyclic molecules. The study of addition reactions due to low temperature autoxidation (**Chapter 4**), was therefore extended to heterocyclic compounds.

Nitrogen containing compounds are most often implicated as the cause of sludge formation due oxidation of fuels (Hardy and Wechter, 1994; Frankenfeld et al., 1983). It was found that the oxidative stability of jet fuels was undermined by the presence of compounds containing a pyrrole ring, such as indoles and carbazoles (Blaster et al., 2006), and analogous observations were reported for synthetic and petroleum derived jet fuel blends (Sobkowiak et al., 2009). The carbon adjacent to the nitrogen in a pyrrole ring is readily oxidized and it ultimately leads to oxidative coupling and the formation of polymeric products (Jones and Bean, 1977). Although pyrroles are generally recognized to be the worst compound class for oxidative instability of fuels, it was pointed out that thiophenes and thiophenols also contributed to deposit formation in jet fuels and diesel fuels (Nixon, 1962). Analogous observations were made in work on oxidative desulfurization (Javadli and De Klerk, 2012b).

This study looked only at heterocyclic compound classes (**Figure 5.1**). The focus was on five-membered heterocyclic compounds that contained sulfur, nitrogen and oxygen. Although pyridinic nitrogen containing compounds were not implicated in oxidative instability, quinoline, a six-membered heterocyclic, was included in the study.

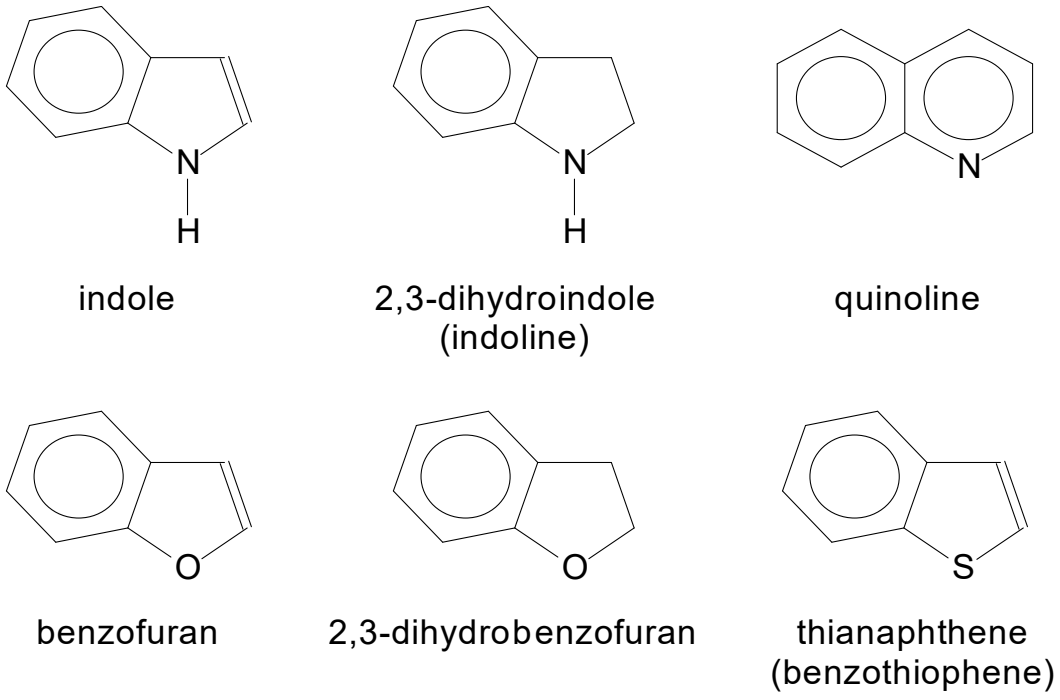

Figure 5.1. Heterocyclic compounds investigated.

5.2 Experimental

5.2.1 Materials

The heterocyclic model compounds that were employed in this study are listed in **Table 5.1**. The purity of the model compounds was confirmed by analysis using gas chromatography with flame ionization detector. Model compounds were selected to be within a narrow carbon number range (C_8–C_9) and boiling point range (173 to 254 °C) to facilitate analysis and comparison. Due to the prevalence of aliphatic ring structures in oilsands bitumen, the aliphatic analogues of the heterocyclic aromatics were included in the study, namely 2,3-dihydroindole and 2,3-dihydrobenzofuran. The exception is 2,3-dihydrothianaphthene, which is difficult to prepare, because it is readily ring-opened on partial hydrogenation (Hartough and Meisel, 1954).

Table 5.1. List of heteroatom containing model compounds used for oxidative coupling.

Name	CASRN [a]	Formula	Normal boiling point (°C)	Purity (wt %)		Supplier
				supplier [b]	analysis [c]	
indole	120-72-9	C_8H_7N	253-254	≥99	99.4	Sigma-Aldrich
2,3-dihydro-indole (indoline)	496-15-1	C_8H_9N	220-221	99	99.4	Sigma-Aldrich
quinoline	91-22-5	C_9H_7N	237	99	98.7	Acros Organics
benzofuran	271-89-6	C_8H_6O	173-175	99	98.6	Sigma-Aldrich
2,3-dihydro-benzofuran	496-16-2	C_8H_8O	188-189	99	99.0	Sigma-Aldrich
thianaphthene (benzothiophene)	95-15-8	C_8H_6S	221-222	98	98.1	Sigma-Aldrich

[a] CASRN = Chemical Abstracts Services Registry Number.

[b] This is the purity of the material guaranteed by the supplier.

[c] This is the purity based on peak area obtained by GC-FID analysis, i.e. without response factor.

Chloroform (98 %, HPLC grade, Fisher Scientific) was used as a general solvent for analyses. Hexachlorobenzene (99 %, analytical standard, Supleco) was used as internal standard for chromatographic analyses. In some of the experiments mixtures were prepared with *n*-decane (>99 %, Sigma-Aldrich). Extra-dry air was purchased in cylinders from Praxair and used as oxidizing agent.

5.2.2 Equipment and Procedure

Pure compounds, as well as mixtures containing 5 wt % *n*-decane were employed as feed materials for the oxidation. The *n*-decane facilitated autoxidation, because it is readily oxidized to produce hydroperoxides and it mimicked autoxidation of the model compounds in mixtures with hydrocarbons. By comparing the oxidation of the pure compounds with the *n*-decane containing mixture, it was possible to evaluate the inherent autoxidation stability of the pure compound relative to the compound in fuel mixtures. All oxidation experiments were performed with air, which results in fairly slow oxidation. Accelerated oxidation, such as with hydrogen peroxide or organic hydroperoxides as oxidants, were not considered.

The procedure was similar to that employed in the study of the oxidation of hydrocarbon compound classes (**Chapter 4**). In a typical experiment 50 g of the feed material was placed in a 250 mL three-necked round bottom flask, which was connected to a reflux condenser. The reflux condenser was cooled with a chilled water supply that was maintained at 10 °C. Air flow was controlled at 120 mL/min at near atmospheric pressure and ambient temperature, which is equivalent to around 145 mL/h air per g of the feed material. Autoxidation of the model compounds was performed at 130 °C for 6 h. The temperature in the flask was controlled using a thermocouple in the solution connected to a Heidolph MR Hei-Standard heat-on-block heater with magnetic stirring. A magnetic stirring bar was used for mixing at 500 revolutions per minute. Small samples, approximately 0.5 g, were withdrawn from the flask at different time intervals to monitor the progress of oxidation. The products were analyzed using chromatographic and spectroscopic techniques. Experiments were performed in triplicate.

The heaviest products from some oxidation products were concentrated by removing the unconverted feed and lighter products by heating under vacuum. The same evaporative procedure was applied to the unoxidized feed material to make sure that the heavy products were not already present in the feed, or formed during heating under vacuum.

5.2.3 Analyses

Oxidation products were identified by gas chromatography with mass spectrometry (GC-MS). The electron impact mass spectra of the oxidation products were compared against the National Institute of Standards and Technology (NIST) library of electron ionization mass spectra, as well as by manual analysis of the mass spectra. The objective was to identify individual compounds if possible, or at least identify the main structural features so that it could be categorized. The categories were:

(a) Primary oxidation products, typically alcohols or ketones of the feed material. Products were classified as primary oxidation products if the product was a single oxygen-containing derivative of the feed. Classification relied on identifying the molecular ion (M^+) in the mass spectrum of the oxidation products, as well as the retention time on the column. If the product eluted shortly after the feed, and had an M^+ that was 14 m/z (for ketones) or 16 m/z (for alcohols) higher than the M^+ of the feed, it was labeled as a primary oxidation product.

(b) Oxidatively dehydrogenated products. Only the dehydrogenation product of the feed was labeled as a dehydrogenation product and the dehydrogenation product had to have an M^+ of 2 m/z less than the M^+ of the feed. Identification of dehydrogenated products was confirmed by mass spectrometry.

(c) Secondary oxidation products were feed molecules that were oxidized more than once, but did not contain more carbon atoms than present in the feed molecules. All products that eluted between the primary oxidation products and addition products were classified as secondary oxidation products.

(d) Addition products were molecules produced by the oxidative addition of two or more feed molecules. These molecules contained more carbon atoms per molecule than the feed and had the longest retention time on the column.

The GC-MS analyses were performed using an Agilent 7820A GC coupled with an Agilent 5977E mass spectrometer. The products were separated on an HP-5 30 m × 0.25 mm × 0.25 μm column. The GC injector temperature was 250 °C, the split ratio was 10:1. Column flow of He

as carrier gas was 2 mL/min and was kept constant. The oven temperature was 75 °C for 0.5 min and then temperature was increased from 75 °C to 325 °C at the rate of 20 °C/min, and finally, temperature was kept constant at 325 °C for 5 min.

Quantification of the products was performed using a gas chromatograph with flame ionization detector (GC-FID). A similar column, DB-5 MS 30 m × 0.25 mm × 0.25 μm, and temperature program as for the GC-MS analysis was employed. The samples were prepared using chloroform as solvent and hexachlorobenzene was added as an internal standard. The FID response factors for the model compounds were experimentally determined (**Table 5.2**) and were higher than values reported in literature (Jorgensen, 1990; Katritzky et al., 1994; Huang et al., 1990). The method by which the FID response factors were determined is explained in Section 4.2.3 of Chapter 4. The response factors were used to calculate the oxidative conversion from GC-FID data.

Table 5.2. Flame ionization detector response factors.

Compound	FID response factor [a]		
	experimental	literature	reference
indole	0.93 ± 0.01	0.81	(Jorgensen, 1990)
2,3-dihydroindole	0.87 ± 0.05		
quinoline	0.94 ± 0.01	0.82	(Katritzky et al., 1994)
benzofuran	0.85 ± 0.01	0.76	(Jorgensen, 1990)
2,3-dihydrobenzofuran	0.84 ± 0.01		
thianaphthene	0.84 ± 0.01	0.75	(Jorgensen, 1990)
hexachlorobenzene	0.32 ± 0.01	0.31	(Huang et al., 1990)

[a] Average and one standard deviation indicated, as measured relative to *n*-heptane, which by definition has a response factor of 1.

The oxygen-containing functional groups that were identified based on GC-MS analysis were verified by identifying the main functional groups observed in the infrared spectra of the products. Infrared analyses were performed using an ABB MB 3000 Fourier transform infrared (FTIR) spectrometer. A small amount of sample was placed on a potassium bromide disc and the spectrum was collected over the wave number range 4000 to 500 cm^{-1} as the average of 120 scans per sample. The spectral resolution was 4 cm^{-1}, signal strength was 70 %, the acquisition mode was absorbance and detector gain was set at 243.

The amount of heavier product formation, which potentially did not elute during GC-FID analysis, was determined by removing the lower boiling fractions from the oxidized compounds using a Heidolph vacuum rotary evaporator. For every determination approximately 15 g of the oxidized sample were transferred to a 500 mL round bottomed flask, pre-weighed on a Mettler Toledo XP 1203S balance (1.2 kg range with 1 mg readability). The lower boiling fractions were removed by heating the mixture in a rotary evaporator. The mass of material that remained was determined by weighing the residue in the flask.

The proton nuclear magnetic resonance (^{1}H NMR) spectra of heterocyclic compounds and the heavier fraction of oxidized heterocyclic samples were measured by using an NMReady 60 spectrometer (Nanalysis Corp., Calgary, Canada). $CDCl_3$ (99.8 % deuterium, Sigma) was used for sample preparation. Samples were analyzed using standard 5 mm NMR tubes (Norell, Landisville, USA). Experimental conditions were: frequency = 60 MHz, spectral range = 14 ppm, number of scans = 32. The threshold shift for classifying hydrogen as aliphatic or aromatic was 6.3 ppm. Values below 6.3 ppm were classified as aliphatic and values above 6.3 ppm were classified as aromatic. In the cases of indole and 2,3-dihydroindole, the hydrogen bonded to nitrogen was integrated separately over the range 3.83 to 4.5 ppm.

5.2.4 Calculations

GC-FID response factor, oxidative conversion and product selectivity were calculated as described in **Chapter 4** (**Section 4.2.3**).

5.3 Results and Discussion

5.3.1 Oxidation of N-Heterocyclic Compounds

The first model compound class that was investigated was the nitrogen-containing heterocyclic compounds, which were represented by indoline, indole, and quinoline (**Figure 5.1**). Indole was selected to represent non-basic nitrogen containing heterocyclic compounds, which are known to readily form oxidative addition products (Jones and Bean, 1977). 2,3-Dihydroindole (indoline) is the partially hydrogenated structural analog of indole, but it is a strong base, because the nitrogen

is aliphatic and the lone pair electrons of nitrogen are no longer involved in an aromatic π-electron structure. Quinoline is also a basic nitrogen-containing heterocyclic compound and the nitrogen is contained in a six-membered pyridine ring. The lone pair electrons on nitrogen are not involved in the aromatic π-electron structure, which accounts for its basicity.

5.3.1.1 Product Identification

Oxidation of indole at 130 °C for 360 min produced two categories of products- primary oxidation product and addition products.

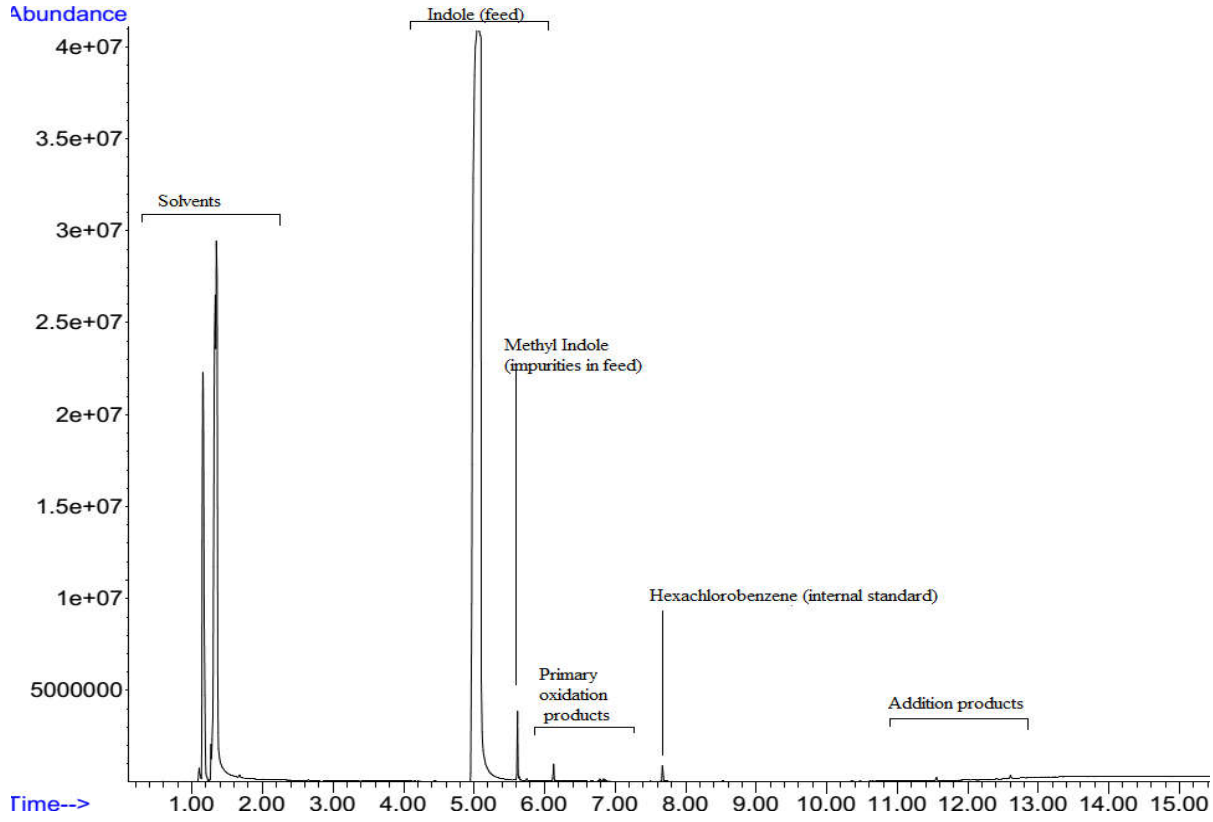

Figure 5.2. Chromatogram (GC-MS) of indole oxidation products after autoxidation at 130 °C for 360 min.

The primary oxidation product was identified as alcohol and ketone of indole. The electron impact mass spectra of primary oxidation product appeared at 6.12 min at **Figure 5.2** is shown in **Figure 5.3**. The m/z gap of 16 (132.9-116.9 =16) and loss of carbon monoxide (m/z gap of 28) from carbonyls was employed as diagnostics for the interpretation of the mass spectra of ketone as primary oxidation product (**Figure 5.3**).

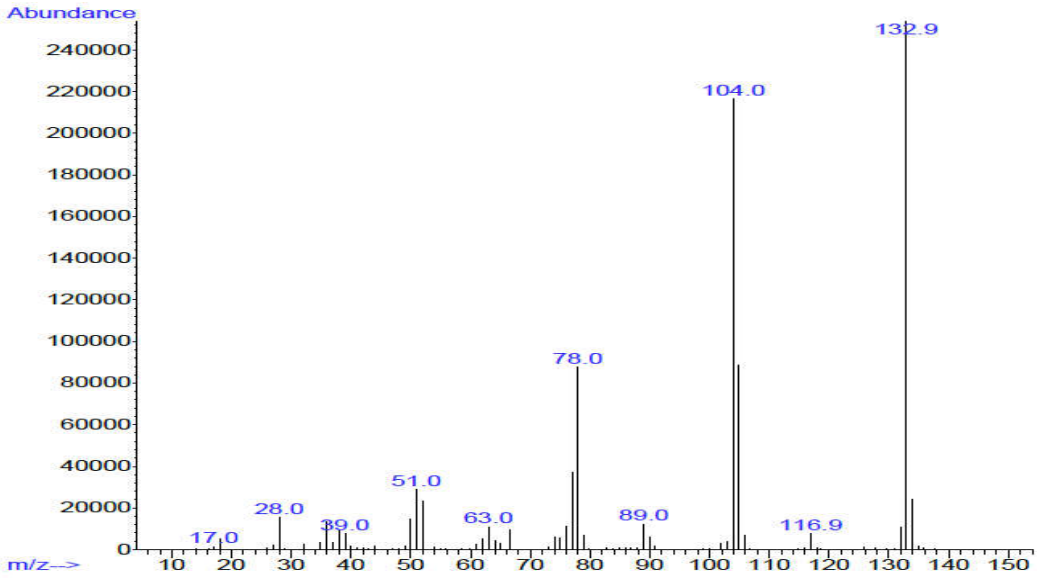

Figure 5.3. Electron ionization mass spectrum of a primary oxidation product (6.13 min retention time) formed during indole oxidation at 130 °C.

Higher molecular weight compounds that were of particular interest were formed due to addition reactions. Since an apolar column was employed for chromatographic separation, heavier compounds tended to elute at longer residence times. Electron ionization chromatograms of addition products appeared at retention time 11.6 min, 12.4 min and 12.6 min (**Figure 5.3**) are shown in **Figure 5.4**, **Figure 5.5**, and **Figure 5.6**, respectively.

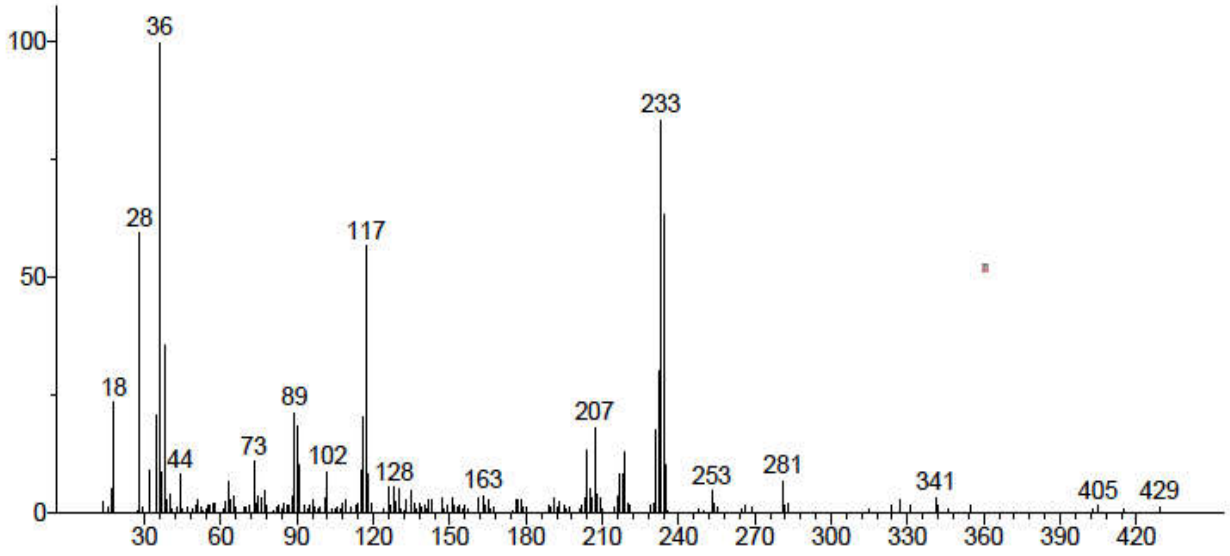

Figure 5.4. Electron ionization mass spectrum of an addition product (11.6 min retention time) formed during indole oxidation at 130 °C.

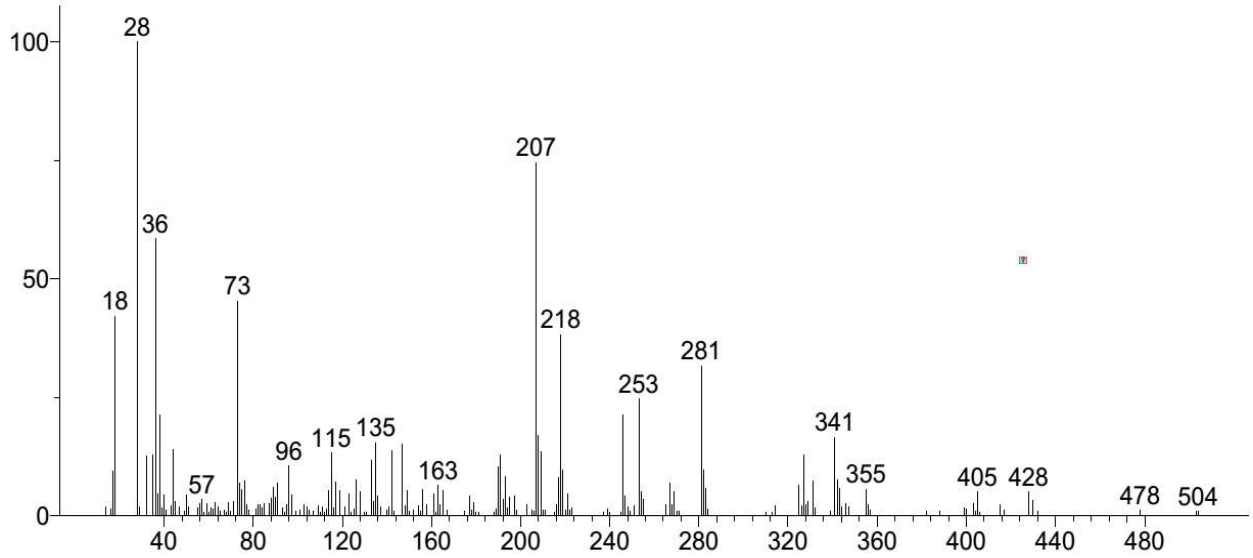

Figure 5.5. Electron ionization mass spectrum of an addition product (12.4 min retention time) formed during indole oxidation at 130 °C.

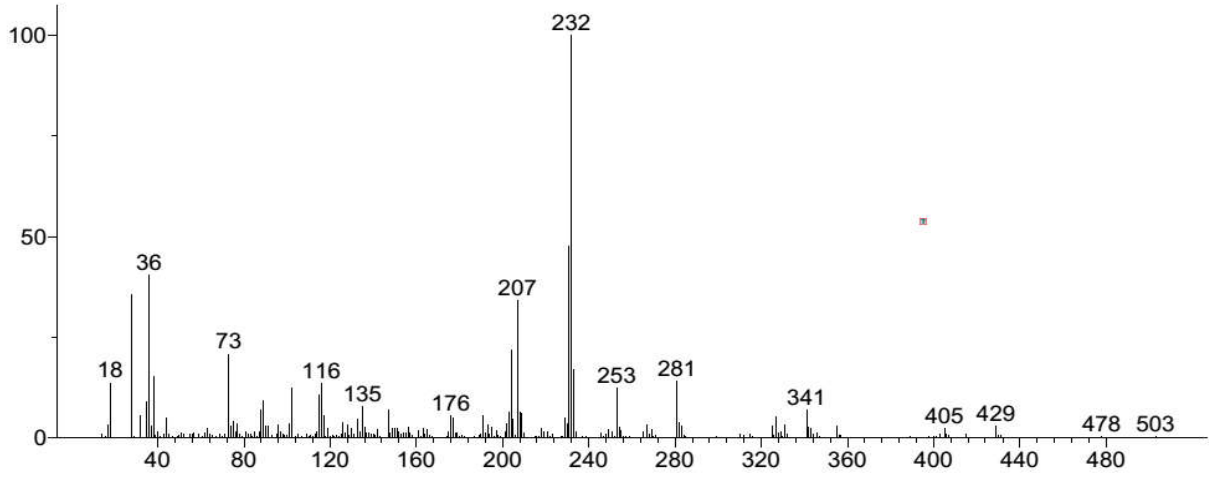

Figure 5.6. Electron ionization mass spectrum of an addition product (12.6 min retention time) formed during indole oxidation at 130 °C.

The addition product claimed at retention time 12.4 min in **Figure 5.2** was very small. However, it is visible in the chromatogram obtained by GC-FID (**Figure 5.7**) having similar column, however, the retention time was slightly different.

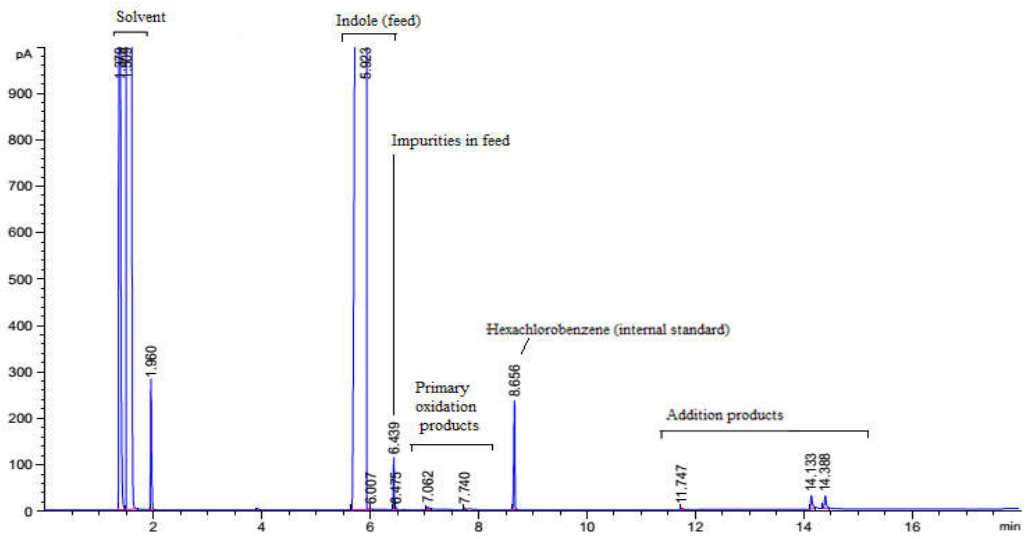

Figure 5.7. Chromatogram (GC-FID) of indole oxidation products after autoxidation at 130 °C for 360 min.

Indoline oxidation at 130 °C produced all four categories of products- oxidatively dehydrogenated products (indole), primary oxidation products, secondary oxidation products, and addition products (**Figure 5.8**).

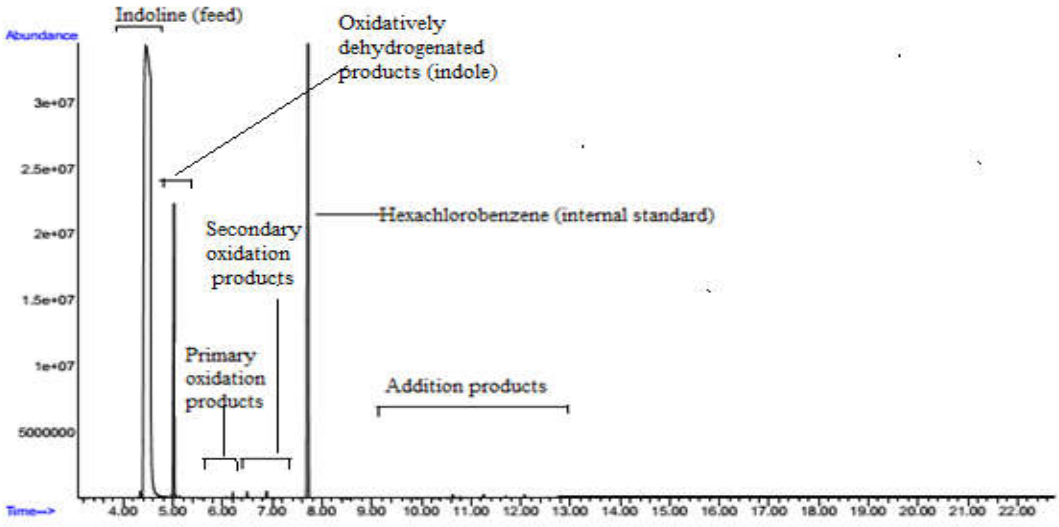

Figure 5.8. Chromatogram (GC-MS) of indoline oxidation products after autoxidation at 130 °C for 360 min.

During indoline oxidation, indole was identified as oxidatively dehydrogenated products. Indole model compound was analyzed to establish reference point in the chromatogram and to

corroborate identification using the electron ionization mass spectra in the National Institute of Standards and Technology (NIST) database. To illustrate the procedure, **Figures 5.2** and **5.8** were compared for the retention time (5.0 min) of indole. Moreover, the electron ionization mass spectrum of the model compound indole (**Figure 5.9**) was compared with the indoline oxidation product that appeared at 5.0 min and was identified as indole (oxidatively dehydrogenated product of indoline) (**Figure 5.10**). The amount of indole formation was much higher compared to other oxidation products.

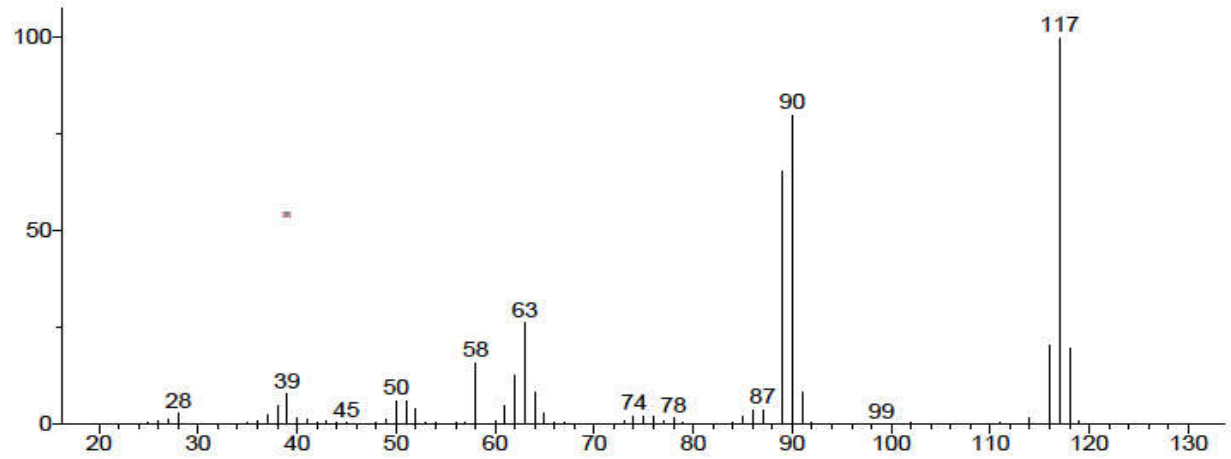

Figure 5.9. Electron ionization mass spectrum of indole (commercially obtained model compound).

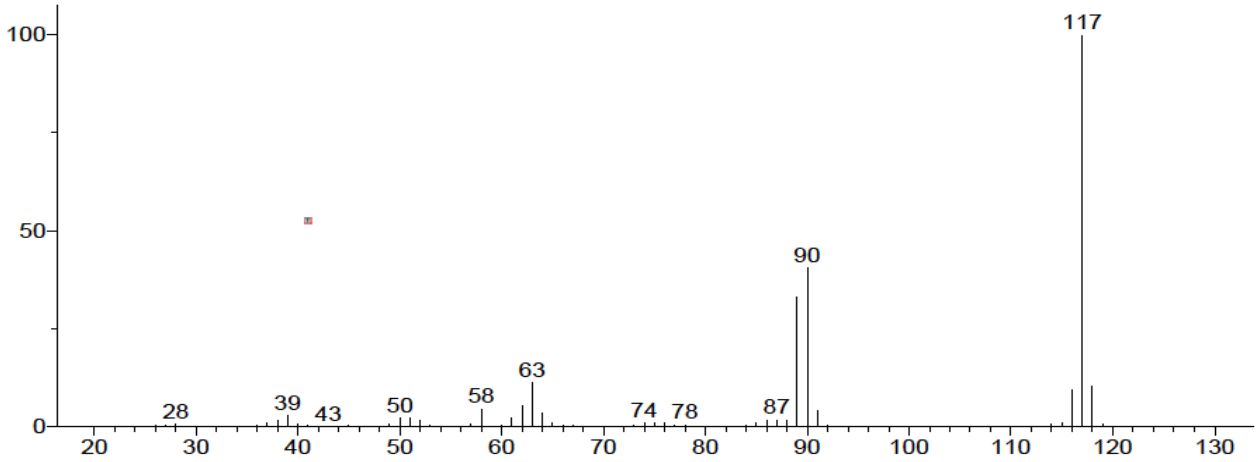

Figure 5.10. Electron ionization mass spectrum of oxidatively dehydrogenated product (5.05 min retention time) formed during oxidation of indoline at 130 °C.

Primary oxidation products from indoline oxidation were alcohols and ketones of indoline and their retention times were between 5.5 min and 6.3 min. In addition to the formation of indole, simple alcohols and ketones, there were also compounds that were secondary oxidation products and had more than one functional group. The loss of water (m/z gap of 18) from alcohols and the loss of carbon monoxide (m/z gap of 28) from carbonyls were employed as diagnostics for the interpretation of the mass spectra of secondary oxidation products (**Figure 5.11**).

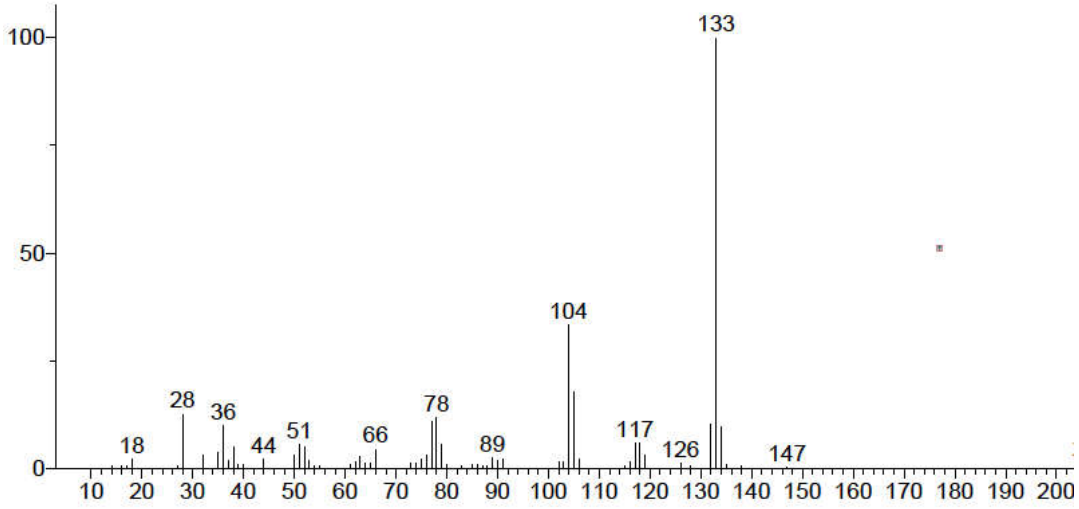

Figure 5.11. Electron ionization mass spectrum of a secondary oxidation product (6.5 min retention time) formed during oxidation of indoline at 130 °C.

Electron ionization mass spectrum of a addition products of indoline (**Figure 5.12**) indicated that the nature of addition was through a C–C bond. This can be explained by the presence of dominant m/z = 234 that was a dimer of m/z = 117. The molecular ion, M^+ at m/z = 281, was less prominent than the $(M+1)^+$ protonated molecular ion at m/z = 282. Carbon monoxide is readily lost to produce the $(M - 28)^+$ ion at m/z = 253 and water is also readily loss to produce $(M - 28\text{-}18)^+$ ion at m/z = 235. This fragment not only indicated that the compound contained alcohol and ketone functional groups, but also that the indoline dimer likely formed by C–C addition and not by an ether linkage. This is analogous to the addition product formation by the oxidation of naphthenic-aromatic compound class (Siddiquee and de Klerk, 2014). Unfortunately the mass spectrum on its own does not completely rule out addition through an ether linkage, because free radical recombination and a weak $(M - 18)^+$ peak are both known to occur in the electron ionization mass spectra of heavy ethers (McLafferty and Tureček, 1993). Oxidation of

indoline showed similar oxidation pattern of tetralin as described in our previous studies with the exception that indoline was easily aromatized to indole (oxidatively dehydrogenated product) (Siddiquee and de Klerk, 2014b).

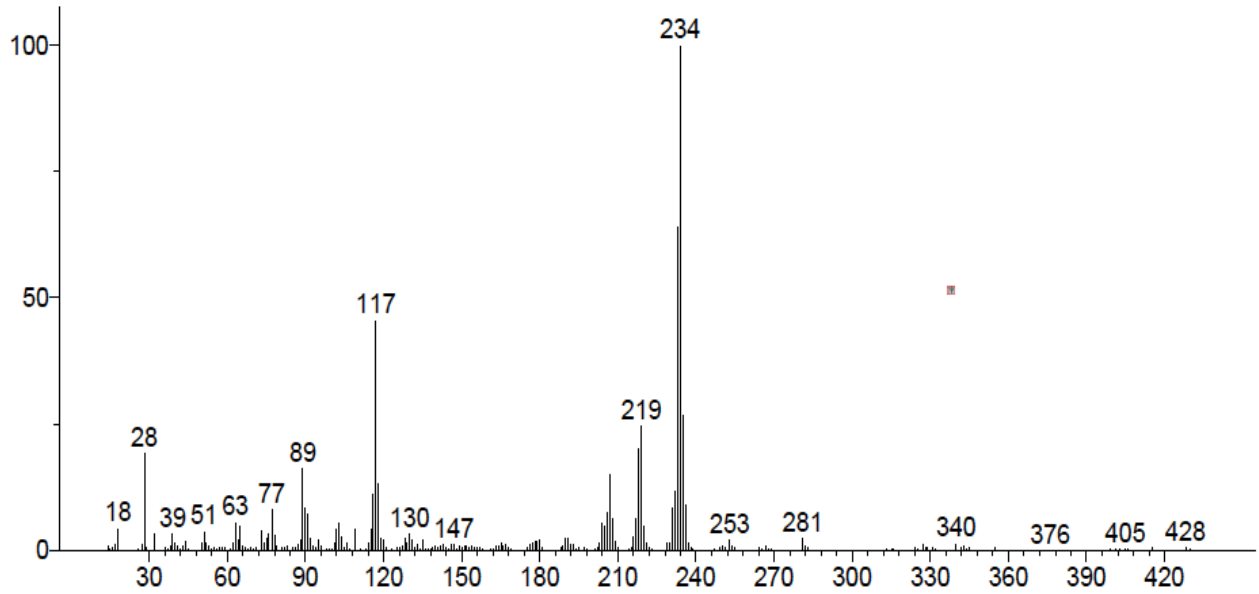

Figure 5.12. Electron ionization mass spectrum of an addition product (11.3 min retention time) formed during indoline oxidation at 130 °C.

Due to particular interest in heavier products, heavier boiling fractions of oxidized indoline was separated and was analyzed with GC-MS. Chromatogram of heavier fraction of oxidized indoline is shown in **Figure 5.13** that clearly shows the presence of heavier fractions (retention time between 9.6 min to 19 min). Some of these were not appeared in the chromatogram of oxidized indoline (**Figure 5.8)** may be due to the low concentration of heavier products.

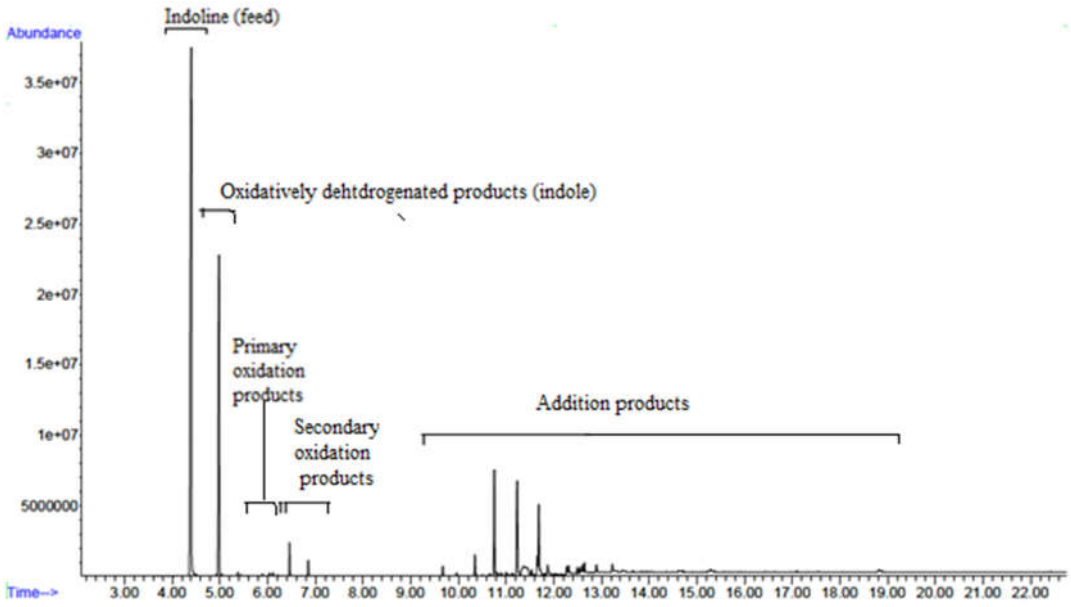

Figure 5.13. Chromatogram (GC-MS) of indoline oxidation products after autoxidation at 130 °C for 360 min.

Electron ionization spectrum (**Figure 5.14**) of heavier products appeared at 13.4 min of **Figure 5.13** showed the addition products formed by four indoline. Fragmentation patterns of **Figures 5.14** and **5.5** indicating indole produced from indoline also contributed to addition product formation and increased the selectivity.

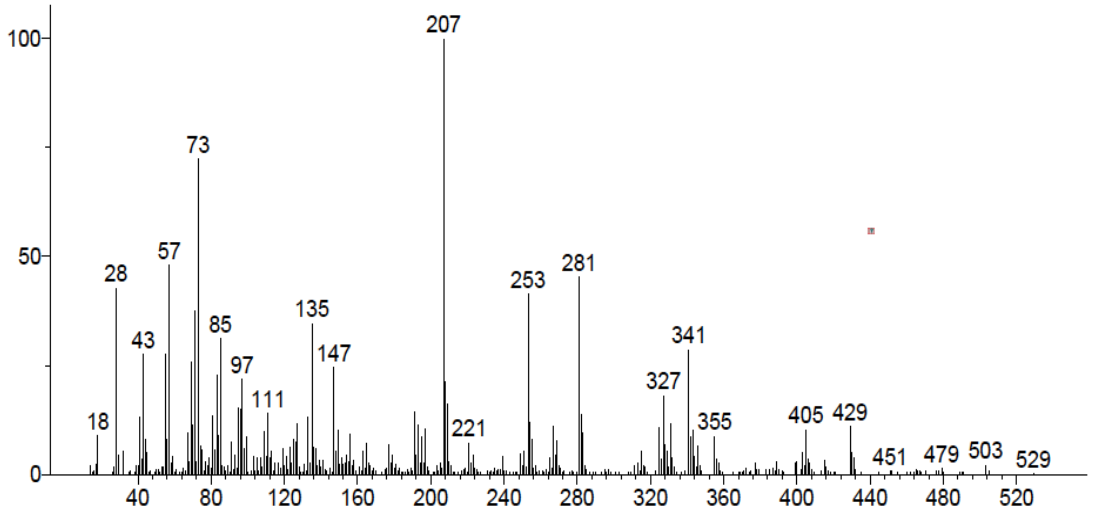

Figure 5.14. Electron ionization mass spectrum of an addition product (13.4 min retention time) formed during indoline oxidation at 130 °C.

Quinoline remained unaffected by autoxidation after 6 hours at 130 °C even in the presence of 5 wt % decane. To make the comparison, the chromatograms of quinoline and quinoline treated with air at 130 °C for 6 h are shown in **Figures 5.15** and **5.16**, respectively.

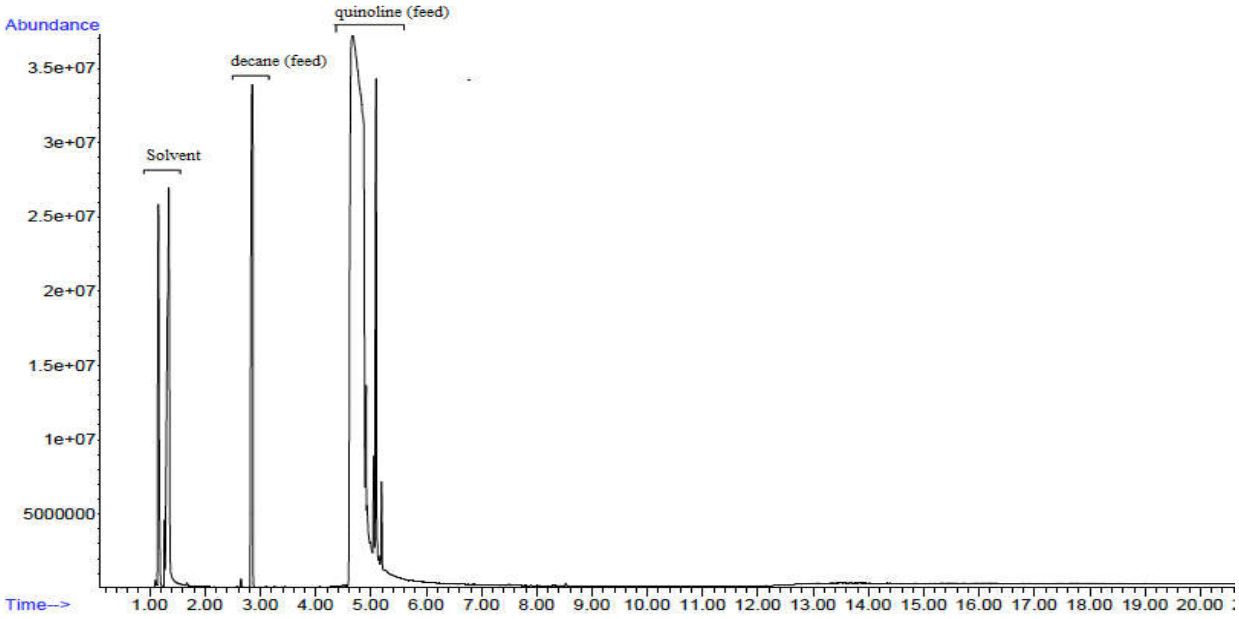

Figure 5.15. Chromatogram of quinoline without oxidation.

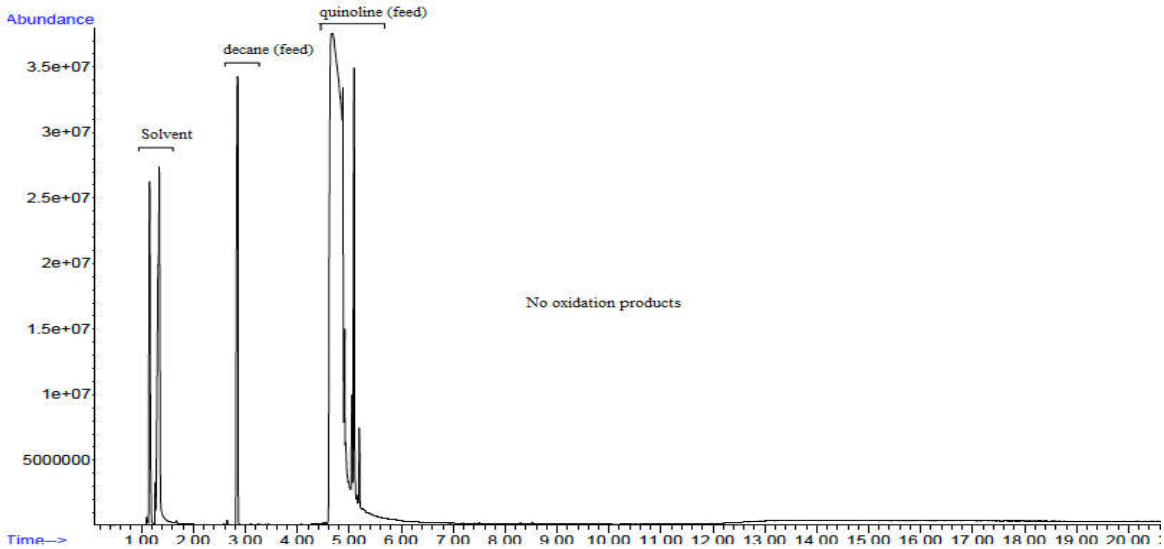

Figure 5.16. Chromatogram (GC-MS) of quinoline oxidation products after autoxidation at 130 °C for 360 min.

5.3.1.2 Conversion and Selectivity

As was anticipated, indole was autoxidized on its own and oxidation was only somewhat faster in the presence of *n*-decane (**Figure 5.17**). The induction time was between 1 and 2 hours, irrespective of whether *n*-decane was present or not. Initially just addition products were found (**Table 5.3**) and monomeric oxidation products were detected only later on during the oxidation. The initial selectivity to oxidative addition products from indole was near complete.

The experimental observations confirmed that indole was very susceptible to oxidative addition reactions, as reported in the literature (Blaster et al., 2006; Sobkowiak et al., 2009; Jones and Bean, 1977). The absence of monomeric primary oxidation products during the initial stages of autoxidation of indole suggested that the addition reaction proceeded directly from an intermediate and not from a primary oxidation product. If monomeric oxidation products had indeed been the intermediates for fast addition, it would not explain the persistence of monomeric oxidation products later on. Very similar results were obtained in the presence and absence of *n*-decane, which further suggested that hydroperoxide formation was not important in the mechanism of oxidative addition of indole.

Oxidation of 2,3-dihydroindole was more rapid than that of indole. The autoxidation induction time was less than 30 min (**Figure 5.17**). The rate of oxidation of 2,3-dihydroindole was very similar when it was oxidized with *n*-decane. Since the induction time of *n*-decane is over 2 hours under the experimental conditions employed (Siddiquee and De Klerk, 2014b), the results indicated that oxygen readily abstracted hydrogen from the aliphatic ring of 2,3-dihydroindole and that *n*-decane was not necessary to initiate oxidation. This was confirmed by the identification of the oxidation products, which had high selectivity for oxidative dehydrogenation of 2,3-dihydroindole to indole (**Table 5.3**). Selectivity towards oxidative dehydrogenation was >80 % throughout the oxidation time period studied.

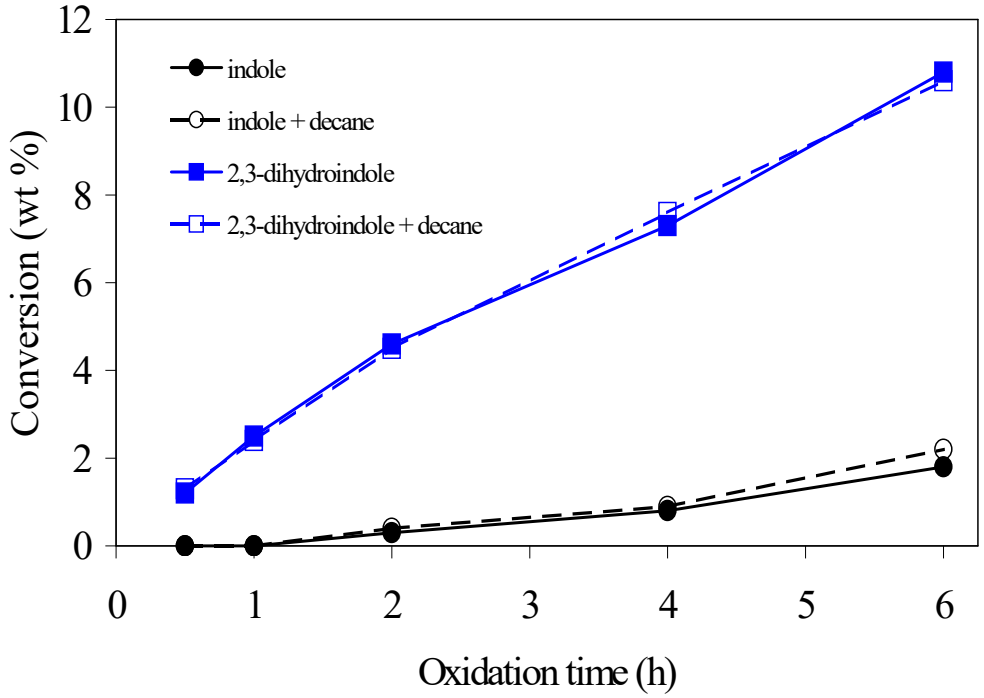

Figure 5.17. Autoxidation conversion of indole (●), indole and decane mixture (○), 2,3-dihydroindole (■), and 2,3-dihydroindole and decane mixture (□) at 130 °C and near atmospheric pressure.

Despite the structural similarity of indole and 2,3-dihydroindole (indoline), oxidation proceeded differently. Apart from the high selectivity to indole, other primary and secondary oxidation products were evident throughout the oxidation (**Table 5.3**). The combined oxidation selectivity to produce other primary and secondary oxidation products exceeded addition product selectivity from the initial stages of the reaction up to 4 hours reaction time. Indole that was formed during the oxidation of 2,3-dihydroindole contributed to the increase in addition product selectivity with increasing oxidation time. During the early stages of oxidation, indole and 2,3-dihydroindole shared no common addition products. After 6 h at oxidation conditions, GS-MS analysis indicated that 7 % of the addition products from the oxidation of 2,3-dihydroindole, matched products previously identified as oxidative addition products of indole. It is likely that these products were derived from the oxidative addition of indole that was formed *in situ* by the oxidative dehydrogenation of 2,3-dihydroindole.

Table 5.3. Product selectivity during the oxidation of indole and 2,3-dihydroindole (indoline) at 130 °C and air flow rate of 145-150 mL h^{-1} per g feed without and with *n*-decane added.

Description	Selectivity (wt %) [a,b]				
	30 min	60 min	120 min	240 min	360 min
Indole					
primary oxidation products (wt %)	0	0	0	3.3	10.3
secondary oxidation products (wt %)	0	0	0	0	0
addition products (wt %)	0	0	100	96.7	89.7
Indole with 5 wt % decane					
primary oxidation products (wt %)	0	0	0	0	10.2
secondary oxidation products (wt %)	0	0	0	0	0
addition products (wt %)	0	0	100	100	89.8
2,3-Dihydroindole					
indole (wt %)	89.9	87.5	85.9	83.5	81.3
primary oxidation products (wt %)	2.5	1.9	1.7	1.1	0.9
secondary oxidation products (wt %)	6.0	6.5	6.0	6.1	6.5
addition products (wt %)	1.6	4.1	6.4	9.3	11.3
2,3-Dihydroindole with 5 wt % decane					
indole (wt %)	95.8	95.6	94.7	92.8	89.5
primary oxidation products (wt %)	2.3	2.2	1.7	0.7	0.8
secondary oxidation products (wt %)	1.5	1.7	1.7	2.9	3.5
addition products (wt %)	0.4	0.5	1.9	3.5	6.2

[a] Average of six analyses of two separate experiments.

[b] Weight percentage of all oxidation products in the liquid, no response factor corrections were applied to the products.

Quinoline was not autoxidized on its own, even after 6 hours at oxidation conditions. Autoxidation of quinoline with 5 wt % *n*-decane did not result in any quinoline oxidation either. It was anticipated that prolonged autoxidation would ultimately yield some quinoline oxidation to produce the quinoline-N-oxide (Katritzky, 1971), but that would require the prior formation of carboxylic acids and hydroperoxides from extensive oxidation of the *n*-decane. This was not demonstrated in the present work.

5.3.1.3 Nature of Addition Products N-Heterocyclic Oxidation

One potential limitation of the selectivity determination based on GC-FID analysis is that the heaviest addition products will not elute and will not be detected. Samples of the products of

indole and 2,3-dihydroindole after 6 hours of oxidation were concentrated by removing the lighter products by heating under vacuum. The amount of heavier oxidation products and the ^{1}H NMR analyses of the heavier products are reported (**Table 5.4**).

Table 5.4. ^{1}H NMR analysis of indole, 2,3-dihydroindole and heavy residues after 6 h oxidation at 130 °C and air flow rate of 145-150 mL h^{-1} per g feed.

Description	Heavy residue (wt %) [a]	^{1}H NMR analysis (%)		
		aliphatic C-H	aliphatic N-H	aromatic
Indole				
calculated from structure		0	0	100
feed (no oxidation)	0	0.7 ± 0.5	- [b]	99.3 ± 0.5
after 6 h oxidation	16.6	1.3 ± 0.5	- [b]	98.7 ± 0.5
2,3-Dihydroindole				
calculated from structure		44.4	11.1	44.4
feed (no oxidation)	0	42.4 ± 1.4	12.9 ± 0.4	44.7 ± 1.3
after 6 h oxidation	3.9	17.9 ± 2.1	9.0 ± 1.0	73.1 ± 2.6

[a] Based on total mass.

[b] Could not be unambiguously differentiated from aliphatic C–H.

The amount of residue that was found supported the observations in **Table 5.3** and indicated that the yield of oxidative addition products was higher during autoxidation of indole, compared to 2,3-dihydroindole.

The progression of the addition reaction of indole (**Table 5.3**) suggested that addition was caused by autoxidation, but that oxidised products were not intermediates. Talbi et al. (1998) proposed that addition mechanism of indole proceeded through the formation of a radical cation intermediate and the mechanism did not require the participation of oxygen as reagent, only that the indole be oxidized to produce a radical cation. The oxidation products found after catalytic oxidation of indole suggested that oxygen incorporation and hydrogen disproportionation took place during addition reactions (Linhares et al., 2014). However, the purely aromatic nature of the indole addition products (**Table 5.4**) and the lack of C=O and C–O absorption bands in the infrared spectra (**Figure 5.18**) indicated that neither of these processes occurred to a significant extent in our study. Since C=O absorptions in the 1760 to 1700 cm^{-1} region are particularly strong (Colthup et al., 1990), the near absence of absorption in this range suggests that little, if

any, carbonyl groups were formed during the oxidative addition of indole. In fact, the infrared spectrum of the heavy product from indole oxidation (**Figure 5.18**) closely matched the reported infrared spectrum of polyindole that was obtained by electrochemical synthesis (Talbi et al., 1997).

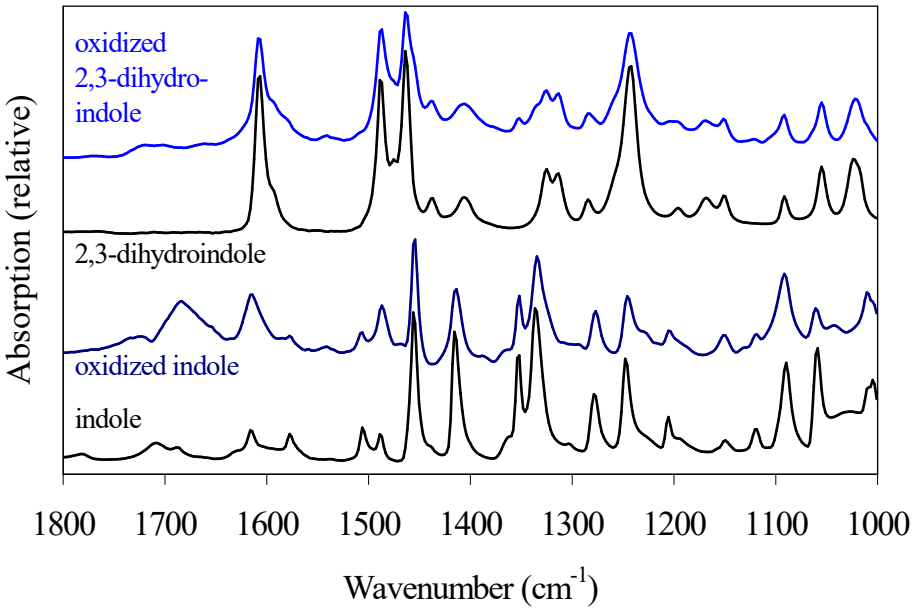

Figure 5.18. Infrared spectra of indole, 2,3-dihydroindole and the heavy residues (oxidative addition products) after 6 h oxidation of each.

A pertinent observation from literature is that when an alkyl group is present on the indole-ring, the C–C coupling takes place via the alkyl-carbon to an indole ring-carbon (Berti et al., 1969). The progression of oxidation of 2,3-dihydroindole and comparison of the oxidation products with that of indole indicated that oxidative addition proceeded differently. The ^{1}H NMR analysis (**Table 5.4**) showed that the heavy oxidative addition products of 2,3-dihydroindole were partly dehydrogenated. Literature suggested that dimerization took place by C–C bond formation between the pyrrolic rings of indole and 3-oxo-3*H*-indole 1-oxide as intermediates (Kovalev et al., 2014). The conditions in the present study was less severe and the infrared spectrum of the heavy oxidative addition products (**Figure 5.18**) show a slight increase in the absorption in the carbonyl region. The ^{1}H NMR results also suggest that the addition products are mainly dimers of indole and 2,3-dihydroindole (**Figure 5.19**), which have a calculated hydrogen distribution of 21.4 % aliphatic C–H (17.9 ± 2.1 % observed), 7.2 % aliphatic N–H (9.0 ± 1.0 % observed) and

71.4 % aromatic (73.1 ± 2.6 % observed). The C–C coupling is between the indole-rings.

The electron impact mass spectra of addition products had 207 m/z, 232 m/z, and/or 234 m/z as dominant features (**Figures 5.4–5.7**). The suggested main addition product (**Figure 5.19**) has a molar mass of 234 g mol^{-1} and could produce the fragments observed: M^+ – HCN = 207 m/z, M^+ – H_2 = 232 m/z, and M^+ = 234 m/z. Although these observations do not rule out other possibilities, collectively it indicates that oxidative addition is likely a consequence of free radical addition to pyrrolic ring. The C–C bond formation due to free radical addition, rather than the formation of oxygenates, is the dominant process involved in the formation of heavier products during 2,3-dihydroindole oxidation.

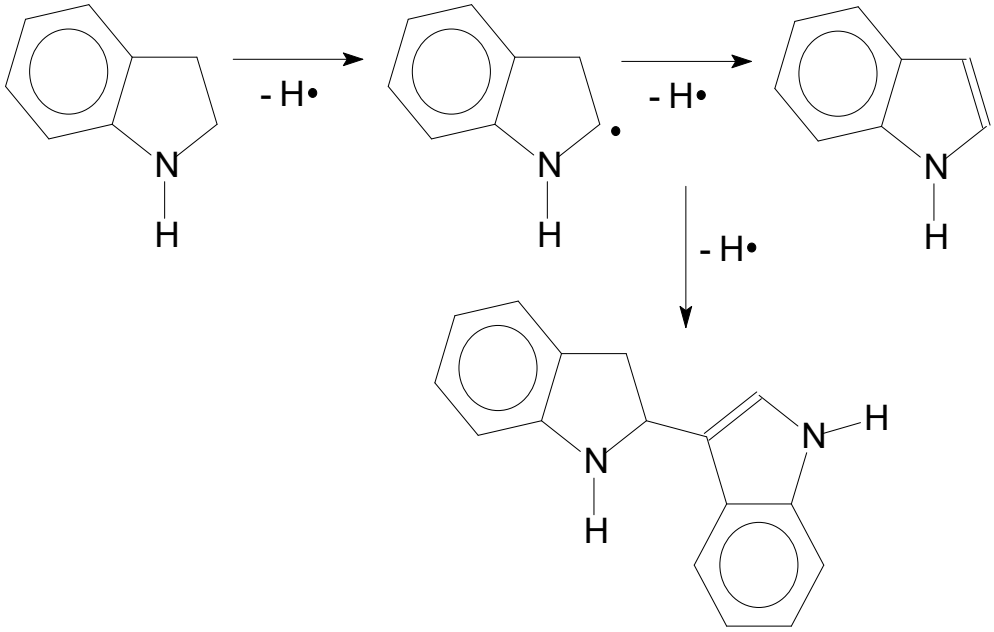

Figure 5.19. Dimerization of 2,3-dihydroindole due to hydrogen abstraction during autoxidation.

Oxidation studies through the formation of carbocation can lead to the different reaction pathways (Poniatowski and Floreancig, 2010; Sevov and Wiest, 2010; Clausen and Floreancig, 2012; Wang et al., 2014), but any chemicals that potentially form carbocation was not considered.

5.3.2 Oxidation of O-Heterocyclic Compounds

Benzofuran and 2,3-dihydrobenzofuran (**Figure 5.1**) represented the O-containing heterocyclic compounds found in bitumen. Benzofuran and 2,3-dihydrobenzofuran were autoxidized at 130 °C and the samples were collected at different oxidation times to monitor the progress of oxidation.

5.3.2.1 Product Identification

Oxidation of 2,3-benzofuran produced three categories of products (**Figure 5.20**)- primary oxidation products, secondary oxidation products and addition products.

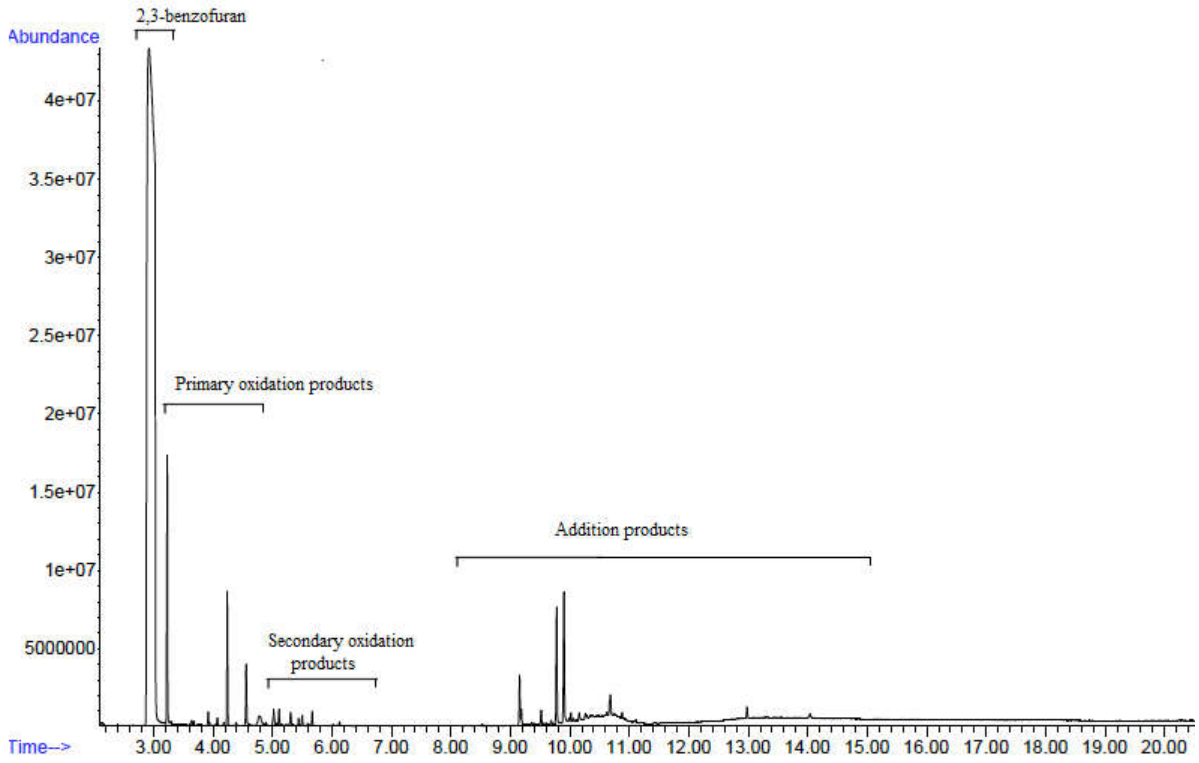

Figure 5.20. Chromatogram (GC-MS) of 2,3-benzofuran oxidation products after autoxidation at 130 °C for 360 min.

As shown in **Figure 5.20,** retention time of 2,3-benzofuran was 2.9 min. Oxidation of 2,3-benzofuran produced primary oxidation products [ketones (4.2 min) and alcohols (4.5 min) of 2,3-benzofuran]. Compounds having multiple functional groups were identified between retention times 5.0 – 6.8 min. Addition products were identified between 8.0-15.0 min. The EI

mass spectrum of addition products that appeared at 10.7 min is shown in **Figure 5.21**. This clearly shows the presence of at least a dimer m/z=235 of m/z=118 (benzofuran) that might be through C–C linkages not through C–O–C linkage. Also, this oxidative product has more than one functional group as this fragmentation pattern shows the loss –CO [m/z =28] and loss of H_2O [m/z = 18].

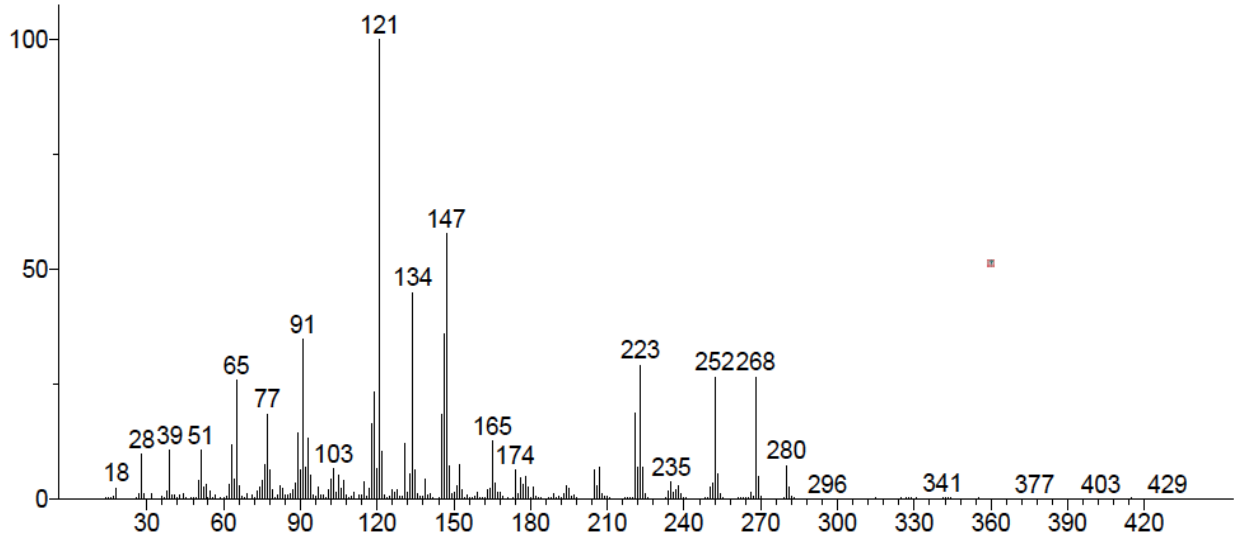

Figure 5.21. Electron ionization mass spectrum of an addition product (10.7 min retention time) formed during oxidation of 2,3-benzofuran at 130 °C.

The chromatogram of the oxidation products from 2,3-dihydrobenzofuran oxidation (**Figure 5.22**) showed a similar grouping of oxidation products as that for indoline oxidation. As shown in **Figure 5.22,** retention time of 2,3-dihydrobenzofuran was 3.5 min. Oxidation of 2,3 dihydrobenzofuran produced the oxidatively dehydrogenated product, 2,3-benzofuran (2.9 min), and primary oxidation products, ketones (4.4 min) and alcohols (4.6 min) of 2,3 dihydrobenzofuran. Compounds having multiple functional groups (secondary oxidation products) were identified between retention times 5.0–7.0 min. Addition products were identified between 9.0–13.0 min. The EI mass spectrum of addition products that appeared at 9.7 min is shown in **Figure 5.23**. This clearly shows the presence of at least a dimer m/z=236 of m/z=118 (benzofuran) that might be through C–C linkages not through C–O–C linkage. Also, this oxidative product has more than one functional group as this fragmentation pattern shows the loss –CO [m/z =28] and loss of H_2O [m/z = 18].

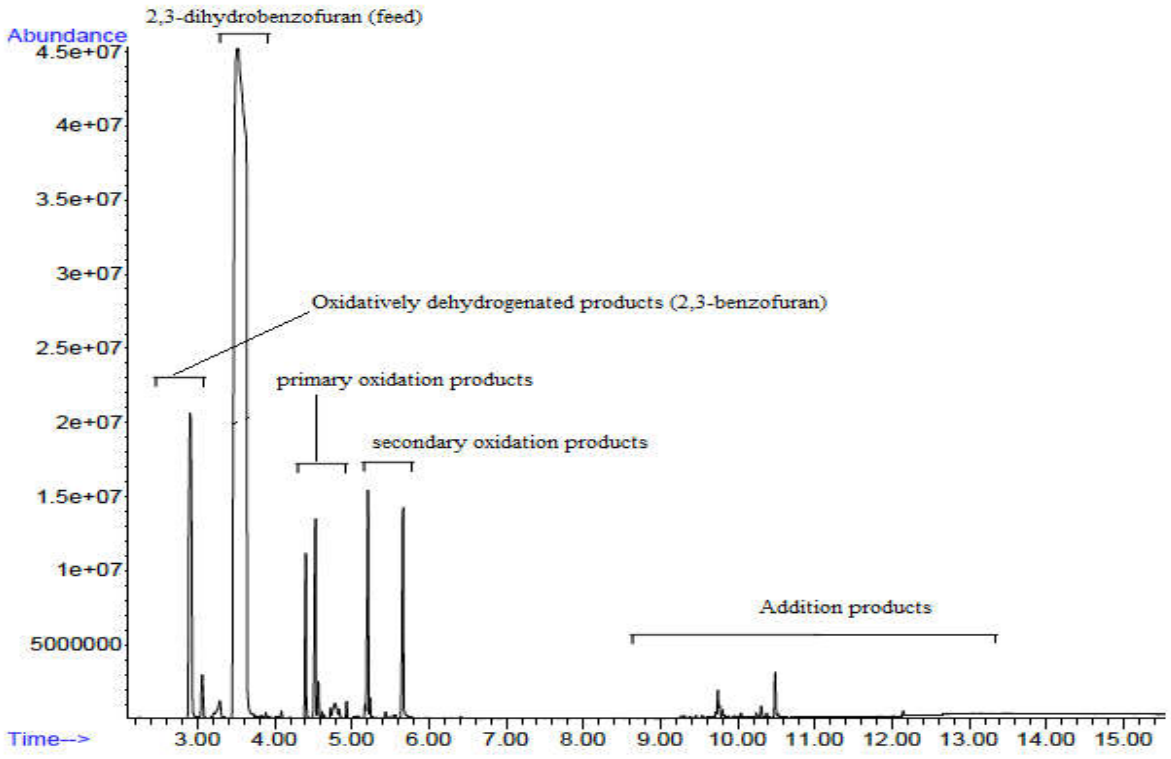

Figure 5.22. Chromatogram (GC-MS) of 2,3-dihydrobenzofuran oxidation products after autoxidation at 130 °C for 360 min.

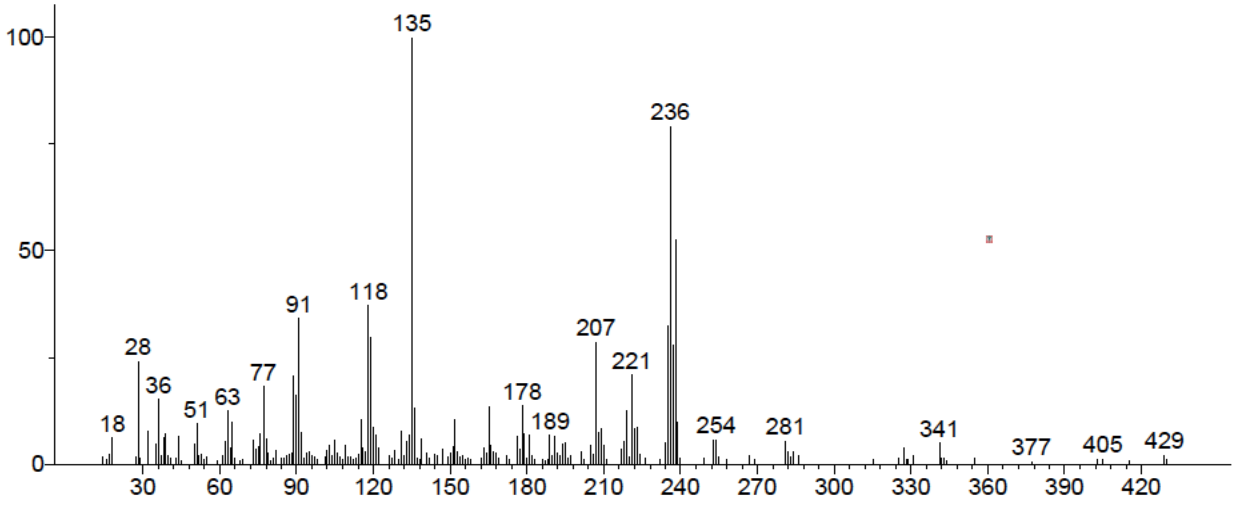

Figure 5.23. Electron ionization mass spectrum of an addition product (9.7 min retention time) formed during oxidation of 2,3-dihydrobenzofuran at 130 °C.

5.3.2.2 Conversion and Selectivity

The oxidation of 2,3-dihydrobenzofuran took place at a faster rate than that of benzofuran (**Figure 5.24**). This was anticipated, because 2,3-dihydrobenzofuran has an aliphatic ring structure. What was not anticipated, was that benzofuran would be so easily oxidised. The oxidation of benzofuran with air is not reported on in standard texts (Elderfield and Meyer, 1951). The literature suggests that oxidation of benzofuran requires a catalyst and the primary aim of most of the investigations were to facilitate oxidative addition (coupling) reactions (Dwight et al., 2007; Do and Daugulis, 2009; Truong et al., 2010; Pereira et al., 2013; Dao-Huy et al., 2014). Although the possible presence of metals in trace quantities were not rigorously excluded in our work, no metals or other forms of catalysts were deliberately added either.

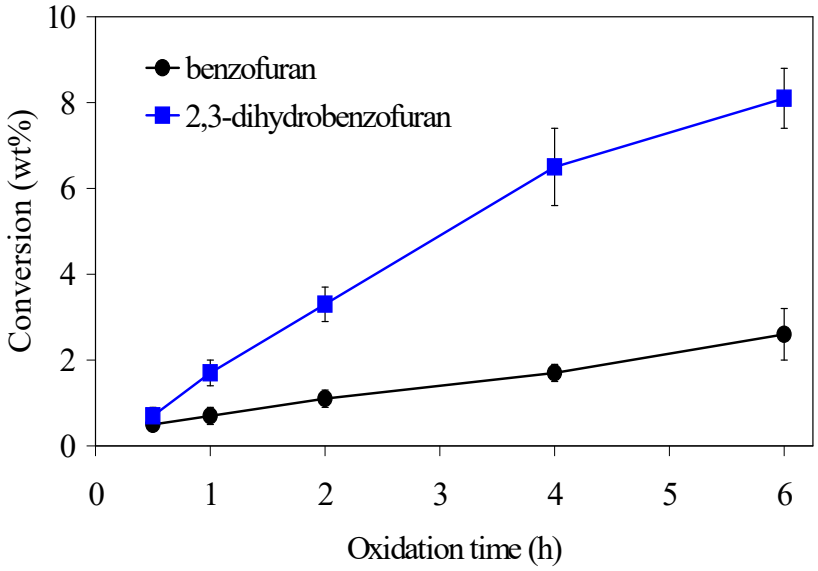

Figure 5.24. Autoxidation conversion of benzofuran (●) and 2,3-dihydrobenzofuran (■) at 130 °C and near atmospheric pressure. Error bars indicate one sample standard deviation of experiments in triplicate.

The selectivity to oxidative addition reactions of benzofuran was in the range 30 to 35 % (**Table 5.5**) and benzofuran conversion was < 3 %. The yields were therefore much lower than the yields reported for some of the catalyzed benzofuran dimerisation reactions mentioned before (Do and Daugulis, 2009; Truong et al., 2010). Most of the products in this work were monomeric oxidised derivatives of benzofuran, which meant that oxygen was added to the benzofuran. The

main products were identified using electron impact mass spectrometry.

Table 5.5. Product selectivity during the oxidation of benzofuran and 2,3-dihydrobenzofuran at 130 °C and air flow rate of 145-150 mL h^{-1} per g feed.

Description	Selectivity (wt %) [a,b]				
	30 min	60 min	120 min	240 min	360 min
Benzofuran					
primary oxidation products (wt %)	51.9	50.6	50.0	50.7	50.3
secondary oxidation products (wt %)	16.0	16.1	15.9	15.4	14.5
addition products (wt %)	32.1	33.3	34.1	33.9	35.3
2,3-Dihydrobenzofuran					
primary oxidation products (wt %)	87.2	85.7	83.7	81.5	80.0
secondary oxidation products (wt %)	12.8	13.4	14.6	14.9	14.1
addition products (wt %)	0.0	0.9	1.7	3.6	5.9

[a] Average of six analyses of two separate experiments.

[b] Weight percentage of all oxidation products in the liquid, no response factor corrections were applied to the products.

5.3.2.3 Nature of Addition Products O-Heterocyclic Oxidation

The electron impact mass spectra of the addition products of benzofuran were complex. The most prominent fragments observed were 121 (dominant), 147 and 134 m/z. On the heavier end of the spectrum 223, 252 and 268 m/z were prominent. It suggests that coumaran-3-one or coumaran-2-one, the coumaranone isomers, are likely intermediates. This type of oxidative conversion was suggested before for photodegradation, which is also a free radical oxidation process (Amalric et al., 1995). Aldol condensation of coumaran-3-one with itself in the presence of air leads to the formation of the leuco compound of oxindirubin (Elderfield and Meyer, 1951). Depending on the intermediate, C–C coupling through the 2- or 3-position on the furan-ring leads to the addition product. Under oxidative conditions further dehydration and oxidative dehydrogenation is possible to ultimately lead to oxindirubin and heavier derivatives of oxindirubin. It is speculated that oxidative addition of benzofuran may take place through coumaranone as intermediate to produce oxindirubin-type products, as shown in **Figure 5.25**.

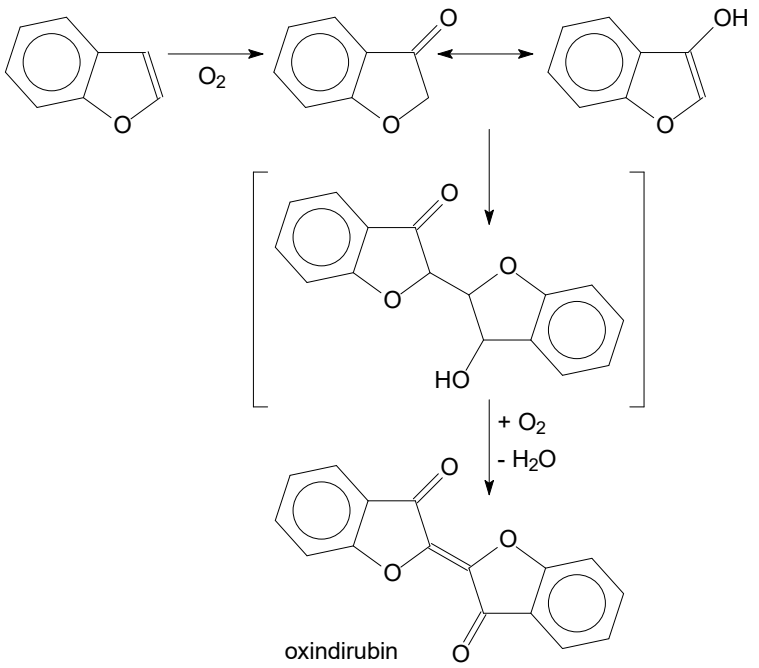

Figure 5.25. Oxidative dimerization of benzofuran that proceeds through coumaranone.

The addition products of 2,3-dihydrobenzofuran had strong 233 (dominant) and 117 m/z fragments. The molar mass of benzofuran is 118 g mol^{-1} and the fragmentation pattern suggested that a C–C coupled addition product was formed in an analogous fashion to 2,3-dihydroindole as shown in **Figure 5.19**. However, unlike in 2,3-dihydroindole oxidation where indole was a major product, benzofuran was not a major product during oxidation of 2,3-dihydrobenzofuran. The addition chemistry is therefore not the same.

The primary oxidation product selectivity was >80 % (**Table 5.5**). Coumaranone is an important primary oxidation product of 2,3-dihydrobenzofuran. Another reaction that takes place during oxidation of 2,3-dihydrobenzofuran is hydrogen abstraction. One plausible reaction sequence is the dimerization of two free radical intermediates (**Figure 5.26**). Another plausible reaction sequence is that the free radical intermediate reacts with the enol tautomer of coumaranone, which has a C=C double bond and that is susceptible to free radical addition (**Figure 5.26**). The net reaction is the addition of two molecules of 2,3-dihydrobenzofuran and the oxidative elimination of hydrogen to produce two molecules of water. Irrespective of the reaction pathway, 3-3-, 2-3- and 2-2-addtion reactions are also possible.

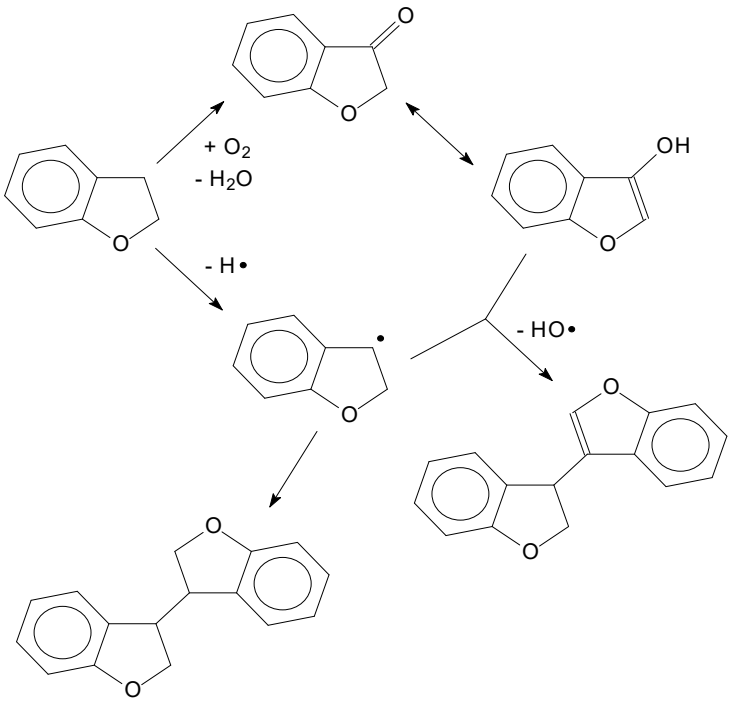

Figure 5.26. Dimerization of 2,3-dihydrobenzofuran.

The heavy addition products that were produced after 6 hours at oxidation conditions were separated from the rest of the product by evaporating the lighter material under vacuum. The heavy addition products were analyzed by ^{1}H NMR (**Table 5.6**). It is possible that further reaction took place during evaporation, because the amount of heavy products exceeded the yield of heavy products calculated from analysis of the product before evaporation (**Table 5.5**). However, it is also possible that some of the heaviest products were too heavy to be eluted during gas chromatography.

The heavier products of benzofuran contained a small amount, 4 %, of aliphatic hydrogen (**Table 5.6**). It suggested that addition did not lead to complete oxidative dehydrogenation to oxindirubin (**Figure 5.25**), but that at least some of the aldol condensation product remained. The ratio of the aliphatic to aromatic hydrogen in the addition product of 2,3-dihydrobenzofuran was 39:61 (**Table 5.6**) that is close to 43:57, which is the calculated aliphatic to aromatic hydrogen ratio for a 2,3-dihydrobenzofuran dimer. This implies that recombination of free radical intermediates after oxidative dehydrogenation (**Figure 5.26**) is the dominant reaction pathway for addition reactions during oxidation of 2,3-dihydrobenzofuran.

Table 5.6. ^{1}H NMR analysis of benzofuran, 2,3-dihydrobenzofuran and heavy residues after 6 h oxidation at 130 °C and air flow rate of 145–150 mL h^{-1} per g feed.

Description	Heavy residue (wt %) [a]	^{1}H NMR analysis (%)	
		aliphatic	aromatic
Benzofuran			
calculated from structure		0	100
feed (no oxidation)	0	0	100
after 6 h oxidation	4.8	3.8 ± 0.9	96.2 ± 0.9
2,3-Dihydrobenzofuran			
calculated from structure		50	50
feed (no oxidation)	0	48.7 ± 0.3	51.3 ± 0.3
after 6 h oxidation	3.5	38.6 ± 4.3	61.4 ± 4.3

[a] Based on total mass.

5.3.3 Oxidation of S-Heterocyclic Compounds

Thianaphthene (**Figure 5.1**), also known as benzothiophene, was selected as representative of aromatic sulfur-containing compounds in bitumen. Thianaphthene and benzofuran are iso-structural, differing only in the heteroatom. When thianaphthene was kept at 130 °C for 6 h under oxidation conditions, no measurable oxidative conversion was observed. Even when the experiment was performed in the presence of 5 wt% decane to provide a facile pathway for hydroperoxide formation, no measurable oxidation of the thianaphthene was observed. To make the comparison, the chromatograms of thianaphthene and thianaphthene treated with air at 130 °C for 6 h are shown in **Figures 5.27** and **5.28**, respectively.

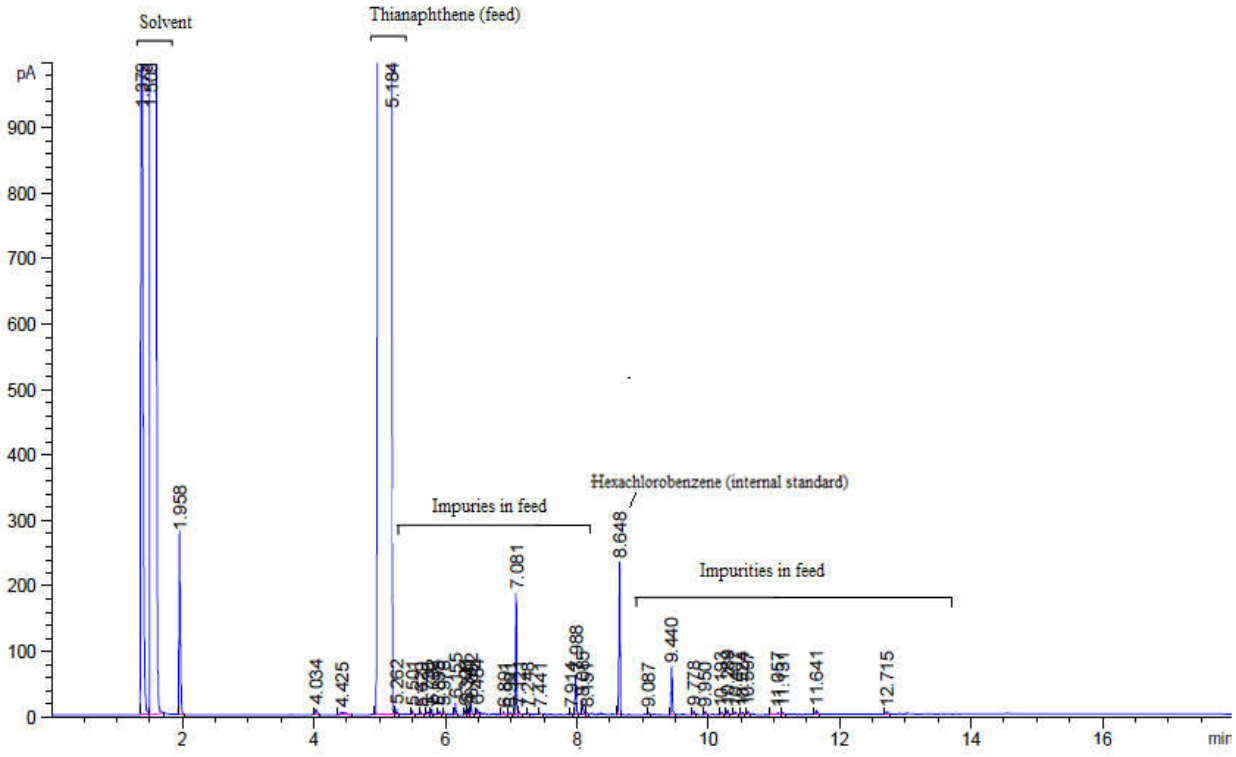

Figure 5.27. Chromatogram of thianaphthene without oxidation.

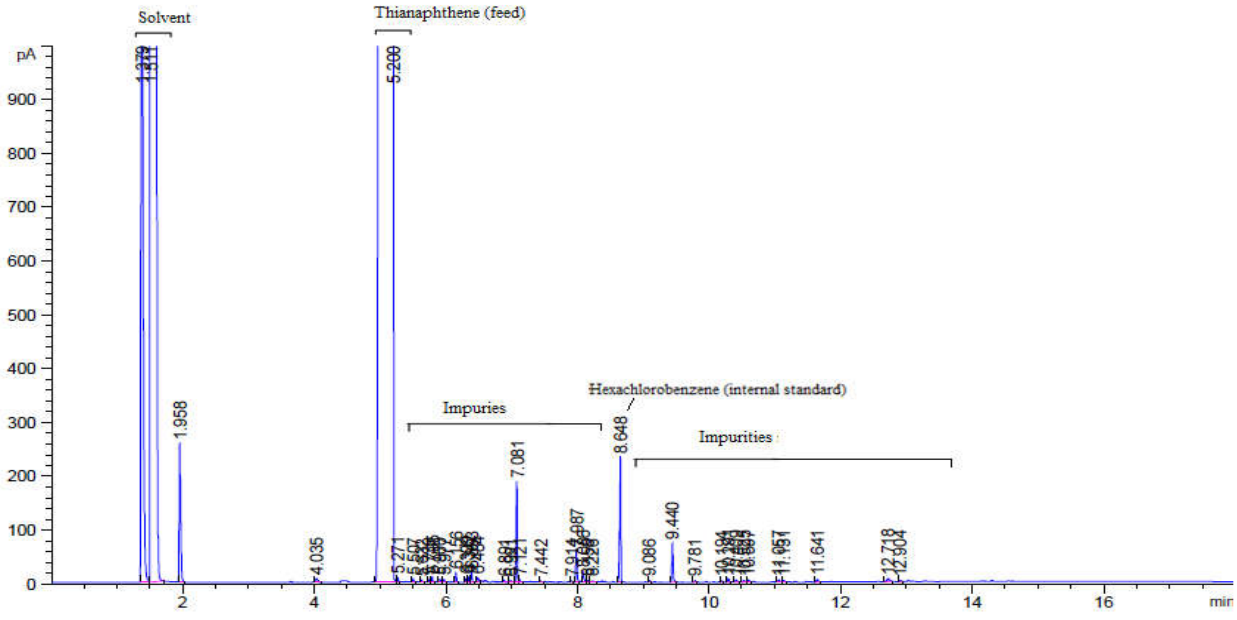

Figure 5.28. Chromatogram of thianaphthene oxidized by air at 130 °C for 6 hour.

These observations were somewhat surprising, since thiophenic compounds are readily oxidized to their corresponding sulfones in diesel fuels (Ismagilov et al., 2011). It was reported that oxidation of thiophenic sulfur in the presence of electron withdrawing groups is difficult (Rajappa and Gumaste, 2014), but thianaphthene does not have any substituents. In fact, the preparation of thianaphthene-1,1-dioxide from thianaphthene is readily achieved by reaction with hydrogen peroxide in dilute acetic acid (Hartough and Meisel, 1954). However, thianaphthene was less reactive towards oxidation when compared to dimethyldibenzothiophene, methyldibenzothiophene, and dibenzothiophene (Ismagilov et al., 2011), which contained electron donating groups and had a higher electron density due to the additional aromatic ring.

In previous work (Javadli and De Klerk, 2012b), oxidative addition reactions of dibenzothiophene in a dilute mixture with *n*-heptane was investigated to elucidate sediment formation during oxidative desulfurization, albeit at more severe conditions. Sulfones and addition products of sulfones were found in the oxidised product. It was therefore anticipated that thianaphthene will ultimately also produce analogous products.

Thianaphthene is oxidised, but the rate of oxidation of thianaphthene is clearly much slower than that observed for the other five-membered heterocyclic compounds studied (**Figures 5.17** and **5.24**).

5.3.4 Implications for Low Temperature Autoxidation Processes

In both Chapters 4 and 5 the compounds were selected to be within the kerosene boiling range and the same oxidation conditions were employed. With the exception of compounds that contained a pyrrole-ring (e.g. indole), which were known to readily polymerize under oxidative conditions (Jones and Bean, 1977), the propensity of other compounds classes to form oxidative addition products was not clear from the literature. A comparison of the oxidative addition yields is presented in **Table 5.7**, and is ranked relative to the oxidative addition yield of indole.

Table 5.7. Oxidative addition product yield after 6 hours of oxidation at 130 °C and an air flow rate of 145-150 mL h^{-1} per g feed.

Compound	Oxidative addition	
	yield (wt %)	relative to indole
indene [a]	5.8	3.6
indole	1.6	1
indan [a]	1.3	0.80
2,3-dihydroindole	1.2	0.76
benzofuran	0.9	0.57
tetralin [a]	0.8	0.47
2,3-dihydrobenzofuran	0.5	0.30
cis/*trans*-decalin [a]	0.1	0.07
p-cymene [a]	0.1	0.05
thianaphthene	0.0	<0.01
n-decane [a]	0	0
naphthalene [a]	0	0
quinoline	0	0

[a] Taken from (Chapter 4).

Compounds that contain a five-membered ring-structure were found to be more susceptible to oxidative addition reactions than six-membered ring-structures, or acyclic compounds. Among the five-membered heterocyclic compounds, the propensity to form oxidative addition products increased in the order: S << O < N. Although the study did not investigate secondary interactions between compound classes, sulfur-containing compounds are the least likely to produce addition products.

Another surprising observation was that five-membered naphtheno-aromatic compounds are very susceptible to oxidative addition. In fact, the oxidation addition propensity of indene was 3.6 times more than that of indole, while indan was only somewhat lower in addition propensity to indole (**Table 5.7**). Five-membered naphtheno-aromatic hydrocarbons, indene and indan, were more prone to oxidative addition than even their pyrrolic analogues, indole and 2,3-dihydroindole!

The implication for low temperature oxidation is far reaching. The compound classes that are most likely to be responsible for oxidative addition reactions are pyrrolic nitrogen-containing

compounds and naphtheno-aromatic hydrocarbons with a five-membered ring. Although sulfur-containing compounds may be observed in fouling layers, sludges and precipitates, the role of sulfur-containing compounds is more likely to be that of a free radical initiator. In applications dealing with hydrotreated materials, it is compounds with an indan-motif that will dominate oxidative addition. Furthermore, the oxidative addition is really a free radical addition reaction and free radical addition is not necessarily restricted to oxidation. In all instances the addition products were C–C coupled by free radical addition. Any processing conditions that will give rise to free radical formation at temperatures where addition dominates cracking, typically at temperatures of 400 °C and below, will be susceptible to addition product formation if the material contains naphtheno-aromatic hydrocarbons with a five-membered ring.

5.4 Conclusions

Oxidative addition reactions of heterocyclic compounds were investigated by making use of model compounds to represent different compound classes. The following conclusions were drawn from the experimental work and comparison of the results with oxidative addition reactions of hydrocarbons:

(a) The oxidative addition susceptibility of compounds containing a pyrrolic-ring was confirmed. Indole had ~90 % selectivity to oxidative addition product formation. The addition mechanism did not require oxygen incorporation and no evidence for oxygen incorporation in the addition products from indole was observed.

(b) Oxidation of 2,3-dihydroindole produced indole with a selectivity of 80–90 %. However, most of the addition products from 2,3-dihydroindole oxidation were not produced via the indole, but by a different reaction pathway. The dimers of 2,3-dihydroindole were partly dehydrogenated and analysis suggested that an oxidative dehydrogenation took place by free radical combination and/or addition to indole. The increase of addition selectivity as the concentration of indole increased, suggested that free radical addition to indole was the dominant addition pathway. There was little evidence of oxygen incorporation in the addition products.

(c) Under the oxidation conditions studied, autoxidation at 130 °C for 6 hours, quinoline was not oxidised at all.

(d) Benzofuran was susceptible to oxidation and oxidative addition products were formed with a selectivity of 30–35 %. The formation of coumaranone ketone produced by oxidation of benzofuran, appeared to be a key intermediate in addition reactions. Coumaranone is capable of keto-enol tautemerism and aldol condensation, which appeared to be responsible for addition reactions.

(e) The oxidation of 2,3-dihydrobenzofuran did not produce benzofuran as major product. The addition products were different. Although coumaranone formation and aldol condensation could contribute to the formation addition products, free radical recombination resulted in products that better matched the analysis of addition products.

(f) Thianaphthene was not as easily oxidised as either indole or benzofuran. Under the oxidation conditions studied, very little conversion was observed.

(g) Among the five-membered heterocyclic compounds, the propensity to form oxidative addition products increased in the order: S << O < N.

(h) Surprisingly, the five-membered naphtheno-aromatic hydrocarbons, indene and indan, were more prone to oxidative addition reactions than even their pyrrolic analogues, indole and 2,3-dihydroindole.

5.5 Literature Cited

Amalric, L.; Guillard, C.; Pichat, P. The photodegradation of 2,3-benzofuran and its intermediates, 2-coumaranone and salicylaldehyde, in TiO_2 aqueous suspensions. *J. Photochem. Photobiol. A* **1995**, *85*, 257–262.

Balster, L. M.; Zabarnick, S.; Striebich, R. C.; Shafer, L. M.; West, Z. J. Analysis of polar species in jet fuel and determination of their role in autoxidative deposit formation. *Energy Fuels* **2006**, *20*, 2564–2571.

Berti, G.; Da Settimo, A.; Di Colo, G.; Nannipieri, E. A dimeric autoxidation product of 2,3-dimethylindole. *J. Chem. Soc. C* **1969**, 2703–2710.

Clausen, D. J.; Floreancig, P. E. Aromatic cations from oxidative carbon hydrogen bond cleavage in bimolecular carbon carbon bond forming reactions. *J. Org. Chem.* **2012**, *77*, 6574 6582.

Colthup, N. B.; Daly, L. H.; Wiberley, S. E. *Introduction to infrared and Raman spectroscopy*, 3ed; Academic Press: San Diego, CA, 1990.

Dao-Huy, T.; Haider, M.; Glatz, F.; Schnürch, M.; Milhovilovic, M. D. Direct arylation of benzo[*b*]furan and other benzo-fused heterocycles. *Eur. J. Org. Chem.* **2014**, 8119–8125.

Do, H-Q.; Daugulis, O. An aromatic Glaser-Hay reaction. *J. Am. Chem. Soc.* **2009**, *131*, 17052–17053.

Dwight, T. A.; Rue, N. R.; Charyk, D.; Josselyn, R.; DeBoef, B. C–C bond formation via double C–H functionalization: Aerobic oxidative coupling as a method for synthesizing heterocoupled biaryls. *Org. Lett.* **2007**, *9*, 3137–3139.

Elderfield, R. C.; Meyer, V. B. Benzofuran and its derivatives. In *Heterocyclic compounds. Vol. 2. Polycyclic five- and six-membered compounds containing one O or S atom*; John Wiley & Sons: New York, 1951, pp1–67.

Fedorak, P. M.; Foght, J. M.; Gray, M. R. Conversion of heavy oil and bitumen to methane by chemical oxidation and bioconversion, US Patent Application 2009/0130732.

Frankenfeld, J. W.; Taylor, W. F.; Brinkman, D. W. Storage stability of synfuels from oil shale. 1. General features of sediment formation in model fuel systems. *Ind. Eng. Chem. Prod. Res. Dev.* **1983**, *22*, 608–614.

Green, U.; Aizenshtat, Z.; Metzger, L.; Cohen, H. Field and laboratory simulation study of hot spots in stockpiled bituminous coal. *Energy Fuels* **2012**, *26*, 7230–7235.

Hardy, D. R.; Wechter, M. A. Characterization of soluble macromolecular oxidatively reactive species (SMORS) from middle distillate diesel fuels: Their origin and role in instability. *Energy Fuels* **1994**, *8*, 782–787.

Hartough, H. D.; Meisel, S. L. *The chemistry of heterocyclic compounds. Compounds with condensed thiophene rings*; Interscience: New York, 1954.

Huang, Y.; Ou, Q.; Yu, W. Characteristics of flame ionization detection for the quantitative analysis of complex organic mixtures. *Anal. Chem.* **1990**, *62*, 2063–2064.

Ismagilov, Z.; Yashnik, S.; Kerzhentsev, M.; Parmon, V.; Bourane, A.; Al-Shahrani, F. M.; Hajji, A. A.; Koseoglu, O. R. Oxidative desulfurization of hydrocarbon fuels. *Catal. Rev. Sci. Eng.* **2011**, *53*, 199–255.

Jones, R. A.; Bean, G. P. *The chemistry of pyrroles*; Academic Press: London, 1977.

Javadli, R.; De Klerk, A. Desulfurization of heavy oil – Oxidative desulfurization (ODS) as potential upgrading pathway for oil sands derived bitumen. *Energy Fuels* **2012b**, *26*, 594–602.

Jia, N.; Moore, R. G.; Mehta, S. A.; Van Fraassen, K.; Ursenbach, M. G.; Zalewski, E. Compositional changes for Athabasca bitumen in the presence of oxygen under low temperature conditions. *J. Can. Petrol. Technol.* **2005**, *44* (9), 51–56.

Jorgensen, A. D. Prediction of gas chromatography flame ionization detector response factors from molecular structures. *Anal. Chem.* **1990**, *62*, 683–689.

Katritzky, A. R.; Lagowski, J. M. *Chemistry of the heterocyclic N-oxides*; Academic Press: London, 1971.

Katritzky, A. R.; Ignatchenko, E. S.; Barcock, R. A.; Lobanov, V. S.; Karelson, M. Prediction of gas chromatographic retention times and response factors using a general qualitative structure-property relationships treatment. *Anal. Chem.* **1994**, *66*, 1799–1807.

Kovalev, I. S.; Kopchuk, D. S.; Zyryanov, G. V.; Rusinov, V. L.; Chupakhin, O. N. Nucleophilic dimerization of indoline under oxidative conditions. *Mendeleev Commun.* **2014**, *24*, 40–41.

Linhares, M.; Rebelo, S.L.H.; Simões, M.M.Q.; Silva, A.M.S.; Graça, M.; Neves, P.M.S.; Cavaleiro, J.A.S.; Freire, C. Biomimetic oxidation of indole by Mn(III)porphyrins. *Appl. Catal. A* **2014**, *470*, 427–433.

McLafferty, F. W.; Tureček, F. *Interpretation of mass spectra*, 4ed; University Science Books: Mill Valley, CA, 1993.

Nixon, A. C. Autoxidation and antioxidants of petroleum. In *Autoxidation and antioxidants. Vol. II*; Lundberg, W. O. Ed.; Interscience: New York, 1962, p. 695–856.

Pereira, K. C.; Porter, A. L.; Potavathri, S.; LeBris, A. P.; DeBoef, B. Insight into the palladium-catalyzed oxidative arylation of benzofuran: heteropoly acid oxidants evoke a Pd(II)/Pd(IV) mechanism. *Tetrahedron* **2013**, *69*, 4429–4435.

Poniatowski, A. J.; Floreancig, P. E. Radical cation fragmentation reactions in organic synthesis. In *Carbon-Centered Free Radicals and Radical Cations: Structure, Reactivity, and Dynamics, 1st ed*; Forbes, M. D. E. Ed.; Wiley: New Jersey, 2010, p 43-60.

Rajappa, S.; Gumaste, V. K. Reactivity of thiophene, oligothiophenes and benzothiophenes. *Adv. Heterocyclic Chem.* **2013**, *108*, 1–161.

Ren, S.; Zhao, H.; Dang-Vu, T.; Xu, Z.; Masliyah, J. H. Effect of weathering on oil sands processability. *Can. J. Chem. Eng.* **2009**, *87*, 879–886.

Sevov, C. S.; Wiest, O. Selectivity in radical cation cycloadditions. In *Carbon-Centered Free Radicals and Radical Cations: Structure, Reactivity, and Dynamics, 1st ed*; Forbes, M. D. E. Ed.; Wiley: New Jersey, 2010, p 61-82.

Siddiquee, M. N.; De Klerk, A. Hydrocarbon addition reactions during low temperature autoxidation of oilsands bitumen. *Energy Fuels* **2014b**, *28*, 6848–6859.

Sobkowiak, M.; Griffith, J. M.; Wang, B.; Beaver, B. Insight into the mechanisms of middle distillate fuel oxidative degradation. Part 1: On the role of phenol, indole, and carbazole derivatives in the thermal oxidative stability of Fischer-Tropsch/Petroleum jet fuel blends. *Energy Fuels* **2009**, *23*, 2041–2046.

Strausz, O. P.; Lown, E. M. *The chemistry of Alberta oil sands, bitumens and heavy oils*; Alberta Energy Research Institute: Calgary, AB, 2003.

Talbi, H.; Monard, G.; Loos, M.; Billaud, D. Theoretical study of indole polymerization. *Theochem.* **1998**, *434*, 129–134.

Talbi, H.; Ghanbaja, J.; Billaud, D.; Humbert, B. Vibrational properties and structural studies of doped and dedoped poluindole by FTIR, Raman and EEL spectroscopies. *Polymer* **1997**, *38*, 2099–2106.

Truong, T.; Alvarado, J.; Tran, L. D.; Daugulis, O. Nickel, manganese, cobalt, and iron-catalyzed deprotonative arene dimerization. *Org. Lett.* **2010**, *12*, 1200–1203.

Van Krevelen, D. W. *Coal. Typology–Physics–Chemistry–Constitution*, 3ed; Elsevier: Amsterdam, 1993, p. 627–658.

Wang, Z. L.; Li, H. L.; Ge, L. S.; An, X. L.; Zhang, Z. G.; Luo, X.; Fossey, J. S.; Deng, W. P. DDQ-mediated oxidative coupling: an approach to 2,3-dicyanofuran (thiophene). *J. Org. Chem.* **2014**, *79*, 1156 1165.

CHAPTER 6 – LIQUID PHASE OXIDATION IN MICROFLUIDIC REACTOR TO MANIPULATE OXYGEN AVAILABILITY TO CONTROL OXIDATION RATE AND PRODUCT SELECTIVITY INDEPENDENTLY [6]

Abstract

Tetralin, a simple naphthenic-aromatic hydrocarbon, was oxidized with oxygen over the temperature range of 120–160 °C. The objectives were to investigate how oxygen availability could be manipulated during oxidation and how it was related to both oxidation rate and product selectivity. Oxygen availability was mainly manipulated by changing hydrodynamics of a rectangular glass microfluidic reactor operated in the Taylor flow region and also by changing reactor types. Ketone-to-alcohol selectivity in primary oxidation products was increased by an order of magnitude from less than 1:1 to 14:1 by increasing oxygen availability in the liquid phase at near constant conversion, oxygen partial pressure and temperature. Higher ketone selectivity could be explained in terms of the oxidation of alcohol and/or alkoxy radicals formed. Selectivity to alcohols and addition products increased at lower oxygen availability. Effects of temperature and initiator (di-*tert*-butyl peroxide) on oxidative conversion and product selectivity were also reported.

Keywords: Microfluidic reactor, slug flow, tetralin oxidation, conversion, oxygen availability, product selectivity

[6]Reprinted from Siddiquee, M. N.; De Klerk, A.; and Nazemifard, N. Application of microfluidics to control product–selectivity during non-catalytic oxidation of naphthanic–aromatic hydrocarbon (submitted to publish in Reaction Chemistry and Engineering).

6.1 Introduction

Liquid phase oxidation of hydrocarbons is widely applied for the production of petrochemicals (Pina et al., 2013; Dimitratos et al., 2014; Suresh et al., 2000). Many of these processes employ oxidation catalysts, but not all feed materials are amenable to catalytic conversion. Homogeneous oxidation catalysts used for the production of fine chemicals generate wastes; catalyst deactivation and recycling are also problematic (Hill and Kholdeeva, 2013). When dealing with complex mixtures that contain potential fouling agents and catalyst poisons, it may be necessary to resort to non-catalytic oxidation. The challenge in free radical oxidation is to achieve good selectivity.

At low temperature some reaction pathways are not favoured, because they require higher activation energies, but in free radical processes selectivity cannot always be controlled by just the kinetics. In practice, oxidation selectivity is governed by temperature in combination with oxygen availability (De Klerk, 2003; Goosen and Morgan, 1994; Jevtic et al., 2009). It is the local concentration of oxygen in proximity to the free radical intermediates that influences selectivity and hence reference to oxygen availability rather than oxygen partial pressure (Suresh et al., 2000; Hobbs et al., 1972; Lundberg, 1961). Although it is convenient to think in terms of bulk concentrations, the reactions that determine selectivity are local events. Yet, despite the industrial importance of selective liquid phase oxidation of hydrocarbons, only few studies dealt with reaction engineering (Suresh et al., 2000; De Klerk, 2003; Hobbs et al., 1972; Jevtic et al., 2010; Leclerc et al., 2008; Fischer et al., 2010).

Oxygen availability is influenced by mass transport. The transport of oxygen from the gas phase to liquid phase, as well as the transport of oxidation intermediates between the bulk liquid and the gas-liquid interface are likely important. The oxidation intermediates are oxygenates that may be surface active in an apolar hydrocarbon medium (De Klerk, 2003). A proper description of oxygen availability and how it is influenced by mass transport must therefore take oxygen and oxygenate transport into account.

During liquid-phase oxidation of hydrocarbons with molecular oxygen, various oxygenates like hydroperoxides, alcohols and ketones are produced as primary oxidation products (De Klerk,

2003; Emanuel et al., 1967; Twigg, 1954). Secondary oxidation products (oxidized multiple times), and in some cases addition products (dimerized/oligomerized) are also generated (Siddiquee and De Klerk, 2014). Oxidation proceeds via a free radical mechanism, which is well studied and reviewed in literature (De Klerk, 2003; Emanuel et al., 1967; Twigg, 1954) and the key elements were summarized in **Chapter 2**. Alkyl free radicals ($R^{\cdot}$) are formed (initiation) during the induction period, but initiation has no appreciable effect on product selectivity (De Klerk, 2003). The reaction between alkyl radicals ($R^{\cdot}$) and molecular oxygen (O_2) is very fast and follows zero order kinetics at an oxygen partial pressure above 13 kPa (Suresh et al., 2000; Hobbs et al., 1972; Lundberg, 1961). Once the propagation starts, selectivity to form oxidation products is changed depending on the oxidation conditions and structure of hydrocarbons. Alcohols and ketones are generally formed at 1:1 ratio for primary and secondary hydrocarbons (De Klerk, 2003; Emanuel et al., 1967); however, depending on the oxygen availability, this ratio changes. During industrial applications, low conversion (less than 5 %) is preferred to control selectivity of hydrocarbon autoxidation; otherwise, different kinds of by-products are produced (Hermans et al., 2008). It is desirable to control selectivity and preferable to control selectivity independent from conversion.

Continuous-flow liquid phase oxidation in microreactors has received a lot of attention as the miniaturized reactor provides high interfacial areas resulting in enhanced heat and mass transfer rates, safe use of hazardous oxidants, and scale-up potential. The objective of the present study was to investigate how oxygen availability could be manipulated during liquid-phase oxidation of naphthenic-aromatic hydrocarbon with molecular oxygen and how it was related to both oxidation rate and product selectivity. In order to have a clearly defined and measurable gas-liquid interface area, most of the experimental work in this investigation was conducted using a microfluidic reactor.

One of the advantages of using microchannel-based reactors (e.g. microfluidic reactor) is the exact control of liquid and gas flowrates, as well as channel geometry and dimensions. This made it possible to calculate the exact gas-liquid interfacial area and film thickness by performing experiments in the Taylor flow region. The Taylor flow region (also known as slug flow) is characterized by a liquid-gas two-phase flow in which the gas phase exists as bubbles separated by liquid “slugs”. The internal circulation within the liquid slug ensures good mixing

(Vanoye et al., 2013; Günther et al., 2004; Doraiswamy and Üner, 2014; Sobieszuk et al., 2012), and more importantly, could transport the oxygenates from the interface to the bulk liquid. Moreover, the short radial diffusion length of microfluidic reactors ensures better mixing and it leads to a narrow residence time distribution (RTD) (Kiwi-Minsker and Renken, 2012). These are potentially advantageous for preventing the over-oxidation of oxygenates in consecutive processes and for controlling the product selectivity. Another important advantage of microfluidic reactor is that oxidation can be conducted using pure oxygen with reduced risk of explosion (Jevtic et al., 2010; Vanoye et al., 2013; Hamano et al., 2012).

6.2 Experimental

6.2.1 Materials

The list of chemicals used in this study is given in **Table 6.1**. Tetralin, known as hydrogen-donor solvent, was selected as the model hydrocarbon due to its relevance to the energy industry and the richness of kinetic data. Di-*tert*-butyl peroxide (DTBP) was used as an initiator for few experiments to overcome initiation limitation.

Table 6.1. List of chemicals used in microfluidic study.

Name	CASRN [a]	Formula	Purity (wt %)		Supplier
			supplier [b]	analysis [c]	
tetralin	119-64-2	$C_{10}H_{12}$	99	98.9	Sigma-Aldrich
di-*tert*-butyl-peroxide	110-05-4	$C_8H_{18}O_2$	99	--[d]	Acros Organics
1,2,3,4-tetrahydro-1-naphthol	529-33-9	$C_{10}H_{12}O$	97	--[d]	Aldrich
α-tetralone	529-34-0	$C_{10}H_{10}O$	97	--[d]	Aldrich
hexachlorobenzene	118-74-1	C_6Cl_6	99	99.1	Supleco
chloroform	67-66-3	$CHCl_3$	99.1	98.1	Fisher Scientific

[a] CASRN = Chemical Abstracts Services Registry Number.

[b] This is the purity of the material guaranteed by the supplier.

[c] This is the purity based on peak area obtained by GC-FID analysis.

[d] Compounds were decomposed or were partially converted during GC-FID analysis and purity was not determined

The oxidized model compounds of tetralin-1,2,3,4-tetrahydro-1-naphthol and α-tetralone were used for identification by GC-MS (gas chromatography-mass spectrometry). Hexachlorobenzene (99 %, analytical standard, Supleco) was used as an internal standard in GC-FID (gas

chromatography with a flame ionization detector) analysis for conversion calculation and chloroform (98 %, HPLC grade, Fischer Scientific) was used as a solvent for GC analysis. Extra-dry oxygen (99.6 % molar purity, Praxair Inc., Canada) was used as an oxidizing agent and nitrogen (99.999 % molar purity, Praxair Inc., Canada) was used to control backpressure. Properties of oxygen and tetralin for all the experimental conditions are reported in **Appendix B** (**Table B.1**).

6.2.2 Equipment and Procedure

6.2.2.1 Oxidation in Microfluidic Reactor

A 1000 µl glass rectangular microfluidic reactor (**Figure 6.1**) having a mixing channel of depth = 1240 µm, width = 161 µm, length = 536 mm and reaction channel of depth = 1240 µm, width = 391 µm, length = 1844 mm were used for oxidation.

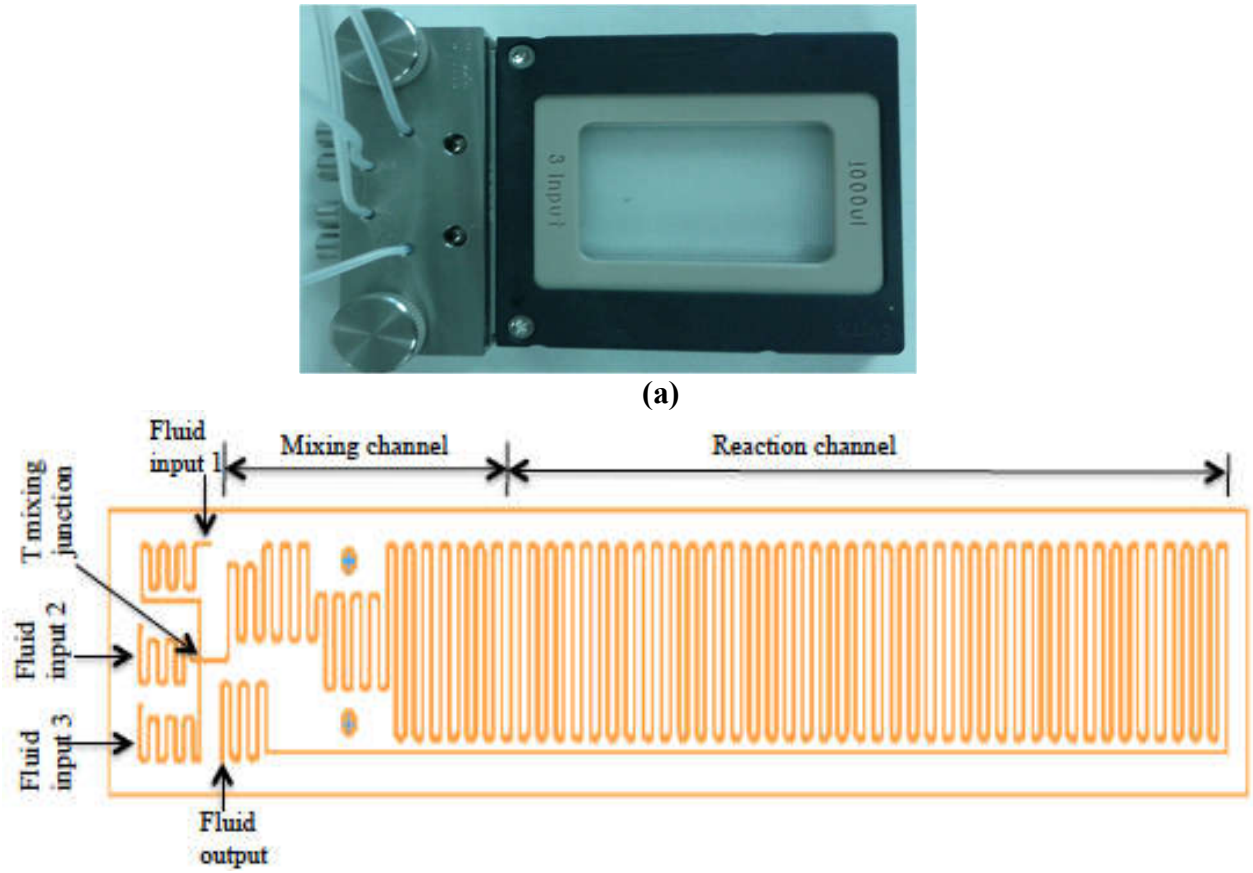

Figure 6.1. Microfluidic reactor (a) used in tetralin oxidation and its sketch (b).

The reactor had three inlet ports and one outlet port. Oxygen and tetralin were injected into the reactor using fluid input 1 and fluid input port 2, respectively, and port 3 was blocked. The dimensions of the reactor lead to a hydraulic diameter of the reaction channel of d_H=6.0×10^{-4} m and aspect ratio of the reaction channel of width/depth = 0.32. The experimental setup employed for this investigation is shown in **Figure 6.2**.

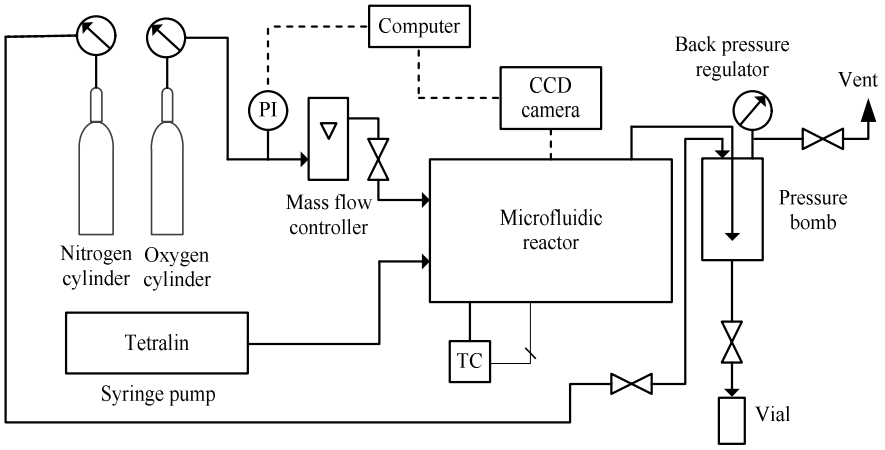

Figure 6.2. Experimental setup for tetralin oxidation by molecular oxygen.

The microfluidic experimental setup consisted of a microfluidic reactor (Dolomite Microfluidics, Charlestown, MA, USA), syringe pump (KDS-210, KD Scientific, USA), gas cylinder, pressure transducer (Swagelok, Canada), gas flow meter (Swagelok, Canada), pressure bomb (Swagelok, Canada), and backpressure regulator (Swagelok, Canada). A syringe pump and syringes (Model: 1005TLL, Hamilton Co., USA) were used to inject the tetralin into reactor at the desired flowrate. A Heidolph MR Hei-Standard hot plate (Model: 505-20000-01-2, Heldolph Instruments, Germany) was used to control the temperature of the microfluidic reactor system. An aluminum block was used to limit the gap between the hotplate and the reactor. Thermal adhesive (Dow Corning Corporation, Midland, MI, USA) was used to ensure better heat transfer between the aluminum block and the microfluidic reactor. Microfluidic reactor temperature was monitored using a surface mounted thermocouple (Model: CO 1, Cement-on Thermocouple, Omega Engineering, Inc., USA). A Flea3FL3-U3-13E4M camera (Point Grey Research Inc., Canada) was used to capture the images of gas bubbles and liquid slugs. A Fiber–Lite lamp (Model: 3100, Dolan-Jenner Industries, Inc., USA) was employed to improve lighting and thereby the image quality. The reactor was connected to the syringe pump, gas flow meter, and

pressure bomb through PTFE tubing, 1/16″ OD x 0.8 mm ID (Dolomite Microfluidics, Charlestown, MA, USA).

Oxidations were performed at low temperatures (120–160 °C) and pressure to control product selectivity. The barometric pressure at the test location was 90 95 kPa. Taylor flow conditions were maintained in which tetralin slugs were separated by elongated oxygen bubbles (**Figure 6.3**). In a typical experiment, tetralin was loaded into the 5 ml syringe. After the syringe was loaded and before tetralin was fed through the system, the system was pressurized to 90 kPa gauge by flowing pure oxygen through the system. Tetralin was then fed into the system using a syringe pump.

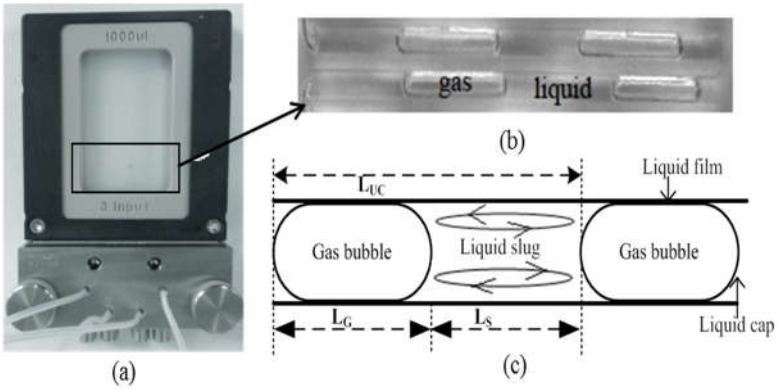

Figure 6.3. (a) Microfluidic reactor; (b) typical gas-liquid (tetralin-oxygen) slugs in a microfluidic reactor; (c) sketch of gas bubble-liquid slug to represent length of gas (oxygen) bubble (L_G), length of liquid (tetralin) slug (L_S), unit cell length (L_{UC}), liquid film and liquid cap. Liquid can circulate within liquid slug.

Gas-liquid slugs were formed due to the co-feed of tetralin and oxygen and applied backpressure using a backpressure regulator and nitrogen gas. The flowrate of the gas-liquid slug was controlled by observing the flow of gas-liquid slug and by changing the setting of backpressure regulator. The flow patterns of the gas and liquid were monitored during the experiment using a digital camera mounted above the microfluidic reactor. Tetralin and oxygen co-feed in Taylor flow condition was continued for twenty minutes, and the system was then depressurized. After the reaction, oxidized tetralin was collected from the pressure vessel using a needle valve, and stored for the instrumental analyses. After each experiment the reactor was flushed with acetone and dried by flowing nitrogen. Oxygen availability was manipulated by performing experiments at different injection rates (1 to 15 µL/min) of tetralin. Liquid slugs and gas bubbles of different

sizes were obtained. All of the experiments were performed in triplicate. Ten different slugs and gas bubbles from each experiment were used to calculate hydrodynamic parameters, mass transfer characteristics and oxygen availability. Oxidative conversion and product selectivity were calculated from the triplicate gas chromatographic analyses of the liquid phase products from each experiment.

6.2.2.2 Oxidation in Semi-Batch and Batch Reactor

Oxidation of tetralin with molecular oxygen was performed in a semi-batch reactor to determine the induction period for oxidation by measuring oxygen consumption, and to compare oxidative conversion and product selectivity achieved using the microfluidic reactor. The oxidation procedure was similar to that employed in the study of low-temperature autoxidation of various hydrocarbon classes (Siddiquee and De Klerk, 2014). Approximately 50 g of the tetralin was placed in a 250 mL three-necked round bottom flask, which was connected to a reflux condenser having a supply of chilled water (10 °C). Oxygen flow was controlled at 110 mL/min at near atmospheric pressure and ambient temperature, which is equivalent to about 125 mL oxygen /h per g of tetralin. Oxidation was performed at 150 °C for one hour. The temperature in the flask was controlled using a thermocouple in the solution connected to a Heidolph MR Hei-Standard heat-on-block heater. Small samples, approximately 0.5 g, were withdrawn from the flask at different time intervals to monitor the progress of oxidation. A cold trap was employed to ensure liquid free off-gas, which was then passed through a preweighed and pre-dried calcium chloride (Fisher Scientific, Canada) bed to absorb water vapor. Oxygen consumption and CO_2 production were continuously monitored by measuring liquid free off-gases using an O_2 and CO_2 analyzer (Series 9600, Alpha Omega Instruments, USA). Liquid free off-gases were also analyzed continuously using a mass spectrometer (Extorr XT Series RGA, XT300 M, Extorr, Inc., New Kensington, PA, USA).

In order to confirm that it is free radical conversion process one could perform control experiments by using radical trap. Also a control experiment with N_2 could indicate the thermal effect in free radical oxidation process. A free radical trap was not used in this study, but a control experiment of tetralin was performed with nitrogen and no products were identified via GC-MS analysis.

A 25 ml batch reactor manufactured from 316 standard stainless steel Swagelok fittings and tubing was used to compare the tetralin conversion and product selectivity with a microfluidic reactor. The reactor was equipped with a thermocouple and a pressure gauge to monitor the operating temperature and pressure, respectively. The batch reactor setup is shown in **Figure 6.4**.

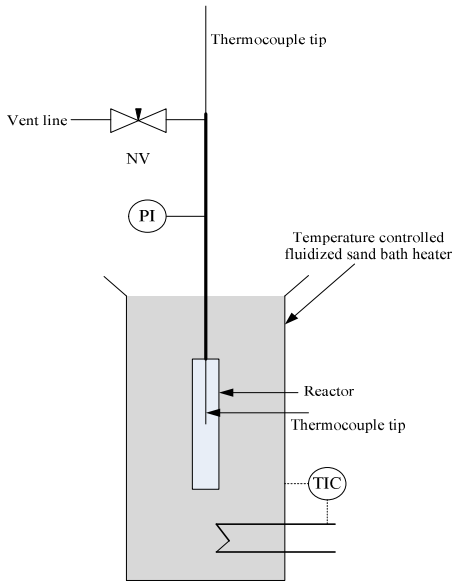

Figure 6.4. Batch reactor setup used in oxidation experiments.

Oxidation was performed at 130 °C for 2 min and 5 min after reaching the internal temperature within 1 °C of the heater temperature. The heat-up time required to reach an internal temperature within 1 °C of the heater temperature was six minutes. Tetralin was first charged into reactor, and then oxygen was introduced into the reactor by maintaining the liquid-to-gas volume and the operating pressure was the same value as used for the microfluidic reactor. The reactor was then submerged into a temperature controlled preheated sand-bath heater (Model: FSB-3, Omega Engineering, Inc., USA) to control the oxidation temperature. The reactor was removed from sand bath heater at the end of oxidation and allowed to cool for 10 minutes. Sands from the surface of the reactor were cleaned. The reactor was depressurized and liquid oxidation products were collected for chromatographic analyses to calculate oxidative conversion and product selectivity. A balance (Mettler-Toledo Model XP1203S, 1.2 kg weighing range, with 1 mg readability) was used to record the mass of the complete microreactor system after each step of the experiment.

6.2.3 Analyses

Gas chromatography with a flame ionization detector (GC-FID) and GC with mass spectrometry (GC-MS) were used to quantify and identify the oxidation products of tetralin. The analyzing procedure and conditions were similar to Sections 4.2.3(a) and 4.2.3(b). Details of product identification are available in Section 4.3.2.1.

A high-pressure differential scanning calorimeter (HP DSC) was used to evaluate the thermal behavior of the initiator (di-*tert*-butyl-peroxide). The instrument, Mettler-Toledo HP DSC 1, was equipped with an FRS-5 sensor employing 56 thermocouples, a Chiller (JULABO GmbHE, Germany) and a 400 W power amplifier. In a typical analysis, approximately 10 mg of sample was placed in an aluminum crucible with a pin (40 µL). The lid was pierced with a needle on a clean rubber surface and the crucible was sealed with a Mettler crucible sealing press. Measurements were conducted under a nitrogen atmosphere and at 1 MPa pressure. The temperature program was to heat the sample from 25 to 250 °C at different heating rates: 5 °C/min, 10 °C/min, 15 °C/min and 20 °C/min. These results are reported in Appendix B.

6.2.4 Calculations

Different hydrodynamic parameters and mass transfer coefficients were calculated from the captured images of flow in the microfluidic reactor as follows:

(a) Gas liquid interfacial area per unit liquid slug volume, a: this was calculated from the dimension of the rectangular channel reactor (h x w) and image analysis of gas bubbles and liquid slugs as shown in **Figure 6.3(c)**.

Surface area of gas bubble: $S_G = 2\left(wL_{G,actual} + \quad L_{G,actual}\right) + 4\pi((w + \quad)/4)^2$ (6.i)

$$L_{G,actual} = L_G \quad (w + \quad)/2 \tag{6.ii}$$

Volume of liquid slug: $V_L = w \;\; L_S + w \;\; [(w + \quad)/2] \quad (4/3)\pi[(w + \quad)/4]^3$ (6.iii)

Gas liquid interfacial area per unit liquid slug volume, $a = \; S_G/V_L$ (6.iv)

Here, S_G is the surface of the gas bubble, L_G and L_S are the lengths of the gas bubble and liquid slug respectively, and w and h are the width and depth of the reactor channel, respectively.

Approximated radius of the cap (**Figure 6.3(c)**) of liquid slug:

$$r_{cap} = (w + \quad)/4 \tag{6.v}$$

The approximation was made since geometry formed by the two liquid caps is not a complete sphere.

(b) Superficial liquid slug velocity, U_L and gas bubble velocity, U_G: these were calculated from the distance travelled by the slug and bubble in a particular time. Two phase superficial velocity (U_{TP}) was calculated as follows:

$$U_{TP} = \varepsilon_G U_G + (1 \quad \varepsilon_G) U_L \tag{6.vi}$$

Here, the volume fraction of gas bubble: $\varepsilon_G = \frac{V_G}{V_G + V_L}$ (6.vii)

V_L is the volume of liquid slug was calculated according to equation (6.iii).

V_G is the volume of gas bubble:

$$V_G = w \; L_{G,actual} + (4/3)\pi((w + \quad)/4)^2 \tag{6.viii}$$

(c) Average residence time: this was calculated from the two-phase superficial velocity (U_{TP}) and the reactor length.

(d) Liquid film thickness surrounding a gas bubble, δ: this was calculated from the captured images and also using the correlations provided by Yun et al. (2010) for a rectangular microchannel as follows:

$$\frac{\delta_{\max}}{D_h} = 0.39\, We^{0.09} \tag{6.ix}$$

$$\frac{\delta_{\min}}{D_h} = 0.02\, We^{0.6\ 2} \tag{6.x}$$

Here, Weber number, $We = \frac{D_h U_T^2 \rho_l}{\sigma_l}$ (6.xi)

Hydraulic diameter of the channel (m), $D_h = 2[w \;/(w + \quad)]$ (6.xii)

$\delta_{\max}$ and $\delta_{\min}$ are the maximum and minimum thicknesses of the liquid film (m), respectively.

U_{TP} (m/s) is the two phase superficial gas velocity, ρ_l is the density of liquid and σ_l is the surface tension of liquid (N/m).

w and h are the width and depth of the reactor channel, respectively.

(e) Volumetric mass transfer coefficient, $k_L a$ (s^{-1}): this was calculated using film theory (Doraiswamy and Üner, 2014; Gemoets et al., 2016):

$$k_L = \frac{D_A}{\delta} \quad \text{(6.xiii)}$$

Here, D_A is the diffusivity of oxygen in tetralin, δ is the thickness of liquid film surrounding the oxygen bubble.

Calculations performed using of the results obtained by analysis of the products using gas chromatography were:

(f) Product selectivity: this was calculated from the relative peak area of the products as follows:

$$\text{Product selectivity (\%)} = \frac{\text{relative peak area of specific product}}{\text{sum of relative peak area of all the products}} \text{ x } 100\% \quad \text{(6.xiv)}$$

Ketone-to-alcohol selectivity in primary oxidation products was calculated from the relative peak areas of ketones and alcohols as determined by GC-FID in primary oxidation products.

(g) Calculation of GC-FID response factor and tetralin conversion is included in **Appendix B (Tables B2 and B3)**. Flame ionization detector response factors for the feed materials were used to calculate conversion. Response factors for products were not used in the selectivity calculations, due to the diversity of oxidation products.

6.3 Results

6.3.1 Role of Oxygen Availability on Conversion and Selectivity

The experimental parameter that influenced oxygen availability most, without changing the oxygen partial pressure, is the gas-liquid interfacial area. A series of experiments were conducted at different flow conditions to evaluate the role of oxygen availability on conversion and selectivity. Conditions of low conversion were selected so that initial product selectivity values could be obtained.

6.3.1.1 Reactor Hydrodynamics

It was necessary to characterize the hydrodynamic behavior of the microfluidic reactor. This was accomplished by taking pictures of the flow under different flow conditions of interest. Five different flow conditions were employed. Flow conditions were manipulated to achieve a range of gas-liquid interfacial areas (*a*), Series A having the largest *a*, and Series E having the lowest *a*.

The measurements and calculated film thickness, gas-liquid transfer area and mass transfer coefficient are reported. **Tables 6.2A** and **6.2B** show hydrodynamic parameters, mass transfer coefficients and gas-liquid interfacial area (oxygen availability) for the oxidation performed at 150 °C and 90 kPa gauge by using pure oxygen as oxidizing agent.

Two-phase superficial velocity (U_{TP}) varied with different sizes of the slugs and gas bubbles and was a consequence of the manipulation of gas-liquid flow ratio. The highest two-phase superficial velocity was 2.6×10^{-2} m/s, which was obtained in the case of smaller liquid slugs and larger gas bubbles (series A). Residence time decreased with increasing two-phase superficial velocity (U_{TP}).

Table 6.2A. Hydrodynamic properties, mass transfer coefficients and oxygen availability during tetralin oxidation performed with oxygen at 150 °C and 90-95 kPa gauge pressure.

Series	experimental [a]						
	length of liquid slug, $L_S\times10^3$ (m)	length of bubble, $L_G\times10^2$ (m)	superficial liquid velocity, $U_S\times10^2$ (m/s)	superficial bubble velocity, $U_G\times10^2$ (m/s)	two-phase superficial velocity, $U_{TP}\times10^2$ (m/s)	residence time (min)	gas-liquid interfacial area, a $\times10^{-4}$ (m^2/m^3)
A	1.6 ± 0.5	2.1×10^1 ± 5.3	2.6 ± 1.0	2.6 ± 1.0	2.6 ± 1.0	1.5 ± 0.4	3.0×10^1 ± 5.2
B	2.7 ± 0.3	9.8 ± 4.1	2.1 ± 0.4	2.1 ± 0.4	2.1 ± 0.4	1.8 ± 0.4	1.5×10^1 ± 4.7
C	4.9 ± 1.9	5.1 ± 1.5	2.0 ± 0.7	2.0 ± 0.7	2.0 ± 0.7	2.0 ± 0.7	6.2 ± 1.8
D	4.3 ± 0.6	$1.1 \pm 4.1\times10^{-1}$	1.6 ± 0.5	1.6 ± 0.5	1.6 ± 0.5	2.4 ± 0.8	$1.6 \pm 5.8\times10^{-1}$
E	4.9 ± 0.6	$0.4 \pm 6.0\times10^{-2}$	1.1 ± 0.2	1.1 ± 0.2	1.1 ± 0.2	3.5± 0.7	$5.4\times10^{-1} \pm 1.3\times10^{-3}$

[a] based on 30 different slugs of each series of experiments

Table 6.2B. Hydrodynamic properties, mass transfer coefficients and oxygen availability during tetralin oxidation performed with oxygen at 150 °C and 90-95 kPa gauge pressure.

Series	calculated based on equation (x) [a]			calculated based on equation (ix)[a]		
	film thickness, $\delta_{min}\times10^6$ (m)	mass transfer coefficient, $k_L\times10^3$ (m/s) [b]	liquid side volumetric mass transfer coefficient, $k_La\times10^{-2}$ (s^{-1})	film thickness, $\delta_{max}\times10^4$ (m)	mass transfer coefficient, $k_L\times10^4$ (m/s) [b]	liquid side volumetric mass transfer coefficient, $k_La\times10^{-1}$ (s^{-1})
A	$5.4 \pm 3\times10^{-2}$	$6.3 \pm 3.1\times10^{-2}$	1.9×10^1 ± 3.3	$1.6 \pm 9.0\times10^{-2}$	$2.2 \pm 1.1\times10^{-1}$	6.4 ± 1.2
B	$5.4 \pm 2\times10^{-2}$	$6.3 \pm 2.4\times10^{-2}$	9.6 ± 2.9	$1.5 \pm 4.8\times10^{-2}$	$2.2 \pm 7.4\times10^{-2}$	3.4 ± 1.1
C	$5.4 \pm 3\times10^{-2}$	$6.3 \pm 3.8\times10^{-2}$	3.9 ± 1.1	$1.5 \pm 1.0\times10^{-1}$	$2.3 \pm 1.5\times10^{-1}$	$1.4 \pm 4.1\times10^{-1}$
D	$5.4 \pm 3\times10^{-2}$	$6.3 \pm 4.0\times10^{-2}$	$1.0 \pm 3.0\times10^{-1}$	$1.4 \pm 9.8\times10^{-2}$	$2.4 \pm 1.7\times10^{-1}$	3.7×10^{-1} ± 1.3×10^{-1}
E	$5.3 \pm 2\times10^{-2}$	$6.4 \pm 2.3\times10^{-2}$	$3.4\times10^{-1} \pm 8.0\times10^{-2}$	$1.3 \pm 5.4\times10^{-2}$	$2.5 \pm 1.0\times10^{-1}$	1.4×10^{-1} ± 3.0×10^{-2}

[a] based on 30 different slugs of each series of experiments

[b] based on film theory and $k_L = {}^{D_A}/_{\delta}$

The maximum and minimum thicknesses of liquid film surrounding the gas bubble were calculated, respectively, based on Equations (6.ix) and (6.x). Minimum film thickness was

almost identical for all test conditions at 5.4×10^{-6} m and maximum film thickness was ~1.4×10^{-4} m for all experimental conditions.

Liquid side volumetric mass transfer coefficient was calculated using Equation (6.xiii). The mass transfer coefficient increased with increasing gas-liquid interfacial area, which was calculated using Equation (6.iv). The maximum liquid side volumetric mass transfer coefficient was 1.9×10^{3} s^{-1} and was obtained for minimum film thickness at the largest gas-liquid interfacial area, 3×10^{5} m^2/m^3 (Series A).

6.3.1.2 Conversion and Selectivity

The conversion and product selectivity data for the oxidation of tetralin with oxygen at different hydrodynamic conditions were determined (**Table 6.3**).

Table 6.3. Oxidative conversion and product selectivity of tetralin oxidation with oxygen at 150 °C and 90-95 kPa gauge pressure at different oxygen availabilities.

series	oxidative conversion [a] $\times10^{1}$(wt %)	selectivity of oxidation products (wt %) [a] primary	secondary	addition	ketone to alcohol in primary oxidation products [a]
A	7.4 ± 1.5	100	0	0	1.4×10^{1} ± 2.2
B	2.1 ± 1.0×10^{-1}	100	0	0	7.0 ± 2.0×10^{-1}
C	1.7 ± 1.0×10^{-1}	100	0	0	1.6 ± 2.0×10^{-1}
D	1.2 ± 1.0×10^{-1}	100	0	0	1.3 ± 1.0×10^{-1}
E	1.6 ± 1.0×10^{-1}	100	0	0	1.3 ± 1.0×10^{-1}

[a] calculated based on the GC-FID relative peak area of triplicate runs of each experiment

Conversion rates were very close at low gas-liquid interfacial area (**Figure 6.5**). When the gas-liquid interfacial area was increased by a factor ~5 it resulted in an increase in tetralin conversion by a factor ~8. Despite the magnitude of change in conversion rate, overall conversion remained low.

Selectivity of the products varied with gas-liquid interfacial area (**Figure 6.5**). Addition products and secondary oxidation products were not identified at the low conversion levels reported (**Table 6.3**). The ketone-to-alcohol selectivity in primary oxidation products increased by an order of magnitude as the gas-liquid interfacial area increased.

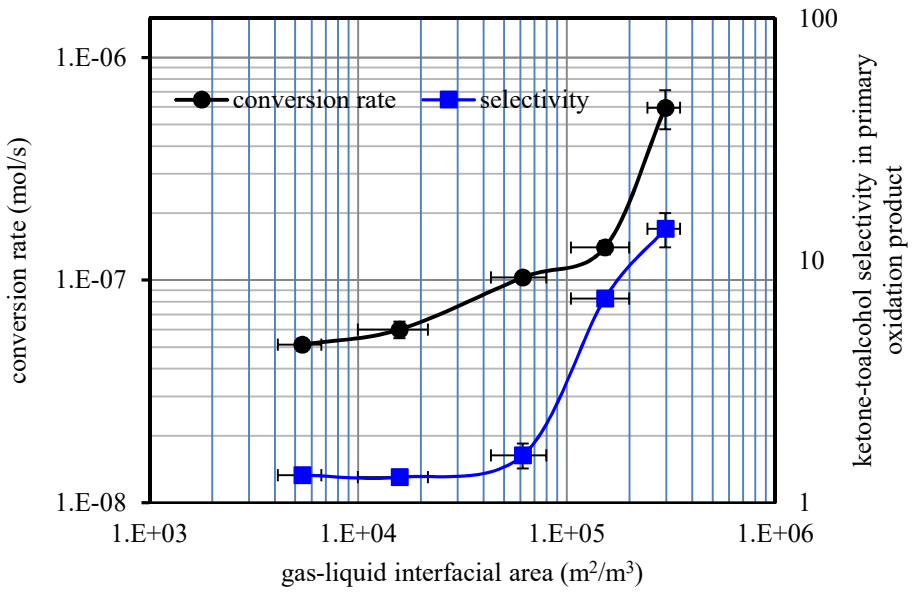

Figure 6.5. Effect of oxygen availability during tetralin oxidation with oxygen at 150 °C and 90-95 kPa gauge pressure [triplicate results for the experiment series A-E: (●) conversion rate and (■) product selectivity].

One could predict the mass transfer limitation due to the increase in slow conversion with interfacial area (oxygen availability). But the prediction could be misleading as the induction period at the level of oxygen was unknown. This could also be true for the change in selectivity with gas-liquid interfacial area.

The chromatograms of tetralin oxidized at 150 °C (Series A and Series E) are reported in **Appendix B** (**Figure B.1**) to illustrate the ketone-to-alcohol selectivity in the primary oxidation product**.**

6.3.2 Effect of Temperature and Initiator on Conversion and Selectivity

The conversion levels that could be achieved when manipulating the gas-liquid interfacial area in the microfluidic reactor were limited to less than 1 wt %. Although it enabled initial reaction selectivities to be determined, it did not provide any information on the influence on secondary oxidation. Secondary oxidation required somewhat higher conversion. The conversion range could be extended in two ways. First, by adding an oxidation initiator to reduce the initiation period. Second, by increasing the temperature of oxidation. Both strategies were explored.

Di-*tert*-butyl peroxide was used as an initiator and five different temperatures (120–160 °C) were maintained. Liquid flow rate was constant at 10 µL/min. Like oxygen availability investigation, experiments were performed at low pressure (90-95 kPa gauge) and oxygen was used as oxidizing agent.

6.3.2.1 Reactor Hydrodynamics

Hydrodynamic parameters, mass transfer coefficients and gas-liquid interfacial area (oxygen availability) for the oxidation performed to investigate the effects of temperatures and initiator are reported (**Tables 6.4A** and **6.4B**).

Table 6.4A. Hydrodynamic properties, mass transfer coefficients and oxygen availability of tetralin oxidized at 90-95 KPa gauge pressure and different temperature using oxygen as oxidizing agent.

series	reactants	temperature (°C)	experimental [a]						
			length of liquid slug, L_S $\times 10^3$ (m)	length of gas bubble, L_G $\times 10^3$ (m)	liquid slug velocity, $U_S \times 10^2$ (m/s)	bubble velocity, U_G $\times 10^2$ (m/s)	two-phase superficial velocity, U_{TP} $\times 10^2$ (m/s)	residence time (min)	gas-liquid interfacial area, a $\times 10^{-4}$ (m^2/m^3)
F	Tetralin	120	3.5 ± 0.4	8.0 ± 1.7	1.1 ± 0.1	1.1 ± 0.1	1.1 ± 0.1	3.4 ± 0.7	$1.4 \pm 3.1 \times 10^{-1}$
G		130	3.8 ± 0.5	8.4 ± 2.8	1.8 ± 0.1	1.8 ± 0.1	1.8 ± 0.1	2.0 ± 0.7	$1.4 \pm 4.5 \times 10^{-1}$
H		140	3.7 ± 0.3	8.7 ± 2.4	1.3 ± 0.1	1.3 ± 0.1	1.3 ± 0.1	2.9 ± 1.1	$1.4 \pm 3.8 \times 10^{-1}$
I		150	4.3 ± 0.6	$1.1 \times 10^1 \pm 4.1$	1.6 ± 0.5	1.6 ± 0.5	1.6 ± 0.5	2.4 ± 0.8	$1.6 \pm 5.8 \times 10^{-1}$
J		160	3.7 ± 0.4	9.4 ± 2.3	1.4 ± 0.1	1.4 ± 0.1	1.4 ± 0.1	2.7 ± 1.3	$1.5 \pm 3.7 \times 10^{-1}$
K [b]	Tetralin with 0.5 wt% DTBP [c]	120	3.4 ± 0.4	8.2 ± 2.2	1.5 ± 0.1	1.5 ± 0.1	1.5 ± 0.1	2.4 ± 0.6	$1.4 \pm 4.5 \times 10^{-1}$
L [b]		130	3.6 ± 0.4	7.9 ± 2.3	2.0 ± 0.8	2.0 ± 0.8	2.0 ± 0.8	2.0 ± 0.8	$1.3 \pm 4.2 \times 10^{-1}$
M [b]		140	3.7 ± 0.5	7.8 ± 3.0	1.9 ± 0.1	1.9 ± 0.1	1.9 ± 0.1	2.0 ± 0.7	$1.3 \pm 5.1 \times 10^{-1}$
N [b]		150	3.7 ± 0.3	6.9 ± 1.6	1.4 ± 0.4	1.4 ± 0.4	1.4 ± 0.4	2.6 ± 0.7	$1.2 \pm 2.7 \times 10^{-1}$
O [b]		160	4.1 ± 0.3	9.8 ± 2.8	1.5 ± 0.0	1.5 ± 0.0	1.5 ± 0.0	2.5 ± 0.7	$1.4 \pm 3.4 \times 10^{-1}$

[a] based on 30 different slugs of each series of experiments
[b] the experiments performed in the presence of 0.5 wt% initiator (di-*tert*-butyl peroxide)
[c] DTBP(di-*tert*-butyl peroxide) was used as an initiator

Table 6.4B. Hydrodynamic properties, mass transfer coefficients and oxygen availability of tetralin oxidized at 90-95 KPa gauge pressure and different temperature using oxygen as oxidizing agent.

series	reactants	temperature (°C)	calculated based on equation (x) [a]			calculated based on equation (ix) [a]		
			film thickness, δ_{min} $\times 10^6$ (m)	mass transfer coefficient, k_L $\times 10^3$ (m/s) [d]	liquid side volumetric mass transfer coefficient, $k_L a \times 10^{-1}$ (s^{-1})	film thickness, δ_{max} $\times 10^4$ (m)	mass transfer coefficient, k_L $\times 10^4$ (m/s) [d]	liquid side volumetric mass transfer coefficient, $k_L a$ (s^{-1})
F	Tetralin	120	$5.3 \pm 1.8 \times 10^{-2}$	$4.0 \pm 1.4 \times 10^{-2}$	5.6 ± 1.3	$1.3 \pm 5.1 \times 10^{-2}$	$1.6 \pm 6.0 \times 10^{-2}$	$2.2 \pm 5.0 \times 10^{-1}$
G		130	$5.4 \pm 2.6 \times 10^{-2}$	$4.7 \pm 2.2 \times 10^{-2}$	6.4 ± 2.1	$1.5 \pm 7.8 \times 10^{-2}$	$1.7 \pm 9.2 \times 10^{-2}$	$2.4 \pm 8.5 \times 10^{-1}$
H		140	$5.4 \pm 3.3 \times 10^{-2}$	$5.5 \pm 3.3 \times 10^{-2}$	7.7 ± 2.0	$1.4 \pm 9.4 \times 10^{-2}$	$2.1 \pm 1.4 \times 10^{-1}$	$3.0 \pm 7.9 \times 10^{-1}$
I		150	$5.4 \pm 3.3 \times 10^{-2}$	$6.3 \pm 4.0 \times 10^{-2}$	9.9 ± 3.6	$1.5 \pm 9.8 \times 10^{-2}$	$2.4 \pm 1.7 \times 10^{-1}$	3.7 ± 1.3
J		160	$5.4 \pm 3.3 \times 10^{-2}$	$7.3 \pm 4.4 \times 10^{-2}$	$1.1 \times 10^{1} \pm 2.7$	$1.4 \pm 9.3 \times 10^{-2}$	$2.8 \pm 1.9 \times 10^{-1}$	4.3 ± 1.1
K [b]	Tetralin with 0.5 wt% DTBP [c]	120	$5.4 \pm 1.8 \times 10^{-2}$	$4.0 \pm 1.4 \times 10^{-2}$	5.9 ± 1.8	$1.4 \pm 5.4 \times 10^{-2}$	$1.5 \pm 5.9 \times 10^{-2}$	$2.2 \pm 6.7 \times 10^{-1}$
L [b]		130	$5.4 \pm 3.5 \times 10^{-2}$	$6.3 \pm 4.1 \times 10^{-2}$	8.4 ± 2.6	$1.5 \pm 1.1 \times 10^{-1}$	$2.3 \pm 1.6 \times 10^{-1}$	$3.0 \pm 9.0 \times 10^{-1}$
M [b]		140	$5.4 \pm 2.7 \times 10^{-2}$	$5.5 \pm 2.7 \times 10^{-2}$	7.1 ± 2.8	$1.5 \pm 8.0 \times 10^{-2}$	$2.0 \pm 1.1 \times 10^{-1}$	2.6 ± 1.0
N [b]		150	$5.4 \pm 2.5 \times 10^{-2}$	$6.3 \pm 3.0 \times 10^{-2}$	7.6 ± 1.7	$1.4 \pm 7.5 \times 10^{-2}$	$2.4 \pm 1.2 \times 10^{-1}$	$2.9 \pm 6.1 \times 10^{-1}$
O [b]		160	$5.4 \pm 2.4 \times 10^{-2}$	$7.0 \pm 4.3 \times 10^{-2}$	$1.0 \times 10^{1} \pm 2.7$	$1.4 \pm 7.3 \times 10^{-2}$	$2.6 \pm 2.2 \times 10^{-1}$	$3.8 \pm 9.2 \times 10^{-1}$

[a] based on 30 different slugs of each series of experiments
[b] the experiments performed in the presence of 0.5 wt% initiator (di-*tert*-butyl peroxide)
[c] DTBP(di-*tert*-butyl peroxide) was used as an initiator
[e] based on film theory and $k_L = {}^{D_A}/_{\delta}$

Reported parameters were varied due to the variation of temperatures and the presence of initiator. Size of liquid slugs varied between 3.4×10^{-3} m (Series K) and 4.3×10^{-3} m (Series I). Gas bubbles changed within 6.9×10^{-3} m (Series N) and 1.1×10^{-3} m (Series I). Slugs and gas bubbles of different sizes resulted variation in superficial liquid velocity (U_S), superficial bubble velocity (U_G), two-phase superficial velocities (U_{TP}), residence times and gas-liquid interfacial area (a). Gas-liquid interfacial area varied between 1.2×10^4 m^2/m^3 (Series N) and 1.6×10^4 m^2/m^3 (Series I).

Like the observations made when manipulating oxygen availability, the calculated minimum thicknesses of liquid film surrounding the gas bubble was almost identical for all experimental conditions, 5.4×10^{-6} m and maximum film thickness was ~1.4×10^{-4} m for all experimental conditions.

Liquid side mass transfer coefficient (k_L) was increased from 4×10^{-3} m/s to 7×10^{-3} m/s for minimum film thickness and 2.2 m/s to 4.3 m/s for maximum film thickness as temperature increased from 120 °C to 160 °C. Liquid side volumetric mass transfer coefficient ($k_L a$) was increased with increasing temperature and gas-liquid interfacial area, which was calculated using

Equation (6.iv). The maximum liquid side volumetric mass transfer coefficient was 1.1×10^{2} s^{-1} and was obtained at 160 °C and at 1.5×10^{5} m^2/m^3 (Series J) gas-liquid interfacial area.

6.3.2.2 Conversion and Selectivity

As anticipated, conversion rate increased with oxidation temperature for both tetralin and tetralin with initiator (**Figure 6.6**) at temperatures higher than 130 °C. Conversion rates were almost constant at temperatures below 130 °C. Maximum conversion rate was 1.6×10^{-6} mol/s for tetralin oxidized with 5 wt % initiator at a temperature of 160 °C, and conversion rate was 2×10^{-7} mol/s for tetralin oxidized without initiator at a temperature of 160 °C. Conversion rate at 160 °C was increased by an order of magnitude due to the use of 5 wt % initiator. Selectivity of ketone-to-alcohol was also changed with conversion (**Figure 6.6**).

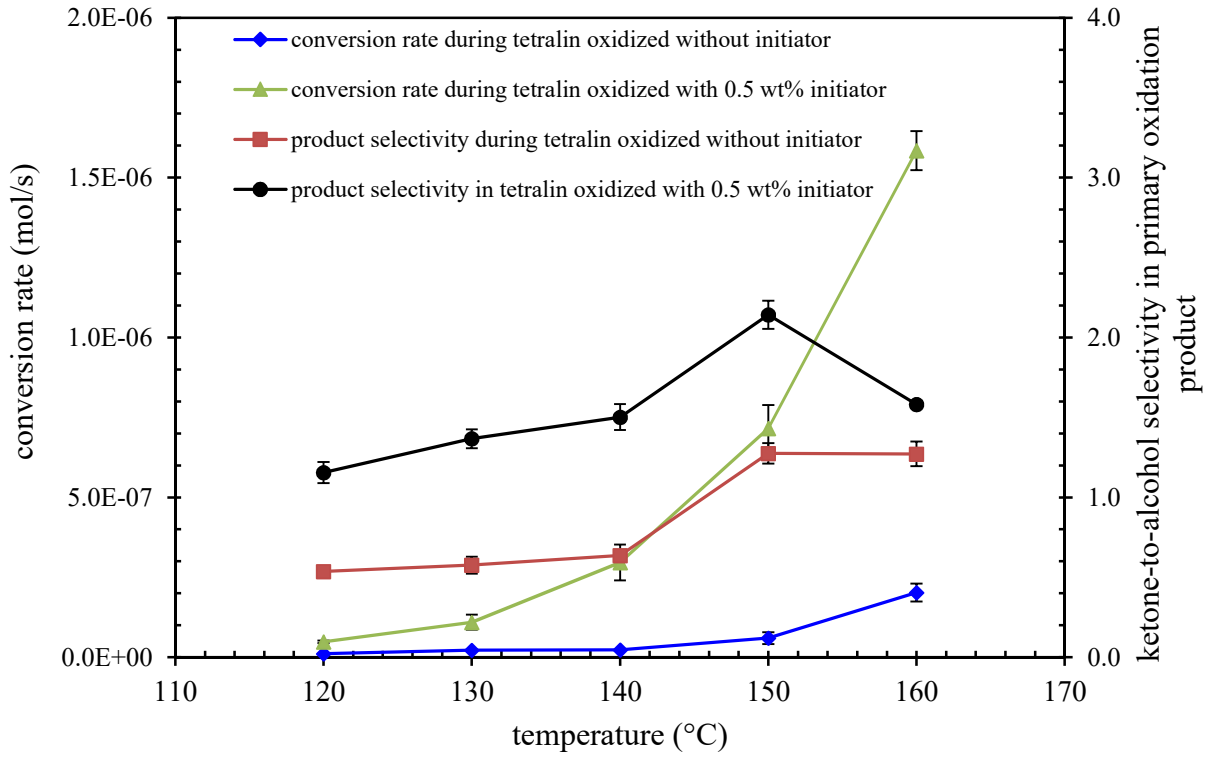

Figure 6.6. Effect of temperature on conversion rate [triplicate results: tetralin ( ) and tetralin with initiator (▲)] and product selectivity [triplicate results: tetralin (■) and tetralin with initiator (●)] during tetralin oxidation with oxygen in the presence or absence of initiator (0.5 wt % di-*tert*-butyl peroxide) at 90 kPa gauge pressure.

Table 6.5. Product selectivity during tetralin oxidation with oxygen at 150 °C and 90-95 KPa gauge pressure in the presence/ absence of initiator (di-*tert*-butyl peroxide).

series	T (°C)	oxidative conversions [b, c] × 10^2 (wt %)	selectivity of oxidation products (wt %) [b, c]			ketone-to-alcohol in primary oxidation products [b] ($\times 10^1$)
			primary	secondary	addition	
F	120	3.0 ± 1.0	100	0	0	$5.4 \pm 1.0 \times 10^{-1}$
G	130	4.0 ± 1.0	100	0	0	$5.7 \pm 5.0 \times 10^{-1}$
H	140	6.0 ± 1.0	100	0	0	$6.4 \pm 3.0 \times 10^{-1}$
I	150	$1.2 \times 10^1 \pm 4.0$	100	0	0	$1.3 \times 10^1 \pm 6.0 \times 10^{-1}$
J	160	$4.4 \times 10^1 \pm 6.0$	100	0	0	$1.3 \times 10^1 \pm 8.0 \times 10^{-1}$
K [a]	120	$1.0 \times 10^1 \pm 1.0$	100	0	0	$1.2 \times 10^1 \pm 6.0 \times 10^{-1}$
L [a]	130	$1.8 \times 10^1 \pm 4.0$	100	0	0	$1.4 \times 10^1 \pm 6.0 \times 10^{-1}$
M [a]	140	$5.0 \times 10^1 \pm 9.0$	100	0	0	$1.5 \times 10^1 \pm 8.0 \times 10^{-1}$
N [a]	150	$1.6 \times 10^2 \pm 1.6 \times 10^1$	95.5	2.8	1.4	$2.1 \times 10^1 \pm 9.0 \times 10^{-1}$
O [a]	160	$3.3 \times 10^2 \pm 1.3 \times 10^1$	90.0	5.1	4.9	$1.6 \times 10^1 \pm 2.0 \times 10^{-1}$

[a] the experiments conducted in the presence of 0.5 wt% initiator (di-*tert*-butyl peroxide)
[b] calculated based on the GC-FID relative peak area of triplicate runs of each experiment
[c] selectivity and conversion of tetralin oxidized in presence of 0.5 wt% initiator (di-*tert*-butyl peroxide) was calculated by subtracting the product formed due to the initiator before oxidation in microfluidic reactor

Table 6.5 summarizes the oxidative conversion product selectivity of tetralin oxidized at different temperatures and oxygen availabilities with and without initiator. Primary products (alcohol and ketone) were observed in all cases; but secondary and addition products were observed during tetralin oxidation performed with 0.5 wt % initiator at temperatures 150 °C and 160 °C. Ketone-to-alcohol formation was varied with temperature and initiator (di-*tert*-butyl peroxide). In the case of tetralin oxidation at temperatures 120–140 °C without initiator, alcohol formation dominated over ketone formation (**Table 6.5**), however, at temperatures 150–160 °C, tetralin oxidations without initiator formed ketones as major products compared to alcohols in the primary oxidation products. Oxidation performed in the presence of initiator resulted in dominant ketone formation compared to alcohol as primary oxidation products. Maximum ketone-to-alcohol selectivity in the primary oxidation product was 2.1 (Series N) which was obtained at the temperature of 150 °C, but the ratio decreased to 1.6 (Series O) at the temperature 160 °C.

6.3.3 Microfluidic Reactor Compared to Batch and Semi-batch Reactors

Gas-liquid interfacial area and hence oxygen availability was also manipulated by using reactors of different geometries. Oxidation was performed in batch and semi-batch reactors to compare

the oxidative conversion and product selectivity with oxidation performed in a microfluidic reactor. Oxidation induction period was also determined from the oxidation performed in a semi-batch reactor.

Oxidation performed in all three reactors in our experiments showed very low conversion (about 0.1 wt %) after 2 to 6 minutes at oxidation conditions (**Table 6.6**). Low oxidation conversion enabled direct comparison of selectivities and provided information about the initial selectivity of oxidation in the different reactors.

Table 6.6. Comparison of oxidative conversion and product selectivity during tetralin oxidation performed in different reactors.

reactor type	series	temperature	residence/ oxidation time (min)	gas-liquid interfacial area [d] (a, m^2/m^3)	oxidative conversion (wt%) [e]	selectivity of oxidation products (wt %) [e]			ketone to alcohol in primary oxidation products [e]
						primary	secondary	addition	
microfluidic [a]	G	130	2.0	1.4×10^4	0.1	100	0	0	0.6
	I	150	2.4	1.6×10^4	0.1	100	0	0	1.3
batch [b]	P	130	2	2.4×10^1	0.1	100	0	0	0.6
	Q	130	5	2.4×10^1	0.1	100	0	0	0.8
semi-batch [c]	R1	150	2	9.8×10^2	0.1	100	0	0	1.3
	R2	150	4	9.8×10^2	0.1	100	0	0	1.3
	R3	150	6	9.8×10^2	0.1	100	0	0	1.4
	R4	150	10	9.8×10^2	0.2	100	0	0	1.8
	R5	150	15	9.8×10^2	0.5	100	0	0	2.0
	R6	150	30	9.8×10^2	2.0	96	1	3	2.0
	R7	150	45	9.8×10^2	2.9	91	2	7	2.0
	R8	150	60	9.8×10^2	4.5	88	1	11	1.1

[a] oxidation performed with pure oxygen at 90-95 KPa pressure gauge at the tetralin input rate of 10 µL/min.
[b] oxidation performed with pure oxygen at 90-95 kPa pressure gauge using tetralin-to-oxygen volume identical to microfluidic reactor
[c] oxidation performed with pure oxygen at near atmospheric pressure.
[d] calculated based on the geometry of the reactors
[e] calculated based on the GC-FID relative peak area of triplicate runs

Ketone-to-alcohol selectivity in primary oxidation products was identical (0.6:1.0) for the oxidation performed at 130 °C in microfluidic and batch reactor for two minutes. Identical ketone-to-alcohol selectivity (1.3:1.0) was also observed for the oxidation completed in microfluidic reactor and semi-batch batch reactor (series R1–R3) at 150 °C.

Induction time was fourteen min (**Figure 6.7**) for the oxidation of tetralin in a semi-batch reactor at 150 °C having an oxygen flowrate of 124–130 mL/h per g tetralin. During the induction period, oxygen consumption and oxidation rate was low; ketone-to-alcohol selectivity in primary oxidation products was 1.3:1.0 in first 6 minutes.

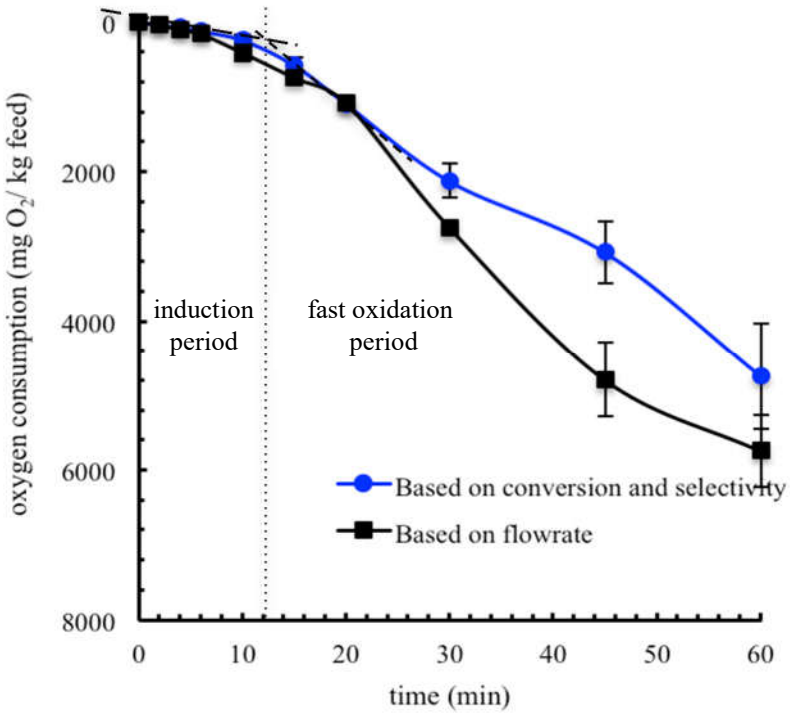

Figure 6.7. Oxygen consumption over time during the oxidation of tetralin at 150 °C using 124-130 mL oxygen/ h per g feed [triplicate results: (●) based on conversion and product selectivity (water generation was not considered)) and (■) based on oxygen flowrates].

6.3.4 Changes in Selectivity with Conversion

Tetralin was oxidized in a semi-batch reactor at 150 °C at near atmospheric pressure for longer oxidation time (**Table 6.6**) to understand the role of conversion on selectivity beyond the induction time.

Oxidation rate was increased after the induction time (14 minutes). Maximum conversion of 4.5 wt % was obtained after one hour oxidation (Series R). Multifunctional groups containing oxidation products (secondary products) and addition products (dimerized products containing

functional groups) were observed after 30 minutes of oxidation in semi-batch reactor. Those products were not observed in case of microfluidic and batch reactor at the studied experimental conditions. Maximum addition product selectivity was 11 wt % which was observed after one hour of oxidation at 150 °C (Series R).

After the induction period (15–45 minutes), ketone-to-alcohol selectivity in primary oxidation products was constant at 2.0:1.0, but the ratio decreased to 1.1:1.0 after 45 minutes of oxidation indicating increasing alcohol production compared to ketone. Similar observation was noticed for the oxidation of tetralin in microfluidic reactor in the presence of di-*tert*-butyl peroxide initiator (**Figure 6.6** and **Table 6.5**).

Approximately 1000 mg H_2O/kg tetralin was produced in the course of 1–hour oxidation of tetralin in semi-batch reactor at 150 °C having an oxygen flowrate of 124–130 mL/h per g tetralin. The change in CO_2 was insignificant (0.4 mg CO_2/kg tetralin) and no acid product was identified during one hour of oxidation. The online mass spectrometer also did not detect any other gases except feed gases.

6.4. Discussion

6.4.1 Oxidation Selectivity

It is clear from all the selectivity data that alcohol and ketones are the two main primary oxidation products regardless of experimental conditions and of the reactor types. Although alcohols and ketones are generally formed at 1:1 ratio according to Reaction (6.6) of **Table 6.7** for compounds having secondary carbons (De Klerk, 2003; Emanuel et al., 1967; Russell, 1957), different alcohol to ketone selectivities are observed that describe the nature of the propagation and termination. Alcohol and ketone selectivities are discussed separately:

6.4.1.1 Alcohol Selectivity

Chain propagation by the decomposition of alkyl hydroperoxide (ROOH) can play a role in alcohol selectivity. In addition to the thermal homolytic decomposition of alkyl hydroperoxides shown in Reaction (6.3) of **Table 6.7**, bimolecular decomposition according to Reaction (6.7)

and radial induced decomposition shown as Reaction (6.8) can also occur (De Klerk, 2003; Emanuel et al., 1967). Alcohol is produced during radial induced decomposition of hydroperoxide in Reaction (6.8).

Table 6.7. Free radical mechanism of tetralin oxidation with molecular oxygen and corresponding activation energy, pre-exponential factor, and reaction rate constant (Emanuel et al., 1967).

reaction		activation energy, $E_a \times 10^{-1}$ (kJ/mol)	pre-exponential factor (A) [b]	reaction rate constant (k_r) [b]
$RH + O_2 + RH \xrightarrow{k_i} 2\dot{R} + H_2O_2$	(6.0)	8.7[1]	3.5×10^{3} L^2/mol^2. s	7.1×10^{-8} L^2/mol^2. s
$R^{\cdot} + O_2 \xrightarrow{k_1} R\dot{O}_2$	(6.1)	0.0	6.8×10^{7} L/mol. s	6.8×10^{7} L/mol. s
$R\dot{O}_2 + RH \xrightarrow{k_2} ROOH + R^{\cdot}$	(6.2)	1.9	2.5×10^{4} L/mol. s	120 L/mol. s
$ROOH \xrightarrow{k_3} R\dot{O} + O\dot{H}$	(6.3)	1.0×10^{1}	9.3×10^{8} s^{-1}	2.29×10^{-4} s^{-1}
$R^{\cdot} + R^{\cdot} \xrightarrow{k_4} R{-}R$	(6.4)	1.1	5.5×10^{8} L/mol. s	2.5×10^{7} L/mol. s
$R\dot{O}_2 + R^{\cdot} \xrightarrow{k_5} ROOR$	(6.5)	-[a]	-[a]	-[a]
$R\dot{O}_2 + R\dot{O}_2 \xrightarrow{k_6} ROH + R_1COR_2 + O_2$	(6.6)	1.7×10^{-1}	4.2×10^{7} L/mol. s	2.6×10^{7} L/mol. s

[a] not reported
[b] calculated for the reaction temperature, 150 °C.

$$2ROOH \longrightarrow R\dot{O} + R\dot{O}_2 + H_2O \quad (6.7)$$

$$ROOH + R\dot{O}_2 \longrightarrow ROH + R\dot{O} + O_2 \quad (6.8)$$

Alkoxy radicals ($RO^{\cdot}$) form in all cases and it plays an important role in changing the product selectivity. It can form alcohol via hydrogen abstraction from α-position of aromatic ring of tetralin as illustrated by generic Reactions (6.9) and (6.10) (De Klerk, 2003).

$$R\dot{O} + RH \longrightarrow ROH + \dot{R} \quad (6.9)$$

$$ROOH + RH \longrightarrow [R\dot{O} + H\dot{O}] + RH \longrightarrow ROH + \dot{R} + H\dot{O} \quad (6.10)$$

Alkoxy radicals can also form alcohol through hydrogen disproportionation, Reaction (6.11), and alkyl peroxide via free radical addition, Reaction (6.12) (Tolman et al., 1989).

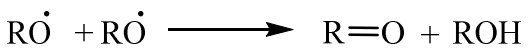

(6.11)

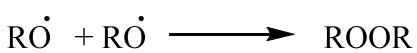

(6.12)

Alcohols can readily form by Reaction (6.8). The Reactions (6.9) and (6.10) result in alcohol only if the alkoxy radical ($RO^{\cdot}$) exists without *in situ* reaction within the molecular cage (De Klerk, 2003). Alcohol production through Reaction (6.11) also produces ketone in 1:1 ratio and cannot be the cause of higher alcohol than ketone selectivity. Hence, Reaction (6.8) would explain the higher alcohol than ketone selectivity during the oxidation of tetralin without initiator at low temperatures (series F-H in **Table 6.5** and series G, P, Q in **Table 6.6**).

6.4.1.2 Ketone Selectivity

In addition to the ketone formation mentioned in Reactions (6.6) and (6.11), ketones are formed by the Reactions (6.13) and (6.14) (De Klerk, 2003; Emanuel et al., 1967; Hendry et al., 1976). Ketone formation by Reaction (6.14) involves formation of alkyl peroxy radicals via hydrogen abstraction from the C-H bond adjacent to peroxy groups. Ketone formation via Reaction (6.13) depends on the reaction within the molecular cage. Reactions (6.8), (6.10), (6.13) and (6.14) take place in direct competition because these are involved with the consumption of alkyl hydroperoxide (ROOH). Hence, the Reactions (6.13) and (6.14) do not explain higher ketone than alcohol selectivity.

(6.13)

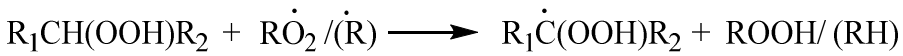

(6.14 A)

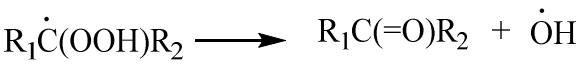

(6.14 B)

At very high oxygen availability Reaction (6.15) takes place and produces ketone and hydroperoxy radical (Bennett et al., 1987). Hydroperoxy radical can react with other free radicals by Reaction (6.16) or tetralin by Reaction (6.17).

$$R\dot{O} + O_2 \longrightarrow R{=}O + H\dot{O}_2 \quad (6.15)$$

$$H\dot{O}_2 + R\dot{O}_2 \longrightarrow ROOH + O_2 \quad (6.16)$$

$$RH + H\dot{O}_2 \longrightarrow \dot{R} + H_2O_2 \quad (6.17)$$

Tolman and co-workers, however, reported that oxidation of alcohol formed during oxidation (**Figure 6.8**) would result in higher ketone-to-alcohol ratio rather than Reaction (6.15) (Tolman et al., 1989). They heated a solution of dicyclohexyl peroxide (ROOR) at 160 °C under N_2 and under 3.45 MPa (500 psi) O_2, and obtained dominant alcohol (ketone-to-alcohol (K/A) = 1/4) and dominant ketone (K/A= 15/1) selectivities, respectively. In order to support their claim, they added cyclopentyl alcohol in their experiments and found no cyclopentanone under N_2; but 80 % cyclopentyl alcohol was converted to cyclopentanone under O_2. This explained that autoxidation of alcohol to ketone led to higher ketone-to-alcohol ratio.

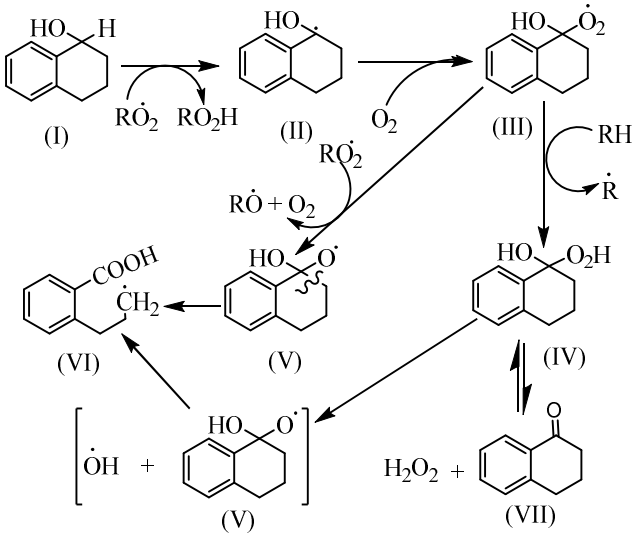

Figure 6.8. Illustration of oxidation of 1-tetranol (alcohol of tetralin).

Oxidation of alcohol not only produces ketone, but also leads to the formation of ring opening products (**Figure 6.8**). Alcohols can readily lose hydrogen from the C–H bond of the α-position that is also the α-position from the benzene ring (Tolman et al., 1989). Ring opening products (structure VI) can also be formed; but those were not observed at the studied experimental conditions.

Higher amounts of ketone can also be formed by the oxidation of alcohol to produce ketone and water (Reaction 6.18).

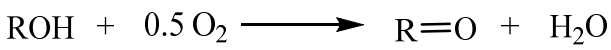

(6.18)

Oxidation of the alkoxy radical by reaction (6.15) and oxidation of the alcohol (**Figure 6.8** and Reaction (6.18)) are the two main aspects that explain higher ketone formation compared to alcohol. Although oxidation of alcohol can be dominant for cyclohexane oxidation, Reaction (6.15) can be dominant for tetralin oxidation due to the longevity of alkoxy radical ($RO^{\cdot}$) of tetralin. For naphthenic compounds such as cyclohexane and decalin, the alkoxy radical ($RO^{\cdot}$) might not exist for a long time at the cage condition to react with oxygen to form ketone as shown in Reaction (6.15) (Siddiquee and De Klerk, 2014b). However, longevity of $RO^{\cdot}$ from tetralin (a naphthenic-aromatic compound) would be longer due to resonance stabilization by the aromatic ring (Siddiquee and De Klerk, 2014b). This alkoxy radical ($RO^{\cdot}$) could react with oxygen to form a ketone. Confirmation of the higher ketone formation pathway was beyond the scope of current study.

6.4.2 Parameters that Affected Oxidation Selectivity

In the introduction it was postulated that temperature and that reactor hydrodynamics would affect oxidation selectivity. Based on all of the results presented, the following parameters appeared to affect oxidation selectivity at near constant conversion:

6.4.2.1 Temperature

Form **Tables 6.5** and **6.6** it is clear that temperature influences product selectivity. The main reasons could be an increase in formation of free radical intermediates during induction period for the oxidation to take place and an increase in oxidation rate (conversion rate) with temperature. Diffusion coefficient of oxygen into tetralin also increases with temperature, but the diffusion coefficient varies only to a limited extent (**Table B.1**) and is not considered for the discussion on product selectivity.

Although hydrocarbon oxidation with oxygen is exothermic, few initial steps especially free radical formation steps via bond dissociations are endothermic, slow, and require activation energy (**Table 6.7)** (Suresh et al., 2000; Emanuel et al., 1967; Tolman et al., 1989). During the induction period, hydrogen abstraction via C–H bond dissociation and decomposition of peroxides (O–O) are two main free radical formation steps that are influenced by temperature. Free radicals are formed from the hydrocarbon via C–H bond dissociation. C–H bond strength varies (typically 300–420 kJ/mol) depending on the carbon type, for example, primary, secondary, tertiary, aromatic, or benzylic (Emanuel et al., 1967; Tolman et al., 1989; Pryor, 1966). Tetralin has four aromatic C–H bonds which are very strong, four aliphatic C-H bonds of intermediate strength and four benzylic C–H bonds which are weak by comparison. Hydrogen can be readily abstracted from benzylic C–H by increasing temperature. Bond strength of peroxides (O–O) (typically 150–180 kJ/mol) varies depending on the group attached to the oxygen atom and decomposes typically at temperature about 150 ºC (De Klerk, 2003, Emanuel et al., 1967; Tolman et al., 1989; Pryor, 1966). This was experimentally confirmed by DSC analysis (**Figure B.2**). Decomposition of peroxides increases the formation of free radical intermediates. Hence, the formation of free radical intermediates would increase with temperature that would change the product selectivity.

After the induction period, sufficient free radical intermediates are available for autocatalytic oxidation to proceed and temperature has comparatively less effect on free radical formation. For instance, hydroxyl radicals ($HO^{\cdot}$) formed from the decomposition of hydroperoxides is strong enough to abstract hydrogen exothermically from paraffinic hydrocarbons, and hydrogen abstraction by alkoxy radicals is mildly endothermic (Tolman et al., 1989). Ketone formation also facilitates peroxide decompositions (Emanuel et al., 1967; Tolman et al., 1989). However, our focus was on initial product selectivity during the induction period.

The strength of O–H bond that is formed via hydrogen abstraction would determine the degree of product selectivity (Tolman et al., 1989). Regardless of the reactor types, alcohol selectivity (initial product selectivity) was dominating at temperatures below 140 ºC; but ketone selectivity was higher at temperatures of 150 ºC or higher (**Tables 6.5** and **6.6**). As discussed earlier, Reaction (6.8) would explain the higher alcohol selectivity during the oxidation of tetralin without initiator at low temperatures (series F-H in **Table 6.5** and series G, P, Q in **Table 6.6**),

and oxidation of alkoxy radical (Reaction 6.15) or oxidation of alcohol (**Figure 6.8** and Reaction 6.18) would explain dominant ketone selectivity compared to alcohol.

6.4.2.2 Oxygen Availability

It is clear from **Tables 6.3** and **6.7,** and from the discussion on alcohol and ketone selectivity that oxygen availability affects product selectivity.

Free radicals formed via H–abstraction during initiation would react depending on the oxygen availability by Reactions (6.1) and (6.4) of **Table 6.7**. If oxygen is present, Reaction (6.1) will take place, because it requires zero activation energy (**Table 6.7**). In the absence of oxygen or oxygen partial pressure below 13 kPa, Reaction (6.4) would take place (Suresh et al., 2000; Hobbs et al., 1972; Lundberg, 1961). Although it indicates the product immediately after the initiation, it could happen for the reaction between any free radicals and/or oxygen.

Both aspects to describe higher ketone formation (oxidation of alkoxy radical and oxidation of alcohol) require oxygen. But ketone formation via Reaction (6.15) would require oxygen at the molecular cage where the alkoxy radical ($RO^{\cdot}$) is formed. The highest ketone-to-alcohol ratio in the primary oxidation product (14:1, series A, **Table 6.3**) was obtained at gas-liquid interfacial area 3.0×10^5 m^2/m^3 (**Table 6.2**) where oxygen availability was the highest. Due to the longer gas bubbles (**Table 6.2**) and the smaller film thickness a higher amount of oxygen was available for the oxidation to take place at the cage conditions. Hence, the Reaction (6.15) could be dominant pathway to form more ketone. As noted earlier, longevity of alkoxy radical ($RO^{\cdot}$) might play an important role for such high ketone selectivity in tetralin (14:1).

At the cage condition if oxygen is available the Reactions (6.9), (6.10), (6.11) and (6.12) would not take place because the reaction between alkoxy radical and oxygen would be very fast. This would also support the higher ketone formation via Reaction (6.15). If alcohol is formed, however, as described earlier (Reactions (6.8), (6.9), (6.10), and (6.11)), the oxidation of alcohol would be the dominant reaction for the higher ketone formation.

In case of constant oxygen supply, oxygen availability would change with conversion and oxidation time, which could lead to different product selectivities. This aspect is evaluated in following sections.

6.4.2.3 Conversion and Oxidation Time

Influence of conversion and oxidation time on product selectivity is clear from the series R5–R8 of **Table 6.6**. This explains how product selectivity would change after the induction period at constant temperature and at constant supply of oxygen.

It is mentioned earlier that sufficient free radical intermediates are available for autocatalytic oxidation after the induction period. The concentration of free radical intermediates would increase with oxidative conversion and oxidation time. Immediately after the induction period (14 minutes), dissolved oxygen and supplied oxygen might be sufficient for the available free radical intermediates to produce more ketones compared to alcohol (2:1). However, a further increase in free radical intermediates and decrease in dissolved oxygen would influence the product selectivity. This situation is found 15 minutes after the induction time (series R6–R8 of **Table 6.6**) when secondary oxidation products and addition products are observed.

A near constant amount of oxygen was supplied as bubbles in the semi-batch reactor. Yet, the oxygen distribution might not be homogeneous due to transport effects and local consumption of oxygen in the presence of a higher concentration of free radicals. Hence, some parts would oxidize more to produce secondary oxidation products; but some parts would form addition products due to oxygen starvation. This would explain the secondary and addition product formation after 30 minutes of oxidation (series R6–R8). Addition products could form via olefin formation as reported in our previous study in **Chapter 4** (Siddiquee and De Klerk, 2014b).

Another notable observation was decrease in ketone-to-alcohol selectivity (2.0:1.0 to 1.1:1.0) in primary oxidation products (series R8 of **Table 6.6**). It indicates ketone-to-alcohol selectivity changed and had a local maximum (series R of **Table 6.6**) during oxidation. A similar observation was also made in our previous study of autoxidation (oxidation with air) of tetralin in a semi-batch reactor at 130 °C for 6 hour (**Table C.4**) (Siddiquee and De Klerk, 2014). The decrease in ketone-to-alcohol selectivity can be explained by the oxygen starvation compared to

free radical intermediates available at higher conversion and longer oxidation time. This observation also explains addition product formation at low oxygen availability.

6.4.2.4 Initiator Concentration

Effect of initiator on product selectivity is clear from the **Table 6.5**. As experiments were performed at different temperatures, and conversion was increased, it was anticipated that initiator would have the same accelerating effect on conversion and on product selectivity.

It is worthwhile to mention here that tetralin was partly oxidized immediately after adding the initiator (**Table 6.8**) without performing oxidation in the microfluidic reactor and the main identified products were addition products of tetralin. Ketone was not observed at 0.03 wt % and 0.1 wt % di-*tert*-butyl peroxide. Lower amount of ketone compared to alcohol was formed at 0.5 wt % di-*tert*-butyl peroxide. Secondary oxidation products were not identified in any cases. As described earlier, oxygen unavailability could play a role for such product selectivities. However, 0.5 wt % initiator was selected to perform experiments as it was the amount which could provide higher conversion without interfering too much with product identification.

Table 6.8. Selectivity of tetralin oxidized at room temperature (21 °C) at different initiator (di-*tert*-butyl peroxide) concentrations.

di-tert-butyl peroxide in tetralin (wt %)	Tetralin conversion $\times 10^2$ (wt%) [a]	selectivity of oxidation products (wt %)[a]			ketone-to-alcohol in primary oxidation products
		primary	secondary	addition	
0.03	7.0 ± 2.0	22.5	0	77.5	-[b]
0.1	1.0×10^1 ± 1.0	19.1	0	80.9	-[b]
0.5	2.2×10^1 ± 1.0	18.7	0	81.3	0.8

[a] calculated based on the GC-FID relative peak area of triplicate runs
[b] ketone to alcohol ratios were not reported as no ketone was identified

Conversion rate was greatly increased in the presence of the initiator (di-tert-butyl peroxide) at 150 °C or higher temperatures that affected the product selectivity (series N and O). Two distinct observations in product selectivity were noticed: secondary and addition products formation increased and ketone-to-alcohol ratio passed through a maximum with increasing temperature (**Figure 6.6**). These can be explained by the decomposition temperature of the initiator (di-*tert*-butyl peroxide) and peroxides formed during oxidation.

The decomposition temperature of di-*tert*-butyl peroxide was reported at 150 °C by thermal screening unit (TSu) and thermokinetic parameters of DTBP were measured by accelerating rate calorimeter (ARC) and reported as heat of reaction = 4.6×10^2 kJ/kg, reaction order n=1, activation energy (E_a)= 1.70×10^2 kJ/mol and pre-exponential factor (A) = 1.06×10^{20} s^{-1} (Jiayu et al., 2012). Our DSC experiments performed in N_2 atmosphere at different heating rates showed that decomposition started at a temperature greater than 133 °C (**Figure B.2**). At 150 °C or higher, the initiator would decompose. Hydroperoxide (ROOH) and/or (HOOH) formed via oxidation would also decompose at this temperature or higher. As mentioned earlier, the decomposition of peroxides leads to formation of free radical intermediates that would help in subsequent oxidations and would increase the oxidative conversion and also affect product selectivity.

The most noticeable changes in product selectivities were observed for the oxidation performed at 150 °C and 160 °C with equal amount of oxygen supply. But, supplied oxygen might not be sufficient for converting the free radicals produced at 160 °C into oxygenates and that might be the cause of the decrease in ketone-to-alcohol selectivity at 160 °C and increase in addition product formation. However, decreasing ketone-to-alcohol selectivity at 160 °C does not mean that there was a decrease in the yield of alcohol and ketone, it is just the ratio that changed. Overall yield of alcohol and ketone at 160 °C was much higher than that obtained at 150 °C.

The changes in product selectivities at higher conversion were analogous to the observation reported for tetralin oxidation after the induction time in a semi-batch reactor (series R5–R8 of **Table 6.6)** and in our previous study (**Table 6.9**). **Table 6.9** shows the additional data of tetralin oxidation reported in **Table 4.4** (**Chapter 4**). These illustrate that oxidation performed in different reactors could proceed in a similar way regardless of oxidants (air or oxygen) and temperatures. However, manipulating oxygen availability could change the product selectivity.

The influence of temperature, oxygen availability, conversions and reaction time were anticipated from literature (De Klerk, 2003; Goosen and Morgan, 1994; Jevtic et al., 2009; Jevtic et al., 2010; Emanuel et al., 1967; Tolman et al., 1989). Our interest was mainly in the influence of oxygen availability, which is related to reactor hydrodynamics.

Table 6.9. Conversion and selectivity of tetralin oxidized in a semi-batch reactor at 130 °C and atmospheric pressure using air as oxidizing agent (additional information on **Table 4.4** of **Chapter 4**).

oxidation time (h)	tetralin conversion (wt%)[a, c]	selectivity of oxidation products (wt %)[a,b, c]			ketone to alcohol in primary oxidation products [a, c]
		Primary	Secondary	Addition	
0.5	0.8	100	0	0	1.76
1	1.1	99	1	0	2.58
2	2.1	95	5	0	2.55
4	4.4	86	7	5	1.58
6	6.9	84	5	11	0.90

[a] average of two runs
[b] weight percentage of all oxidized products in the liquid
[c] not reported in **Table 4.4** of **Chapter 4**.

6.4.3 Mass Transfer Coefficients

The first parameter that affected oxidation selectivity and that was affected by hydrodynamics, is the mass transfer coefficient. The mass transfer coefficient is affected by film thickness and gas-liquid-interfacial area, which is related to the reactor design and operation.

Improving the mass transfer coefficient would increase the oxygen transfer to tetralin and hence increase the oxygen availability in the liquid phase. Oxygen transfer to tetralin can be described by three different models: film model, penetration model, and surface renewal model (Danckwerts, 1970, Kaštánek et al., 1993; Cussler, 2009). The main parameter that changes with different models is liquid side mass transfer coefficient (k_L) (Doraiswamy and Üner, 2014; Danckwerts, 1970). In most cases the results are very similar (Kaštánek et al., 1993; Cussler, 2009; Völkel, 2009; Suresh et al., 1988). Film theory is simple and was used in this study to explain the process. According to film theory, the liquid side mass transfer coefficient is $k_L = \frac{D_A}{\delta}$ and it is assumed that film is stagnant and uniform (Doraiswamy and Üner, 2014; Danckwerts, 1970, Cussler, 2009). Hence, the oxygen transfer rate to tetralin can be presented as:

$$J_A = k_L a\,(C_A \quad C_b) = \frac{D_A}{\delta}\, a\,(C_A \quad C_b) \tag{6.xv}$$

Here, J_A is the mass transfer rate across the gas-liquid interface (mol/m^3.s), D_A is the diffusivity of oxygen in tetralin (m^2/s), k_L is the liquid side mass transfer coefficient, (m/s), a is the gas-liquid interfacial area, (m^2/m^3), δ is the film thickness (m), C_A is the concentration of gas at the interface, (mol/m^3); C_b is the concentration of gas in bulk liquid (mol/m^3). As D_A and C_A can be changed only to a limited extent, δ and a are the two most important parameters to enhance the gas-liquid mass transfer because. These two aspects are discussed separately:

6.4.3.1 Film Thickness

Thin film thickness ensures shorter radial diffusion path and hence would increase the mass transfer as shown in Equation (6.xv). Film thickness could influence hydrodynamic conditions in the microfluidic reactor and this aspect had to be evaluated.

Liquid film thickness depends on reactor geometry, liquid agitation, interfacial properties of the channel, etc (Danckwerts, 1970; Sobieszuk et al., 2012). For a rectangular microchannel, liquid film thickness (δ) surrounding a gas bubble is expected to be different at different positions: diagonally, laterally, and at the top and bottom of the bubble (**Figure 6.9**) depending on the channel aspect ratio *w/h* (Sobieszuk et al., 2012; Yun et al., 2010; Völkel, 2009). It can be explained by the Capillary number, Equation (6.xvi). Generally, film thickness increases with the Capillary number (Hessel et al., 2005).

Capillary number, $Ca = U_G \mu / \sigma$ (6.xvi)

Where, U_G is superficial bubble velocity, μ is the viscosity of liquid, σ is the surface tension.

Figure 6.9. Sketch of bubble profiles in a rectangular channel under different flow conditions: (a) Interface shape at $Ca < 10^{-3}$; (b) bubble shape at $Ca > 10^{-3}$ in rectangular channel with aspect ratio, width (w)/depth (h) >1.5 (Völkel, 2009; Hazel and Heil, 2002; Wong et al., 1992).

For values of Ca less than 10^{-3}, the film surrounding the gas bubble would be very thin except in the corners (**Figure 6.9a**) For values of Ca greater than 10^{-3} the liquid film occupies a significant portion of the microchannel (**Figure 6.9b**) (Völkel, 2009; Hazel and Heil, 2002). Since Ca is a function of bubble velocity, increasing velocity would increase the film thickness. Moreover, thicknesses would be different laterally and at the top and bottom of the channel due to the velocity differences. In this study, the calculated Ca value of 2.1×10^{-4} – 5.4×10^{-4} (**Table 6.10**) suggests that **Figure 6.9(a)** would represent the most likely film thickness pattern.

Table 6.10. Dimensionless numbers for the oxidation of tetralin with molecular oxygen at 150 °C and 90-95 kPa gauge pressure in a microfluidic reactor.

dimensionless number	value
$Re_L = U_L d_H \rho_L / \mu_L$	9–27
$Re_G = U_G d_H \rho_G / \mu_G$	0.5–0.2
$Re_{TP} = U_{TP} d_H \rho_L / \mu_L$	9–27
$We = D_h U_{TP}^2 \rho_L / \sigma_L$	2.2×10^{-3}–1.7×10^{-2}
$Ca = U_G \mu_L / \sigma_L$	2.1×10^{-4}–5.4×10^{-4}
$Bo = (\rho_L \quad \rho_g) d_H^2 g / \sigma$	1.1×10^{-1}–1.4×10^{-1}
$Pe_L = \delta_L^2 U_L / D_A$	8.2×10^{-6} –2.2×10^{-5} [(a)]
	5.2×10^{-3}–2.0×10^{-2} [(b)]
$M_H = \delta\sqrt{k_r C_A / D_A}$	32–33[(a) (c)]
	800–984[(b) (c)]
$Da = (k_r C_A \delta^2) / D_A$	1.0×10^{3}–1.1×10^{3} [(a) (c)]
	6.4×10^{5}–9.4×10^{5} [(b) (c)]

[(a)] based on minimum film thickness.
[(b)] based on maximum film thickness.
[(c)] calculated for Reaction (6.1) Table 6.7.

Film thickness could also vary axially from the head side to the tail side of the bubble when inertial effects are not negligible (Sobieszuk et al., 2012; Yun et al., 2010). The bubble caps can be assumed to be spherical at low Capillary number (Ca), but ripples start to form at the tail side with increase in Ca (Hessel et al., 2005). At $Ca > 10^{-3}$, the effect of inertia cannot be ignored and with increase in Reynolds number amplitude of ripples increases and the tail side becomes flattened, which would result in increased film thickness (Hessel et al., 2005). It would not be the case, however, in this study due to the $Ca < 10^{-3}$(Table 6.10).

Yun et al. (2010) investigated the variation in film thickness for a rectangular microchannel experimentally and suggested correlations (Equations (6.ix) and (6.x)) to calculate maximum and minimum film thickness. As calculated maximum film thickness δ_{max} (~1.6×10^{-4} m) is ~ 30 times higher than the minimum film thickness δ_{min}, (~5.4×10^{-6} m), both are considered during analysis of results.

Film thicknesses (lateral) calculated from the captured images were identical to those calculated using the correlation for δ_{min}, Equation (6.x). It was difficult to measure exact film thickness, because proper film thickness determining methods, for instance, Laser Induced Fluorescence (LIF) or confocal Laser Scanning Microscopy (LSM) (Fries et al., 2008), were not available to us. Our intention was also to know only the order of magnitude of film thickness instead of investigating film thickness per se.

Since the thickness of liquid film calculated using either Equation (6.ix) or (6.x) was almost identical (**Table 6.2B**) and diffusivity of oxygen in tetralin was expected to be constant at 150 °C, a change in liquid side volumetric mass transfer coefficient ($k_L a$) was mostly due to increase in interfacial area. Hence, gas-liquid interfacial area would be the most important parameter to assess the role of oxygen availability during the oxidation of tetralin with molecular oxygen.

6.4.3.2 Gas-Liquid Interfacial Area

Since it was concluded that mass transfer coefficient ($k_L a$) under different hydrodynamic conditions in the microfluidic reactor was due to the change in gas-liquid interfacial area (a), this aspect had to be evaluated.

Gas-liquid interfacial area proportionally increases the mass transfer as shown in equation (6.xv). It is clear from **Table 6.2** that gas-liquid interfacial area influences the mass transfer coefficient that increases the oxygen availability. The impact of gas-liquid interfacial area on conversion rate and product selectivity is clear from the **Figure 6.3.** Conversion rate rather than conversion was calculated, because conversion is affected by flow rate.

At the inflexion point, liquid film formation (not the film thickness, rather the length of film) was increased (series B, **Table 6.2A**) compared to the series C, D and E (**Table 6.2A**). Increased film formation ensured higher gas-liquid interfacial area and hence oxygen availability for the oxidation to take place, and resulted in higher conversion rate and it changed the product selectivity. As explained earlier, due to very high oxygen availability, higher ketone compared to alcohol selectivity (14:1) was attributed to either the oxidation of alkoxy radical or alcohol with molecular oxygen.

Although gas-liquid interfacial areas were also manipulated by performing oxidation with different reactor geometries (**Table 6.6**), initial ketone-to-alcohol selectivities were not changed due to the longer induction period (14 minutes) at the studied oxygen availability. Then, it was quite suspiring to get order of magnitude higher ketone (series A, **Table 6.3**) at very high oxygen availability, but even shorter residence time. Two possible things could happen: induction time changed at very high oxygen supply at 150 °C, or alcohol and/or alkoxy radicals reacted very fast at very high oxygen availability to increase ketone formation.

Mass transfer coefficient is greatly influenced by gas-liquid interfacial area compared to film thickness. Gas-liquid interfacial area and hence oxygen availability can be manipulated by changing reactor geometry and operating conditions that would change the product selectivity.

6.4.4. Potential of Taylor Flow in Liquid Phase Oxidation

In Taylor flow, gas bubbles (**Figure 6.3b**) are separated from liquid slugs and thin liquid films on the channel walls (Gemoets et al., 2016; Vanoye et al., 2013; Günther et al., 2004; Doraiswamy and Üner, 2014; Sobieszuk et al., 2012). Thin liquid films facilitate the radial diffusion and ensure higher oxygen availability in the films. Hence, increase the length of gas bubbles and decrease the length of liquid slugs would ensure higher film area and facilitate the higher oxygen availability per unit reactor volume. Another advantage of Taylor flow in liquid phase oxidation is the presence of internal circulation within the liquid slugs and gas bubbles, which arises from the interfacial friction and slip velocity (Gemoets et al., 2016; Vanoye et al., 2013; Günther et al., 2004; Doraiswamy and Üner, 2014; Sobieszuk et al., 2012). This internal

circulation enhances the mixing and facilitates the gas-liquid mass transfer. More importantly, internal circulation could prevent the over oxidation of primary oxygenates into liquid slugs (**Figure 6.3c**). The short radial diffusion length of microfluidic reactors ensures better mixing and it leads to a narrow residence time distribution (RTD) (Kiwi-Minsker and Renken, 2012; Gemoets et al., 2016). All these are potentially advantageous for preventing the over-oxidation of oxygenates in consecutive processes and for controlling the product selectivity.

In the case of larger gas bubbles and smaller liquid slugs (Series A, Table 7.2A), the presence of liquid film per unit reactor volume was higher. Moreover, due to the smaller slug and higher superficial liquid velocity (**Series A of Table 7.2A**), the circulation with in the liquid was expected to be higher. The effect of increased film and internal circulation was noticed in the higher ketone formation (**Series A of Table 7.3** and **Figure 6.5**). This can be explained by the change in induction period at higher oxygen availability and facilitate ketone formation (described in Section 6.4.1.2).

6.4.5. Additional Effects

Additional effects that can potentially influence the product selectivity and that are affected by reactor hydrodynamics are pressure drop and residence time distribution. However, these aspects were not investigated.

6.4.6 Characteristic Dimensionless Numbers

Although hydrodynamics of microscale reactors can be explained by the principles used for macroscale reactors, many physical characteristics, for instances, surface tension forces, viscous forces, area-to-volume ratio and diffusion, cannot be scaled up linearly. Different characteristic dimensionless numbers may be useful to approximate the gas-liquid two-phase flow behaviour in microchannel reactors.

Characteristic dimensionless numbers (**Table 6.10**) were calculated from the studied gas-liquid systems.

Reynolds numbers (Re) from 9 to 27 indicate laminar flow throughout the microchannel that was typical for Taylor flow in microchannels (Günther et al., 2004; Hessel et al., 2005). Smaller Re also indicated that viscous forces dominated over inertial forces.

The smaller Weber numbers (We) indicated that inertial forces were not high enough to overcome surface tension forces and to break down the slug between two phases.

Capillary number (Ca) characterizes the relative importance of viscous forces relative to surface tension forces. Smaller Ca indicated that surface tension had a larger effect than viscous force. Both the Ca and We indicated surface tension is dominant and that slug formation should be anticipated. As noted earlier, film thickness would be estimated from these numbers.

Peclet number (Pe) represents the relative importance of diffusive and convective transport. For both minimum and maximum film thickness, $Pe<<1$ which suggests diffusive transport far outweighs convective transport through the thin film.

Bond number (Bo) estimates the magnitude of gravitational forces over surface tension forces. Bo values of 1.1×10^{-1}–1.4×10^{-1} (**Table 6.10**) suggests that values of surface tension have a larger influence on the system than gravitational forces.

Hatta modulus (M_H) and Damköhler number (Da) indicate whether a reaction is kinetically controlled or mass transfer limited. Since calculated $M_H>>3$ and $Da>>1$ for the Reaction (6.1) (**Table 6.7**), the reaction would be mass transfer limited and based on these values the reaction would be completed in the film (Kaštánek et al., 1993; Hartman et al., 2011; Rebrov et al., 2012). This would true for any reaction between a free radial and oxygen molecule. The experimental observations do not support such an interpretation, since it was possible to manipulate ketone-to-alcohol selectivity through microfluidic reactor operation to control oxygen availability in the liquid phase at near constant conversion, oxygen partial pressure and temperature. The other reactions shown in **Table 6.7** can also lead to incorrect prediction. The calculation based on oxygen consumption rate can also result discrepancies (discussed in Chapter 7).

6.4.7 Application of Microfluidic Devices to Control Selectivity

6.4.7.1. Upgrading of Oilsands Bitumen

To the best of our knowledge, oxidation of bitumen in a microfluidic reactor is not reported in literature. High viscosity is the main challenge in using bitumen in a microfluidic setup. Recently, the Sinton-group developed a microfluidic platform to measure CO_2 diffusivity in bitumen (Fadaei et al., 2011). The judicial use of solvent and/or temperature might help to study the oxidation of bitumen in a microchannel reactor. Although the application of microfluidic for studying the upgrading of oilsands derived bitumen is challenging, the fundamental understanding from this research would be useful to select suitable reactor and reaction conditions for processes where mass transport affects selectivity.

6.4.7.2. Pharmaceutical Products

Order of magnitude increase in ketone formation in this study indicates that microfluidic reactors have that potential to improve selectivity for small volume, high value products, such as pharmaceutical products. Literature also pointed out the suitability of microfluidic reactors for the production of pharmaceuticals (Hamano et al., 2012; Snead and Jamison, 2015). Some complex processes could be modified to simpler and faster ones. For instance, ibuprofen can be synthesized only in three minutes in a microfluidic reactor (Snead and Jamison, 2015); traditional ibuprofen synthesis involves highly complex oxidation process (Rothenberg, 2008). More importantly, pharmaceutical industries generate huge amount of wastes (E-factor: 20–100) compared to other chemical industries (Rothenberg, 2008). Microfluidic reactors could be useful to control the product selectivity and to mitigate waste generation in processes where selectivity is influenced mass transport.

6.4.7.3. Petrochemical Products

Microfluidic reactors could potentially be used for the production of fine chemicals from petroleum with improved product selectivity for dyes, fragrances and polymer intermediates. For instance, selective oxidation of cyclohexane to produce caprolactum (a precursor to nylon-6) and adipic acid requires higher ketone-to-alcohol selectivity (Dimitratos, 2014; Alsters et al., 2014).

As mentioned earlier, operation with low single pass conversion is practiced industrially to achieve a mixture of alcohol and ketone that converted later to cyclohexanone via catalytic oxidation (Dimitratos, 2014; Sheldon and Kochi, 1981). Capillary and micro-structured reactors were investigated for cyclohexane oxidation, although these studies did not specifically investigate how oxygen availability controls product selectivity (Jevtic et al., 2010; Leclerc et al., 2008; Fischer, 2010). The fundamental understandings from this study could be applied to produce cyclohexanone more selectively (ketone of cyclohexane) by ensuring very high oxygen availability. Selective oxidation can also be performed to synthesize chemicals that are not readily available commercially. For example, the diketone of tetralin could be produced by oxidizing the tetralin or ketone (or alcohol) of tetralin with air or oxygen in a microfluidic reactor.

Oxidation in microfluidic reactor can also be performed to reduce the environmental impact caused by strong oxidizing agents. For instance, chromium trioxide and sulfuric acid are used traditionally for the production of benzophenone from diphenyl methanol. E-factor for the process is 9.1×10^{-1} (almost 1 kg waste/ kg product) (Rothenberg, 2008), but this process could potentially be completed in microfluidic reactor using air or oxygen as oxidant.

Overall, microfluidic devices have potential to control the product selectivity where mass transport influences selectivity.

6.5 Conclusions

Oxidation of a naphthenic-aromatic compound (tetralin) was investigated mainly in a microfluidic reactor to understand how product selectivity could be manipulated by ensuring oxygen availability and how mass transfer would affect the oxidation process. The main observations and conclusions are as follows:

(a) Liquid phase mass transfer (k_La) in the microfluidic reactor could be manipulated over two orders of magnitude. This was possible mainly through changing the gas-liquid interfacial area (a). The mass transfer coefficient (k_L) was fairly insensitive to changes in operation.

(b) It was possible to increase the ketone-to-alcohol ratio in the product by an order of magnitude at near similar conversion, pressure and temperature. This was possible through microfluidic reactor operation only.

(c) The influence of operating conditions on oxidation selectivity could be explained in terms of the reaction network. The ketone-to-alcohol selectivity ratio was strongly affected by oxygen availability in the liquid phase, which promoted alcohol and/or alkoxy radical oxidation to produce ketones. This showed how engineering could affect the chemistry.

(d) Addition products were not observed during tetralin oxidation at high oxygen availability. For example, when oxidation was performed with oxygen instead of air in a microfluidic reactor no addition products were observed. When oxygen availability decreased, or the reaction rate was increased to decrease oxygen availability in relation to reaction rate, addition products were observed. Hence, some addition products were noticed in the presence of initiator (di-*tert*-butyl peroxide) at higher temperature (150 °C and higher). Addition products were also observed after 30 minutes of tetralin oxidation performed in a semi-batch reactor. There was also a concomitant increase in alcohol selectivity with an increase in addition product selectivity. This was anticipated from the reaction network that favored ketone selectivity at high oxygen availability, but favored alcohol and addition product selectivity at lower oxygen availability.

(e) Higher Damköhler number (Da) and Hatta modulus (M_H) suggested that gas-liquid oxidation might take place at liquid film surrounding the gas bubbles rather than liquid bulk. This was not consistent with the experimental observations, which recorded meaningful selectivity control based on control of oxygen availability in the liquid phase through microfluidic reactor operation at near constant conversion, pressure and temperature.

6.6 Nomenclature

a	gas-liquid interfacial area, (m^2/m^3)
A	pre-exponential factor
Bo	Bond number, $Bo = (\rho_L \quad \rho_g) d_H^2 g/\sigma$
Ca	Capillary number, $Ca = U_G \mu/\sigma$

C_A	concentration of gas at the interface, (mol/m^3)
C_b	concentration of gas in bulk liquid (mol/m^3)
Da	Damköhler number; Da $= (k_r\, C_A \delta^2)/D_A$
D_A	diffusivity of oxygen in tetralin (m^2/s)
d_H	hydraulic diameter; $d_H = 2[w\ /(w +\ )]$, (m)
DTBP	di-tert-butyl peroxide
E_a	activation energy, (kJ/mol)
FID	flame ionization detector
GC	gas chromatography
	depth of the reactor, (m)
HP DSC	high-pressure differential scanning calorimeter
HPLC	high performance liquid chromatography
J_A	mass transfer rate across the gas-liquid interface (mol/m^3.s)
k_L	mass transfer coefficient; $k_L = D_A/\delta$, (m/s)
k_La	overall mass transfer coefficient, (s^{-1})
k_r	reaction rate constant
L_G	length of gas bubble, (m)
L_S	length of liquid slug, (m)
M_H	Hatta modulus; $\mathrm{M}_H = \delta\sqrt{k_r\, C_A/D_A}$
MS	mass spectrometry
NIST	National Institute of Standards and Technology
Pe_L	Peclet number; $Pe_L = \delta_L^2 U_L/D_A$
PTFE	Poly tetra fluoro ethylene
Re_G	gas-phase Reynolds number; $Re_G = U_G d_H \rho_G/\mu_G$
Re_L	liquid-phase Reynolds number; $Re_L = U_L d_H \rho_L/\mu_L$
Re_{TP}	two-phase Reynolds number; $Re_{TP} = U_{TP} d_H \rho_L/\mu_L$
RTD	residence time distribution
S_G	surface area of gas bubble, (m^2)
U_G	superficial gas bubble velocity, (m/s)
U_L	superficial liquid slug velocity, (m/s)
U_{TP}	two phase superficial velocity, (m/s)
V_G	volume of gas bubble, (m^3)
V_L	volume of liquid slug, (m^3)
w	width of the reactor, (m)
We	Weber number; $We = D_h U_{TP}^2 \rho_L/\sigma_L$

Greek letters

δ	thickness of liquid film, (m)
ε_G	volume fraction of gas bubble

ρ_G	density of gas, (kg/m^3)
ρ_l	density of liquid, (kg/m^3)
μ_G	gas viscosity, (Pa.s)
μ_L	liquid viscosity, (Pa.s)
σ	surface tension, (N/m)

Subscripts

b	bulk
G	gas
L	liquid
TP	two-phase

6.7 Literature Cited

Alsters, P. L.; Aubry, J. M.; Bonrath, W.; Daguenet, C.; Hans, M.; Jary, W.; Letinois, U.; Nardello-Rataj, V.; Netscher, T.; Rarton, R.; Schütz, J.; Van Soolingen, J.; Tinge, J.; Wüstenberg, B. Selective oxidation in DSM: Innovative catalysts and technology. In *Handbook of Advanced Methods and Processes in Oxidation Catalysis: From Laboratory to Industry*; Duprez, D., Cavani, F. Eds.; Imperial College Press: London, 2014; pp 382–419.

Bennett, J. E.; Brunton, G.; Smith, J. R. L.; Salmon, T. M. F.; Waddington, D. J. Reactions of alkylperoxyl radicals in solution. Part 2-A kinetic and product study of self-reactions of 2-propylperoxyl radicals between 253 and 323 K. *J. Chem. Soc., Faraday Trans. 1* **1987**, *83*(8), 2433–2447.

Cussler, E. L. *Diffusion: Mass Transfer in Fluid Systems,* 3rd ed.; Cambridge University Press: Cambridge, 2009.

Danckwerts, P. V. *Gas-Liquid Reactions*; McGraw-Hill: New York, 1970.

De Klerk, A. Continuous- mode thermal oxidation of Fischer-Tropsch waxes. *Ind. Eng. Chem. Res*. **2003,** *42*, 6545–6548.

Dimitratos, N.; Lopez-Sanchez, J. A.; Hutchings, G. J. Supported metal nanoparticles in liquid-phase oxidation reactions. In *Handbook of Advanced Methods and Processes in Oxidation Catalysis: From Laboratory to Industry*; Duprez, D., Cavani, F. Eds.; Imperial College Press: London, 2014; pp 631–678.

Doraiswamy, L.K.; Üner, D. *Chemical Reaction Engineering, Beyond the Fundamentals*; CRC Press: Boca Raton, 2014.

Emanuel, N. M.; Denisov, E. T.; Maizus, Z. K. *Liquid-phase oxidation of hydrocarbons*; Plenum Press: New York, 1967.

Fadaei, H., Scarff, B.; Sinton, D. Rapid microfluidics-based measurement of the CO_2 diffusivity in bitumen. *Energy Fuels* **2011,** *25*, 4829–4835.

Fischer, J.; Lange, T.; Boehling, R.; Rehfinger, A.; Klemm, E. Uncatalyzed selective oxidation of liquid cyclohexane with air in a microcapillary reactor. *Chem. Eng. Sci.* **2010**, *65*, 4866–4872.

Fries, D. M.; Trachsel, F.; von Rohr, P. R. Segmented gas–liquid flow characterization in rectangular microchannels. *Int. J. Multiphase Flow* **2008**, *34*, 1108–1118.

Gemoets, H. P. L.; Su, Y.; Shang, M; Hessel, V.; Luque, R. Noël, T. Liquid phase oxidation chemistry in continuous flow microreactors, *Chem. Soc. Rev.* **2016**, ***45***, 83–117.

Goosen, A.; Morgan, D. H. Autoxidation of nonane and decane: A product study. *J. Chem. Soc., Perkin Trans.* **1994**, *2*, 557–562.

Günther, A.; Khan, S. A.; Thalmann, M.; Trachsel, F.; and Jensen, K. F. Transport and reaction in microscale segmented gas–liquid flow. *Lab Chip* **2004**, *4*, 278–286.

Hamano, M.; Nagy, K. D.; Jensen, K. F. Continuous flow metal-free oxidation of picolines using air. *Chem. Comm.* **2012,** *48*, 2086–2088.

Hartman, R.L.; McMullen, J.P.; Jensen, K.F. Deciding whether to go with the flow – evaluating the merits of flow reactors for synthesis. *Angew Chemie Int. Ed*. *Angew Chemie Int. Ed*. **2011,** *50*, 7502–7519.

Hazel, A. L.; Heil, M. The steady propagation of a semi-infinite bubble into a tube of elliptical or rectangular cross-section. *J. Fluid Mech.* **2002**, *470*, 91–114.

Hendry, D. G.; Gould, C. W.; Schuetzle, D.; Syz, M. G.; Mayo, F. R. Autoxidations of cyclohexane and its autoxidation products. *J. Org. Chem.* **1976**, *41*(1), 1–10.

Hermans, I.; Peeters, J.; Jacobs, P. A. Autoxidation of Hydrocarbons: From Chemistry to Catalysis. *Top Catal.* **2008**, *50*, 124–132.

Hessel, V.; Angeli, P.; Gavriilidis, A.; Löwe, H. Gas-liquid and gas-liquid-solid microstructured reactors: contacting principles and applications. *Ind. Eng. Chem. Res.* **2005**, *44,* 9750–9769.

Hill, C. L.; Kholdeeva, O. A. Selective liquid phase oxidation in the presence of supported polyoxometalates. In *Liquid Phase Oxidation via Heterogeneous Catalysis: Organic*

Synthesis and Industrial Applications, First Edition; Clerici, M. G., Kholdeeva, O. A. Eds.; Wiley: Hoboken, 2013; pp 263–319.

Hobbs, C. C.; Drew, E. H.; Van't Hof, H.A.; Mesich, F. G.; Onore, M. J. Mass transfer rate-limitation effects in liquid-phase oxidation. *Ind. Eng. Chem. Prod. Res. Develop.* **1972**, *11*(2), 220–225.

Jevtic , R.; Ramachandran, P.A.; Dudukovic, M. P. Effect of oxygen on cyclohexane oxidation: A stirred tank study. *Ind. Eng. Chem. Res.* **2009**, *48*, 7986–7993.

Jevtic , R.; Ramachandran, P.A.; Dudukovic, M. P. Capillary reactor for cyclohexane oxidation with oxygen. Chem. Eng. Res. Des. **2010**, *88*, 255–262.

Jiayu, L.; Wanghua, C.; Liping, C.; Yingtao, T.; Xin, S. Thermal decomposition analysis and safety study on di-tert-butyl peroxide. *Procedia Eng.* **2012,** *43*, 312–317.

Kaštánek, F.; Zaharadník, J.; Kratochvíl, J.; Čermák, J. *Chemical Reactors for Gas-Liquid Systems*, 1st ed.; Ellis Horwood: West Sussex, 1993.

Kiwi-Minsker, L.; Renken, A. Microstructured reactors for catalytic reactions. *Catal. Today* **2005,** *110,* 2–14.

Leclerc, A.; Alame, M.; Schweich, D. Pouteau, P. Delattreb, C. de Bellefon, C. Gas–liquid selective oxidations with oxygen under explosive conditions in a micro-structured reactor. *Lab Chip*, **2008**, *8*, 814–817.

Lundberg, W. O. Autoxidation and antioxidants, Vol I. Wiley: New York, 1961.

Pina, C. D.; Falletta, E.; Rossi, M. Liquid phase oxidation of organic compounds by supported metal-based catalysts with a focus on gold. In *Liquid Phase Oxidation via Heterogeneous Catalysis: Organic Synthesis and Industrial Applications,* First Edition; Clerici, M. G.; Kholdeeva, O. A. Eds.; Wiley: Hoboken, 2013, 221–262.

Pryor, W. A. *Free Radicals*; McGraw Hill: New York, 1966.

Rebrov, E.V.; Duisters, T.; Löb, P.; Meuldijk, J.; Hessel, V. Enhancement of the liquid-side mass transfer in a falling film catalytic microreactor by in-channel mixing structures. *Ind. Eng. Chem. Res.* **2012**, *51*(26), 8719–8725.

Rothenberg, G. *Catalysis: Concepts and Green Applications*; Wiley: Weinheim, 2008; pp 1–38.

Russell, G. A. Deuterium-isotope effects in the autoxidation of aralkyl hydrocarbons. Mechanism of the interaction of peroxy radicals. *J. Am. Chem. Soc.* **1957**, *79*, 3871–3877.

Sheldon, R. A.; Kochi, J. K. *Metal-Catalyzed Oxidations of Organic Compounds*; Academic Press: New York, 1981.

Siddiquee, M.N.; De Klerk, A. Hydrocarbon addition reactions during low temperature autoxidation of oilsands bitumen. *Energy Fuels* **2014b**, *28*, 6848–6859.

Snead, D. R.; Jamison, T.F. A three-minute synthesis and purification of ibuprofen: pushing the limits of continuous-flow processing. *Angew. Chem. Int. Ed.* **2015***, 54*(3), 1521–3773.

Sobieszuk, P.; Aubin, J.; Pohorecki, R. Hydrodynamics and mass transfer in gas-liquid flows in microreactor. *Chem. Eng. Tech.* **2012**, *35*(8), 1346–1358.

Suresh, A. K.; Sharma, M. M.; Sridhar, T. Engineering aspects of industrial liquid-phase air oxidation of hydrocarbon. *Ind. Eng. Chem. Res.* **2000,** *39,* 3958–3997.

Suresh, A. K.; Sridhar, T.; Potter, O. E. Autocatalytic oxidation of cyclohexane- mass transfer and chemical reaction. *AIChE J.* **1988**, *34*(1), 81–93.

Tolman, C. A.; Druliner, J. D.; Nappa, M. J.; Herron, N. Alkane oxidation studies in du Pont's central research department. In *Activation and Functionalization of Alkanes*; Hill C. L. Ed.; Wiley: New York, 1989; pp 303–360.

Twigg, G. H. The mechanism of liquid-phase oxidation. *Chem. Eng. Sci. Suppl.* **1954**, *8*, 5–16.

Vanoye, L.; Aloui, A.; Pablos, M.; Philippe, R.; Percheron, A.; Favre-Réguillon, A.; de Bellefon, C. A safe and efficient flow oxidation of aldehydes with O_2. *Org. Lett.* **2013**, *15*(23), 5978–5981.

Völkel, N. Design and Characterization of Gas-Liquid Microreactors. Ph.D. Thesis, Universite de Tolousé, December 2009.

Wong, H.; Morris, S.; Radke, C. J. Three-dimensional menisci in polygonal capillaries. *J. Colloid Interf. Sci.* **1992**, *148*(2), 317–336.

Yun, J.; Lei, Q.; Zhang, S.; Shen, S.; Yao, K. Slug flow characteristics of gas-miscible liquids in a rectangular microchannel with cross and T-shaped junctions. *Chem. Eng. Sci.* **2010**, *65*, 5256–5263.

CHAPTER 7 – ENGINEERING ASPECTS OF LIQUID PHASE AUTOXIDATION OF HYDROCARBON: EXPERIMENTAL STUDY[7]

Abstract

Liquid phase autoxidation (oxidation with air) of indan, a simple naphthenic–aromatic hydrocarbon, was performed in a flat interface reactor (FIR) at 50 °C. The objectives were to experimentally confirm whether or not the gas–liquid oxidation was mass transfer limited or kinetically controlled, where the limitation was if there was mass transfer limitation and what its extent was. An oxygen phase fluorometer was employed to measure *in situ* oxygen partial pressure in the liquid phase to achieve the goals. During the induction period, oxygen partial pressure in the liquid phase was increased from 0 kPa to the saturated value (19.2 kPa) and no detectable oxidation was observed. This indicated kinetically control phenomenon as oxidation rate was very slow compared to mass transfer rate. The maximum rates of O_2 transfer to the indan phase was 1.9×10^{-6} mol/(m^2.s) or 1.5×10^{-3} mol O_2/(m^3.s) and the overall mass transfer coefficient obtained from the experimental measurements was 1.0×10^{-3} s^{-1} during autoxidation of indan in a flat interface reactor at 50 ˚C and 19.2 kPa O_2 partial pressure. Different levels (1–9.2 wt %) of di-*tert*-butyl peroxide initiator were added to shorten the exceedingly long induction period. In the cases of 5.1 wt % and 9.2 wt % of di-*tert*-butyl peroxide, oxygen partial pressure in the liquid phase was decreased from the saturated value (19.2 kPa) to zero kPa indicating mass transfer limitation. The underlying cause behind the occurrence might be the sudden increase in free radical intermediates and the higher oxidation rate between free radical intermediates and molecular oxygen. These results also indicated that the rate of oxidation compared to mass transport was so high that reaction would be gas–liquid interface (film) dominated. The reaction rate threshold was 2.6×10^{-3} (mol/m^3.s) or 3.4×10^{-6} (mol/m^2.s) for the reaction to occur in the film instead of the bulk.

Keywords: Flat interface reactor, indan, oxygen transport, oxidation rate, film, liquid phase.

---

[7]Reprinted from "Siddiquee, M. N.; De Klerk, A. *In situ* measurement of liquid Phase oxygen during oxidation. (Submitted to publish in Industrial and Engineering Chemistry Research).

7.1 Introduction

Liquid phase autoxidation (oxidation with air) of hydrocarbons are industrially important. Large volume industrial processes that employ liquid phase oxidation include the oxidation of cyclohexane to cyclohexanone and cyclohexanol, which are used for adipic acid manufacturing, and the oxidation of cumene for the production of phenol. These oxidation reactions can proceed without a catalyst, but catalysts are often used to accelerate the reaction rate (Centi et al., 2001; Centi and Perathoner, 2002; Clerici and Kholdeeva, 2013). Despite the use of catalysts, the oxidation mechanism is a free radical mechanism (Clerici and Kholdeeva, 2013; Emanuel et al., 1967; Sheldon and Kochi, 1981).

Reaction engineering of liquid phase autoxidation deals mainly with two issues: improving the selectivity of the oxidation reaction to the target products and ensuring adequate mass transport of oxygen from the gas phase to the liquid phase (Suresh et al., 2000). The oxidation selectivity is influenced by the overall conversion (Suresh et al., 2000), and by oxygen availability (De Klerk, 2003; Chapter 6). Oxygen availability is determined by the mass transport of oxygen relative to reaction rate. Hence, oxygen transport influences both oxidative conversion and product selectivity simultaneously, which is a potential challenge for the engineering of such gas–liquid reactions (Suresh et al., 2000; Hobbs et al., 1972; Chapter 6).

The rate of gas–liquid reaction depends on the mass transfer through the gas–liquid interface (film) and on the reaction kinetics (Doraiswamy and Üner, 2014). Thus, liquid phase oxidation can be kinetically controlled, mass–transfer limited, or limited by both the reaction kinetics and mass transport rate, with neither dominating the reaction process.

In the case of kinetically controlled oxidation, the rate oxygen transfer to the liquid phase would be high and the concentration of oxygen in liquid phase would be close to saturation (Emanuel et al., 1967; Hobbs et al., 1972). The oxidation rate in a kinetically controlled reaction system would be slow compared to the mass transport rate and oxidation would occur predominantly in the bulk liquid phase. Oxygen availability would be governed by the oxygen partial pressure and oxygen solubility in the liquid phase.

When mass transport is limiting, the contribution of oxidation that is taking place at the gas–liquid interface increases and for very fast oxidation reactions, the oxidation takes place almost exclusively in the film (Emanuel et al., 1967). Oxygenates produced during oxidation might be surface active (De Klerk, 2003), and the rate of diffusion of the oxygenates might also be slow in comparison to the oxidation rate. Thus the local concentration of oxidized material at the interface could be higher than in the bulk liquid phase. As a consequence conversion at the gas–liquid interface may influence oxidation selectivity differently to conversion in the bulk liquid phase. The surface active nature of the oxidation products and slow diffusion rate of the oxidation products in the liquid can exacerbate the influence of mass transport limited oxidation on oxidation selectivity.

Oxidation of hydrocarbons with oxygen was reported to be kinetically controlled during the induction period and mass transfer limited after the induction period (Suresh et al., 2000; Suresh et al., 1988a; Fischer et al., 2010). It was somewhat surprising was to find that there was very little literature on mass transport of oxygen during liquid phase oxidation.

Most liquid phase oxidation studies dealt with oxygen transport in a theoretical fashion only and relied on engineering calculations, rather than experimental measurements, to draw conclusions about oxygen availability in the liquid phase. For example, Fischer et al. (2010) applied a concentration–time dependent mass transfer model to evaluate the mass transfer limitation during cyclohexane autoxidation and calculated the Hatta number to assess the extent of mass transfer limitation. Likewise, Rebrov et al. (2012) calculated the Hatta number to understand the mass transfer limitation during catalytic oxidation of octanal with oxygen.

Experimental investigations were more limited, possibly because they are experimentally challenging to perform. Suresh et al. (1988a, 1988b) experimentally investigated oxygen transport during liquid phase oxidation. They systematically oxidized cyclohexane in a bubble column and in a flat interface reactor to investigate the influence of mass transfers on liquid–phase oxidation at 0 to 2 MPa and 20 to 150 °C. They calculated oxygen consumption for the oxidation performed in bubble column reactor from the oxygen content of inlet and outlet gas streams. The bubble column reactor had inherent lag time between reaction and analysis by the oxygen analyzer and it was reported that changes could only be observed accurately for higher

oxygen consumption. In the case of flat interface with stirring system, they collected liquid samples at different time intervals and desorbed the gases from solution by lowering the pressure. Desorbed gases were analyzed using a gas chromatograph (GC) and thereby the dissolved oxygen content in liquid phase could be determined indirectly. They observed that there were discrepancies between the theoretical evaluation of oxygen transport and the experimental measurements. Fischer et al. (2010) mentioned that Schäfer (2005) also observed discrepancies between experimental measurements and calculated prediction of the mass transfer during liquid phase oxidation.

Our investigation into the selectivity of tetralin oxidation in the Taylor flow region in a microfluidic reactor also found contradictions between experimental observations and theoretical analysis of the mass transfer limitation based on calculating Hatta number (Chapter 6). A high value for the Hatta number was calculated, which indicated that there was a meaningful mass transfer limitation and that oxidation occurred mainly in the film, i.e. at the gas–liquid interface (Rebrov et al, 2012; Kaštánek et al., 1993). Yet, despite the high calculated Hatta numbers, it was possible to manipulate the product selectivity at near constant conversion, oxygen partial pressure and temperature, by changes in the reactor hydrodynamics (Chapter 6). The experimental observations suggested that oxygen availability was changed, but that should not have been possible; the Hatta number indicated that reaction could only take place in the film with essentially no dissolved oxygen in the bulk liquid.

The discrepancies between experimental observations and predictions that were based on calculated Hatta numbers were troubling. It was decided to experimentally determine the oxygen availability in the bulk liquid phase during autoxidation of hydrocarbons. In this respect there appears to be a gap in the experimental literature. Not only is there little experimental literature as mentioned before, but no reports were found that conducted *in situ* measurements of liquid phase oxygen content during liquid phase autoxidation of hydrocarbons. The aim of the current study was to address this shortcoming.

Indan, a naphthenic–aromatic compound, and benzene, an aromatic compound, were autoxidized in a flat interface reactor equipped with oxygen phase fluorimeter to measure the dissolved oxygen content in the bulk liquid phase. Di-*tert*-butyl peroxide was used as an initiator to

shorten the induction period during indan oxidation and manipulate the oxidation rate independent of oxygen availability during the initial stages of oxidation.

7.2 Experimental

7.2.1 Materials

Table 7.1 shows the list of chemicals used in this study. Indan was selected because it is readily oxidized and because it is a naphthenic–aromatic compound with high addition product selectivity (Chapter 4). The reason for selecting a compound with high addition product selectivity is to better discriminate between free radical addition and free radical oxidation. Benzene was selected as control, because it is impervious to oxidation at the oxidation conditions studied. Benzene could therefore be used as an inert aromatic liquid to calibrate the fluorimeter that was used to determine the dissolved oxygen content. Properties of indan and benzene are listed in Appendix C (**Table C.1**)

Table 7.1. Chemicals employed in mass transfer study.

Name	CASRN [a]	Formula	Purity (wt %)		Supplier
			supplier [b]	analysis [c]	
indan	496-11-7	C_9H_{10}	95	96.7	Aldrich
1-indanol	51-10-06	$C_9H_{10}O$	98	87.5	Aldrich
1-indanone	83-33-0	C_9H_8O	≥99	99.4	Aldrich
1,2-indandione	16214270	$C_9H_6O_2$	97	98.5	Sigma-Aldrich
1,3-indandione	606235	$C_9H_6O_2$	97	99.5	Sigma-Aldrich
benzene	71-43-2	C_6H_6	≥99	99.9	Sigma-Aldrich
di-*tert*-butyl-peroxide	110-05-4	$C_8H_{18}O_2$	99	--[d]	Sigma-Aldrich
hexachlorobenzene	118-74-1	C_6Cl_6	99	99.1	Supleco
chloroform	67-66-3	$CHCl_3$	99.1	98.1	Fisher Scientific

[a] CASRN = Chemical Abstracts Services Registry Number.

[b] This is the purity of the material guaranteed by the supplier.

[c] This is the purity based on peak area obtained by GC-FID analysis.

[d] Compounds were decomposed while GC-FID analysis and purity was not determined

Di-*tert*-butyl peroxide (DTBP) was used as an initiator to shorten the exceedingly long induction period at 50 °C without any phase separation.

The oxidized model compounds of 1-indanol, 1-indanone, 1,2-indandione, and 1,3-indandione were used only to assist with the identification of products during analysis by gas chromatography with mass spectrometry (GC-MS). Hexachlorobenzene was used as an internal standard for quantification using gas chromatography with flame ionization detector (GC-FID) in order to calculate conversion and selectivity. Chloroform was used as a solvent for GC-FID and GC-MS analyses, as well as mobile phase during high performance liquid chromatography (HPLC).

Extra-dry air (Praxair Inc., Canada) was used as an oxidizing agent and nitrogen (99.999 % molar purity, Praxair Inc., Canada) was used to calibrate the fluorimeter to determine the dissolved oxygen content in the bulk liquid.

7.2.2 Equipment and Procedure

A three-necked round bottom glass flask was employed as flat interface reactor (**Figure 7.1**). Autoxidation of indan was performed in semi-batch mode where liquid was batch and air flow was continuous. The gas was introduced above the liquid so that there was no bubbling of the gas through the liquid phase. The gas–liquid interface was therefore clearly defined and it could be accurately measured. The gas flow rate was monitored by gas flow meters (Bel-Art, NJ, USA). Off gases were passed through the cold trap to obtain a liquid-free off gas, which was passed through a calcium chloride bed to remove any water present in the off gas. An online oxygen and carbon dioxide analyzer (Series 9600, Alpha Omega Instruments, USA) and mass spectrometer (Extorr XT Series RGA, XT300 M, Extorr, Inc., PA, USA) were used to analyze off gas. Liquid samples (~ 0.5 g) were collected at different times during the experiment from the bottom of the reactor for chromatographic analysis. A balance, Denver Instruments (SI–403, capacity of 400 g with readability of 0.001 g) was used for all weight determinations in this study.

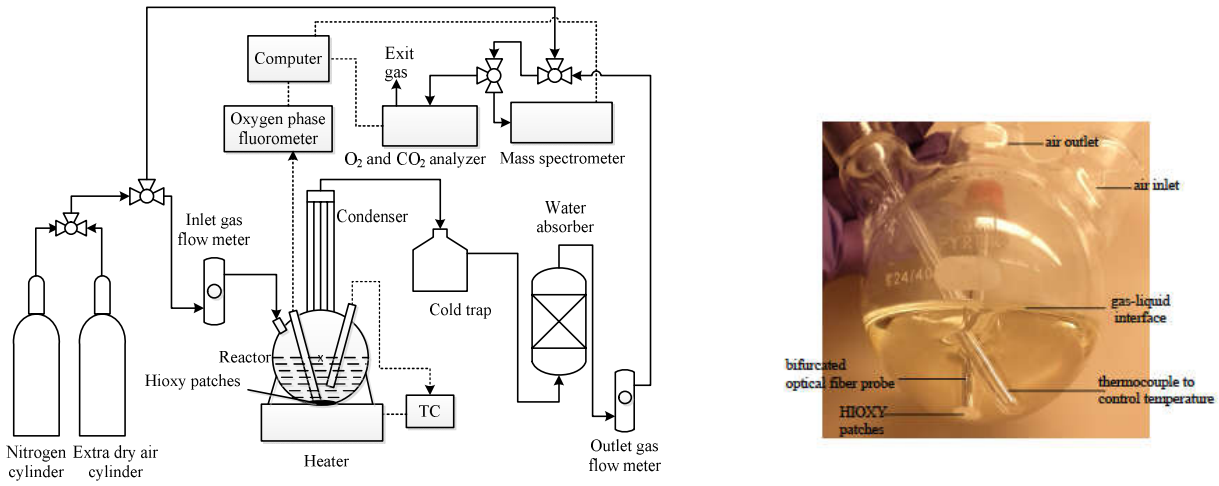

(a) (b)

Figure 7.1. Experimental setup for the autoxidation of hydrocarbon (a) and a flat interface reactor (FIR) used for the oxidation study (b).

In a typical experiment, cleaned and pre–weighted parts of the reactor system were connected and purged with nitrogen to eliminate the oxygen present in the system. The online oxygen analyzer and online mass spectrometer were used to confirm this. Approximately 65 g of indan (or benzene) was then transferred to a three-neck round bottom flask followed by nitrogen purging through the reactor at room temperature for twenty minutes to displace oxygen present in the liquid phase. In the presence of nitrogen flow, the reactor was heated to 50 °C by using a Heidolph MR Hei-Standard heat-on-block heater. A thermocouple measured the temperature of the solution and it was connected to the heater controller to control the temperature in the flask. A HIOXY patch was attached to the bottom of the reactor (**Figure 7.1**) for *in situ* oxygen measurement and it is described in Section 7.2.3 on dissolved oxygen analysis.

A stable fluorescence decay value was corresponding to 0 kPa oxygen was determined under nitrogen flow. Nitrogen flow was then replaced by the controlled flow of air and the liquid phase was given time to equilibrate with the oxygen in air. At this point, a stable decay value that corresponding to the maximum oxygen partial pressure was determined. During the calibration with benzene, several flow cycles of alternating nitrogen and air were used to verify the response of the system, which tracked the dissolved oxygen content over time. These cycles were also useful for determining the mass transfer coefficient of oxygen from the gas to the liquid.

For oxidation experiments using indan, from 1 to 9.2 wt % di-*tert*-butyl peroxide was added after reaching the saturated value. The di-*tert*-butyl peroxide was used instead of hydrogen peroxide to avoid phase separation during the oxidation process. Hydrogen peroxide (50 wt % aqueous solution, Fischer Scientific) was used in preliminary experiments to reduce the induction period, but it was found that the hydrogen peroxide not only complicated the interpretation of results, but also interacted with the HIOXY patch to affect the measurements.

Experiments were repeated at least two times except for the experiment using 1 wt % and 3 wt % di-*tert*-butyl peroxide.

In order to confirm that it is free radical conversion process one could perform control experiments by using radical trap. Also a control experiment with N_2 could indicate the thermal effect in free radical oxidation process. A free radical trap was not used in this study, but a control experiment of indan was performed with nitrogen and no products were identified via GC-MS analysis. In fact, indan was not oxidized during autoxidation of 36 hours at 50 °C.

7.2.3 Dissolved Oxygen Analysis

A fluorometer (Ocean Optics Inc., FL, USA) was used to measure dissolved oxygen (O_2) in the liquid phase *in situ* at experimental conditions. There are two components to the system, one is the fluorometer with bifurcated optical fiber probe and the other is the oxygen-sensitive fluorescing material. The fluorometer uses a light emitting diode with blue emission at 450 nm to excite the oxygen sensitive material. The fluorescence of the oxygen sensitive material is quenched by interaction with oxygen and the extent of quenching of the fluorescence is a measure of the dissolved oxygen concentration. The fluorescence is affected by temperature and the temperature of the liquid must be controlled, or factored into the calibration. In this work the temperature was controlled.

The oxygen sensitive material that was employed was a polycarbonate HIOXY patch supplied by Ocean Optics Inc. The HIOXY patch incorporated a noble metal porphyrin complex in the membrane material. No oxygen is consumed during analysis, but with use there is some decay in the fluorescence. Due to the decay in fluorescence with use, the baseline over time is not constant, but sloped; the magnitude of the slope is dependent on the oxygen sensitive material.

The fluorescence decay rate reported by the manufacturer for HIOXY patches is 0.007 % per hour. In the experimental work the slope was determined by regularly repeating 0 kPa oxygen measurements.

Most of the experimental work was conducted at 50 °C. Oxidation experiments were conducted at 150, 140 and 100 °C, but the service lifetime of the HIOXY patches were short at these temperatures, making it difficult to obtain accurate data over time. It appeared that not only excitation at 450 nm, but also high temperature, cause a deterioration in the fluorescence of the oxygen sensitive material.

Benzene, which is not oxidized by air at the conditions tested, was used with air (0.209 mol O_2/mol) and nitrogen (0 mol O_2/mol) to calibrate the measurement scale at controlled temperature. The calibration for liquid phase oxygen content was therefore measured in terms of the oxygen partial pressure. The liquid phase oxygen concentration was a derived value that was proportional to the oxygen partial pressure and it was calculated based on application of Henry's Law as is explained in the Calculations section, Section 7.2.5.

7.2.4 Product Analyses

In addition to the online analyzers noted in the Equipment and Procedure section, the liquid products collected during the oxidation experiments were analyzed offline using the following instrumental techniques:

(a) An Agilent 7890A gas chromatograph with flame ionization detector (GC-FID) was used for quantitative analysis. The instrument was equipped with DB-5 MS 30 m × 0.25 mm × 0.25 μm column. The sample injection volume was 1 μL with a split ratio of 10:1. Helium was used as carrier gas with a flow of 2 mL/min, which was kept constant during the experiment. The oven temperature was 75 °C for 0.5 minutes and then temperature was increased from 75 °C to 325 °C at a rate of 20 °C/min, and finally, the temperature was kept constant at 325 °C for 5 minutes. Chloroform was used as solvent and hexachlorobenzene was added as an internal standard when samples were prepared for analysis.

In a typical GC–FID analysis, approximately 50 µL (~89 µg) sample was mixed with ~1 µL (~1.7 g) solution of hexachlorobenzene in chloroform (0.04 wt/wt %). Eppendorf research plus micropipettes of 100 and 1000 µL were used for the sample transfer in a 1.5 mL GC vial (Agilent Technologies Canada Inc., Mississauga, ON). An analytical balance (Mettler Toledo, Model XS105 Dual Range with 105 g capacity and 10 µg readability) was used to record the mass of the samples. A 0.04 wt/wt % solution of hexachlorobenzene in chloroform was prepared using a Mettler Toledo Model XP1203S (1.2 kg capacity, with 1 mg readability) and the solution was stored in a refrigerator prior to use for the GC–FID analyses.

(b) A gas chromatograph coupled with mass spectrometer (GC-MS) consisting of an Agilent 78820A GC system (Agilent Technologies Canada Inc., Mississauga, ON) and an Agilent 5977E MSD (Agilent Technologies Canada Inc., Mississauga, ON) mass spectrometer was used to identify the oxidation products. An HP-5 30 m × 0.25 mm × 0.25 µm column was employed to separate the products. The HP-5 and DB-5 MS columns have similar separation characteristics. The same temperature program as employed for GC-FID analyses was used to facilitate the product identification. Oxidation products were classified as primary, secondary and addition products. Primary and secondary oxidation products were identified using the electron impact mass spectra and analysis of the commercially available oxidation products of indan listed in **Table 7.1**. Identification of products from the mass spectra was assisted by making use of the NIST library. Further details related to product identification of indan oxidation are available in Chapter 4.

(c) A high performance liquid chromatograph (HPLC) consisting of a Waters e2695 Separation Module, Waters 2998 Photodiode Array Detector, and Waters 2414 Refractive Index Detector, were employed to identify the possible addition products. Separation was performed using a µBondapak TM NH_2 10µm 125A, 3.9 × 300 mm column (Waters, Ireland). The column temperature was 30 °C. Chloroform was used as mobile phase. The HPLC was operated in an isocratic mode for 50 minutes and the flow rate of the mobile phase was 1 mL/min.

7.2.5 Calculations

(a) The rate of oxygen transfer was calculated using Equation (7.1) (Hobbs et al., 1972):

$$-\frac{dC^b}{dt} = k_L a(C^b - C^*)$$ Equation (7.1)

where, C^b is the oxygen concentration in the bulk liquid (mol/m^3), C^* is the oxygen concentration in the gas–liquid interface (mol/m^3), k_L is the mass transfer coefficient (m/s) and a is the gas–liquid interfacial area (m^2/m^3).

(b) The overall mass transfer coefficient (k_La) was calculated from experiments where the liquid was first deoxygenated by flowing nitrogen. At $t = 0$, when $C^b = 0$, nitrogen flow was switched to air flow. Equation (7.1) was integrated (derivation provided in Appendix C) with the boundary conditions as stated and using the experimental measurements over time the mass transfer coefficient was determined.

$$\ln(C^* - C^b) = -k_L a t + \ln C^*$$ Equation (7.2)

(c) Concentration of oxygen in liquid phase was calculated from the measured oxygen partial pressure using Henry's law (Equation 7.3):

$$C^* = H \times P_{O2}$$ Equation (7.3)

where, C^* is the oxygen concentration in the gas-liquid interface (mol/m^3), H is the Henry's law constant (mol/(m^3.kPa)) and P_{O_2} is oxygen partial pressure in gas phase (kPa).

The Henry's law constant for benzene was available from literature, no Henry's law constant for indan could be found. The Henry's law constant for tetralin ($C_{10}H_{12}$) was available and tetralin as has only one CH_2 more in the cycloalkane ring than indan (C_9H_{10}). The value for the Henry's law constant of tetralin in this study were determined by interpolating data published over the temperature range 10 to 100 °C (**Table C.2**), whereas data for benzene was available at 50 °C (Emanuel et al., 1967; Battino et al.; 1983; Bateman et al., 1951; Mayo and Miller; 1958). Henry's law constants of $H = 7.6\times10^{-2}$ mol/(m^3.kPa) and $H = 9.2\times10^{-2}$ mol/(m^3.kPa) were used for indan and benzene respectively (detail calculation is provided in Appendix C). It is important to point out that any error in the values of H would not affect the trends observed, although it would cause a proportional bias in the absolute values that were calculated.

(d) Gas–liquid interfacial area (a) was calculated from the cross sectional area of the reactor (m^2) and the volume of the liquid (m^3).

(e) Oxidative conversion was calculated using flame ionization detector response factor of indan using conversion factors shown in Appendix C (**Table C.3**) that were obtained from a previous study (Siddiquee and De Klerk, 2014b).

(f) The oxygen consumption rate ($mol/m^3.s$) was calculated from the indan conversion (mol/m^3) and the O_2 consumption ratio (mol O_2/mol indan):

$$\text{oxidation rate} = \frac{\text{indan conversion} \times \text{O}_2 \text{ consumption ratio}}{\text{oxidation time}} \qquad \text{Equation (7.4)}$$

(g) Product selectivity was calculated from the relative peak area of the products and response factors of products were not used in the selectivity calculations due to the diversity of oxidation products.

$$\text{Product selectivity (\%)} = \frac{\text{relative peak area of a specific product}}{\text{sum of relative peak area of all the products}} \times 100\ \% \qquad \text{Equation (7.5)}$$

The ketone-to-alcohol selectivity in primary oxidation products was calculated from the ratio of the relative peak areas of ketones and alcohols in the primary oxidation products.

(h) The diffusion coefficient of oxygen transfer was calculated using Fick's Law, Equation (7.6):

$$J_A = -D_A \frac{dC^b}{dx} \qquad \text{Equation (7.6)}$$

where, J_A is the diffusion flux through the gas–liquid interface ($mol/m^2.s$); C^b is the oxygen concentration in the bulk liquid (mol/m^3), x is the diffusion path length (m) and D_A is the diffusion coefficient (m^2/s). Calculation has shown in **Appendix C (C.10)**.

7.2.6 Calibrations

(a) Oxygen and carbon dioxide analyzer was calibrated by using nitrogen and extra dry air. Nitrogen was passed through the experimental setup for about an hour and it showed zero kPa oxygen partial pressure and zero ppm carbon dioxide. Extra dry air was then passed through the setup until a stable value was obtained and it was set as the maximum oxygen partial pressure.

The calibration was later confirmed by switching nitrogen and air flow. The calibration for carbon dioxide was not verified in the same way, but the instrument indicated 0–2 ppm CO_2 during the calibration performed by using nitrogen and extra dry air.

(b) Oxygen phase fluorometer was calibrated during the oxidation experiment by using air and nitrogen as described in Section 7.2.2. The mol fraction O_2 in the cylinder air was 0.209 mol O_2/mol air. The maximum oxygen partial pressure was had to take the actual atmospheric pressure in Edmonton, Alberta (on average around 93 kPa, or 699 mm Hg) into account, which was lower than atmospheric pressure at sea level (101 kPa, or 760 mm Hg). The pressure in the laboratory was measured using a digital manometer (255W2 Traceable, Fischer Scientific, Canada). The values were also cross-checked against the atmospheric pressure reported at the Edmonton City Center Airport.[7] The maximum oxygen partial pressure was 19.2 kPa.

Additional verification of the calibration was obtained from experiments using benzene. The benzene was inert to oxidation at the conditions investigated. By changing between air and nitrogen flow cycles, values at zero and maximum oxygen partial pressure were recorded that could be compared with the calibration values.

7.3 Results

7.3.1 Benzene Oxidation (Control Experiments)

The first objective of measuring oxygen partial pressure in benzene was to evaluate the performance of oxygen fluorometer for the *in situ* measurement of dissolved oxygen in the liquid. The second objective was to employ air and nitrogen flow cycles to calculate the oxygen transfer rate between gas and liquid phases.

It was found that the fluorometer could be used to track the changes in dissolved oxygen concentration. Changes in oxygen partial pressure during consecutive air and nitrogen flow cycles produced repeatable measurements (**Figure 7.2**), with the dissolved oxygen concentration expressed in terms as equivalent oxygen partial pressure.

[7] http://rp5.ru/Weather_in_Edmonton,_City_Centre_(airport) (Access during performing experiments).

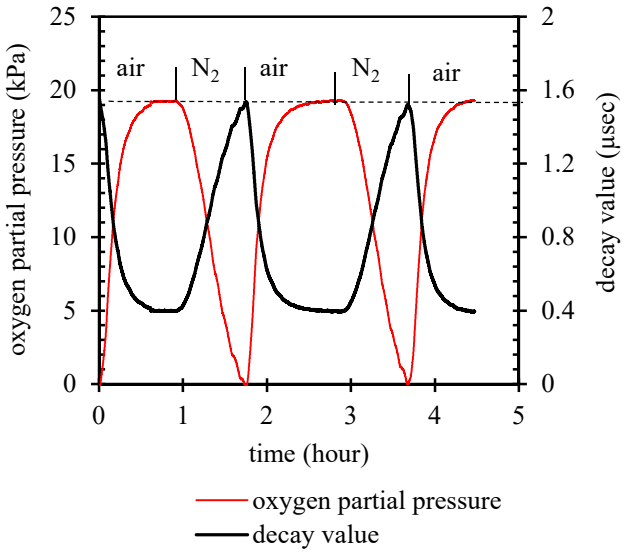

Figure 7.2. Changes in oxygen partial pressure and corresponding decay value during air and nitrogen flow cycles in benzene at 50 °C.

Under constant air flow the dissolved oxygen concentration increased until the benzene was saturated and in equilibrium with the oxygen partial pressure of the air. Under constant nitrogen flow the dissolved oxygen was released from the benzene until no dissolved oxygen was left in the liquid. It was found that removing dissolved oxygen from the benzene by decreasing the oxygen partial pressure to 0 kPa through nitrogen flow was slightly faster than dissolving oxygen in benzene by increasing the oxygen partial pressure to 19.2 kPa through air flow (**Figure 7.3**).

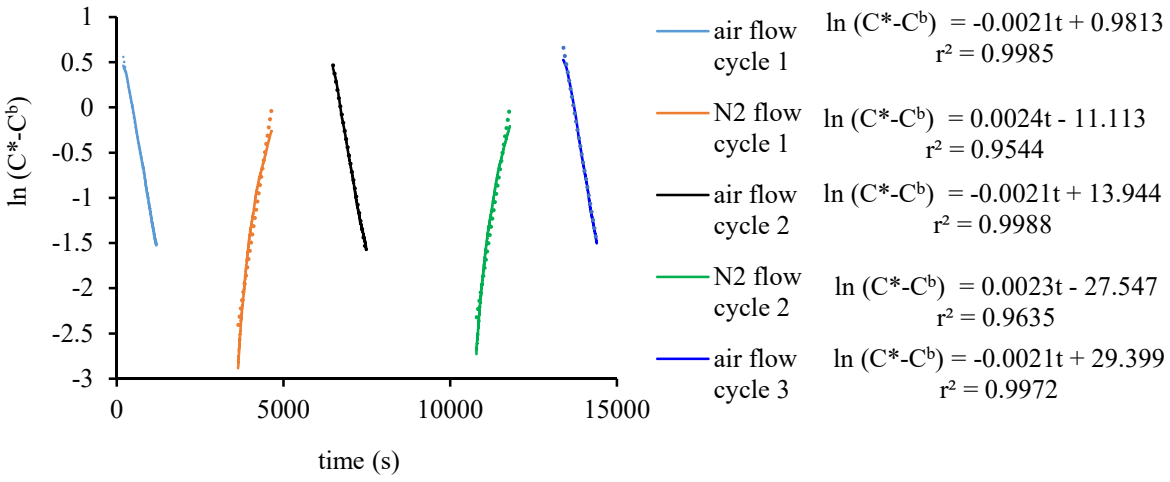

Figure 7.3. $\ln(C^* - C^b)$ vs t plot based on change in oxygen concentration benzene phase with time at 50 °C during air and nitrogen flow cycles shown in Figure 7.2.

The overall mass transfer coefficient (k_La) for oxygen dissolving in benzene at 50 °C was 0.0021 s^{-1}. The correlation coefficient (r^2) was better than 0.99. The gas–liquid interface area (a) was 690 m^2/m^3 during the benzene oxidation and the liquid side mass transfer (k_L) could therefore be calculated: 3.0×10^{-6} m/s.

A slightly higher value for the removal of oxygen from benzene at 50 °C was found, 0.0023-0.0024 s^{-1}. The correlation was 0.95-0.96 and curvature was clearly visible. The poorer fit might be due to the evolution of tiny bubbles as oxygen is released, which would increase the interface area and hence the overall mass transfer coefficient.

As anticipated, benzene was a suitable control and benzene was not oxidized at the studied experimental conditions. Chromatograms of benzene and oxidized benzene are shown in the Appendix C (**Figure C.1**).

7.3.2 Indan Oxidation

The fluorometer was used to measure changes in the dissolved oxygen concentration of indan during oxidation with air at 50 °C. Measurements at higher temperatures were attempted, but the rate of degradation of the oxygen sensitive HIOXY patches were too high to make reliable measurements for experiments lasting several hours. At 50 °C the induction time for autoxidation was very long and it was decided to accelerate induction through the use of di-*tert*-butyl peroxide (DTBP).

The use of DTBP reduced the induction time, but it also caused the oxidation rate to pass through a maximum rate that was much higher than autoxidation on its own. The added benefit of this approach was that it was possible to study different oxidation rates at the same temperature without changing the gas–liquid interface area or oxygen partial pressure. As the DTBP was converted and consumed during the oxidation, the contribution of the DTBP accelerated oxidation diminished over time. Different amounts of DTBP in the range 1 to 9.2 wt% were used to explore oxygen availability in the liquid phase at different reaction rates.

7.3.2.1 Indan with 5.1 wt% di-*tert*-butyl peroxide

The indan was saturated with oxygen over a period of around 1 hour. During this induction period the rate of oxidation was negligible. Oxygen availability was equivalent to an oxygen partial pressure of 19.2 kPa (**Figure 7.4**), which based on the Henry's law calculation (Equation 7.3), is about 1.5 mol O_2/m^3.

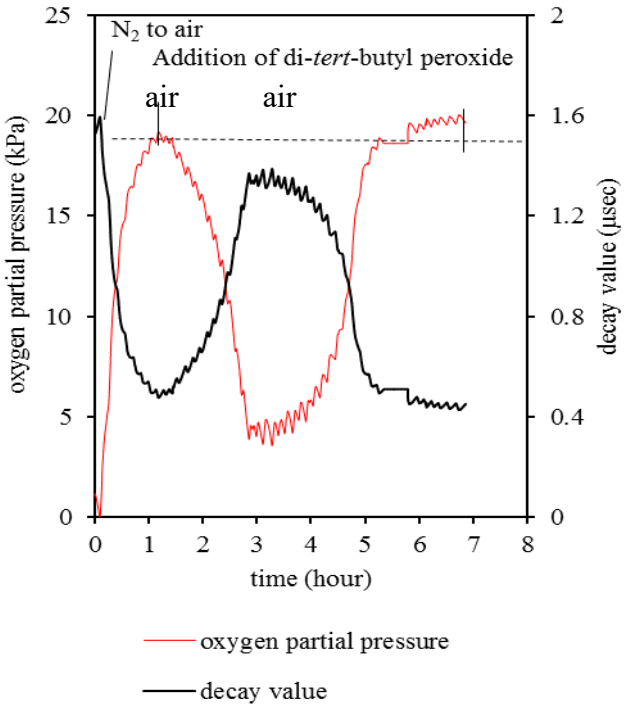

Figure 7.4. Changes in oxygen partial pressure and corresponding decay value during oxidation of indan with air at 50 °C (5.1 wt % di-*tert*-butyl peroxide was added after 1 hour).

When 5.1 wt% DTBP initiator was added to the indan, the oxidation rate was increased. Conversion and selectivity results are reported in Section 7.3.3. The increase in oxidation rate exceeded the rate of mass transport of oxygen from the gas phase and over a period of around 2 hours the oxygen content in the liquid phase decreased from 19.2 kPa O_2 until it remained constant at a value of 4.5 kPa O_2. As the DTBP was consumed that oxidation rate and O_2 consumption decreased again, as can be seen from the increase in oxygen availability after 4 hours, i.e. 3 hours after DTBP was added.

There were two experimental observations in **Figure 7.4** that raised some questions. The minimum oxygen availability in the liquid phase was not zero, but lined out at 4.5 kPa O_2. When oxygen availability in the liquid phase recovered, it recovered to 20.0 kPa O_2, which exceeded the partial pressure of O_2 in the gas phase. It was suspected that during the period of accelerated oxidation, the decay rate of the HIOXY patch increased, so that the calibration changed. If this were the case, the oxygen content in the liquid phase would be lower than calculated from the calibration.

What was particularly important to know, was whether the lowest level of oxygen availability was zero or not. The experiment was repeated, but after 3 hours air flow was switched to nitrogen flow (**Figure 7.5**).

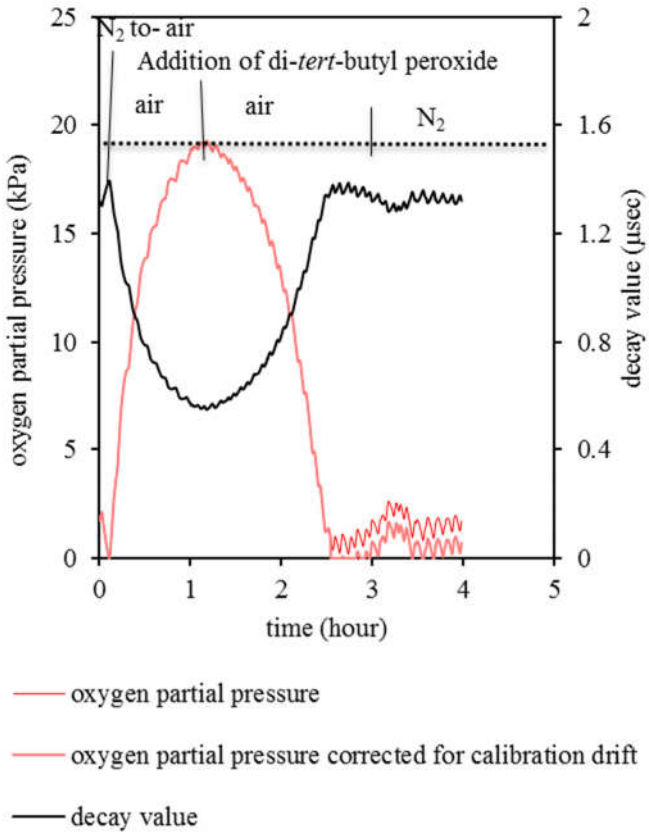

Figure 7.5. Change in oxygen partial pressure and corresponding decay value during oxidation of indan with air at 50 °C (5.1 wt % di-*tert*-butyl peroxide was added after 1 hour and air was switched to N_2 was after 3 hour).

If the lowest measured oxygen availability was above zero, the combined effect of DTBP and absence of oxygen in the gas phase would cause the remaining oxygen in the liquid phase to be eliminated. No further decrease in oxygen availability was found when air flow was switched to nitrogen flow. In this experiment the calibration did not appear to drift much either. The decay value from the calibration was 1.35 μsec, which corresponded to ~1.0 kPa O_2 pressure. The decay value was 1.37 μsec before switching to nitrogen. It was confirmed that oxygen was completely consumed in the liquid phase within 2 hours after adding DTBP.

7.3.2.2 Indan with 1 to 4.7 wt% Di-*tert*-Butyl Peroxide

The preceding experiments (**Figures 7.4 and 7.5**) demonstrated that at high oxidation rate dissolved oxygen in the bulk liquid could be completely depleted. Oxidation of indan using less DTBP was explored to find conditions at which oxygen availability in the liquid phase was not meaningfully decreased. The concentration range from 1 to 4.7 wt % DTBP initiator was explored.

As in the previous experiments, the indan was saturated with O_2 from the air flow to reach an oxygen availability in the liquid phase equivalent to 19.2 kPa. After 1 hour, 1 wt % DTBP was added, but there was no measurable change in the oxygen availability in the liquid phase (**Figure 7.6**). The apparent slight increase in oxygen availability after adding the 1 wt % DTBP is due to the change in the decay value of the HIOXY patch, which was confirmed by introducing nitrogen for 1 hour, followed by air for 1 hour. When the nitrogen was introduced the oxygen availability decreased to zero and when air was introduced the oxygen availability increased again to its previous value. The slight negative slope in the measured decay value is related to the deterioration in the fluorescence of the oxygen sensitive material in the HIOXY patch, as was anticipated and explained in the Experimental section.

When the indan was saturated with O_2 after the nitrogen–air cycle, 1.5 wt% DTBP was added (**Figure 7.6**). The change in liquid phase oxygen availability was barely noticeable and the liquid phase remained near saturated with O_2. To confirm the measurement, the air flow was replaced with nitrogen flow. Apart from the slight anticipated change over time in the decay

value versus liquid phase oxygen concentration response, the calibration remained valid for the duration of the experiment.

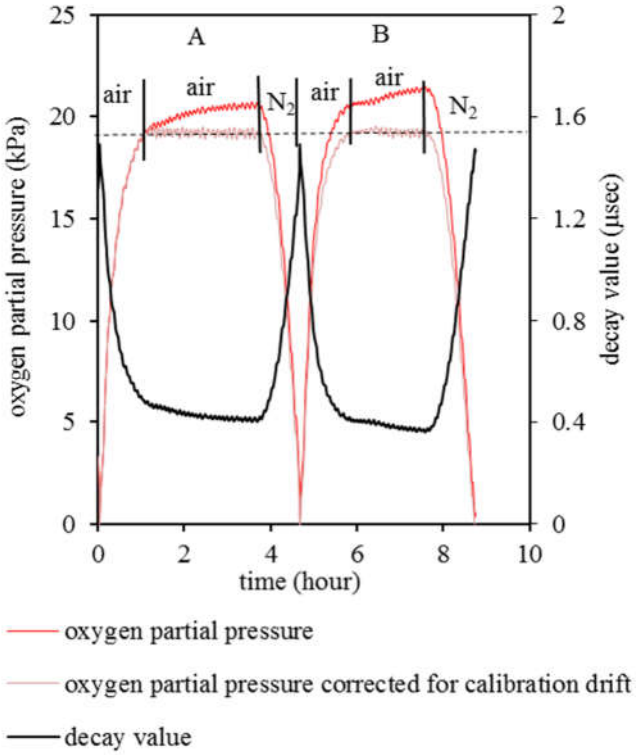

Figure 7.6. Changes in oxygen partial pressure and corresponding decay value during oxidation of indan with air at 50 °C (1 wt % di-*tert*-butyl peroxide was added after 1 hour (A), additional 1.5 wt% added at ~ 6 hour (B)).

The change in oxygen availability in the liquid phase was measured for the addition of 3 wt% DTBP (**Figure 7.7**) and the change in O_2 in the liquid phase was barely noticeable.

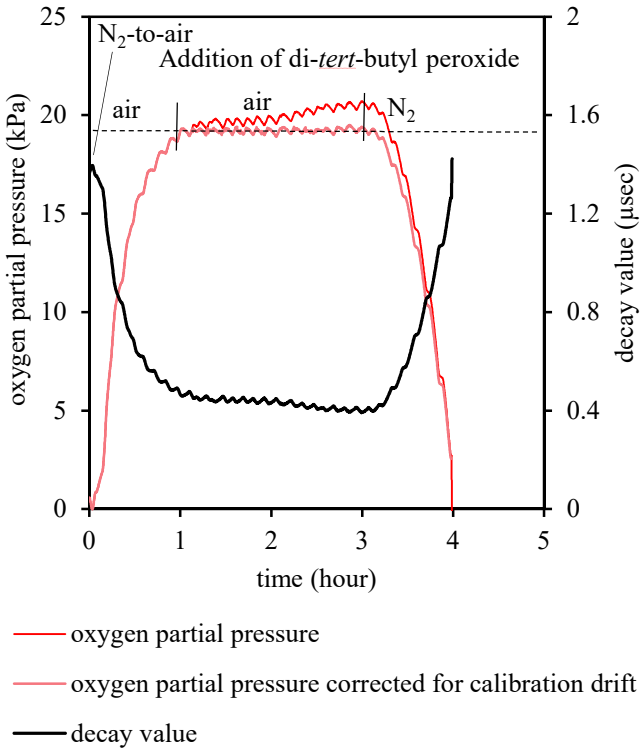

Figure 7.7. Changes in oxygen partial pressure and corresponding decay value during oxidation of indan with air at 50 °C (3 wt % di-*tert*-butyl peroxide was added after 1 hour).

The experiment was repeated with 4.7 wt% DTBP (**Figure 7.8**) and at this concentration of the oxidation initiator, depletion of oxygen in the liquid phase was clearly noticeable. The oxygen in the liquid phase decreased from 19.2 kPa O_2 to around 15 kPa O_2 over a period of 2 hours after the DTBP was added to the indan. As the DTBP was consumed the oxidation rate decreased and liquid phase oxygen content returned to its saturated value. As in previous experiments there was a slight change over time in the calibration.

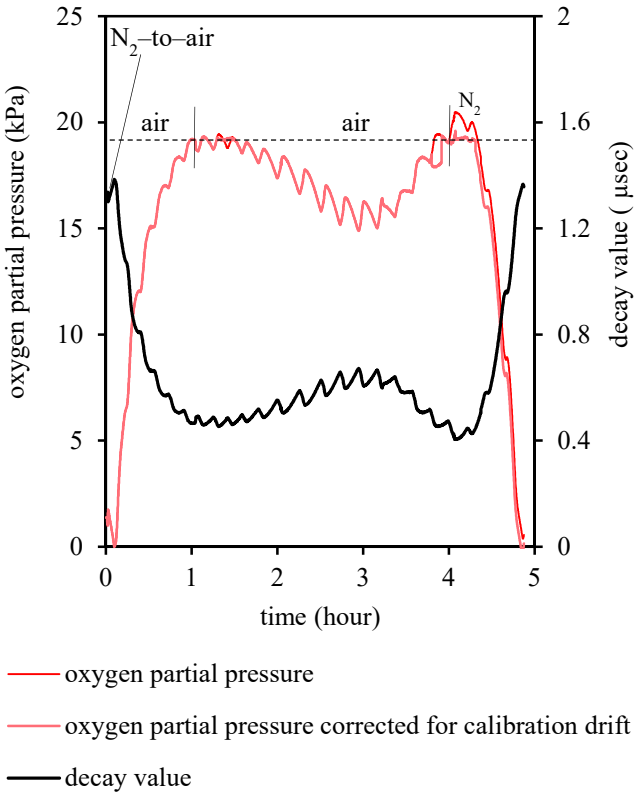

Figure 7.8. Changes in oxygen partial pressure and corresponding decay value during oxidation of indan with air at 50 °C (4.7 wt % di-*tert*-butyl peroxide was added after 1 hour).

Contrary to the experiments using 5.1 wt% DTBP (**Figure 7.5**), at 4.7 wt% DTBP (**Figure 7.8**) the oxidation rate was not high enough to completely deplete the liquid phase of dissolved oxygen. Yet, at 4.7 wt% DTBP addition the oxidation rate was high enough to slightly exceed mass transport of O_2 for about 2 hours, during which there was a decrease in the bulk liquid phase oxygen concentration.

7.3.2.3 Indan with 9.2 wt% Di-*tert*-Butyl Peroxide

To illustrate a situation of severe mass transfer limitation during liquid phase oxidation and to serve as a control experiment, 9.2 wt% DTBP was added to oxygen saturated indan (**Figure 7.9**). In less than 1 hour after the DTBP was introduced, the oxygen dissolved in the liquid phase was completely depleted.

To confirm that the slightly positive and increasing oxygen concentration was due to a change in the response of the decay value to dissolved oxygen, the air flow was replaced with nitrogen flow after 3 hours (**Figure 7.9**). The trend over time in the decay value was uninterrupted and it confirmed that the oxygen content in the liquid phase was zero.

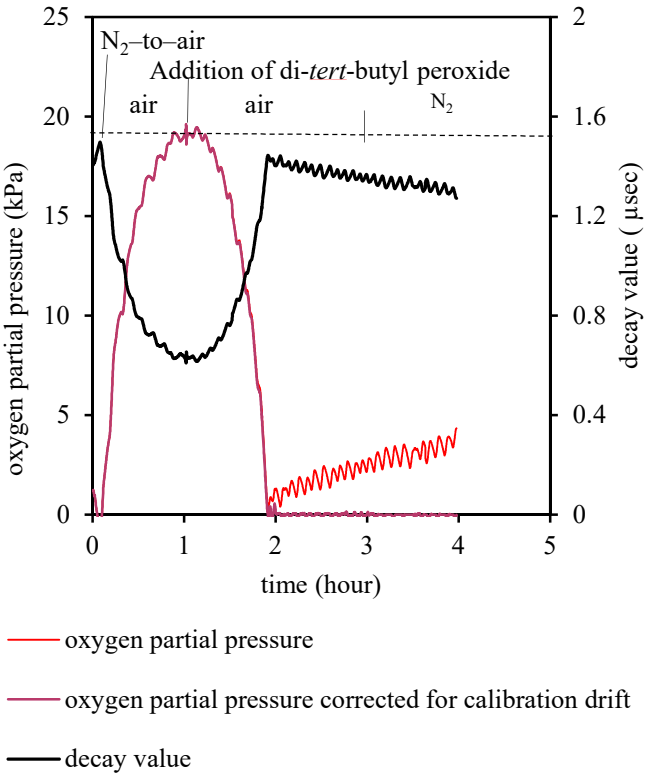

Figure 7.9. Change in oxygen partial pressure and corresponding decay value during oxidation of indan with air at 50 °C (9.2 wt % di-*tert*-butyl peroxide was added after 1 hour and air was switched to N_2 was after 3 hour).

7.3.2.4 Mass Transfer Coefficient

There were seven sets of measurements available to determine the mass transfer coefficient of O_2 from air to indan (**Figure 7.10**). The average overall mass transfer coefficient (k_La) was 1.0×10^{-3} s^{-1}, with a sample standard deviation of 0.1×10^{-3} s^{-1}. During the indan oxidation experiments the gas–liquid interface area was 770 m^2/m^3, so that the liquid side mass transfer coefficient (k_L) could be calculated: 1.3×10^{-6} m/s.

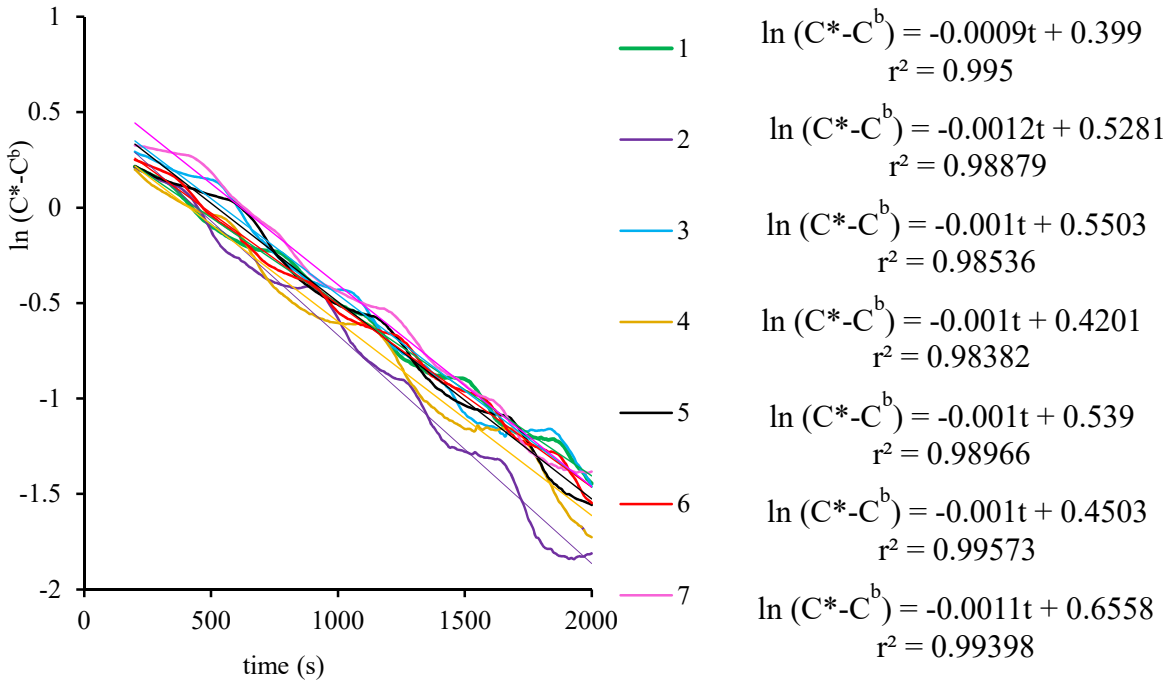

Figure 7.10. $\ln(C^* - C^b)$ vs t plot based on change in dissolve oxygen content with time during oxidation of indan with air at 50 °C.

The maximum rate of O_2 transfer to the liquid phase is when there is no dissolved oxygen in the bulk liquid, i.e. $C^b = 0$, and it can be calculated using Equation (7.1). The O_2 concentration at the interface (C^*) in equilibrium with the O_2 partial pressure in the gas phase was calculated from Henry's law, (Equation 7.3). For indan at 50 °C with 19.2 kPa O_2 partial pressure $C^* = 1.46$ mol/m^3. Using the mass transfer coefficient obtained from the experimental measurements, it was calculated that the maximum rate of O_2 transfer to the liquid phase was 1.9×10^{-6} mol/(m^2.s), with an uncertainty of 0.2×10^{-6} mol/(m^2.s).

At the experimental conditions employed, this meant that the maximum oxygen transfer rate was 1.5×10^{-3} mol O_2/(m^3.s), given that the gas–liquid interface area of the flat interface reactor was known and constant during the indan oxidation experiments.

7.3.2.5 Diffusion Coefficient

Diffusion coefficient of oxygen transfer from the air to the indan phase was 6.6×10^{-8} (m^2/s), with an uncertainty of 3.8×10^{-9} (m^2/s). Interfacial area of 770 m^2/m^3 and a diffusion path length of 5 cm were used in calculating the diffusion coefficient.

7.3.3 Conversion and Selectivity Measurements

The conversion of indan, as well as the selectivity to different oxidation products over time was determined from analysis of the liquid products (**Table 7.2**). The reaction times indicated, were measured from the time that the DTBP oxidation initiator was added, i.e. one hour after the start of the reaction, and not from the start of the experiment.

Samples taken just before addition of DTBP confirmed that no measurable oxidation was found after exposing the indan to air at 50 °C for one hour. In fact, at 50 °C the induction period for the indan oxidation with air was exceedingly long. Very limited change was observed at 50 °C even after 36 hours at oxidation conditions, as can be seen from the chromatograms provided in Appendix C (**Figure C.2**).

The oxidation products were lumped into three categories: primary oxidation products, secondary oxidation products and addition products. The primary oxidation products were indan that was oxidized either to the alcohol or ketone derivative of indan, namely, indanol and indanone. The secondary oxidation products were all of the other oxidation products with the same or less carbon atoms as than indan and were mostly indan with two oxygen atoms per molecule. An example of a typical secondary oxidation product is the diketone of indan, 1,2-indadione. The addition products were products with more carbon atoms per molecule than indan and were mostly oxidative dimerization products. It is noteworthy that some of the addition products contained no oxygen containing functional groups. The formation of addition products was also confirmed by HPLC analysis (**Figure C.3**).

A detailed description of product identification can be found in previous work (Chapter 4), as well as the Appendix C. It was anticipated that DTBP could interfere with the product identification due the decomposition of weak peroxide bond to form *tert*-butyl oxy-radicals and ultimately *tert*-butanol and *tert*-butoxy-derivatives, but it was possible to identify and segregate the oxidation products from indan and DTBP using GC-MS analysis (**Figures C.4** to **C.6**).

Table 7.2. Product selectivity and O_2 consumption during the oxidation indan in a flat interface reactor at 50 °C and air flow rate of ~110 mL/h per g liquid.

Description	Conversion and Selectivity [a]			
Time (min)	30 min	60 min	120 min	180 min
Indan with 1 wt % DTBP				
Indan conversion	0.02	0.05	0.07	0.1
Indan conversion in interval	0.02	0.03	0.02	0.02
primary oxidation products (wt %) [b]	100.0	100.0	100.0	100.0
secondary oxidation products (wt %) [b]	0.0	0.0	0.0	0.0
addition products (wt %) [b]	0.0	0.0	0.0	0.0
ketone to alcohol in primary oxidation products	1.2	1.2	1.2	1.2
oxygen consumption rate (mol/m^3.s)	6.9×10^{-5}	3.1×10^{-5}	2.0×10^{-5}	1.6×10^{-5}
Indan with 3 wt % DTBP				
Indan conversion	0.04	0.34	0.8	1.3
Indan conversion in interval	0.04	0.3	0.5	0.5
primary oxidation products (wt %) [b]	100.0	18.9	13.6	14.0
secondary oxidation products (wt %) [b]	0.0	2.1	1.9	1.8
addition products (wt %) [b]	0.0	79.0	84.5	84.2
ketone to alcohol in primary oxidation products	1.5	1.5	1.3	1.5
oxygen consumption rate (mol/m^3. s)	4.8×10^{-5}	4.6×10^{-4}	4.7×10^{-4}	3.6×10^{-4}
Indan with 4.7 wt % DTBP				
Indan conversion	0.2	1.6	3.7	5.4
Indan conversion in interval	0.2	1.4	2.1	1.7
primary oxidation products (wt %) [b]	100.0	14.5	10.1	12.6
secondary oxidation products (wt %) [b]	0.0	2.7	2.5	2.9
addition products (wt %) [b]	0.0	82.8	87.4	84.5
ketone to alcohol in primary oxidation products	1.39	1.13	1.12	1.14
oxygen consumption rate (mol/m^3. s)	5.0×10^{-4}	2.0×10^{-3}	1.9×10^{-3}	1.2×10^{-3}
Indan with 5.1 wt % DTBP [b]				
Indan conversion	0.8	2.3	4.8	7.2
Indan conversion in interval	0.8	1.5	2.5	2.4
primary oxidation products (wt %) [b]	40.7	56.3	38.5	42.7
secondary oxidation products (wt %) [b]	1.5	1.4	2.8	4.2
addition products (wt %) [b]	57.8	42.3	58.6	53.1
ketone to alcohol in primary oxidation products	1.7	1.6	1.4	1.6
oxygen consumption rate (mol/m^3. s)	1.6×10^{-3}	2.4×10^{-3}	2.6×10^{-3}	1.9×10^{-3}
Indan with 9.2 wt % DTBP				
Indan conversion	3.0	5.1	6.7	8.4
Indan conversion in interval	3.0	2.1	1.6	1.7
primary oxidation products (wt %) [b]	43.1	10.9	18.8	10.7
secondary oxidation products (wt %) [b]	9.9	3.0	5.4	2.8
addition products (wt %) [b]	47.0	86.1	75.8	86.5
ketone to alcohol in primary oxidation products	1.3	1.4	1.4	1.3
oxygen consumption rate (mol/m^3. s)	6.5×10^{-3}	3.0×10^{-3}	1.5×10^{-3}	1.2×10^{-3}

[a] Average of at least triplicate GC-FID runs. The reaction times started from the time that DTBP was added and analysis just before adding the DTBP found no oxidation. Products formed immediately after adding DTBP were subtracted from the corresponding products formed at different oxidation time to calculate the reported conversion and selectivity in the presence of DTBP.

[b] Weight percentage of all oxidized products in the liquid

The online MS identified no gases other than the feed gases. The online O_2 and CO_2 analyzer did not detect any carbon dioxide production (CO_2), regardless of the experiment. A small amount of water was observed in indan phase after completion of the experiment in the presence of 9.2 wt% DTBP.

7.4 Discussion

7.4.1 Oxidation in the Film or in the Bulk?

It is customary to classify reactions as kinetically controlled or mass transport controlled. Mass transport is definitely controlling when the oxygen consumption rate reaches the maximum oxygen transport rate. In this experimental study it was possible for the oxygen consumption rate to exceed the maximum oxygen transport rate (**Figure 7.11**), because the liquid phase was pre-saturated with oxygen. There was a dynamic depletion of oxygen in the liquid phase at high oxidation rate as shown in **Figures 7.4, 7.5, 7.8 and 7.9**.

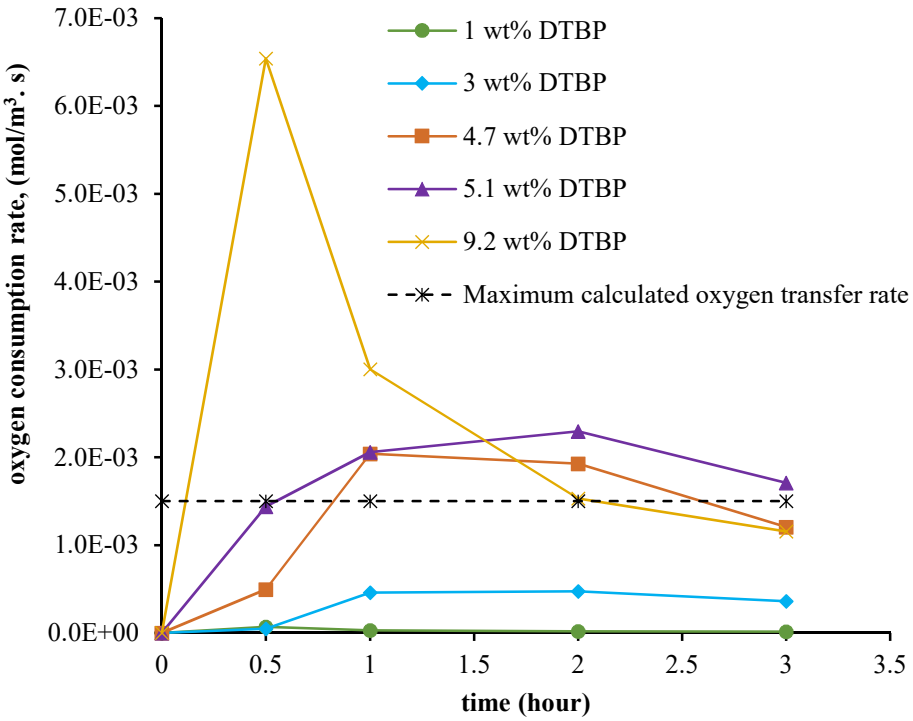

Figure 7.11. Oxygen consumption rates of indan autoxidation performed in the presence of 1–9.2 wt % di-*tert*-butyl peroxide (DTBP) at 50 °C (DTBP was added after 1 hour and considered as 0 time).

Once all of the dissolved oxygen in the bulk liquid phase is consumed, the oxygen consumption rate is limited to the maximum oxygen transfer rate. This was experimentally observed in the reaction with 9.2 wt% DTBP, which depleted all of the dissolved oxygen within 60 minutes. After this period there was no more oxygen available in the bulk liquid (**Figure 7.9**) and the oxygen consumption rate had to decrease to a value that was at most equal to the maximum oxygen transfer rate. This is indeed what was found (**Table 7.2** and **Figure 7.11**), with the oxygen consumption rate in the reaction period from 60 to 90 minutes after DTBP was added decreasing to 1.5×10^{-3} mol $O_2/(m^3.s)$ and remaining at or below this value.

The situation is more complex when the oxygen consumption rate that is less than the maximum oxygen transfer rate. In practice mass transport always influences liquid phase autoxidation. The driving force for transport of oxygen from the gas phase to the liquid phase is the difference in the oxygen concentration at the gas–liquid interface and the bulk liquid, $(C^* - C^b)$ in Equation (7.1). Only when oxidation rate is negligible, does the bulk liquid phase remain saturated with oxygen. Otherwise, a dynamic equilibrium is established between the oxygen consumption rate that is equal to oxygen mass transport rate and both rates are related to the bulk liquid phase oxygen concentration.

Thus, with the exception of an oxygen consumption rate equal to the maximum oxygen mass transfer rate, the bulk liquid phase will always have some dissolved oxygen. The relative contribution of oxidation in the film and oxidation in the bulk liquid is related to the relative volumes of the film and bulk and the oxygen concentration in each. The film has an oxygen concentration profile with oxygen concentration between C^* and C^b, whereas the bulk has an oxygen concentration that is by definition equal to C^b.

7.4.2 Phenomenon of Liquid Phase Oxidation

Kinetically controlled and mass transfer limited phenomenon of liquid phase autoxidation was confirmed from the *in situ* measurement of the oxygen level in the liquid phase at experimental conditions. The comparison of oxidation rate and mass transfer rate, and addition product formation would yield additional information about the impact of oxygen availability during liquid phase oxidation

It is apparent from the **Figures 7.2, 7.6** and **7.7** that oxygen level in the liquid phase did not decrease except in case of N_2 flow cycles. It indicates benzene oxidation and indan oxidation in the presence of 1–3 wt % of di-*tert*-butyl peroxide were kinetically controlled. Although 1–3 wt % of di-*tert*-butyl peroxide would create free radical intermediates, those might not be enough for the notable changes in oxygen consumption. All the reported indan oxidations (**Figures 7.4**–7.**9**) during first one hour (before adding di-*tert*-butyl peroxide) were kinetically controlled as oxygen level in the liquid phase did not observably change. Hence, addition of 0–3 wt % of di-*tert*-butyl peroxide can be considered as kinetically controlled. Kinetic control is typical of the induction period and slow oxidation, as reported previously in liquid phase oxidation studies (Suresh et al., 2000; Hobbs et al., 1972; Fischer et al., 2010; Suresh et al., 1988c).

As oxygen level decreased after adding di-*tert*-butyl peroxide of 4.7 wt % or higher (**Figures 7.4, 7.5, 7.8** and **7.9**), was influenced by mass transfer. This can be explained by the higher concentration of free radical intermediates that consumed dissolved oxygen and reduced the oxygen level in bulk liquid phase. This could be true for any liquid phase autoxidation.

The above mentioned kinetic and mass transfer phenomenon was also evaluated by comparing mass transfer rate and oxidation rate of the reported experiments. It is clear from the **Figures 7.12–7.16** that mass transfer rate was higher compared to the oxidation rate during the induction period (before adding di-*tert*-butyl peroxide). Higher mass transfer rate compared to oxidation rate supports the kinetically controlled nature of the initial stages of liquid phase oxidation.

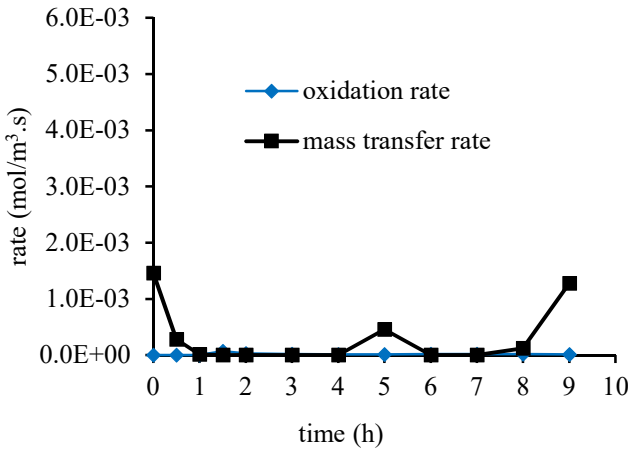

Figure 7.12. Comparison of oxygen transport and consumption rates of indan autoxidation in the presence of 1.0 wt % (1–6 hour) and 2.5 wt % (6–9 hour) di-*tert*-butyl peroxide at 50 °C. DTBP was added after 1 hour. Data points representing oxidation rate are the average of three GC-FID run of single experiment.

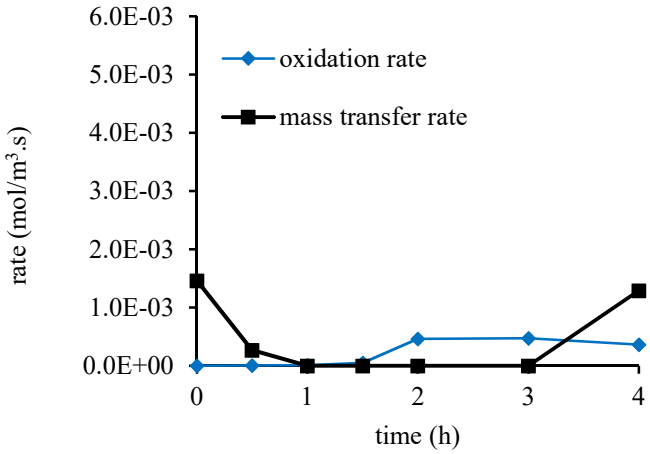

Figure 7.13. Comparison of oxygen transport and consumption rates of indan autoxidation in the presence of 3.0 wt % di-*tert*-butyl peroxide at 50 °C. DTBP was added after 1 hour. Data points representing oxidation rate are the average of three GC-FID run of single experiment.

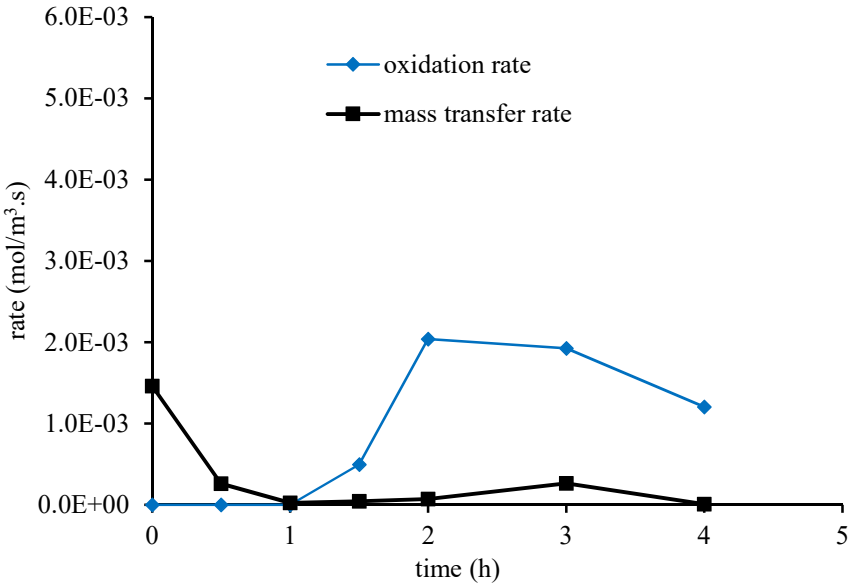

Figure 7.14. Comparison of oxygen transport and consumption rates of indan autoxidation in the presence of 4.7 wt % di-*tert*-butyl peroxide at 50 °C. DTBP was added after 1 hour. Data points representing oxidation rate are the average of three GC-FID run of single experiment.

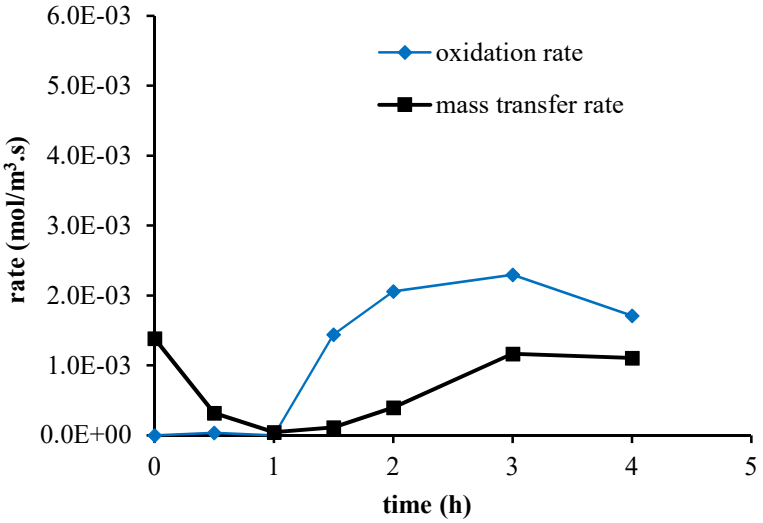

Figure 7.15. Comparison of oxygen transport and consumption rates of indan autoxidation in the presence of 5.1 wt % di-*tert*-butyl peroxide at 50 °C. DTBP was added after 1 hour. Data points are average of six GC-FID run of repeating experiments.

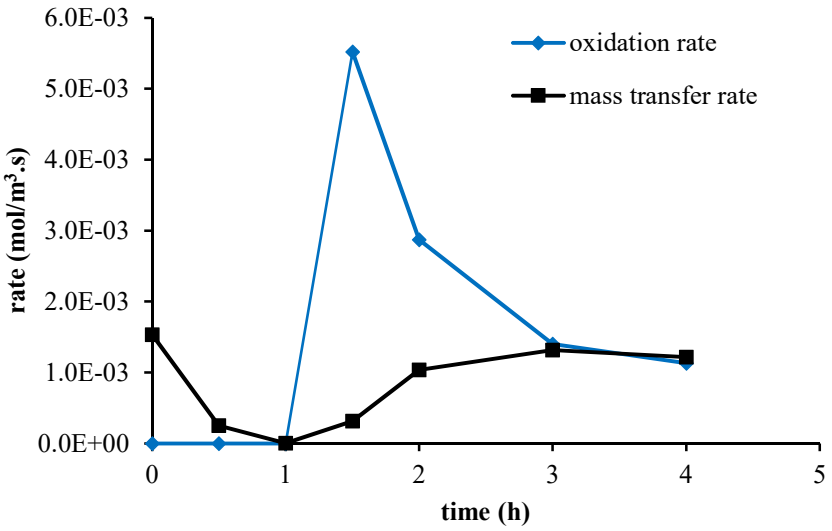

Figure 7.16. Comparison of oxygen transport and consumption rates of indan autoxidation in the presence of 9.2 wt % di-*tert*-butyl peroxide at 50 °C. DTBP was added after 1 hour. Data points are the average of six GC-FID run of repeating experiments.

Higher mass transfer rate presented in **Figures 7.12** to **7.16** can be explained by the concentration gradient before indan was saturated. Initially oxygen concentration was zero mol/m^3 in liquid phase, which resulted in highest concentration gradient and mass transfer rate was higher. Mass transfer rate was then decreased as oxygen concentration increased in liquid phase, which decreased the concentration gradient. Liquid phase becomes saturated with oxygen. The main reason of the saturation would be the constant and mild airflow to indan and no consumption of oxygen in the liquid phase during the induction period. This would also be true for oxygen transport in benzene.

Mass transfer coefficient influences the oxygen transport from air to liquid phase (Chapter 6; Suresh et al., 1988a). Mass transfer coefficients of benzene were comparatively higher than that of indan. It might de due to the higher solubility of oxygen in benzene compared to the indan as described in Section 7.2.4. It was interesting to observe higher mass transfer coefficient of N_2 transport in benzene compared to the O_2 transport in benzene. It might be due to the higher solubility of N_2 in benzene (partial molal volume of N_2 in benzene at 25 ºC= 53 cm^3/mol) compared to O_2 in benzene (partial molal volume O_2 in benzene at 25 ºC= 46 cm^3/mol) (Reid et al., 1987). It could also have been due to the formation of microscopic bubbles releasing the

oxygen, as previously indicated. In fact, many liquids show similar behaviour. However, mass transfer coefficients (k_L) obtained in this study are ranges from 1.2×10^{-6}–3.5×10^{-6} m/s (**Table C.4**) that are comparatively smaller than to the reported k_L values 2.5×10^{-4}–4.1×10^{-4} m/s of cyclohexane autoxidation (Suresh et al., 1988a; Fischer et al., 2010). It might be due to the different reaction conditions and/or reactor system. Suresh et al. (1988a) found k_L values of 3.1×10^{-4}–4.1×10^{-4} m/s during autoxidation of cyclohexane at 150 °C (473 K) and 1 MPa (10 bar) pressure in a stirred tank reactor. Fischer et al. (2010) reported via modeling that k_L value must be at least 2.5×10^{-4} m/s for the cyclohexane–air oxidation (rate constant of 9.49×10^{-1} s^{-1}) in a micro capillary reactor at 200 °C (473 K), 8.0 MPa pressure. Changes in temperature and pressure, the presence of stirring and airflow that changes the interfacial area would influence the mass transfer rate. It was beyond the scope of the current study.

Mass transfer rate was zero when indan was saturated with oxygen (**Figures 7.12**–7.**13**). Oxidation rate could be higher than zero (**Figure 7.13**). But it would not be mass transfer limited because of the constant oxygen level in the liquid phase. Hence, theoretical calculation without knowing oxygen level in the liquid phase could be misleading. It is highly important to know the oxygen content and its change in the bulk liquid phase to evaluate the engineering aspect of liquid phase autoxidation.

During the induction period, no detectable oxidation rate at 50 °C can be explained by the strength of C–H bond energy. Indan has four C–H bonds that are part of aromatic structure and are very strong. It also has six C–H bonds that are comparatively less strong but 50 °C is not enough to abstract hydrogen from these C–H bonds. It also explains the inertness of benzene containing six C–H bonds which all are part of aromatic structure.

It is clear from the **Figures 7.14**–7.**16** that oxygen transport rate was increased indicating decreasing oxygen level in liquid phase from its saturated value after adding di-*tert*-butyl peroxide of 4.7 wt % or higher. But these rates were much less than the oxidation rate. Moreover, mass transfer rate can only be changed to a limited extent (maximum 1.5×10^{-3} $mol/m^3.s$ for air cycles during indan oxidation in this study), but oxidation rate could be much higher. Higher oxidation rate compared to mass transfer influenced the liquid phase autoxidation after the induction period.

Higher oxidation rate after adding di-*tert*-butyl peroxide can be explained by the formation of free radical intermediates by the H–abstraction. Free radical intermediates (R) would react with oxygen present in the liquid phase as shown in Reaction (7.1). This reaction is very fast and with respect to O_2 it is reported as zero order kinetics at higher oxygen availability (Chapter 6; Suresh et al., 2000, 1988c; Hobbs, 1972; Doraiswamy and Üner, 2014; Lundberg, 1961). The rate equation can be presented as presented in Equation (7.7).

$R + O_2 \rightarrow ROO$ Reaction (7.1)

$-r = k_r[R][O_2]$ Equation (7.7)

During the induction period, the oxygen concentration was higher compared to the concentration of alkyl radical (R) which was rate limiting. Due to the sudden increase in free radicals after adding di-*tert*-butyl peroxide of 4.7 wt % or higher, free radical concentration was higher and oxygen became rate limiting. At low oxygen availability the rate of Reaction (7.1) and hence overall propagation rate would become first order in oxygen (Suresh et al., 2000, 1988c). Oxygen depletion in liquid phase could lead to the formation of addition product as represented by Reaction (7.2) (Chapter 6; Suresh et al., 2000; Partenheimer, 1995). This explains why addition products were dominant after the induction period (**Table 7.2**).

$R + R \rightarrow R–R$ Reaction (7.2)

It was established in our previous study that changes in ketone-to-alcohol selectivity and increases in addition product formation indirectly indicate the oxygen availability in the liquid phase (Chapter 6).

Mass transport can influence the oxidation by changing the oxygen availability in the liquid phase. For a liquid pre-saturated with oxygen, even when the oxidation rate exceeds the mass transfer rate the oxidation rate is not necessarily mass transfer limited (**Figure 7.14**). However, the oxidation rate became mass transfer limited only once the oxygen content in the liquid phase became depleted. Figure 7.16 illustrates how the rate of reaction and rate of transport becomes balanced, i.e. mass transfer limited.

7.4.3 Extent of Mass Transfer Limitation

The extent of mass transfer limitation was also confirmed from the *in situ* change in oxygen partial pressure in the liquid phase during autoxidation. It would help to confirm experimentally whether the oxidation takes place in the film (gas–liquid interface) or in the bulk (liquid phase).

It is clear from the discussion in Section 7.4.2 that liquid phase autoxidation was affected by mass transfer as observed by the decrease in oxygen level in liquid phase after the induction period (in the presence of di-*tert*-butyl peroxide of 4.7 wt % or higher). Oxygen partial pressure decreased from 19.2 kPa to zero kPa considering post calibration (**Figures 7.5** and **7.6**). Oxygen level of zero kPa indicates extreme oxygen transport limitation in the gas–liquid interface (film). In other words, oxidation represented by Reaction (7.1) takes place completely in the in the film. Time required to reach the oxygen partial pressure of zero kPa, however, would depend on the free radicals present in the system (**Figures 7.5** and 7.**6**). More free radicals were expected to be produced via H–abstraction using 9.2 wt % di–*tert*–butyl peroxide (DTBP) compared to 5.1 wt % DTBP. It is clear from the **Figures 7.5** and **7.6** that the experiment performed using 9.2 wt % DTBP required comparatively less time to reach zero kPa. It indicates that liquid phase autoxidation might experience extreme limitation by mass transfer (zero kPa oxygen partial pressure) at some point after exhausting dissolved oxygen by the free radical intermediates.

It is not always obvious that mass transfer limitation would be extreme and continue for long time. The influence of mass transport due to the use of 4.7 wt % di-*tert*-butyl peroxide was mild because oxygen level was decreased only by ~4 kPa (from 19.2 kPa to 15 kPa) and liquid phase was saturated with oxygen again after a certain period of time (**Figure 7.8**). In case of mild transport effect, oxidation represented by reaction (7.1) would take place both in film and in bulk liquid. Hence, extent of mass transfer limitation would depend on the relative amount of free radical intermediates and oxygen content in the system.

Free radical intermediates were created by adding di-*tert*-butyl peroxide in this study and it was expected that free radical concentration would decrease at some point as the initiator was consumed by reaction. Free radicals concentration might not decrease when induction period was not manipulated using initiator and autocatalytic oxidation started after the induction period.

Decrease in free radicals to propagate oxidation would lead to increase in oxygen partial pressure in liquid phase. This aspect was apparently observed in the case of adding 4.7 wt % of di-*tert*-butyl peroxide (**Figure 7.8**). It was also clear from the **Figure 7.4**, where oxygen partial pressure reached to 19.2 kPa from zero kPa due to the continuation of air cycles after 3 hours. This aspect was somewhat observed in **Figure 7.5** during 2.75 hour to 3.25 hours, before switching air supply to nitrogen supply for the post calibration purpose. The reaction rate threshold was 2.6×10^{-3} (mol/m^3.s) or 3.4×10^{-6} (mol/m^2.s) for the reaction to occur in the film instead of the bulk.

It is a common practice in gas–liquid reaction to evaluate the mass transfer limitation and/or its extent by calculating Hatta Number (Chapter 6; Doraiswamy and Üner, 2014; Fischer et al.; 2010; Rebrov et al.; 2012). Hatta number was originally derived considering the reaction between CO_2 and KOH as fast reaction and the reaction between CO_2 and K_2CO_3 as moderate reaction (Hatta, 1932). Liquid phase autoxidation involves multiple free radical reactions having different activation energies and reaction speeds (Chapter 6; Suresh et al., 2000; Emanuel et al.; 1967). The rate of free radical forming reactions can also be changed during oxidation process depending on the reaction conditions. Hatta number would be different for different free radical reactions. For all these reasons Hatta number can overestimate the mass transfer limitation and its extent during liquid phase autoxidation.

One aspect of the Hatta-number criterion that is pointed out in the literature, is that it is a steady-state criterion. However, oxidation reactions do not reach steady state, because the limiting reagent that is transported is O_2, but the reactions consuming O_2 keep on changing. Furthermore, in an oxygen pre-saturated liquid, the reaction rate can exceed the mass transfer rate, because O_2 is available both from the liquid phase and the gas phase. Unless the liquid phase starts off with no O_2 and the O_2 consumption rate remains equal to the maximum O_2 transfer rate, the liquid phase will always have some dissolved O_2. Whenever the O_2 consumption rate is less than the maximum O_2 transfer rate, some O_2 will be transferred to the liquid phase. The O_2 concentration in the liquid phase will therefore increase to a level such that the mass transfer rate is equal to reaction consumption rate. The important conclusion from this is that the Hatta-number provides a steady state estimate comparing reaction rate to transport rate, but one can only say something

about reaction in the film versus reaction in the bulk if the maximum transfer rate (i.e. $C^b = 0$) is known.

7.5 Conclusions

Autoxidation of indan and benzene were performed at 50 ºC in a flat interface reactor to experimentally confirm the kinetic and mass transfer phenomenon during liquid phase autoxidation and determine their extents. The main conclusions and observations from the work are:

(a) The overall mass transfer coefficients obtained from the experimental measurements were 2.1×10^{-3} s^{-1} for benzene and 1.0×10^{-3} s^{-1} for indan during autoxidation in a flat interface reactor at 50 ˚C and 19.2 kPa O_2 partial pressure. The maximum rates of O_2 transfer to the indan phase was 1.9×10^{-6} mol/(m^2.s) or 1.5×10^{-3} mol O_2/(m^3.s) at 19.2 kPa O_2 partial pressure.

(b) Liquid phase oxidation was kinetically controlled during the induction period of liquid phase autoxidation of indan. This phenomenon was experimentally confirmed by measuring *in situ* oxygen partial pressure in the liquid phase. Indan reached to complete saturation with air (19.2 kPa O_2) during this period.

(c) Liquid phase autoxidation was influenced by mass transfer after the induction period (after adding di-*tert*-butyl peroxide of 4.7 wt % or higher). It was confirmed from the decreasing oxygen partial pressure after the induction period. The reason of mass transfer effect would be the very fast reaction of oxygen with available free radicals.

(d) It was possible to confirm the extent of mass transfer limitation from the *in situ* change in oxygen partial pressure in the liquid phase. An oxygen partial pressure of zero kPa indicated that the reaction was mass transfer limited. In other words, oxidation takes place completely in the film. The reaction rate threshold was 2.6×10^{-3} (mol/m^3.s) or 3.4×10^{-6} (mol/m^2.s) for the reaction to occur in the film instead of the bulk.

(e) Product selectivity was changed due to the influence of mass transfer on oxygen availability in the liquid phase in indan autoxidation.

7.6 Literature Cited

Bateman, L.; Bolland, J. L.; Gee, G. Determination of absolute rate constants for olefinic oxidations by measurement of photochemical pre- and after-effects. Part II.– At "low" oxygen pressures. *Trans. Faraday Soc.* **1951**, *47*, 274–285.

Battino, R.; Rettich, T. R.; Tominaga, T. The solubility of oxygen and ozone in liquids. *J. Phys. Chem. Ref. Data* **1983**, *12* (2), 163–178.

Clerici, M. G.; Kholdeeva , M. G. *Liquid phase oxidations via heterogeneous catalysis. Organic synthesis and industrial applications*; Clerici, M. G., Kholdeeva, O. A. Eds.; Wiley: Hoboken, NJ, 2013.

Centi, G.; Cavani, F.; Triffò, F. *Selective Oxidation by Heterogeneous Catalysis.* Kluwer/Plenum: New York, 2001.

Centi, G; Perathoner, S. Selective oxidation—industrial. In *Encyclopedia of Catalysis;* Wiley, 2002.

De Klerk, A. Continuous- mode thermal oxidation of Fischer-Tropsch waxes. *Ind. Eng. Chem. Res*. **2003,** *42*, 6545–6548.

Doraiswamy, L.K.; Üner, D. *Chemical Reaction Engineering, Beyond the Fundamentals*; CRC Press: Boca Raton, 2014.

Emanuel, N. M.; Denisov, E. T.; Maizus, Z. K. *Liquid-phase oxidation of hydrocarbons*; Plenum Press: New York, 1967.

Fischer, J.; Lange, T.; Boehling, R.; Rehfinger, A.; Klemm, E. Uncatalyzed selective oxidation of liquid cyclohexane with air in a microcapillary reactor. *Chem. Eng. Sci.* **2010**, *65*, 4866–4872.

Hatta, S. On the absorption velocity of gases by liquids–II: Theoretical considerations of gas absorption due to chemical reaction. *Technological Reports of Tôhoku University* **1932**, *10*, 613–622.

Hobbs, C. C.; Drew, E. H.; Van't Hof, H.A.; Mesich, F. G.; Onore, M. J. Mass transfer rate-limitation effects in liquid-phase oxidation. *Ind. Eng. Chem. Prod. Res. Develop.* **1972**, *11*(2), 220–225.

Kaštánek, F.; Zaharadnĭk, J.; Kratochvĭl, J.; Čermák, J. *Chemical Reactors for Gas-Liquid Systems*, 1st ed.; Ellis Horwood: West Sussex, 1993.

Knotnerus, J.; Bitumen durability-measurement by oxygen absorption. *Ind. Eng. Chem. Prod. Res. Develop.* **1972**, *11*(4), 411–422.

Lundberg, W. O. Autoxidation and antioxidants, Vol I. Wiley: New York, 1961.

Mayo, F. R.; Miller, A. A. The oxidation of unsaturated compounds. VI. The effect of oxygen pressure on the oxidation of a-methylstyrene. *J. Am. Chem. Soc.* **1958**, *80*, 2480–2493.

Partenheimer, W. Methodology and scope of metal/bromide autoxidation of hydrocarbons. *Catal. Today* **1995**, *23* (2), 69–158.

Rebrov, E.V.; Duisters, T.; Löb, P.; Meuldijk, J.; Hessel, V. Enhancement of the liquid-side mass transfer in a falling film catalytic microreactor by in-channel mixing structures. *Ind. Eng. Chem. Res.* **2012**, *51*, 8719–8725.

Reid, R.C.; Prausnitz, J. M.; Poling, B, E. The properties of gases and liquids, 4th ed, McGraw-Hill, New York, 1987, pp 332–336.

Schäfer, R. Bubble size distributions and reaction kinetics for the autocatalytic oxidation of cyclohexane in a bubble column reactor. PhD Thesis, Universität of Stuttgart, Germany, **2005**.

Sheldon, R. A.; Kochi, J. K. *Metal-Catalyzed Oxidations of Organic Compounds*; Academic Press: New York, 1981.

Siddiquee, M. N.; De Klerk, A.; Nazemifard, N. Application of microfluidics to enhance gas-liquid mass transfer during selective oxidation of hydrocarbons. *Reaction and Engineering Chemistry Research* (Submitted).

Siddiquee, M.N.; De Klerk, A. Hydrocarbon addition reactions during low temperature autoxidation of oilsands bitumen. *Energy Fuels* **2014b**, *28*, 6848–6859.

Suresh, A. K.; Sharma, M. M.; Sridhar, T. Engineering aspects of industrial liquid-phase air oxidation of hydrocarbon. *Ind. Eng. Chem. Res.* **2000,** *39,* 3958–3997.

Suresh, A. K.; Sridhar, T.; Potter, O. E. Mass transfer and solubility in autocatalytic oxidation of cyclohexane. *AIChE J.* **1988a**, *34*(1), 55–68.

Suresh, A. K.; Sridhar, T.; Potter, O. E. Mass transfer and solubility in autocatalytic oxidation of cyclohexane. *AIChE J.* **1988c**, *34*(1), 69–80.

CHAPTER 8 – CONCLUSION

8.1 Introduction

Oilsands bitumen autoxidation (oxidation with air) is a potential *in situ* upgrading strategy to facilitate microbial digestion produce higher value products at low cost. Bitumen hardening, however, is a potential challenge to make the upgrading process viable. The interest of this study was to get a better fundamental understanding of oxidation to prevent or reduce hardening as generic problem faced by low temperature free radical conversion processes. This would help to develop a bitumen oxidation strategy for the efficient and economical *in situ* conversion of oilsands derived bitumen.

The major conclusions and new insights that will contribute to the field of oxidative upgrading of oilsands derived materials and the liquid phase autoxidation in general are highlighted.

8.2 Significance, Major Conclusions and Key Insights

8.2.1 Oxidative Addition during Liquid Phase Autoxidation

It is well known that oxidation of bitumen can cause hardening. There are also studies that in some way relate the hardening to composition. However, oxidative degradation of bitumen is also reported. In order to assess the potential hardening problem, oilsands derived bitumen was autoxidized at different temperatures and oxidation times and products were characterized. Although viscosity was anticipated to increase, the viscosity increase was severe (11 times higher) and bitumen became very hard (17 times harder) during bitumen autoxidation at 130 ºC for 229 hours. Moreover, hydrogen disproportionation was observed during the low temperature bitumen autoxidation in spite of limited change in overall elemental composition.

It was postulated that oxidative addition was the potential cause of hardening, rather than the introduction of specific oxygen-containing functional groups.

A model compound study was planned and the focus was on free radical addition reactions specifically. The underlying chemistry of free radical addition reactions has been described in

literature, but such descriptions are usually independent of application. It was intent to bridge these gaps. Model compounds representing compound classes available in bitumen were systematically investigated to understand which compound classes were responsible to form addition products during low temperature bitumen autoxidation. The reactions pathways to form addition products was interrogated and the nature of the bond formed during free radical addition was determined, i.e. did addition take place by C–C bond formation, or through C–O–C linkages.

The compound classes and structural motifs that were susceptible to free radical addition reactions leading to hardening during low temperature oxidation were identified as naphthenic-aromatic hydrocarbons compounds and heterocyclic N- and O-containing compounds. It was known that pyrrolic N-containing compounds, such as indole, were susceptible to form addition products. It was surprising to observe that five-membered naphtheno-aromatic compounds were even more susceptible to oxidative addition. In fact, the oxidation addition propensity of indene was 3.6 times more than that of indole, while indan was only somewhat lower in addition propensity to indole. The systematic identification of addition product forming pathways was the first contribution from this study to contribute to the field of the oxidative addition. Although some aspects of oxidation addition were known, the propensity for free radical addition of five-membered cycloalkanes in naphtheno-aromatic compounds was not fully appreciated.

Mechanisms of addition product formation of different compound classes were proposed. In all instances the addition products were C–C coupled by free radical addition. It was proposed that the dominant pathway for addition reactions of hydrocarbons is the hydrogen disproportionation of free radicals to produce olefins. Free radical addition to olefins through the formation of C–C bonds explained all of the oxidation selectivity observations from the model compound studies, as well as the addition products identified by GC-MS analysis.

The pathway to addition product formation of N– and O– containing heterocyclic compounds was different. The addition product formation pathway for indole that was proposed in literature, involved the formation of a radical cation intermediate, oxygen incorporation and hydrogen disproportionation. Product analyses, however, suggested that this pathway was not significant in the case of 2,3-dihydroindole under the autoxidation conditions in the current study. The C–C bond formation due to free radical addition, rather than the formation of oxygenates, is the

dominant process involved in the formation of heavier products during 2,3-dihydroindole oxidation.

Oxidative addition of benzofuran may take place through coumaranone as intermediate to produce oxindirubin-type products. Recombination of free radical intermediates after oxidative dehydrogenation is the dominant reaction pathway for addition reactions during oxidation of 2,3-dihydrobenzofuran.

Understanding why the addition products formed and the likely oxidative pathways to form addition products are considered contributions from this study to advance understanding in the field of the oxidative addition.

The implications for the advances made in the understanding of low temperature oxidation is far reaching. Addition products formed by hydrogen disproportionation after free radical formation indicates the oxidative addition is really a free radical addition process and not necessarily restricted to oxidation. At any temperature where C–C bond formation would be thermally stable and thermodynamically favored free radical processes could lead to addition product formation by the pathways described. Processes that were considered for bitumen upgrading, for instance in thermal cracking (visbreaking) and halogenation, that will give rise to free radical formation would be susceptible to addition product formation, particularly if the material contains naphtheno-aromatic hydrocarbons with a five-membered ring.

Naphthenic-aromatic compounds are abundant in oilsands derived bitumen. The increase in bitumen viscosity as a result of low temperature oxidation is therefore understandable, because addition products are readily formed, even at low oxidation extent. This implies that oxidative hardening of bitumen is inevitable and cannot be avoided. It may also explain processes such as natural bitumen weathering and its impact on oilsands bitumen recovery and upgrading.

However, if the mechanism to explain addition reactions via olefin formation is correct, then it should be possible to manipulate addition selectivity during oxidation. The key is to limit the disproportionation reactions that produce olefins. Although direct free radical addition cannot be eliminated, the rate of free radical addition reactions can be reduced. The rates of direct free radical addition as well as the rate of olefin formation by free radical disproportionation are both

dependent on the concentration of carbon-centred free radicals. Reaction engineering approaches that can limit the concentration of carbon-centred free radicals, as opposed to oxygen centred free radicals, will also decrease the selectivity to addition products. This added understanding developed in this study therefore has direct engineering application and value.

8.2.2 Manipulating Product Selectivity during Liquid Phase Autoxidation

Liquid phase oxidation of hydrocarbons is widely applied for the production of petrochemicals. It also has a great potential for oxidative upgrading of fuels and specifically the oxidative degradation of bitumen to enable microbial conversion, which was a specific objective.

Since it was shown that free radical addition reactions were inherent to the autoxidation chemistry of some compound classes, engineering approaches were sought to manipulate oxidation selectivity independent of oxidative conversion. The engineering approach that was of specific interest was to manipulate selectivity through local oxygen availability during liquid phase autoxidation. However, it was found that there was surprisingly little systematic study to describe oxygen availability in terms of transport characteristics to control product selectivity during uncatalyzed liquid-phase oxidation of hydrocarbons.

The approach taken was to study the impact of reactor hydrodynamics on oxidation selectivity. Oxidation selectivity at low conversion was studied using different reactor types, as well as using different hydrodynamic conditions in a rectangular glass microfluidic reactor operated in Taylor flow region. Ketone-to-alcohol selectivity in primary oxidation products could be increased by an order of magnitude from less than 1:1 to 14:1 by increasing oxygen availability in the liquid phase at near constant conversion, oxygen partial pressure and temperature. In this respect the use of a microfluidic reactor proved invaluable.

The higher ketone selectivity was explained in terms of the oxidation of alcohol and/or alkoxy radical formed at higher oxygen availability. Selectivity to alcohols and addition products increased at lower oxygen availability. A crucial insight that came from the study of oxidation selectivity was that the ketone-to-alcohol selectivity was not only affected by oxygen availability, but also an indicator of oxygen availability and the likelihood of free radical addition. A high ketone-to-alcohol selectivity indicated high oxygen availability. When oxygen

availability was high, oxygen preferentially reacted with the R· free radicals to produce ROO species. The intermediate ROO species were more likely to terminate via oxygenate formation (2 ROO → 2 oxygenates) than via free radical addition (2 R → R_2). Increased ketone-to-alcohol selectivity in primary oxidation products makes the discussion applicable to a wide variety of industrial processes involving selective oxidation. The demonstration and description of how to control product selectivity through oxygen availability independent of conversion is another contribution of the current study to advance the field of liquid phase autoxidation.

8.2.3 Engineering Aspects of Liquid Phase Autoxidation

Considering the deleterious impact of oxidative addition and the importance of oxygen availability to manipulate product selectivity, it was important to better understand engineering descriptions relating oxygen transport to liquid phase oxygen availability. In principle an engineering design that ensured high oxygen availability could limit addition reactions.

However, engineering calculations based on the Hatta-number suggested that oxidation is too fast and that autoxidation mainly occurs in the gas-liquid interface (film). If reaction indeed took place in the film, the bulk liquid would always be oxygen depleted and it would not be possible to engineer around the problem of free radical addition reactions. Intuitively this felt wrong, because hydrodynamic manipulation using microfluidic reactors demonstrated that oxygen transport had an influence on product selectivity independent of conversion.

Due to the importance of the problem, it was decided to find a way to experimentally investigate oxygen availability in the bulk liquid phase through *in situ* measurements during autoxidation. This was an experimentally challenging endeavor. There were surprisingly little systematic studies to describe mass transport of oxygen during liquid phase oxidation. Most liquid phase oxidation studies dealt with oxygen transport in an empirical fashion only. Calculated predictions based on the Hatta-number showed discrepancies with the experimental observations.

This study experimentally investigated the mass transfer limitations imposed by oxygen transfer to the liquid phase and how oxygen availability changed during oxidation. The oxygen content of the liquid phase was measured *in situ* during oxidation and a unique experimental

methodology based on a fluorometric approach was developed to do so. Previous studies reported in literature relied on measurements after quenching oxidation.

The maximum mass transport rate of oxygen was determined with good repeatability. It was show that at high oxidation rate, once the dissolved oxygen in the liquid phase was depleted, the oxidation became mass transfer limited and oxidation took place at a rate equal to the maximum mass transport rate of oxygen. However, the liquid phase oxygen content changed dynamically and oxidation in the film required oxygen in the bulk to be consumed first and only if the oxidation rate remained equal to the maximum oxygen transfer rate did oxidation take place mainly in the film. The steady state approximation underlying the calculation of the Hatta-number does not capture the dynamic aspects and process, which can cause misleading inferences based on the Hatta-number.

8.3 Suggested Future Work

- Bitumen autoxidation to correlate viscosity with addition product formation. Electrospray ionisation Fourier transform ion cyclotron resonance mass spectrometry (ESI FT-ICR-MS) can be used to confirm the nature of addition products by measuring the changes of double bond equivalent and molecular mass distribution in relation to oxygen functionality. This would help to evaluate the relative contribution of heavier product formation and changes in oxidative functionality to increase viscosity of bitumen. This would also validate understanding from model compounds studies about addition product during bitumen autoxidation.

- Additional work on the liquid phase oxidation of a five member ring naphthenic-aromatic hydrocarbon in microfluidic reactor can provide additional information on selectivity manipulation. It is suggested that oxidation of indan be performed in a microfluidic reactor and studied under conditions of different flow regime (from Taylor flow to film flow), as well as with and without using initiator to increase oxidation rate. This would help to understand whether or not ensuring higher oxygen availability would produce more oxygenate functional groups and suppress addition product selectivity.

- Oxidation of diluted bitumen in microfluidic reactor. Microfluidic reactor showed promising results producing order of magnitude higher ketone than alcohol during tetralin oxidation and limiting the addition product formation. The main reason to get the higher ketone is the oxygen availability for the oxidation to take place. Mass transfer plays an important role to maximize the oxygen availability by increasing both the gas-liquid interfacial area and mass transfer coefficient. In order to apply this fundamental understanding to bitumen oxidation, bitumen diluted in benzene (an inert solvent to facilitate the flow through the microfluidic reactor) can be oxidized in microfluidic reactor.

- Oxidation in a flat interface reactor (FIR) without using initiator at different oxidation conditions. One limitation of performing experiment in a FIR was that system was not suitable for high temperature operation. A question that still remains is whether there is a temperature range in which autoxidation (without any accelerant) would take place at a reasonable rate, but at a rate that did not deplete bulk phase oxygen when then system is engineered for efficient mass transport. This would help to devise an engineering strategy to prevent or mitigate the heavier product formation.

8.4 Publications and Presentations

1. **Siddiquee, M. N**.; De Klerk, A. Heterocyclic addition reactions during low temperature autoxidation. *Energy Fuels* **2015**, *29* (7), 4236–4244.
2. **Siddiquee, M. N**.; De Klerk, A. Hydrocarbon addition reactions during low temperature autoxidation of oilsands bitumen. *Energy Fuels* **2014,** *28* (11), 6848–6859.
3. **Siddiquee, M. N.**; De Klerk, A. Oxidation of naphthenic-aromatic compounds in bitumen. *Prepr.Pap.-Am. Chem. Soc., Div. Energy Fuels* **2014**, *59* (2), 572–574. [Presented at the 248th ACS National Meeting, 2014, San Francisco, CA, USA]
4. **Siddiquee, M. N**.; De Klerk, A. Bitumen weathering. Oil Sands 2014 symposium, University of Alberta, Edmonton, AB Canada (poster).
5. **Siddiquee, M. N.**; De Klerk, A. Continuous and prolonged oxidation of bitumen for upgrading by microbial digestion. *Prepr. Pap.-Am. Chem. Soc., Div. Energy Fuels* **2013**, *58* (2), 649–651. [Presented at the 246th ACS National Meeting, 2013, Indianapolis, IN, USA]

In addition to these, the following works were submitted for review, but has not yet been accepted for publication:

6. **Siddiquee, M. N**.; De Klerk, A.; Nazemifard, N. Application of microfluidics to control product selectivity during non-catalytic oxidation of naphthenic-aromatic hydrocarbons. *React. Chem. Eng.*
7. **Siddiquee, M. N**.; De Klerk, A. *In situ* measurement of liquid Phase oxygen during oxidation. *Ind. Eng. Chem. Res.*

Bibliography

Alsters, P. L.; Aubry, J. M.; Bonrath, W.; Daguenet, C.; Hans, M.; Jary, W.; Letinois, U.; Nardello-Rataj, V.; Netscher, T.; Rarton, R.; Schütz, J.; Van Soolingen, J.; Tinge, J.; Wüstenberg, B. Selective oxidation in DSM: Innovative catalysts and technology. In *Handbook of Advanced Methods and Processes in Oxidation Catalysis: From Laboratory to Industry*; Duprez, D., Cavani, F. Eds.; Imperial College Press: London, 2014, pp 382–419.

Amalric, L.; Guillard, C.; Pichat, P. The photodegradation of 2,3-benzofuran and its intermediates, 2-coumaranone and salicylaldehyde, in TiO_2 aqueous suspensions. *J. Photochem. Photobiol. A* **1995**, *85*, 257–262.

Anderson, K. B.; Crelling, J. C.; Huggett, W. W.; Perry, D.; Fullinghim, T.; McGill, P.; Kaelin, P. Oxidative hydrothermal dissolution (OHD) of coal and biomass. *Prepr. Pap.-Am. Chem. Soc., Div. Fuel Chem.* **2011**, *56*(2), 310–311.

Asinger, F. *Paraffins Chemistry and Technology*; Pergamon: Oxford, 1968.

Babu, D. R.; Cormack, D. E. Low temperature oxidation of Athabasca bitumen. *Can. J. Chem. Eng.* **1983**, *61*, 575–580.

Babu, D. R.; Cormack, D. E. Effect of low-temperature oxidation on the composition of Athabasca bitumen. *Fuel* **1984a**, *63*, 858–861.

Babu, D. R.; Cormack, D. E. Effect of oxidation on the viscosity of Athabasca bitumen. *Can. J. Chem. Eng.* **1984b**, *62*, 562–564.

Balster, L. M.; Zabarnick, S.; Striebich, R. C.; Shafer, L. M.; West, Z. J. Analysis of polar species in jet fuel and determination of their role in autoxidative deposit formation. *Energy Fuels* **2006**, *20*, 2564–2571.

Bateman, L.; Bolland, J. L.; Gee, G. Determination of absolute rate constants for olefinic oxidations by measurement of photochemical pre- and after-effects. Part II.– At "low" oxygen pressures. *Trans. Faraday Soc.***1951**, *47*, 274–285.

Battino, R.; Rettich, T. R.; Tominaga, T. The solubility of oxygen and ozone in liquids. *J. Phys. Chem. Ref. Data* **1983**, *12* (2), 163–178.

Bennett, J. E.; Brunton, G.; Smith, J. R. L.; Salmon, T. M. F.; Waddington, D. J. Reactions of alkylperoxyl radicals in solution. Part 2-A kinetic and product study of self-reactions of 2-

propylperoxyl radicals between 253 and 323 K. *J. Chem. Soc., Faraday Trans. 1* **1987**, *83*(8), 2433–2447.

Berti, G.; Da Settimo, A.; Di Colo, G.; Nannipieri, E. A dimeric autoxidation product of 2,3-dimethylindole. *J. Chem. Soc. C* **1969**, 2703–2710.

Betts, A.T.; Uri, N. The conversion of metal catalysts into inhibitors of autoxidation. *Die Makromolekulare Chemie.* **1966**, 95, 22–39.

Bharadwaj, S. S.; Schmidt, L. D. Catalytic partial oxidation of natural gas to syngas. *Fuel Process. Tech.* **1995**, *42*, 109–127.

Bolder, F. H. A.; De Klerk, A.; Visagie, J. L. Hydrogenation of oxidized wax and a process to produce olefins from paraffins by autoxidation, selective hydrogenation, and dehydration. *Ind. Eng. Chem. Res.* **2009,** *48*, 3755–3760.

Calderbank, P.H.; Moo-Young, M.B. The continuous phase heat and mass-transfer properties of dispersions. *Chem. Eng. Sci.* **1961**, *16* (1–2), 39–54.

Chelton, H. M.; Traxler, R. N.; Romberg, J. W. Oxidized asphalts. *Ind. Eng. Chem.* **1959,** *51*, 1353–1354.

Chen, G.; Yuan, Q.; Li, H.; Li, S. CO selective oxidation in a microchannel reactor for PEM fuel cell. *Chem. Eng. J.* **2004,** *101*, 101–106.

Centi, G.; Cavani, F.; Triffò, F. *Selective Oxidation by Heterogeneous Catalysis.* Kluwer/Plenum: New York, 2001.

Centi, G; Perathoner, S. Selective oxidation—industrial. In *Encyclopedia of Catalysis;* Wiley, 2002.

Centi, G.; Malaguti, M.; Stella, G. Low temperature gas-phase selective oxidation of 1-butene to 2- butanone on supported Pd/V_2O_5 Catalysts. In *New Developments in Selective Oxidation II,* Corberan, V. C., Bellón, S. V., Eds.; Elsevier: Amsterdam, 1994.

Clausen, D. J.; Floreancig, P. E. Aromatic cations from oxidative carbon hydrogen bond cleavage in bimolecular carbon carbon bond forming reactions. *J. Org. Chem.* **2012**, *77*, 6574 6582.

Colthup, N. B.; Daly, L. H.; Wiberley, S. E. *Introduction to Infrared and Raman Spectroscopy*, 3ed; Academic Press: San Diego, 1990.

Conaway, L. M. Method for recovering hydrocarbons from tar sands and oil shales. US Patent 6, 251, 290 B1, 2001.

Cussler, E. L. *Diffusion: Mass Transfer in Fluid Systems,* 3rd ed.; Cambridge University Press: Cambridge, 2009.

Danckwerts, P. V. *Gas-Liquid Reactions*; McGraw-Hill: New York, 1970.

Dao-Huy, T.; Haider, M.; Glatz, F.; Schnürch, M.; Milhovilovic, M. D. Direct arylation of benzo[*b*]furan and other benzo-fused heterocycles. *Eur. J. Org. Chem.* **2014**, *36*, 8119–8125.

Das, S. C. A Study of Oxidation Reaction Kinetics During an Air Injection Process. M.E.Sc. Thesis. The University of Adelaide, April 2009.

Davis, M. E.; Davis, R. J. *Fundamental of Chemical Reaction Engineering*; McGraw-Hill: New York, 2003.

Degaleesan, S.; Dudukovic, M.; Pan,Y. Experimental study of gas-induced liquid-flow structures in bubble columns. *Fluid Mech.Trans. Phenom.* **2001,** *47*(9), 1914–1931.

De Klerk, A. *Fischer-Tropsch Refining*, 1st ed.; Wiley VCH: Weinheim, 2011.

De Klerk, A. Continuous- mode thermal oxidation of Fischer-Tropsch waxes. *Ind. Eng. Chem. Res*. **2003,** *42*, 6545–6548.

De Klerk, A.; Gray, M. R.; Zerpa, N. Unconventional oil and gas: Oilsands. In *Future Energy*, 2nd ed; Letcher, T. M., Ed.; Elsevier: Amsterdam, 2014; pp 95–116.

De Man, A. Desulfurization of oxidized bitumen using microorganisms through process-based directed evolution. MSc. Thesis, University of Alberta, Canada, June 2014.

Dietz, W. A. Response factors for gas chromatographic analyses. *J. Chromatogr. Sci.* **1967**, *5* (2), 68-71.

Dimitratos, N.; Lopez-Sanchez, J. A.; Hutchings, G. J. Supported metal nanoparticles in liquid-phase oxidation reactions. In *Handbook of Advanced Methods and Processes in Oxidation Catalysis: From Laboratory to Industry*; Duprez, D., Cavani, F., Eds.; Imperial College Press: London, 2014; pp 631–678.

Do, H-Q.; Daugulis, O. An aromatic Glaser-Hay reaction. *J. Am. Chem. Soc.* **2009**, *131*, 17052–17053.

Dolphin, D.; Wick, A. *Tabulation of Infrared Spectral Data*; Wiley-Interscience: New York, 1977.

Doraiswamy, L.K.; Üner, D. *Chemical Reaction Engineering, Beyond the Fundamentals*; CRC Press: Boca Raton, 2014.

Duyvesteyn, W. P. C.; Morley, R. L. Oxidation of asphaltenes. US Patent Application 2007/0284283.

Dwight, T. A.; Rue, N. R.; Charyk, D.; Josselyn, R.; DeBoef, B. C–C bond formation via double C–H functionalization: Aerobic oxidative coupling as a method for synthesizing heterocoupled biaryls. *Org. Lett.* **2007**, *9*, 3137–3139

Elderfield, R. C.; Meyer, V. B. Benzofuran and its derivatives. In *Heterocyclic Compounds. Vol. 2. Polycyclic Five- and Six-Membered Compounds Containing One O or S Atom*; John Wiley & Sons: New York, 1951, pp1–67.

Emanuel, N. M.; Denisov, E. T.; Maizus, Z. K. *Liquid-Phase Oxidation of Hydrocarbons*; Plenum Press: New York, 1967.

Fadaei, H., Scarff, B.; Sinton, D. Rapid microfluidics-based measurement of the CO_2 diffusivity in bitumen. *Energy Fuels* **2011,** *25*, 4829–4835.

Fedorak, P. M.; Foght, J. M.; Gray, M. R. Conversion of heavy oil and bitumen to methane by chemical oxidation and bioconversion. US Patent Application 2009/0130732 A1, May 21, 2009.

Fischer, J.; Lange, T.; Boehling, R.; Rehfinger, A.; Klemm, E. Uncatalyzed selective oxidation of liquid cyclohexane with air in a microcapillary reactor. *Chem. Eng. Sci.* **2010**, *65*, 4866–4872.

Fletcher, P.D. I.; Haswell, S. J.; Pombo-Villar, E.; Warrington, B.H.; Watts, P.; Wongc, S. Y. F.; Zhanga, X. Micro reactors: principles and applications in organic synthesis. *Tetrahedron,* **2002,** *58,* 4735–4757.

Foght, J. M. Anaerobic biodegradation of aromatic hydrocarbons: pathways and prospects. *J. Mol. Microbiol. Biotechnol.* **2008**, *15*, 93–120.

Frankenfeld, J. W.; Taylor, W. F.; Brinkman, D. W. Storage stability of synfuels from oil shale. 1. General features of sediment formation in model fuel systems. *Ind. Eng. Chem. Prod. Res. Dev.* **1983**, *22*, 608–614.

Fries, D. M.; Trachsel, F.; von Rohr, P. R. Segmented gas–liquid flow characterization in rectangular microchannels. *Int. J. Multiphase Flow* **2008**, *34*, 1108–1118.

García Zapata, J. L.; De Klerk, A. Viscosity changes during mild oxidation of oilsands derived bitumen: Solvent effects and selectivity. *Energy Fuels* **2014**, *28*, 6242–6248.

Gemoets, H. P. L.; Su, Y.; Shang, M; Hessel, V.; Luque, R. Noël, T. Liquid phase oxidation chemistry in continuous flow microreactors, *Chem. Soc. Rev.* **2016**, ***45***, 83–117.

Goosen, A.; Morgan, D. H. Autoxidation of nonane and decane: A product study. *J. Chem. Soc., Perkin Trans.* **1994**, *2*, 557–562.

Gray, M.R. Upgrading of oilsands bitumen and heavy oil; The University of Alberta Press: Edmonton, Canada, 2015.

Gray, M.R. Fundamentals of Oil Sands Upgrading; Course notes, University of Alberta, Edmonton, 2010.

Green, U.; Aizenshtat, Z.; Metzger, L.; Cohen, H. Field and laboratory simulation study of hot spots in stockpiled bituminous coal. *Energy Fuels* **2012**, *26*, 7230–7235.

Günther, A.; Khan, S. A.; Thalmann, M.; Trachsel, F.; and Jensen, K. F. Transport and reaction in microscale segmented gas–liquid flow. *Lab Chip* **2004**, *4*, 278–286.

Hamano, M.; Nagy, K. D.; Jensen, K. F. Continuous flow metal-free oxidation of picolines using air. *Chem. Comm.* **2012,** *48*, 2086–2088.

Hardy, D. R.; Wechter, M. A. Characterization of soluble macromolecular oxidatively reactive species (SMORS) from middle distillate diesel fuels: Their origin and role in instability. *Energy Fuels* **1994**, *8*, 782–787.

Hartman, R.L.; McMullen, J.P.; Jensen, K.F. Deciding whether to go with the flow – evaluating the merits of flow reactors for synthesis. *Angew. Chemie Int. Ed*. **2011,** *50*, 7502–7519.

Hartough, H. D.; Meisel, S. L. *The Chemistry of Heterocyclic Compounds. Compounds with Condensed Thiophene Rings*; Interscience: New York, 1954.

Hayashi, J.; Matsuo, Y.; Kusakabe, K.; Morooka, S. Depolymerization of lower rank coals by low-temperature O_2 oxidation. *Energy Fuels* **1997**, *11*, 227–235.

Hazel, A. L.; Heil, M. The steady propagation of a semi-infinite bubble into a tube of elliptical or rectangular cross-section. *J. Fluid Mech.* **2002**, *470*, 91–114.

Head, I. M.; Jones, D. M.; Larter, S. R. Biological activity in the deep subsurface and the origin of heavy oil. *Nature* **2003,** 426, 344–352.

Hendessi, S. Low temperature ozonation of Canadian Athabasca bitumen. MSc. Thesis, University of Alberta, Canada, September 2015.

Hendry, D. G.; Gould, C. W.; Schuetzle, D.; Syz, M. G.; Mayo, F. R. Autoxidations of cyclohexane and its autoxidation products. *J. Org. Chem.* **1976**, *41*(1), 1–10.

Hermans, I.; Peeters, J.; Jacobs, P. A. Autoxidation of Hydrocarbons: From Chemistry to Catalysis. *Top Catal.* **2008**, *50*, 124–132.

Herrington, P. R. Oxidation of bitumen in the presence of a constant concentration of oxygen. *Petrol. Sci. Technol.* **1998**, *16*, 1061–1084.

Herrington, P. R. Effect of concentration on the rate of reaction of asphaltenes with oxygen. *Energy Fuels* **2004**, *18*, 1573–1577.

Hessel, V.; Angeli, P.; Gavriilidis, A.; Löwe, H. Gas-liquid and gas-liquid-solid microstructured reactors: contacting principles and applications. *Ind. Eng. Chem. Res.* **2005**, *44,* 9750–9769.

Hill, C. L.; Kholdeeva, O. A. Selective liquid phase oxidation in the presence of supported polyoxometalates. In *Liquid Phase Oxidation via Heterogeneous Catalysis: Organic Synthesis and Industrial Applications,* First Edition; Clerici, M. G., Kholdeeva, O. A. Eds.; Wiley: Hoboken, 2013; pp 263–319.

Hobbs, C. C.; Drew, E. H.; Van't Hof, H.A.; Mesich, F. G.; Onore, M. J. Mass transfer rate-limitation effects in liquid-phase oxidation. *Ind. Eng. Chem. Prod. Res. Develop.* **1972**, *11*(2), 220–225.

Hofmann, H. Reaction Engineering Problems in slurry reactors. In *Mass Transfer with Chemical Reaction in Multiphase Systems,* Volume II: Three-Phase Systems; Alper, E., Ed.; NATO ASI series: Series E: Applied Sciences-No.73, Martinus Nijhoff Publishers: The Hauge, 1983; pp 171-173.

http://rp5.ru/Weather_in_Edmonton,_City_Centre_(airport) (Access during performing experiments).

Huang, Y.; Ou, Q.; Yu, W. Characteristics of flame ionization detection for the quantitative analysis of complex organic mixtures. *Anal. Chem.* **1990**, *62* (18), 2063-2064.

Hucknall, D. J. *Selective Oxidation of Hydrocarbons*. Academic Press: London, 1974.

Ishihara, A.; Wang, D.; Dumeignil, F.; Amano, H.; Qian, E. W.; Kabe, T. Oxidative desulfurization and denitrogenation of a light gas oil using an oxidation/adsorption continuous flow process. *Appl. Catal. A* **2005**, *279*, 279–287.

Ismagilov, Z.; Yashnik, S.; Kerzhentsev, M.; Parmon, V.; Bourane, A.; Al-Shahrani, F. M.; Hajji, A. A.; Koseoglu, O. R. Oxidative desulfurization of hydrocarbon fuels. *Catal. Rev. Sci. Eng.* **2011**, *53*, 199–255.

Javadli, R.; de Klerk, A. Desulfurization of heavy oil. *Appl. Petrochem. Res.* **2012a,** *1*, 3–19.

Javadli, R.; de Klerk, A. Desulfurization of heavy oil–oxidative desulfurization (ODS) as potential upgrading pathway for oil sands derived bitumen. *Energy Fuels* **2012b,** *26* (1), 594–602.

Jevtic , R.; Ramachandran, P.A.; Dudukovic, M. P. Effect of oxygen on cyclohexane oxidation: A stirred tank study. *Ind. Eng. Chem. Res.* **2009**, *48*, 7986–7993.

Jevtic , R.; Ramachandran, P.A.; Dudukovic, M. P. Capillary reactor for cyclohexane oxidation with oxygen. Chem. Eng. Res. Des. **2010**, *88*, 255–262.

Jha, K. N.; Rao, P. M.; Strausz, O. P.Oxidation of Athabasca oil sand and its reactions. *Prepr. Pap. Am. Chem. Soc., Div. Fuel Chem.* **1978,** *23*(4), 91–97.

Jia, N.; Moore, R. G.; Mehta, S. A.; Van Fraassen, K.; Ursenbach, M. G.; Zalewski, E. Compositional changes for Athabasca bitumen in the presence of oxygen under low temperature conditions. *J. Can. Petrol. Technol.* **2005**, *44*(9), 51-56.

Jiayu, L.; Wanghua, C.; Liping, C.; Yingtao, T.; Xin, S. Thermal decomposition analysis and safety study on di-tert-butyl peroxide. *Procedia Eng.* **2012,** *43*, 312–317.

Johnson, R. M.; Siddiqi, I. W. *The determination of organic peroxides*; Pergamon Press: Oxford, 1970.

Jones, R. A.; Bean, G. P. *The chemistry of pyrroles*; Academic Press: London, 1977.

Jorgensen, A. D. Prediction of gas chromatography flame ionization detector response factors from molecular structures. *Anal. Chem.* **1990**, *62*, 683–689.

Kantarci, N.; Borak, F., Ulgen, K. O. Bubble column reactors. *Process Biochem.* **2005,** *40,* 2263-2283.

Kaštánek, F.; Zaharadník, J.; Kratochvíl, J.; Čermák, J. *Chemical Reactors for Gas-Liquid Systems*, 1st ed.; Ellis Horwood: West Sussex, 1993.

Katritzky, A. R.; Lagowski, J. M. *Chemistry of the heterocyclic N-oxides*; Academic Press: London, 1971.

Katritzky, A. R.; Ignatchenko, E. S.; Barcock, R. A.; Lobanov, V. S.; Karelson, M. Prediction of gas chromatographic retention times and response factors using a general qualitative structure-property relationships treatment. *Anal. Chem.* **1994**, *66*, 1799–1807.

Kiwi-Minsker, L.; Renken, A. Microstructured reactors for catalytic reactions. *Catal. Today* **2005,** *110,* 2–14.

Knotnerus, J.; Bitumen durability-measurement by oxygen absorption. *Ind. Eng. Chem. Prod. Res. Develop.* **1972**, *11* (4), 411–422.

Kovalev, I. S.; Kopchuk, D. S.; Zyryanov, G. V.; Rusinov, V. L.; Chupakhin, O. N. Nucleophilic dimerization of indoline under oxidative conditions. *Mendeleev Commun.* **2014**, *24*, 40–41.

Leclerc, A.; Alame, M.; Schweich, D. Pouteau, P. Delattreb, C. de Bellefon, C. Gas–liquid selective oxidations with oxygen under explosive conditions in a micro-structured reactor. *Lab Chip*, **2008**, *8*, 814–817.

Lee, D. G.; Noureldin, N. A. Effect of water on the low-temperature oxidation of heavy oil. *Energy Fuels* **1989**, *3*, 713–715.

Lerou, J. J.; Tonkovich, A. L.; Silva, L.; Perry, S.; McDaniel, J. Microchannel reactor architecture enables greener processes. *Chem. Eng. Sci.* **2010,** *65,* 380–385.

Lesueur, D. The colloidal structure of bitumen: Consequences on the rheology and on the mechanisms of bitumen modification. *Adv. Colloid Interface Sci.* **2009**, *145*, 42–82.

Linhares, M.; Rebelo, S.L.H.; Simões, M.M.Q.; Silva, A.M.S.; Graça, M.; Neves, P.M.S.; Cavaleiro, J.A.S.; Freire, C. Biomimetic oxidation of indole by Mn(III)porphyrins. *Appl. Catal. A* **2014**, *470*, 427–433.

Liu, J. K.; Gunning, H. E. Syncrude analytical methods manual for bitumen upgrading; AOSTRA, Edmonton, 1991.

Liu, X.; Jensen, K.F. Direct oxidative amidation of aromatic aldehydes using aqueous hydrogen peroxide in continuous flow microreactor systems. *Green Chem.,* **2012,** *14* (5), 1471–1474.

Londry, K.; Foght, J. M.; Fedorak, P. M.; Gray, M. R. Bioconversion of Oil Sands Bitumen, Final report to EnCana, June 11, 2009.

Lundberg, W. O. *Autoxidation and antioxidants*, Vol I. Wiley: New York, 1961.

Mae, K.; Maki, T.; Araki, J.; Miura, K. Extraction of low-rank coals oxidized with hydrogen peroxide in conventionally used solvents at room temperature. *Energy Fuels* **1997**, *11*, 825-831.

Mayo, F. R.; Miller, A. A. The oxidation of unsaturated compounds. VI. The effect of oxygen pressure on the oxidation of a-methylstyrene. *J. Am. Chem. Soc.***1958**, *80* (10), 2480–2493.

McLafferty, F. W.; Tureček, F. *Interpretation of mass spectra*, 4ed; University Science Books: Mill Valley, CA, 1993.

Montgomery, D. S. Bitumen chemistry related to oil production and upgrading. Edmonton, Alberta, 1981.

Moschopedis, S. E.; Speight, J. G. Water-soluble derivatives of Athabasca asphaltenes. *Fuel* **1971a**, *50*, 34-40.

Moschopedis, S. E.; Speight, J. G. The halogenation of Athabasca asphaltenes with elemental halogen. *Fuel* **1971b**, *50*, 58-64.

Moschopedis, S. E.; Speight, J. G. Oxidation of bitumen in relation to its recovery from tar-sand formations. *Fuel* **1974**, *53*, 21-25.

Moschopedis, S.E.; Speight, J.G. Oxidation of bitumen. *Fuel* **1975,** *54* (3), 210–212.

Nixon, A. C. Autoxidation and antioxidants of petroleum. In *Autoxidation and antioxidants. Vol. II*; Lundberg, W. O. Ed.; Interscience: New York, 1962, p. 695–856.

Nji, G. Characterization of heavy oils and bitumens. Ph.D. dissertation, University of Calgary (Canada), Canada. Retrieved January 11, 2012, from Dissertations & Theses: Full Text. (Publication No. AAT NR62165).

Noller, R. C. Chemistry of organic compounds, 3rd Edition. W. B. Saunders Company: London, 1966.

Noureldin, N. A.; Lee, D. G.; Mourtis, F. M.; Jha, K. N. Chemical changes accompanying the low temperature oxidation of heavy oil. *AOSTRA J. Res.* **1987,** *3,* 155–161.

Pan, T.; Lu, Y.; Lloyd, S. Quantum-chemistry study of asphalt oxidative aging: An XPS-aided analysis. *Ind. Eng. Chem. Res.* **2012**, *51*, 7957 7966

Pan, C.-X.; Wei, X.-Y.; Shui, H.-F.; Wang, Z.-C.; Gao, J.; Wei, C.; Cao, X.-Z.; Zong, Z.-M., Investigation on the macromolecular network structure of Xianfeng lignite by a new two-step depolymerization. *Fuel* **2013**, *109*, 49 53.

Partenheimer, W. Methodology and scope of metal/bromide autoxidation of hydrocarbons. *Catal. Today* **1995**, *23* (2), 69–158.

Pereira, K. C.; Porter, A. L.; Potavathri, S.; LeBris, A. P.; DeBoef, B. Insight into the palladium-catalyzed oxidative arylation of benzofuran: heteropoly acid oxidants evoke a Pd(II)/Pd(IV) mechanism. *Tetrahedron* **2013**, *69*, 4429–4435.

Petersen, J. C. Asphalt oxidation - an overview including a new model for oxidation proposing that physicochemical factors dominate the oxidation kinetics. *Fuel Sci. Technol. Int.* **1993**, *11*, 57 87.

Phillips, C. R.; Hsieh, I.-C. Oxidation reaction kinetics of Athabasca bitumen. *Fuel* **1985**, *64*, 985-989.

Pina, C. D.; Falletta, E.; Rossi, M. Liquid phase oxidation of organic compounds by supported metal-based catalysts with a focus on gold. In *Liquid Phase Oxidation via Heterogeneous Catalysis: Organic Synthesis and Industrial Applications,* First Edition; Clerici, M. G.; Kholdeeva, O. A. Eds.; Wiley: Hoboken, 2013, 221–262.

Plesnicar, B. In Oxidation in organic chemistry, 5-C; Trahanovsky, W. S. Ed.; Academic Press: New York, 1978, 211–294.

Poniatowski, A. J.; Floreancig, P. E. Radical cation fragmentation reactions in organic synthesis. In *Carbon-Centered Free Radicals and Radical Cations: Structure, Reactivity, and Dynamics, 1st ed*; Forbes, M. D. E. Ed.; Wiley: New Jersey, 2010, p 43-60.

Prado, G. H. C.; De Klerk, A. Halogenation of oilsands bitumen, maltenes and asphaltenes. *Energy Fuels* **2014**, *28*, 4458–4468.

Pryor, W. A. *Free Radicals*; McGraw Hill: New York, 1966.

Rajappa, S.; Gumaste, V. K. Reactivity of thiophene, oligothiophenes and benzothiophenes. *Adv. Heterocyclic Chem.* **2013**, *108*, 1–161.

Rana, M. S.; Sámano, V.; Ancheyta, J.; Diaz, J. A. I. A review of recent advances on processing technologies for upgrading of heavy oils and residua. *Fuel* **2007**, *86*, 1216-1231.

Rebrov, E.V.; Duisters, T.; Löb, P.; Meuldijk, J.; Hessel, V. Enhancement of the liquid-side mass transfer in a falling film catalytic microreactor by in-channel mixing structures. *Ind. Eng. Chem. Res.* **2012**, *51*(26), 8719–8725.

Reid, R.C.; Prausnitz, J. M.; Poling, B, E. The properties of gases and liquids, 4th ed, McGraw-Hill, New York, 1987, pp 332–336.

Ren, S.; Zhao, H.; Dang-Vu, T.; Xu, Z.; Masliyah, J. H. Effect of weathering on oil sands processability. *Can. J. Chem. Eng.* **2009**, *87*, 879–886.

Rothenberg, G. *Catalysis: Concepts and Green Applications*; Wiley: Weinheim, 2008; pp 1–38.

Russell, G. A. Deuterium-isotope effects in the autoxidation of aralkyl hydrocarbons. Mechanism of the interaction of peroxy radicals. *J. Am. Chem. Soc.* **1957**, *79*, 3871–3877.

Schäfer, R. Bubble size distributions and reaction kinetics for the autocatalytic oxidation of cyclohexane in a bubble column reactor. PhD Thesis, Universität of Stuttgart Germany, **2005**.

Schwartz, D.; Hall, P. J.; Marsh, H. Macromolecular and chemical changes induced by air-oxidation of a medium volatile bituminous coal. *Prepr. Pap.-Am. Chem. Soc., Div. Fuel Chem.* **1988**, *33*(2), 343-351.

Scott, G. Atmospheric Oxidation and Antioxidants; Elsevier Publishing Company: Amsterdam, 1981, 17.

Sevov, C. S.; Wiest, O. Selectivity in radical cation cycloadditions. In *Carbon-Centered Free Radicals and Radical Cations: Structure, Reactivity, and Dynamics, 1st ed*; Forbes, M. D. E. Ed.; Wiley: New Jersey, 2010, p 61-82.

Sheldon, R. A.; Kochi, J. K. *Metal-Catalyzed Oxidations of Organic Compounds*; Academic Press: New York, 1981.

Siddiquee, M. N.; De Klerk, A. Oxidation of naphthenic-aromatic compounds in bitumen. *Prepr.Pap.-Am. Chem. Soc., Div. Energy Fuels* **2014a**, *59*(2), 572–574

Siddiquee, M. N.; De Klerk, A. Hydrocarbon addition reactions during low temperature autoxidation of oilsands bitumen. *Energy Fuels* **2014b**, *28*, 6848–6859.

Siddiquee, M. N.; De Klerk, A.; Nazemifard, N. Application of microfluidics to enhance gas-liquid mass transfer during selective oxidation of hydrocarbons. *Reaction and Engineering Chemistry Research* (Submitted).

Silverstein, R. M.; Webster, F. X.; Kiemle, D.J. *Spectrometric Identification of Organic Compounds,* 7th ed.; John Wiley: New York, 2005.

Snead, D. R.; Jamison, T.F. A three-minute synthesis and purification of ibuprofen: pushing the limits of continuous-flow processing. *Angew. Chem. Int. Ed.* **2015***, 54*(3), 1521–3773.

Sobieszuk, P.; Aubin, J.; Pohorecki, R. Hydrodynamics and mass transfer in gas-liquid flows in microreactor. *Chem. Eng. Tech.* **2012**, *35*(8), 1346–1358.

Sobkowiak, M.; Griffith, J. M.; Wang, B.; Beaver, B. Insight into the mechanisms of middle distillate fuel oxidative degradation. Part 1: On the role of phenol, indole, and carbazole derivatives in the thermal oxidative stability of Fischer-Tropsch/Petroleum jet fuel blends. *Energy Fuels* **2009**, *23*, 2041–2046.

Song, H.; Tice, J.D.; Ismagilov, R.F. A microfluidic system for controlling reaction networks in time. *Angew. Chem. Int. Ed.* **2003,** *42* (7), 768–772.

Speight, J. G. *The Chemistry and Technology of Petroleum,* 4th ed.; CRC Press: Boca Raton, FL, 2006; pp 1-34.

Strausz, O. P.; Lown, E. M. *The chemistry of Alberta oil sands, bitumens and heavy oils*; Alberta Energy Research Institute: Calgary, AB, 2003.

Suresh, A. K.; Sharma, M. M.; Sridhar, T. Engineering aspects of industrial liquid-phase air oxidation of hydrocarbon. *Ind. Eng. Chem. Res.* **2000,** *39,* 3958–3997.

Suresh, A. K.; Sridhar, T.; Potter, O. E. Mass transfer and solubility in autocatalytic oxidation of cyclohexane. *AIChE J.* **1988a**, *34*(1), 55–68.

Suresh, A. K.; Sridhar, T.; Potter, O. E. Autocatalytic oxidation of cyclohexane mass transfer and chemical reaction. *AIChE J.* **1988b**, *34*(1), 81–93.

Suresh, A. K.; Sridhar, T.; Potter, O. E. Autocatalytic oxidation of cyclohexane–modeling reaction kinetics. *AIChE J.* **1988c**, *34*(1), 69–80.

Talbi, H.; Monard, G.; Loos, M.; Billaud, D. Theoretical study of indole polymerization. *Theochem.* **1998**, *434*, 129–134.

Talbi, H.; Ghanbaja, J.; Billaud, D.; Humbert, B. Vibrational properties and structural studies of doped and dedoped poluindole by FTIR, Raman and EEL spectroscopies. *Polymer* **1997**, *38*, 2099–2106.

Thyrion, F.C. Asphalt Oxidation. In Asphaltenes and Asphalts, 2. Developments in Petroleum Sciences, 40B. Eidited by Yen, T.F.; Chilingarian, G.V., 2000, Elsevier Science B. V., Amsterdam, The Netherlands, 445–474.

Tipson, R.S. Oxidation of Polycyclic, Aromatic Hydrocarbons. A review of literature; National Bureau of Standards: NBS monograph 87, Washington, 1965; 1–49.

Tolman, C. A.; Druliner, J. D.; Nappa, M. J.; Herron, N. Alkane oxidation studies in du Pont's central research department. In *Activation and Functionalization of Alkanes*; Hill C. L. Ed.; Wiley: New York, 1989; pp 303–360.

Truong, T.; Alvarado, J.; Tran, L. D.; Daugulis, O. Nickel, manganese, cobalt, and iron-catalyzed deprotonative arene dimerization. *Org. Lett.* **2010**, *12*, 1200–1203.

Twigg, G. H. The mechanism of liquid-phase oxidation. *Chem. Eng. Sci. Suppl.* **1954**, *8*, 5–16.

Van Krevelen, D. W. *Coal. Typology–Physics–Chemistry–Constitution*, 3ed; Elsevier: Amsterdam, 1993, p. 627–658.

Vanoye, L.; Aloui, A.; Pablos, M.; Philippe, R.; Percheron, A.; Favre-Réguillon, A.; de Bellefon, C. A safe and efficient flow oxidation of aldehydes with O_2. *Org. Lett.* **2013**, *15*(23), 5978–5981.

Völkel, N. Design and Characterization of Gas-Liquid Microreactors. Ph.D. Thesis, Universite de Tolousé, December 2009.

Wang, L.; Zachariah, A.; Yang, S.; Prasad, V; De Klerk, A. Visbreaking oilsands derived bitumen in the temperature range 340-400 °C. *Energy Fuels* **2014**, *28*(8), 5014-5022.

Wang, Z. L.; Li, H. L.; Ge, L. S.; An, X. L.; Zhang, Z. G.; Luo, X.; Fossey, J. S.; Deng, W. P. DDQ-mediated oxidative coupling: an approach to 2,3-dicyanofuran (thiophene). *J. Org. Chem.* **2014**, *79*, 1156 1165.

Waters, W. A. *Mechanisms of oxidation of organic compounds*; Methuen: London, 1964.

Webster, A. B.; Small, N. J. H.; Rigby, R. Desulfurization of heavy oils. Patent US 3,163,593 (1964, Shell).

Whitehurst, D. D.; Mitchell, T. O.; Farcasiu, M. *Coal liquefaction. The chemistry and technology of thermal processes*; Academic Press: New York, 1980.

Wichert, G. C.In situ upgrading of heavy oils by low-temperature oxidation in the presence of caustic additives; MSc dissertation, University of Calgary, 1996.

Williams, D. H.; Fleming. *Spectrometric Methods in Organic Chemistry,* 4th ed. revised; McGraw-Hill: New York, 1989.

Wilms, D.; Klos, J.; Frey, H. Microstructured reactors for polymer synthesis: a renaissance of continuous flow processes for Tailor-Made macromolecules? *Macromol. Chem. Phys.* **2008,** *209,* 343–356.

Wong, H.; Morris, S.; Radke, C. J. Three-dimensional menisci in polygonal capillaries. *J. Colloid Interf. Sci.* **1992**, *148*(2), 317–336.

Xu, H. H.; Okazawa, N. E.; Moore, R. G.; Mehta, S. A.; Laureshen, C. J.; Ursenbach, C. J.; Ursenbach, M. G.; Mallory, D. G. In situ upgrading of heavy oil. *J. Can. Pet. Technol.* **2001,** *40* (8), 45–53.

Yen, T.F.; Chilingarian, G.V. Introduction. In Asphaltenes and Asphalts,1. Developments in Petroleum Sciences, 40A. Eidited by Yen, T.F.; Chilingarian, G.V., 1994, Elsevier Science B. V., Amsterdam, The Netherlands, 1–6.

Yun, J.; Lei, Q.; Zhang, S.; Shen, S.; Yao, K. Slug flow characteristics of gas-miscible liquids in a rectangular microchannel with cross and T-shaped junctions. *Chem. Eng. Sci.* **2010**, *65*, 5256–5263.

Appendix A: Support information of Low-Temperature Autoxidation of Oilsands Bitumen (Chapter 3)

A.1. SARA Fractionation of Bitumen

Bitumen was separated into SARA (saturates, aromatics, resin, and asphaltenes) fractions by Clay-Gel Adsorption chromatography using a modified ASTM D-2007 standard method (ASTM D2007-03). The difference between the procedure followed and the ASTM D-2007 method was the definition of aromatic and polar (resin) compounds. A stronger solvent was used to elute aromatics and therefore aromatics containing more benzene rings were therefore included in the product that eluted as the aromatic fraction.

A.1.1 Activation of Attapulgus Clay

The Attapulgus clay (30-60 mesh size, Univar Canada Ltd) was washed in a beaker with methylene chloride (99.9 %, stabilized HPLC grade, Fisher Scientific) 2-3 times until the wash was colourless. The methylene chloride wash was followed by washing the clay with methanol (99.9 %, HPLC grade, Fisher Scientific), typically 2-3 times until the wash was colourless. Lastly the clay was washed with distilled water until the pH of the water was in the pH range 6-7. The Attapulgus clay was then dried on a metal tray overnight in an oven (vacuum drying oven DP43, Yamato) at 100 °C under vacuum. The prepared clay was then stored in glass jars.

A.1.2 Activation of Silica Gel

Silica gel (28-200 mesh, S157-212, Fischer Scientific) was spread evenly on a metal tray and placed in the oven (vacuum drying oven DP43, Yamato) overnight at 145 °C to activate.

A.1.3 Asphaltene Removal

Approximately 10.0 g of material was placed in 500 ml Erlenmeyer flask, 400 mL pentane (99.7%, Fisher Scientific) was added to precipitate the asphaltenes. The flask was then placed in an ultrasoninc bath (1510 Branson Sonicator) for 45 minutes and allowed to settle overnight. The mixture was then placed in the ultrasoninc bath (1510 Branson Sonicator) for 15 minutes

and the asphaltenes were filtered through a 0.22 μm filter paper (Millipore). The asphaltenes were washed with pentane until the solution runs clear. Asphaltenes were then dried to get constant weight. Pentane was removed from maltenes using a Heidolph vacuum rotary evaporator (HeizbadHei-VAP, P/N: 517-6100-01-0).

Material Balance

Asphaltenes % = (weight (g) asphaltenes/ weight (g) original sample) × 100

Maltenes % = [(weight (g) original sample – weight (g) asphaltenes)/(weight (g) original sample)] × 100

A.1.4 Chromatographic Procedure

The adsorption column was consisted with two identical glass section assembled vertically. All glassware were cleaned and rinsed with methylene chloride first and secondly with pentane. The upper adsorption column was prepared by placing 20 g freshly activated Attapulgus clay (washed) in the column. The lower column was prepared by placing 40 g of activated silica gel in the column and tapping gently with rubber hose to achieve a constant level of packing then a further 10 g of Attapulgus clay was placed on top and tapped down with the rubber hose. The two columns were then assembled with the glass joints making sure the joint was clean of clay or silica. A ground glass control tap was attached to the bottom of each column to control the flow. A clean 100 mL measuring cylinder was placed below each column. Approximately 2 g maltenes (pentane soluble part of bitumen) was weighed in a vial and diluted with 5 mL pentane and swirled to ensure complete dissolution.

A.1.5 Collection of Saturates Fraction

Prior to sample addition, 10 mL of pentane was charged to the top of the column and allowed to percolate into the clay. When all of the pentane had entered the clay, the diluted sample was charged to the top of the column. The vial was washed 2-3 times with pentane and added to the top of the column. After the entire sample had entered the clay, the sides of the column were washed down with more pentane. Approximately 130 mL of pentane was added in order to collect 80 mL of eluent. The addition of pentane was done in several portions. The collected

saturate fraction was placed in a clean 500 mL round bottom flask, and was afterwards stored for solvent removal.

A.1.6 Collection of the Aromatics Fraction

A 50:50 solvent mixture of pentane and toluene (99.7%, HPLC grade, Fisher Scientific), in the amount of 312 mL, was added to the column using 250 mL funnel. The column was allowed to drain. The two columns were separated and the Attapulgus clay from the lower column was added to the Attapulgus of the upper column to enable total recovery of the polar (resin) fraction. The column was then connected to the refluxing assembly and 100 mL of toluene added. The column was refluxed at a rate of 8-10 mL/minute for one hour. The solution from the refluxing flask was added to the rest of the aromatic fraction in a 500 mL bottle.

A.1.7 Collection of the Resin Fraction

The solvent mixture of methanol (99.9%, HPLC grade, Fisher Scientifc) and methylene chloride (60:40) in the amount of 100 mL was added to the clay from both columns (the clay from the lower column was removed carefully from the silica and added to the clay in the upper column) another 50 mL of methanol was added to the column and eluted out.

A.1.8 Solvent Removal

The saturates were transferred to pre-weighed 500 mL round bottomed flask and the cylinder rinsed 2-3 times with pentane and washings were added to the flask. The solvent was removed using a Heidolph vacuum rotary evaporator (HeizbadHei-VAP, P/N: 517-6100-01-0). Similarly, the solvent was removed from the polar (resin) and aromatic fractions. The remaining solvent was removed by placing the flasks in a fume hood. A Mettler Toledo balance (XS 105) was used to determine asphaltene fraction, and a Mettler Toledo balance (XP 1203S) was used to calculate the weight of saturates, resin, and aromatic fractions of bitumen.

A.2 Literature cited

ASTM D2007-03: Standard test method for characteristic groups in rubber extender and processing oils and other petroleum-derived oils by the clay-gel absorption chromatographic method; ASTM: West Conshohocken, PA, 2003.

Appendix B: Support information of Liquid Phase Oxidation in Microfluidic Reactor to Manipulate Oxygen Availability to Control Oxidation Rate and Product Selectivity Independently (Chapter 6)

B.1. Physicochemical Properties of Tetralin and Oxygen

Physicochemical properties of tetralin and oxygen used for the calculation shown in the study are listed **Table B.1**. Most of the properties are interpolated from the values obtained from the reported literatures.

Table B.1. Physicochemical properties of tetralin and oxygen at different experimental conditions.

	Tetralin					Oxygen		
Temper-ature (ºC)	density [c] (kg/m^3)	surface tension [a, e, f] (N/m)	dynamic viscosity [c] (Pa.s)	kinematic viscosity [c] (m^2/s)	dynamic viscosity [d] (Pa.s)	density [b] (kg/m^3)	kinematic viscosity [d] (m^2/s)	D_A [g] (m^2/s)
25	9.66E+02	3.51E-02	1.17E-03	1.21E-06	2.15E-05	2.36E+00	9.08E-06	2.73E-09
120	8.87E+02	2.57E-02	6.36E-04	7.17E-07	2.59E-05	1.79E+00	1.44E-05	2.14E-08
130	8.79E+02	2.48E-02	5.84E-04	6.65E-07	2.64E-05	1.75E+00	1.51E-05	2.52E-08
140	8.71E+02	2.38E-02	5.33E-04	6.13E-07	2.68E-05	1.71E+00	1.57E-05	2.93E-08
150	8.62E+02	2.28E-02	4.83E-04	5.61E-07	2.73E-05	1.67E+00	1.64E-05	3.39E-08
160	8.54E+02	2.18E-02	4.34E-04	5.08E-07	2.78E-05	1.63E+00	1.71E-05	3.90E-08

[a] with respect to air.
[b] density of oxygen was calculated at experimental pressure using ideal gas law.
[c] adapted from Caudwell et al., 2009.
[d] adapted from Schmid, 1942.
[e] adapted from Herz, 1922.
[f] adapted from Grunmach, 1924.
[g] adapted from Díaz et al.,1987.

B.2 Flame Ionization Detector (FID) Response Factors

The flame ionization detector (FID) has different responses to various organic compounds. So, it is required to calculate response factors for accurate quantification of oxidative conversion by GC-FID. The Dietz-method was used to calculate the response factors (Dietz, 1967):

$$Response\ factor\ (RF)_{Dietz} = \frac{(area\ of\ compound)(mass\ of\ standard)}{(mass\ of\ compound)(area\ of\ standard)}$$

Heptane was used as the standard and its response factor was 1.00. The calculated relative response factors are tabulated in **Table B.2**. The calculated relative response factors are very close the response factors reported in literature (Dietz, 1967; Huang et al., 1990; Katritzky et al., 1994). The FID response factors previously reported in literature are also listed in **Table B.2** for comparison.

Table B.2. FID response factors of various compounds.

Compound Name	Retention Time (minute)	Response factor (RF)	Reported RF value
Heptane	1.72	1.00 ± 0.00	1.00 (Dietz, 1967)
$CHCl_3$	1.52	0.09 ± 0.01	
Hexachlorobenzene	8.67	0.32 ± 0.01	0.31(Huang et al., 1990)
Tetralin	4.90	1.08 ± 0.01	1.02 (Katritzky et al., 1994)
1,2,3,4-tetrahydro-1-naphthol	6.35	0.82 ± 0.02	
alpha-tetralone	6.51	0.84 ± 0.01	0.80 (Katritzky et al., 1994)

B.3 Conversion Calculations

Conversion was calculated based on the tetralin disappearance and did not reflect the extent of oxidation. The percentage conversion was calculated as follows (Siddiquee and De Klerk, 2014b):

$$W_i = \frac{A_i * W_{HCB}}{A_{HCB} * RRF_{i,HCB}}$$

Where, $RRF_{i,HCB} = RF_i / RF_{HCB}$

= Relative response factor of model compounds with respect to hexachlorobenzene (internal standard)

RF_{HCB} = Response factor of hexachlorobenzene with respect to heptane

RF_i = Response factor of model compound with respect to heptane

W_i = Weight % of model compounds

W_{HCB} = Weight % of hexachlorobenzene

A_i = Peak area of model compounds

$A_{HCB}A_{HCB}$ = Peak area of hexachlorobenzene

For the conversion less than 1 (wt/wt %), the tetralin conversion was calculated based on the formation of products. A conversion factor was calculated using the data obtained from oxidation of tetralin with air conducted in a semi-batch reactor (**Table B.3**) (Siddiquee and De Klerk, 2014b). Conversion factor was multiplied by sum of relative peak areas of product area to get the conversion. Conversion factor was selected based on the sum of product area.

Table B.3. Conversion data for oxidation of tetralin with air at 130 °C conducted in a semi-batch reactor (Siddiquee and De Klerk, 2014b).

Time	conversion	sum of oxidized products	conversion factor
30 min	0.8	214.8	0.0035
1 hr	1.1	643.3	0.0017
2 hr	2.1	1128.1	0.0019
4 hr	4.5	2922.5	0.0015
6 hr	6.9	4628.7	0.0015

Conversion rate was calculated by multiplying conversion with molar flowrate.

B.4 Diffusion Coefficient Calculation

Different correlations are available in literature to calculate the diffusivities in liquid. Correlation provided by Díaz et al. (1987) can be used to calculate diffusivity of gases in liquid over wide temperature range. This correlation is used to calculate the diffusion coefficient of oxygen in tetralin (D_A) at 150 °C.

Díaz et al. Correlation (Díaz et al., 1987):

$$(D_A)_T = 4.996 \times 10^3 (D_{AB})_{T=25\,^\circ\mathrm{C}} e^{(-2539/T)}$$

Where, $(D_A)_{T=25\,^\circ\mathrm{C}} = 6.02 \times 10^{-5} \frac{V_B^{0.36}}{\mu_B^{0.61} V_A^{0.64}}$

$(D_A)_T$ is the diffusion coefficient of oxygen in tetralin at given temperature in cm^2/s

$(D_A)_{T=25\,^\circ\mathrm{C}}$ is the diffusion coefficient of oxygen in tetralin at 25 °C in cm^2/s

T is the absolute temperature (K) = 423 K

μ_B is the viscosity of tetralin = 2 cp

V_A is the molar volume of oxygen at the normal boiling point temperature ($cm^3/gmol$) = 27.9 $cm^3/gmol$

V_B is the molar volume of tetralin at the normal boiling point temperature ($cm^3/gmol$) = 135.7 $cm^3/gmol$

$$(D_A)_{T= 25\,^\circ\mathrm{C}} = 2.7 \times 10^{-09}\ m^2/s$$

$$(D_A)_{T= 150\,^\circ\mathrm{C}} = 3.4 \times 10^{-08}\ m^2/s$$

B.5 Product identification

GC-FID chromatograms of tetralin oxidized at 150 °C in a microfluidic reactor are shown in **Figure B.1** to illustrate the ketone-to-alcohol selectivity in primary oxidation product.

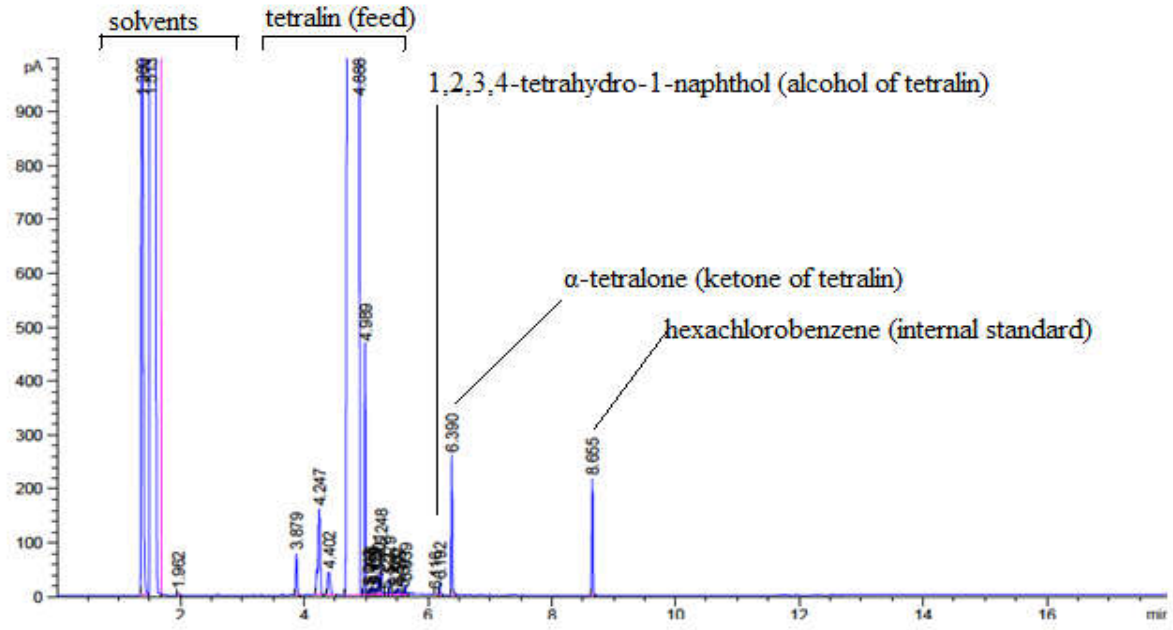

(a)

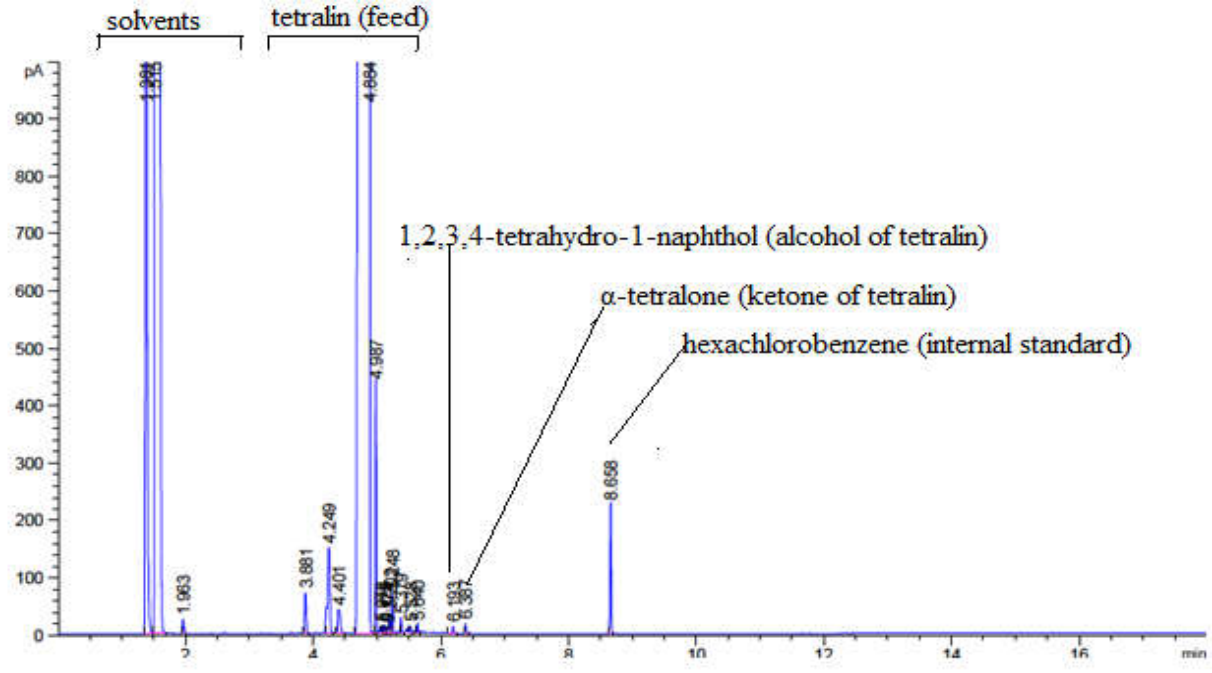

(b)

Figure B.1. GC-FID chromatogram of tetralin oxidized at 150 °C in a microfluidic reactor at gas-liquid interfacial area: (a) $3x10^5$ m^2/m^3 (Series A) and (b) $5\ x10^3$ m^2/m^3 (Series E).

B.6 Thermal Analysis of di-*tert*-Butyl peroxide (initiator)

Typical DSC (differential scanning calorimeter) curves of di-*tert*-butyl peroxide obtained at different heating rates under N_2 atmosphere are shown in **Figure B.2.**

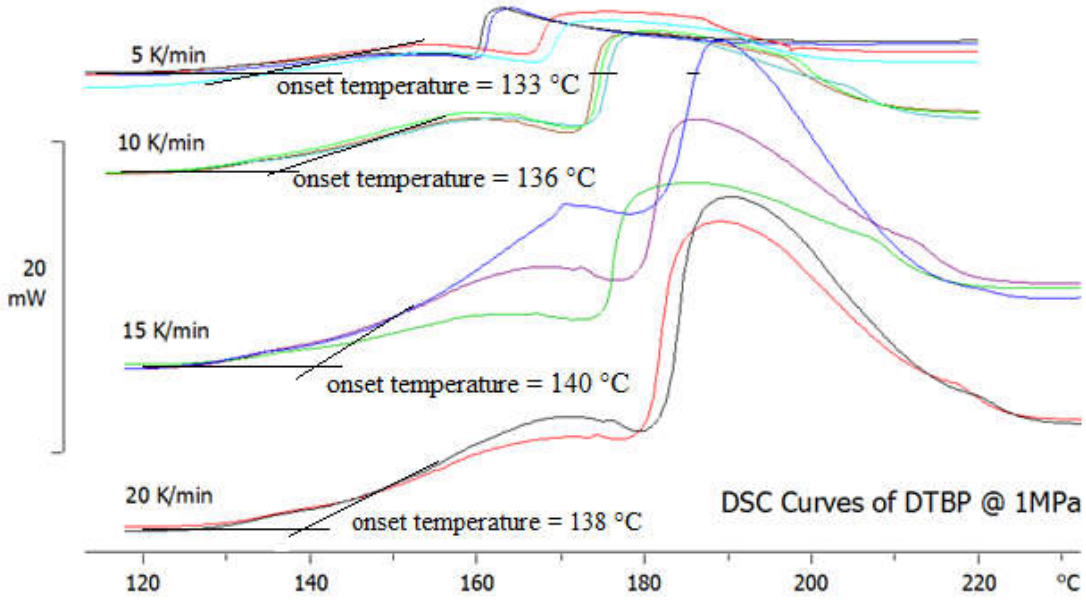

Figure B.2. Typical DSC (differential scanning calorimeter) curves of di-*tert*-butyl peroxide obtained at heating rate of 5-20 °C/min from 25 to 220 (or 230) °C under N_2 atmosphere.

B.7 Literature Cited

Caudwell, D. R.; Trusler, J. P. M.; Vesovic, V.; Wakeham, W. A. Viscosity and density of five hydrocarbon liquids at pressures up to 200 MPa and temperatures up to 473 k. *J. Chem. Eng. Data* **2009**, *54*, 359–366.

Díaz, M.; Vega, A.; Coca, J. Correlation for the estimation of gas-liquid diffusivity, *Chem. Eng. Com.* **1987**, *52*(4-6), 271–281.

Dietz, W. A. Response factors for gas chromatographic analyses. *J. Chromatogr. Sci.* **1967**, *5* (2), 68–71.

Grunmach, S. *Zeitschrift Physikalische Chemie Stoechiometrie Verwandtschaftslehre* **1924**, *113*, 437.

Herz, S. *Zeitschrift Physikalische Chemie Stoechiometrie Verwandtschaftslehre* **1922**, 101, 284.

Huang, Y.; Ou, Q.; Yu, W. Characteristics of flame ionization detection for the quantitative analysis of complex organic mixtures. *Anal. Chem.* **1990**, *62* (18), 2063–2064.

Katritzky, A. R.; Ignatchenko, E. S.; Barcock, R. A.; Lobanov, V. S.; Karelson, M. Prediction of gas chromatographic retention times and response factors using a general qualitative structure-property relationships treatment**.** *Anal. Chem.* **1994**, *66* (11), 1799–1807.

Schmid, C. *Gas. Wasserfach.* **1942** , *85*, 92 –103

Siddiquee, M.N.; De Klerk, A. Hydrocarbon addition reactions during low temperature autoxidation of oilsands bitumen. *Energy Fuels* **2014**, *28*, 6848–6859.

Appendix C: Support information of Engineering Aspects of Liquid Phase Autoxidation of Hydrocarbon: Experimental Study (Chapter 7)

C.1. Calculation of Mass Transfer Coefficient

Mass transfer coefficient was calculated by solving equation (7.1) with the boundary condition, at t=0, C^b=0, C=$-\ln C^*$.

Rate of oxygen transfer, $-\frac{dC^b}{dt} = k_L a(C^b - C^*)$ Equation (7.1)

where, C^b is the oxygen concentration in the bulk liquid (mol/m^3)
C^* is the oxygen concentration in the gas-liquid interface (mol/m^3)
k_L is the mass transfer coefficient (m/s).
a is the gas-liquid interfacial area (m^2/m^3)

By rearranging and integration:

$$\int \frac{dC^b}{(C^* - C^b)} = k_L a \int dt$$

$$-\ln(C^* - C^b) = k_L a t + C \qquad \text{Equation (C.1)}$$

Where, C is an integral constant.

At t=0, C^b=0, C=$-\ln C^*$

Equation (C.1) becomes,

$$-\ln(C^* - C^b) = k_L a t - \ln C^*$$

$$\ln(C^* - C^b) = -k_L a t + \ln C^* \qquad \text{Equation (7.2)}$$

Intercept of Equation (7.2) provided the mass transfer coefficient ($k_L a$).

C. 2. Properties of Indan and Benzene

Properties of indan and benzene used for the calculation shown in the study are listed **Table C.1**. Most of the properties are interpolated from the values obtained from the reported literatures.

Table C.1. Properties of indan and oxygen at different experimental conditions.

	indan		benzene	
temperature (ºC)	density (kg/m^3)	dynamic viscosity (Pa.s)	density (kg/m^3)	dynamic viscosity (Pa.s)
50	9.4×10^{2} (1)	9.2×10^{-4} (1)	8.5×10^{2} (1)(2)(3)	4.4×10^{-4} (1)(3)

[1]Evans, E. B. The viscosities of hydrocarbon. *J. Inst. Petr. Technol.* **1938**, 24, 537–549.

[2]Malek, N. I.; Ijardar, S. P.; Master, Z. R.; Oswal, S. B. Temperature dependence of densities, speeds of sound, and derived properties of cyclohexylamine + cyclohexane or benzene in the temperature range 293.15–323.15 K. *Thermochim. Acta* **2012,** *547*, 106–119.

[3]Song, C.; Shen, H.; Zhao, J.; Wang, L.; Wang, F. Densities and Viscosities of Binary Mixtures of Vitamin K3 with Benzene, Toluene, Ethylbenzene, *o*-Xylene, *m*-Xylene, and *p*-Xylene from (303.15 to 333.15) K. *J. Chem. Eng. Data* **2008,** *53,* 1110–1115.

C. 3. Henry's Law Constant of Tetralin and Benzene

C.3.1 Henry's law constant of tetralin

Henry's law constant of tetralin available in literature is shown in **Table C.2**

Table C.2. Henry's law constant of tetralin available in literature.

Temperature °C	Pressure mm Hg	Pressure kPa	C* mol/m3	Henry's law constant (C*/P) mol/(m3. kPa)
10 [(1)]	758	101.0334211	7.5	7.42E-02
25 [(2)]	760	101.3	7.6	7.50E-02
40 [(1)]	755	100.6335526	7.6255	7.58E-02
65 [(1)]	760	101.3	7.752	7.65E-02
100 [(3)]	760	101.3	9.5	9.38E-02

Extrapolated Henry's law constant at 50 °C **= 7.6× 10^{-2} mol/m^3. kPa**

C.3.1 Henry's law constant of benzene

Battino et al. (1983)[4] reported mole fraction solubility of oxygen in benzene at 101.325 kPa and **50 °C (**323.15 K) is, x_1= 8.57 ×10^{-4}

Density of benzene at 50 °C = 846.3 kg/m^3

Molecular weight of benzene = 78.11 g/mol = 7.811 × 10^{-2} kg/mol

Molar volume of benzene = 9.22959× 10^{-5} m^3/mol

Concentration of O_2 in benzene = 9.29 mol/m^3

Henry's law constant of oxygen in benzene at 50 °C **= 9.17 × 10^{-2} mol/m^3. kPa**

= 9.2 × 10^{-2} mol/m^3. kPa

Source of data:

[1]Bateman, L.; Bolland, J. L.; Gee, G. Determination of absolute rate constants for olefinic oxidations by measurement of photochemical pre- and after-effects. Part II.– At "low" oxygen pressures. *Trans. Faraday Soc.***1951**, *47*, 274–285.

[2]Mayo, F. R.; Miller, A. A. The oxidation of unsaturated compounds. VI. The effect of oxygen pressure on the oxidation of a-methylstyrene. *J. Am. Chem. Soc.***1958**, *80* (10), 2480–2493.

[3]Emanuel, N. M.; Denisov, E. T.; Maizus, Z. K. *Liquid-phase oxidation of hydrocarbons*; Plenum Press: New York, 1967.

[4]Battino, R.; Rettich, T. R.; Tominaga, T. The solubility of oxygen and ozone in liquids. *J. Phys. Chem. Ref. Data* **1983**, *12* (2), 163–178.

C.4. Flame Ionization Detector (FID) Response Factors and Conversion Calculation

Conversion was calculated as described in **Section 4.3.** by using the Flame ionization detector (FID) response factors listed in **Table 4.2.**

For the conversion less than 2 (wt/wt %), the indan conversion was calculated based on the formation of products. A conversion factor was calculated using the data obtained from oxidation of indan with air conducted in a semi-batch reactor (**Table C.3**). Conversion factor was multiplied by sum of relative peak areas of product area to get the conversion. Conversion factor was selected based on the sum of product area.

Table C.3. Conversion data for oxidation of indan with air at 130 °C conducted in a semi-batch reactor. [(1)]

Time	conversion	sum relative area of oxidized products	conversion factor
30 min	2.3	1176	0.0020
1 hr	2.9	1351	0.0021
2 hr	4.9	2933	0.0017
4 hr	9.4	5580	0.0017
6 hr	12.9	8496	0.0015

[1]Siddiquee, M.N.; De Klerk, A. Hydrocarbon addition reactions during low temperature autoxidation of oilsands bitumen. *Energy Fuels* **2014b**, *28*, 6848–6859.

C.5. GC-FID Chromatogram of Benzene and Oxidized Benzene

GC-FID chromatogram of benzene and oxidized benzene are shown in (**Figure C.1**). As anticipated, benzene did not oxidize with air at 50 ºC. Oxidation rate for benzene did not calculate due to inertness of it for oxidation.

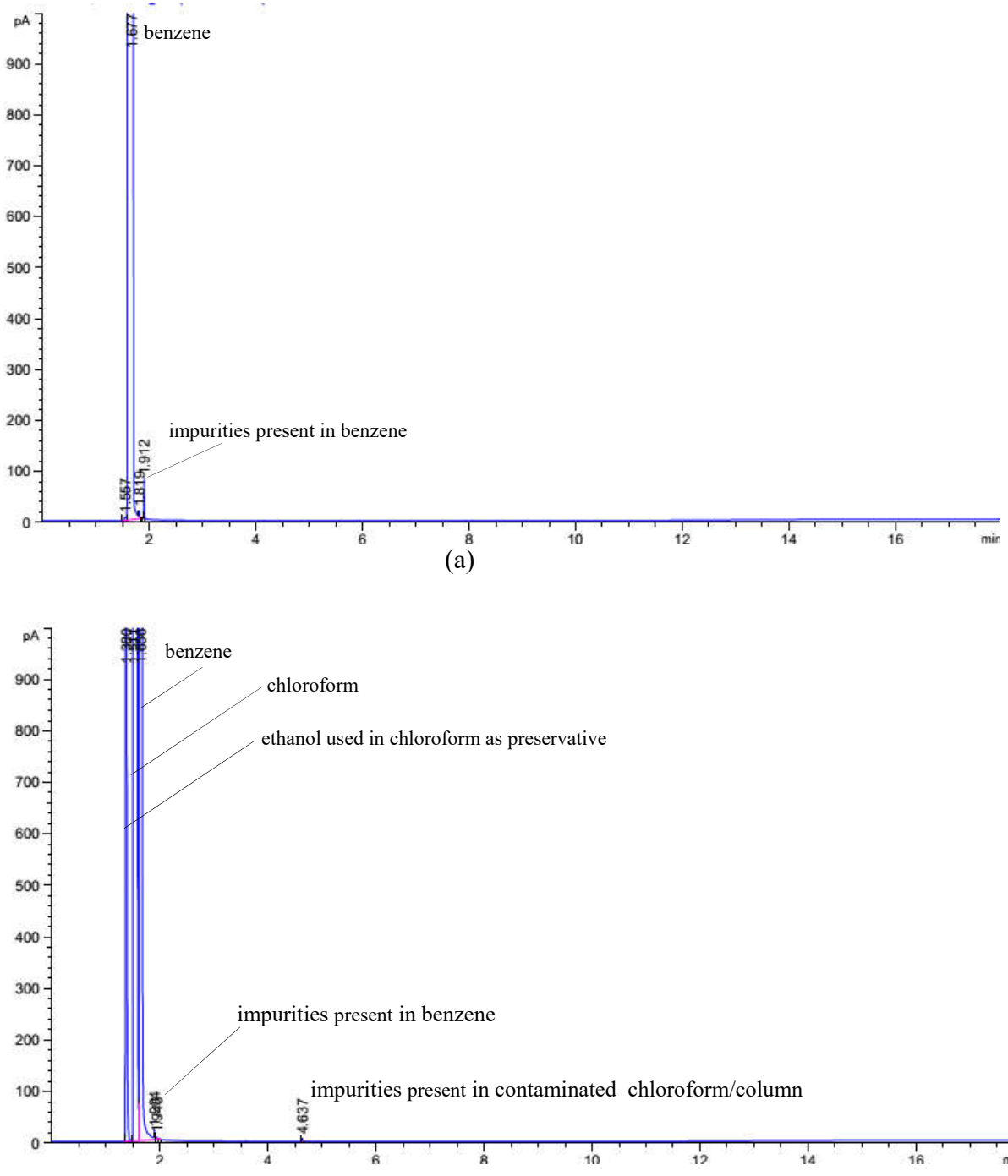

Figure C.1. GC-FID chromatogram of the benzene oxidation at 50 °C: (a) 0 hour (b) 4 hours.

C.6. GC-FID Chromatogram of Indan and Oxidized Indan

GC-FID chromatogram of indan and indan oxidized without di-*tert*-butyl peroxide are shown in (**Figure C.2**). Very limited oxidation observed even after 36 hour oxidation at 50 ºC indicating exceedingly long induction time.

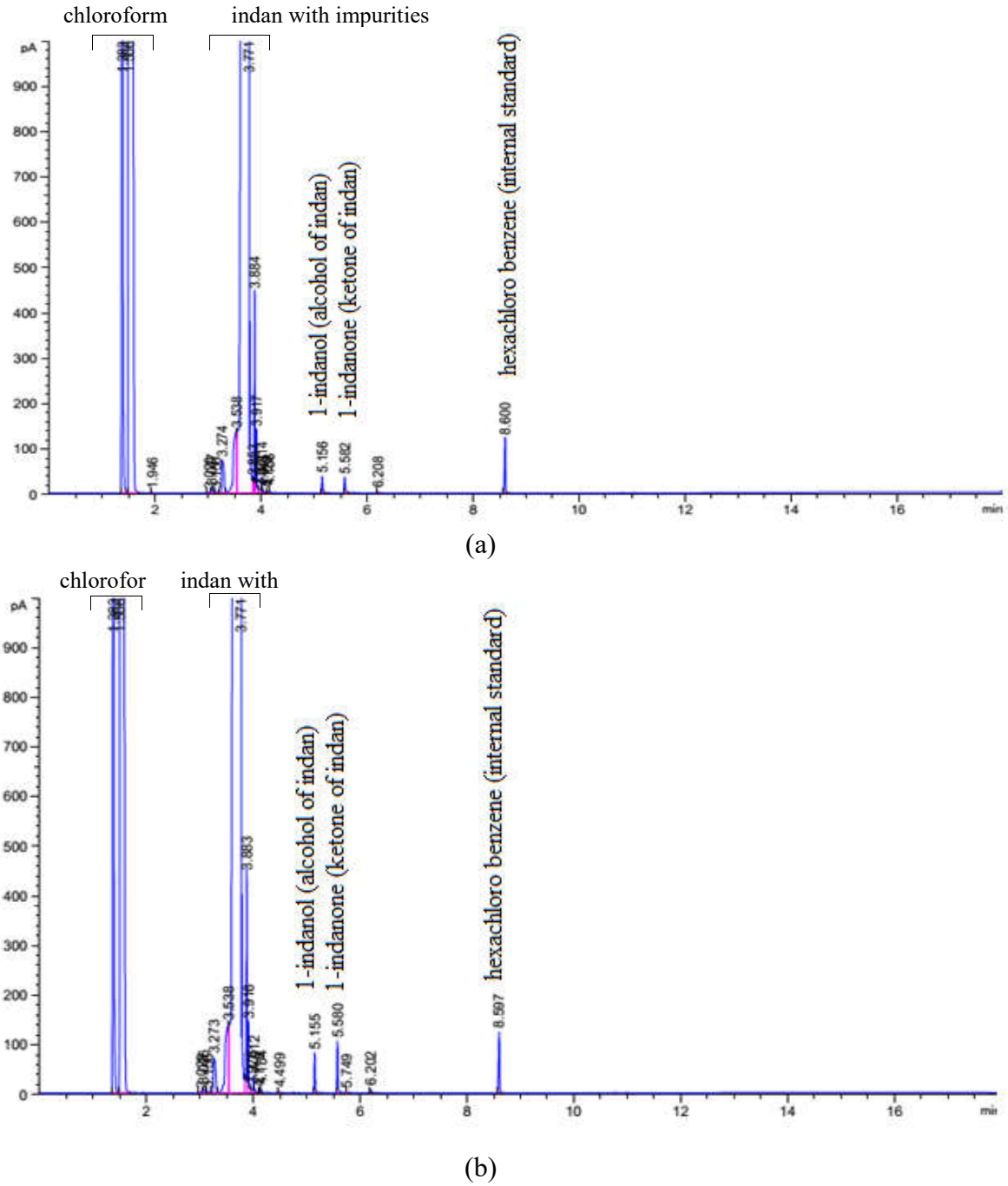

Figure C.2. GC-FID chromatogram of the indan autoxidation at 50 °C: (a) 0 hour (b) 36 hour.

C.7. HPLC Chromatogram of Indan Oxidized in the Presence of Di-*tert*-Butyl Peroxide

Typical HPLC chromatograms of indan and oxidized indan in the presence of di-*tert*-butyl peroxide are shown in **Figure C.3**. Compounds were confirmed from the model compounds except possible addition product between 36–42 minutes of retention time of **Figure C.3(c)**.

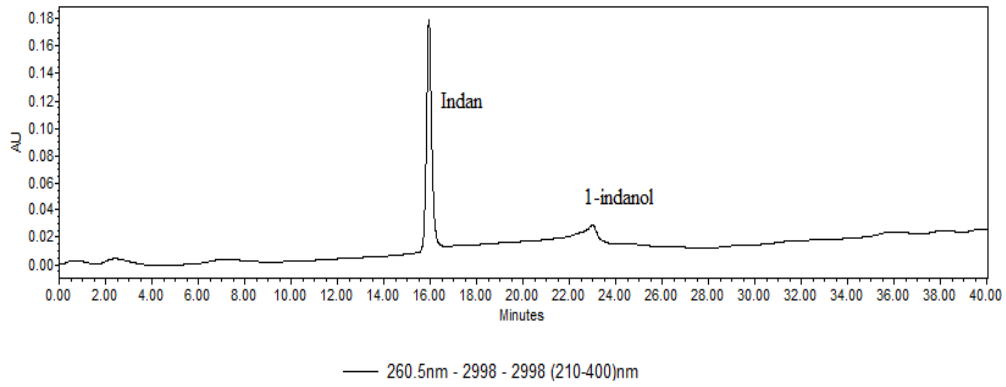

(a)

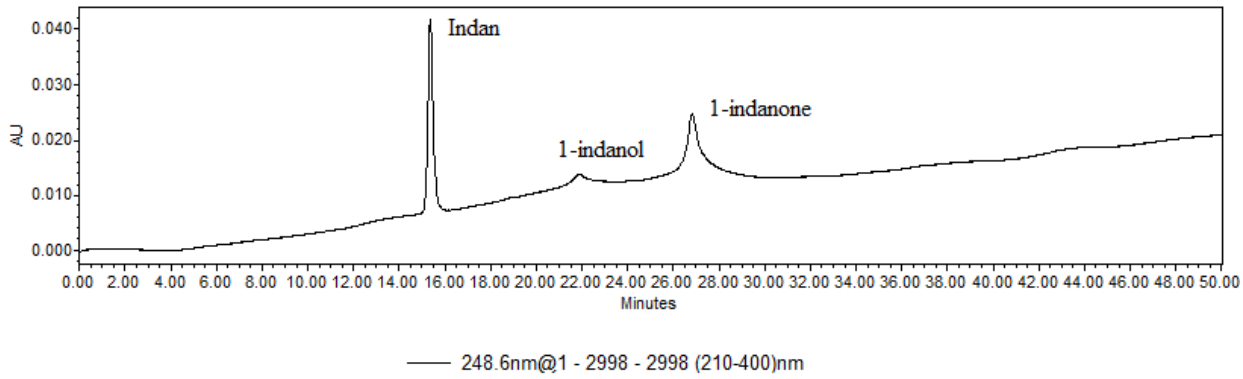

(b)

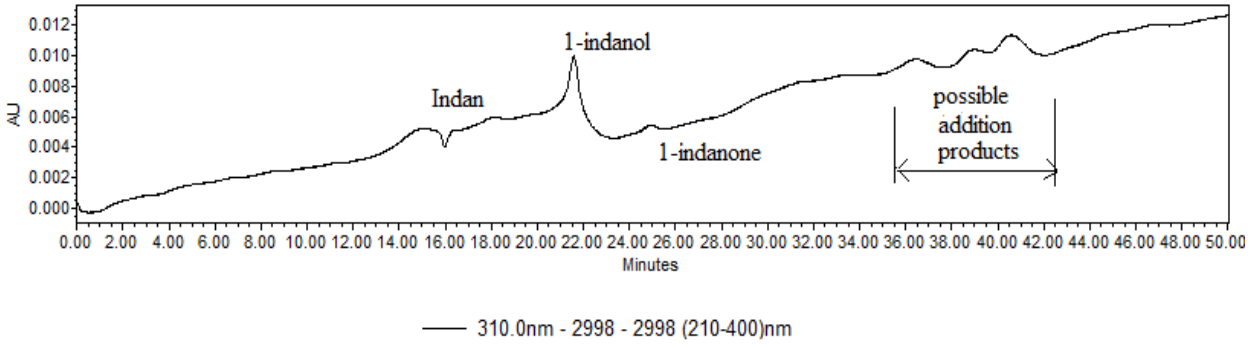

(c)

Figure C.3. Typical HPLC Chromatogram of indan and oxidized indan in the presence of di-*tert*-butyl peroxide: (a) indan, (b) oxidized indan in the presence of di-*tert*-butyl peroxide (chromatogram extracted at 248.6 nm) and (c) possible addition product between 36 42 minutes of retention time (chromatogram extracted at 310 nm).

C.8. Product Identification of Indan Oxidized in the Presence of Di-*tert*-Butyl Peroxide

GC-MS chromatogram of oxidized indan in the presence of 5.1 wt % di-*tert*-butyl peroxide is shown in **Figure C.4**. Compounds leveled as A–J were identified from commercially available compounds using GC-MS. Product (K) was identified based on the fragmentation pattern of compound K (**Figure C.5**) and similar compound suggested in NIST library (**Figure C.6**). Details on addition products (M) can be found in (Chapter 4).

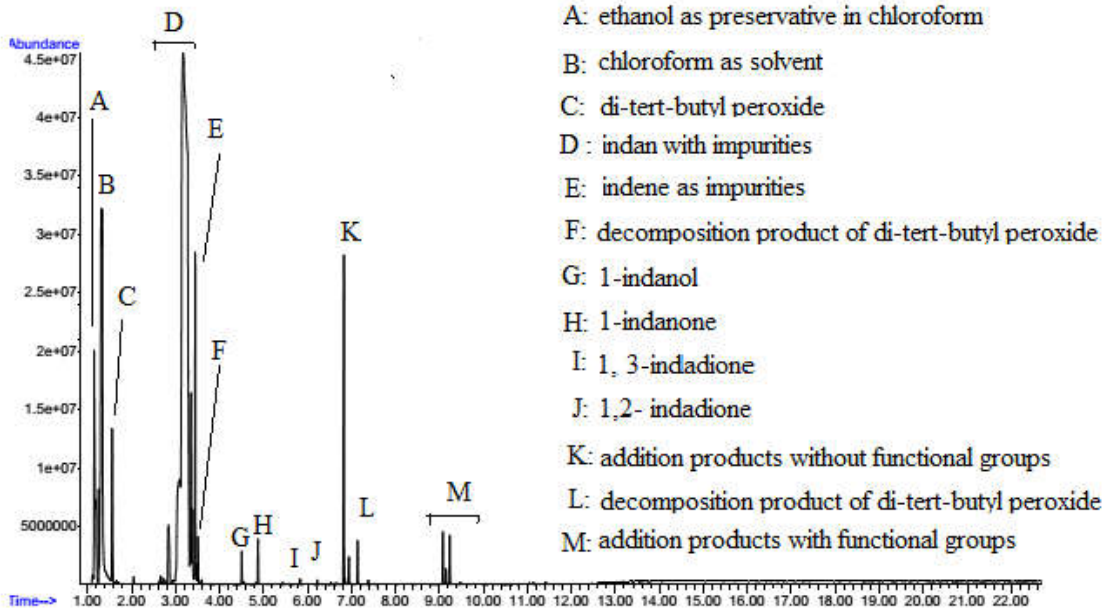

Figure C.4. GC-MS chromatogram of oxidized indan in the presence of 5.1 wt % di-*tert*-butyl peroxide.

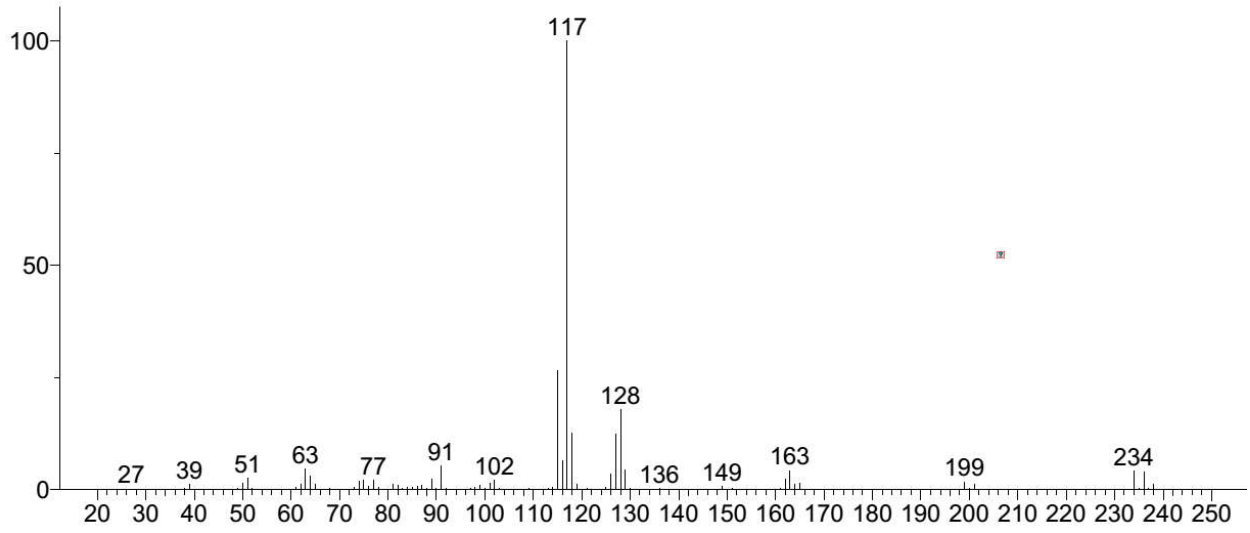

Figure C.5. Fragmentation pattern of addition product appeared at 6.8 minutes of **Figure C.3**.

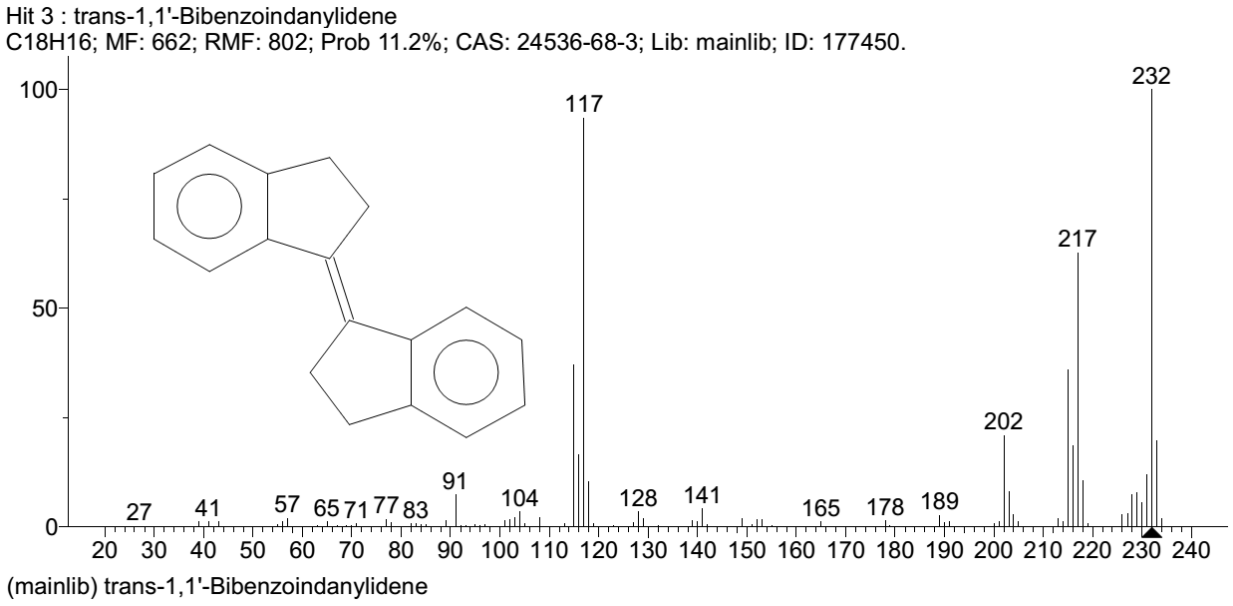

Figure C.6. Fragmentation pattern of an addition compound available in NIST library and close to compound shown in Figure C.5.

C.9 Mass Transfer Coefficients at Different Experimental Conditions

Mass transfer coefficients at different experimental conditions during benzene and indan oxidation are shown in **Table C.4**.

Table C.4. Mass transfer coefficients of benzene and indan at 50 °C and 19.2 kPa O_2 partial pressure.

experiments	gas supply	volumetric mass transfer coefficient, $k_La \times 10^3$ (s^{-1})	liquid side mass transfer coefficient, $k_L \times 10^6$ (m/s)
benzene	air	2.1	3.0
	nitrogen	2.4	3.5
indan with 1.0 wt % di-*tert*-butyl peroxide[a]	air	1.0	1.3
indan with 3.0 wt % di-*tert*-butyl peroxide[a]	air	1.0	1.3
indan with 4.7 wt % di-*tert*-butyl peroxide[a]	air	1.0	1.3
indan with 5.1 wt % di-*tert*-butyl peroxide[a]	air	9.5×10^{-1}	1.2
indan with 9.2 wt % di-*tert*-butyl peroxide[a]	air	1.1	1.4

[a]mass transfer coefficients were calculated before adding di-*tert*-butyl peroxide.

C.10 Calculation of Diffusion Coefficients

The diffusion coefficient of oxygen transfer was calculated using Fick's Law, Equation (7.6):

$$J_A = -D_A \frac{dC^b}{dx} \qquad \text{Equation (7.6)}$$

where, J_A is the diffusion flux through the gas–liquid interface (mol/m^2.s); C^b is the oxygen concentration in the bulk liquid (mol/m^3), x is the diffusion path length (m) and D_A is the diffusion coefficient (m^2/s).

By rearranging the Equation 7.6,

$$J_A dx = -D_A dC^b \qquad \text{Equation (C.2)}$$

By integrating Equation C.2 and rearranging,

$$J_A x = D_A (C_A^* - C^b) \qquad \text{Equation (C.3)}$$

The slope of $J_A x$ vs $(C_A^* - C^b)$ provides the diffusion coefficient (D_A). Figure C.7 illustrates the procedure to get diffusion coefficient which is 6.6×10^{-8} (m^2/s).

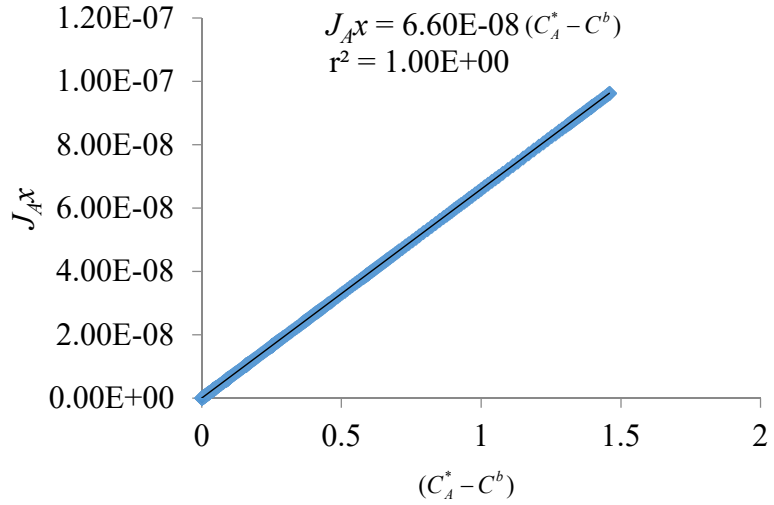

Figure C.7. $J_A x$ vs $(C_A^* - C^b)$ plot based on change in oxygen concentration in indan phase with time at 50 °C during air flow cycles shown in Figure 7.7.